VNiVERSiDAD
D SALAMANCA

CAMPUS DE EXCELENCIA INTERNACIONAL

VNiVERSiDAD DE SALAMANCA

FACVLTAD DE CiENCiAS QVíMiCAS

DEPARTAMENTO DE iNGENiERíA QVíMiCA Y TEXTiL

ESTVDiO TERMODiNÁMiCO DE VN PROCESO SEDS PARA LA PRECiPiTACiÓN DE FÁRMACOS

ANTONIO TABERNERO DE PAZ

2014

ESTVDiO TERMODiNÁMiCO DE VN PROCESO SEDS PARA LA PRECiPiTACiÓN DE FÁRMACOS

Memoria para optar al grado de Doctor por la Universidad de Salamanca realizada por el licenciado

ANTONIO TABERNERO DE PAZ

Salamanca 2014

VNiVERSiDAD D SALAMANCA

CAMPUS DE EXCELENCIA INTERNACIONAL

El Dr. D. Miguel Ángel Galán Serrano, Catedrático de Ingeniería Química de la Universidad de Salamanca y la Dra. Dña. Eva María Martín del Valle, Profesora Titular de Ingeniería Química de la Universidad de Salamanca,

Informan:

Que la memoria titulada: "Estudio termodinámico de un proceso SEDS para la precipitación de fármacos" que para optar al Grado de Doctor en Ingeniería Química, Programa de Doctorado "Ingeniería Química y Medio Ambiente (2006/2008)", presenta D. Antonio Tabernero de Paz, ha sido realizado bajo la dirección de los mismos en el Departamento de Ingeniería Química y Textil de la Universidad de Salamanca y que considerando que constituye un trabajo de tesis autorizan:

Su presentación ante tercer ciclo de la Universidad de Salamanca.

Y para que así conste, firman el presente informe, en Salamanca a 24 de Marzo de 2013.

D. Miguel Ángel Galán Serrano

Dña. Eva María Martín del Valle

Agradecimientos

En primer lugar quiero agradecer a mis directores de tesis, los profesores Eva Martín del Valle y Miguel Ángel Galán, la paciencia, la confianza y la cercanía con la que han intentado enseñarme todo su conocimiento sobre los fluidos supercríticos. Asimismo, agradezco enormemente la libertad que me dieron en ciertos momentos, que me sirvió para ser capaz de aprender de mis errores. Gracias a ellos creo que he conseguido desarrollar una filosofía de trabajo y aprendizaje y me he formado un poco más como persona. Muchas gracias por todo.

También quiero agradecer a los miembros del Departamento de Ingeniería Química de la Universidad de Salamanca toda la ayuda prestada. Especialmente, destacar a Manolo y a Julián, a quienes les debo mucho más de lo que se creen. Y, por supuesto mención aparte para Chema y Audelino, con quienes disfruté mucho en ratos de asueto

Para finalizar con profesores, quería agradecer al Dr. D. Juan M. Rodríguez Díaz del Departamento de Estadística su amabilidad y disponibilidad para enseñarme diferentes cuestiones estadísticas y a Juan González de microscopía electrónica por hacerme más amenos esos ratos en el SEM.

Gracias también a todos los compañeros de laboratorio que he tenido durante este tiempo, principalmente Raúl, Milena, Rafa, Claudio, Cristina R., Mariano, José V., Jesús Antonio, Montaña y Edgar.

Otra mención especial para Carlos Cordón, Manolo Calvo, Elena Cachaza, Pepe Cerveró (gracias por acordarte siempre de mi), y para Cristina Montejo (te tengo que agradecer muchas cosas ya desde Octubre del año 2000). Siempre me acordaré de vosotros allá donde esté.

Agradecer a Vicente los buenísimos ratos en la cafetería. Me has hecho la vida un poco más divertida. Espero que te haya quedado claro que Sergio Rodríguez es el mejor jugador de baloncesto de Europa.

Also, I would like to thank Prof. Neil Foster from the University of New South Wales (Sydney) for accepting me in his research group. Thank you very much for treating me well. I felt like I was another member of the group and I will never forget those six months in Australia. Thanks to all of the members of that group (Danh, Ibrahim, Firman and Grace). Special thanks to Raffaella (for your concern and for your advice), Andrian and Jane (when are you going to pay me a visit?), and the spaniards I met there: David, Toni and Mapi. I owe all of you a deep gratitude and promise we will see each other again.

Na Australia eu também tive a sorte de conhecer e trabalhar com o Prof. Silvio Vieira de Melo da Universidade Federal da Bahía. Muito obrigado pela sua ajuda com tudo em geral. Espero poder trabalhar mais vezes com você, y poder ver um jogo de futebol lá no Brasil além de melhorar o meu português.

También dar las gracias a mis amigos de siempre de Ponferrada y a los que conocí aquí en Salamanca por su continua preocupación por mi. Un especial agradecimiento a Juan y a María Jesús por todas las comidas que me hicieron en los primeros años al salir del laboratorio. También muchas gracias a Mercedes por su apoyo incondicional al final de esta tesis. Ojalá se cumpla lo que dijiste un día sobre los caminos.

Finalmente, quería aprovechar las últimas líneas para agradecer a mis padres su comprensión y su ánimo en todas las decisiones que he tomado, así como por no desesperarse conmigo nunca en mis momentos malos. Asimismo, gracias a mi hermano, que para mí es el mejor físico y científico del mundo, por las cosas que me ha enseñado. Sin él no hubiese podido realizar esta tesis.

“The desire for knowledge shapes a man”

Patrick Rothfuss (The wise man´s fear)

Índice

Lista de figuras

Lista de tablas

Resumen

El presente trabajo de investigación está encuadrado dentro del proyecto que lleva a cabo nuestro grupo de investigación sobre la precipitación de fármacos con fluidos supercríticos como antisolventes (proceso SEDS). En este caso concreto se pretende generar de forma semicontinua partículas de acetaminofén y tretinoína, utilizando etanol como disolvente y CO_2sc como antisolvente.

A fin de conocer la viabilidad de este proceso, es fundamental realizar un estudio termodinámico previo de los distintos equilibrios de fase de los sistemas objeto de estudio, es decir del CO_2-etanol-acetaminofén y CO_2-etanol-tretinoína.

Para ello, se empleó la ecuación de estado cúbica de Peng-Robinson con un parámetro de interacción en las reglas de mezcla de Van der Waals para determinar los equilibrios líquido-vapor disolvente-antisolvente, los equilibrios sólido-vapor soluto-antisolvente y los equilibrios sólido-líquido-vapor soluto-disolvente-antisolvente.

Como dispositivo experimental se empleó una celda de equilibrio con ventanas para correlacionar de forma visual los resultados obtenidos del equilibrio líquido-vapor así como para obtener de manera aproximada el porcentaje de precipitación de los sólidos en un proceso discontinuo.

Mediante la ecuación de estado de Peng-Robinson se han descrito los diferentes diagramas de equilibrio, a partir de los cuáles se pudo determinar la posición del punto crítico de mezcla antisolvente-disolvente así como la

ausencia de inmiscibilidades líquido-líquido en los sistemas estudiados debido a la presencia del sólido.

Estos resultados teóricos fueron confirmados con los resultados experimentales obtenidos con la celda de equilibrio, dónde se observó que la adición del sólido no producía ninguna modificación en la posición del punto crítico de mezcla.

Sin embargo, durante el estudio de los equilibrios de fases, se han observado ciertos inconvenientes al emplear ecuaciones de estado cúbicas para ajustar los equilibrios sólido-fluido supercrítico.

El primero de ellos fue el alto error obtenido y los largos algoritmos en el ajuste de los equilibrios. A fin de reducir el error a la vez que emplear un método computacional más corto, se estudió de manera comparativa el uso de diversas ecuaciones semiempíricas como alternativa a las ecuaciones clásicas.

Este estudio proporcionó información acerca de la mejor ecuación semiempírica para ajustar equilibrios sólido-fluido supercrítico dependiendo de las condiciones experimentales de presión y temperatura.

Con la ecuación de Sparks se obtuvo el mejor ajuste de los datos experimentales.

Por otra parte, se observó que el error de ajuste de las ecuaciones semiempíricas empleadas aumentaba para altos intervalos de temperatura, ya que se alcanzaban las cercanías del punto crítico final superior (*"upper critical end point"*). Sin embargo, este tipo de ecuaciones siempre proporcionaron un error inferior al obtenido con ecuaciones de estado cúbicas.

El estudio de las ecuaciones semiempíricas se extendió a los sistemas sólido-fluido supercrítico con cosolventes. Las ecuaciones empleadas en estos sistemas

producían un error alrededor del 10%, aunque este error se incrementó cuando las condiciones experimentales se acercaban al punto crítico de mezcla fluido supercrítico-cosolvente.

A partir de lo anterior, las ecuaciones de González y Reddy-Madras se presentan como la mejor opción, debido a que pueden ser usadas un amplio intervalo de concentraciones con un bajo número de parámetros.

Asimismo, para finalizar el trabajo relacionado con las ecuaciones semiempíricas, éstas se modificaron mediante la utilización de la función exponencial q procedente de la mecánica estadística no extensiva. Los modelos modificados no presentaban inconsistencia teórica con la temperatura que se había encontrado en los modelos originales, aunque ambas ecuaciones (original y modificada) producen el mismo error de ajuste.

El segundo problema observado en el ajuste de los equilibrios sólido-fluido supercrítico está relacionado con la necesidad de la determinación de la presión de sublimación del sólido. La determinación tanto teórica como experimental de esta propiedad es compleja para fármacos debido a sus bajos valores, a la falta de una gran base de datos así como a la falta de un procedimiento de cálculo para este tipo de moléculas.

Por ello, se desarrolló un método de cálculo de la presión de sublimación de sólidos basado en el modelado de datos experimentales de solubilidad del sólido en CO_2sc con ecuaciones semiempíricas y en la aproximación de Clausius-Clapeyron en el punto triple. Este método fue empleado de manera exitosa en el cálculo de la presión de sublimación de varios sólidos.

Para emplear la aproximación de Clausius-Clapeyron es necesario conocer la entalpía de sublimación del sólido. Al igual que ocurre con la presión de sublimación, su determinación (experimental o teórica) es compleja. Con el fin

de solventar este inconveniente, se desarrolló un modelo de contribución de grupos para la estimación de sólidos constituidos por anillos aromáticos y/o policíclicos sustituidos. Este modelo estima la entalpía de sublimación para estos sólidos con un error aceptable (menor del 10%).

El último problema observado referente a la solubilidad de fármacos en CO_2sc está relacionado con la ausencia de un test de consistencia para evaluar su exactitud.

La solubilidad de una molécula polar en CO_2sc suele ser muy baja (alrededor de 10^{-5}-10^{-8} molar) debido a la diferencia de polaridad. Ello se traduce en que dependiendo del procedimiento experimental pueden encontrarse en bibliografía desviaciones muy elevadas (más de dos órdenes de magnitud) entre diferentes estudios para el mismo sólido.

Con el fin de evaluar la solubilidad de compuestos polares en CO_2sc, se desarrolló un test de consistencia basado en una modificación del factor de mejora y la entalpía de sublimación del sólido. De acuerdo al test desarrollado, sólidos con similar entalpía de sublimación tienen el mismo factor de mejora (enhancement factor) modificado para condiciones experimentales similares. Este test puede resultar muy útil para la evaluación de nuevos datos experimentales de solubilidad en CO_2sc.

Finalmente, una vez realizado el estudio termodinámico de los equilibrios de fases correspondientes, y estudiada la solubilidad de fármacos en CO_2sc, se procedió a la precipitación de fármacos con el SEDS.

Mediante la anterior técnica, se procedió a la precipitación de acetaminofén y tretinoina, disminuyendo su tamaño desde 150 micras a 1-5 micras.

Los resultados obtenidos de esta precipitación se relacionaron con los distintos diagramas de equilibrios de fase, regímenes de atomización y coeficientes de transferencia de materia tanto en la película del líquido como en la del sólido.

El mejor resultado experimental (distribución de tamaño más pequeña con ausencia de agregados) se obtuvo en condiciones ligeramente superiores al punto crítico de mezcla del sistema antisolvente-disolvente. En esas condiciones el grado de sobresaturación está cercano al máximo y la resistencia a la transferencia de materia en la película del líquido es mínima, por lo que el antisolvente penetrará mejor en la gota de la disolución formada. Además, esas condiciones implican que exista una nucleación en fase gaseosa, caracterizada por la no aparición de agregados.

A pesar de que la distribución de tamaño es independiente del régimen de desintegración, conseguir un régimen de atomización es beneficioso para este proceso, ya que se obtiene un menor tamaño inicial de gota, así como una mejor dispersión. Ambos fenómenos favorecen la obtención de una distribución de partícula más pequeña con una morfología más adecuada.

Abstract

This thesis belongs to one of the proyects of our research group relating to particle formation of drugs based on a semicontinuous supercritical antisolvent process, called solution enhanced dispersion by supercritical fluids (SEDS). Specifically, acetaminophen and tretoin have been precipitated by using ethanol and CO_2sc as solvent and antisolvent respectively.

To know the feasability of the SEDS process previous its application a thermodynamic study of the phase equilibria of the different systems (CO_2-ethanol-tretinoin and CO_2-ethanol-acetaminophen) must be carried out aiming.

Peng-Robinson equation of state (with one single binary interaction parameter in the classical Van der Waals mixing rule) was used to determine the vapor-liquid antisolvent-solvent, solid-vapor solute-antisolvent and solid-liquid-vapor equilibria.

On the other hand, a windowed equilibrium cell was used with the purpose of proving the vapor-liquid equilibria results as well as obtaining an approach of the solid precipitation percentage with a discontinuous supercritical antisolvent technique.

Different equilibria diagrams were described by using the former equation of state. Upon those diagramas, it was possible to determine the position of the mixture critical point antisolvent-solvent and the no existence of liquid-liquid immiscibilities at all the investigated conditions.

On the other hand, theoretical results were confirmed with the windowed cell. It was possible to check the conditions (pressure and temperature) of the mixture critical point and the neglectable effect of the solid on these conditions.

However, several drawbacks were found regarding the use of cubic equations of state for fitting solubility data of solids in supercritical fluids.

Computing this type of equilibria with cubic equations of state is a tedious task, and in addition those equations produced a high deviation (more than 20-30%). In order to reduce that deviation and to use a shorter algorithm, several semiempirical equations were used as an alternative.

All of this provided us information regarding which is the best semiempirical equation for fitting solid-supercritical fluid equilibria depending on the experimental conditions (pressure and temperature).

Sparks´ equation [1] was the best equation (in terms of deviation) to fit solubility data solid-supercritical fluid.

Moreover, the error increases for all the semiempirical equations when the increment of temperature is big at the experimental conditions. These equations cannot capture the drastic increase of the solubility at high temperatures (the vicinity of the upper critical end point). In spite of this fact, semiempirical equations provide a better fit for the solubility data solid-supercritical fluids in comparison with cubic equations of state.

After that, this study was extended to systems constituted by CO_2sc, solute and cosolvent by using several semiempirical equations.

All of the investigated models provided a deviation around 10%. Nevertheless, this deviation increased when the experimental conditions were closer to the mixture critical point of the sysmt CO_2sc-cosolvent.

González and Reddy-Madras equations [2-3] are the best choice for modelling those experimental data, because they can be used in a great cosolvent concentration range with few parameters.

Finally, we found an inconsistency with the temperature in some semiempirical equations. In order to remove such inconsistency as well as reducing the deviation, those models for fitting solid-supercritical fluid (with or without cosolvent) equilibria were modified by using the q exponential function from the non-extensive statistical mechanics.

The new q models and the former models provided the same deviation, but q models do not include any temperature inconsistency.

The second drawback concerning the solid-vapour equilibria refers to the calculation of the sublimation pressure of the solid.

The estimation of this property for drugs is a difficult task because its value is usually very low, and in addition there is not a standard procedure or a huge data base for its calculation or estimation.

For that reason, a procedure for calculating the sublimation pressure of complex molecules was developed in this thesis. This procedure is based on modelling solubility data of solids in CO_2sc and on the Clausius-Clapeyron approach in the triple point. This method was succesfully used for calculating sublimatin pressures of several solids.

According to this method, it is required a knowledge of the sublimation enthalpy of the solid. However, as happened with the sublimation pressure, the determination of that property is not easy and there is not a group contribution method for its estimation for drugs.

In order to solve the previous shortcoming with the sublimation enthalpy, a group contribution model for estimation that property for solids constituted by aromatic and/or polycyclic aliphatic rings was developed. That model predicted the sublimation enthalpy of this type of solids with a deviation lower than 10%.

The last drawback concerning the solubility of solids in supercritical fluids is the lack of a consistency test for assesing the accuracy of new experimental data.

The solubility of drugs in CO_2sc is usually very low (around 10^{-5}-10^{-8} in molar fraction) due to the different polarity. That is a disadvantage because these data are strongly related to the experimental procedure or the solid impurities.

Then, high deviations (sometimes more than one order of magnitude) can be found between different solubility studies for the same solid depending on the procedure used in its determination.

Therefore, a consistency test based on a modified enhancement factor and the sublimation enthalpy of the solid was developed. According to that test, solids with similar sublimation enthalpies have similar modified enhancement factors at the same experimental conditions. That approach can be useful for distinguishing between accurate and inaccurate experimental data.

Finally, after studying the phase equilibria and the solubility of drugs in CO_2sc, the precipitation of acetaminophen and tretinoin was succesfully performed with a SEDS technique. By using this technique, the particle size distribution of both solids was reduced from 150 microns to 1-5 microns.

Those experimentals results were explained according to the different equilibria diagrams, disintegration regimes and mass transfer coefficients of the liquid and gas films.

The narrowest particle size distribution without aggregates was obtained at experimental conditions near and above the mixture critical point antisolvent-solvent.

At those conditions the degree of supersaturation is close to its maximum. Furthermore, the value of the mass transfer resistence of the liquid film is close to the minimum and there is a gas-to-solid nucleation.

Those phenomena improve the penetration of the antisolvent (CO_2sc) inside the droplet and as a consequence the antisolvent effect.

Results indicate that there is not a clear dependency of the particle size distribution with the disintegration regime. However, an atomization regime is preferred over a sinous wave break-up or a Rayleigh regime because an atomization regime produces a smaller initial droplet size and a finer dispersion. Both facts improve the process outcome.

CAPÍTULO 1.

Concepto e importancia del uso de fluidos supercríticos en la industria farmacéutica

1.1. Importancia de la industria farmacéutica

Como consecuencia de la importancia en el tratamiento de enfermedades, la industria farmacéutica es una de las industrias que más dinero mueve en el mundo.

Así, en el año 2010 las ventas de productos farmacéuticos alcanzaban casi 900 billones americanos de dólares y llegaron a los 1000 billones en el año 2012. Aunque en este sector los ingresos por ventas han disminuido en estos últimos años (figura 1.1) presenta un crecimiento constante, por lo que es considerado como uno de los más beneficiosos e importantes del mundo [1].

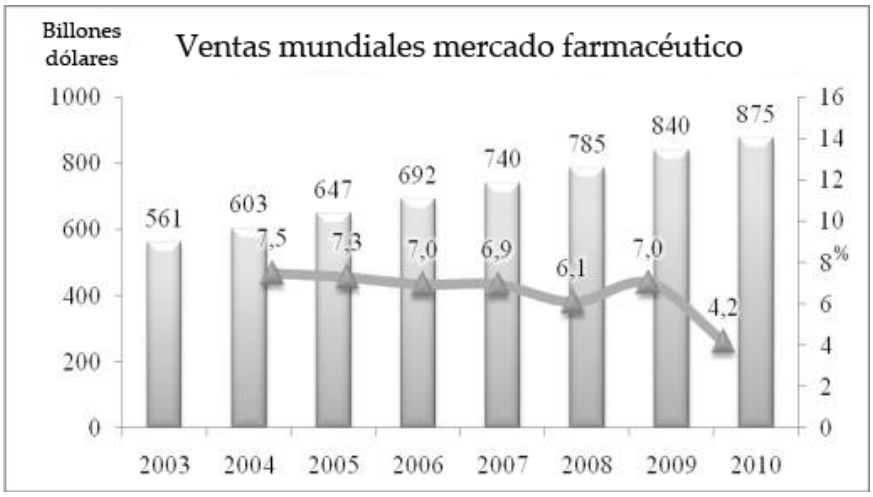

Figura 1.1 Ingresos por ventas en la industria farmacéutica [1].

Todo ello a pesar de que el coste del desarrollo de un fármaco hasta ponerlo en el mercado ha pasado de 139 MM$ en 1975 a 1300 MM$ en el año 2013 debido a diferentes desafíos técnicos y de la autoridad sanitaria [2].

Dentro de esta industria, la mayoría de sus preparaciones como aerosoles, cápsulas, suspensiones o supositorios contienen fármacos en forma particulada.

Por ello, las compañías farmacéuticas centradas en la necesidad de desarrollar nuevos productos y nuevas vías para su administración y ser competitivas, están realizando un gran esfuerzo económico en investigación. Todos esos avances van destinados principalmente a mejorar los mecanismos de eficacia y biodisponibilidad de sus productos, además de reducir sus efectos secundarios y minimizar las dosis necesarias, lo que conduce a un beneficio humano y económico.

Lo anterior determinó que alrededor de los años 30 surjan como gran novedad los fármacos microencapsulados.

Las microcápsulas pueden definirse como una pequeña esfera (en la que el material activo constituye su núcleo) rodeada por un recubrimiento homogéneo (normalmente un polímero).

Este diseño permite el control del mecanismo de liberación del fármaco a través de la membrana, consiguiéndose de esa forma una liberación controlada en el tiempo, como puede observarse en la figura 1.2 [3]

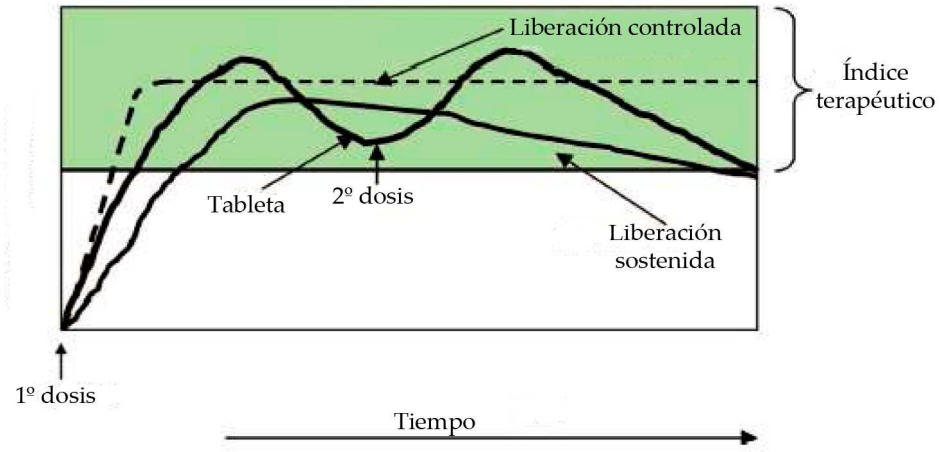

Figura 1.2. Diferentes perfiles de liberación de un fármaco en sangre [3]

Teniendo en cuenta lo anteriormente descrito puede concluirse que durante estos últimos años la investigación en el mercado farmacéutico está

principalmente dirigida hacia el desarrollo de nuevas técnicas para producir nuevos sistemas de liberación de una forma eficaz y no contaminante.

1.1.1. Importancia del tamaño de partícula en la industria farmacéutica.

El tamaño de partícula es una propiedad que condiciona la superficie de la misma, y es de máxima importancia en procesos de liberación de fármacos.

Es bien conocido que en la industria farmacéutica el tamaño más pequeño favorece el porcentaje de fármaco absorbido por el organismo y el aumento de la tasa de disolución del producto. De igual forma, al lograr una disminución del tamaño se pretende también mejorar su metodología de administración del principio activo o la disminución de las dosis necesarias de un tratamiento.

Así, partículas con un intervalo de tamaño entre 0,1-0,3 micras son necesarias para la administración intravenosa, 1-5 micras para inhalación respiratoria y 0,1-100 micras para la administración oral [4-5].

Sin embargo, además del tamaño de partícula del fármaco existen otras propiedades dimensionales y químicas que condicionan el uso de los fármacos, tal como puede observarse en la tabla 1.1.

Tabla 1.1. Propiedades estructurales, dimensionales y químicas de los fármacos y sus efectos [6].

Propiedad	Efecto
Estructural: - Cristalinidad. - Hidratos. - Sales.	- Estabilidad física y química. - Perfil solubilidad y disolución. - Aspectos en procesado
Dimensional: - Tamaño partícula. - Morfología. - Estructura superficie partícula.	Forma de administración al cuerpo humano
Químicas: - Impurezas	Toxicidad

1.1.2. Limitaciones de los métodos convencionales de micronización.

Como se indicó anteriormente en la sección 1.1.1, la investigación en el sector farmacéutico se dirige hacia el desarrollo de nuevas técnicas para la generación de partículas de tamaño cada vez más pequeño y para la producción de nuevos sistemas de liberación de los mismos.

Sin embargo, a pesar de este esfuerzo en investigación se siguen empleando métodos convencionales. Cada uno de estos métodos puede producir ciertas desventajas, como se describe a continuación.

Así, la molienda y el triturado producen una amplia y no uniforme distribución de tamaño de partícula. Otras técnicas, como la molienda con gas (*jet milling*) o el secado por spray (*spray drying*), son procesos altamente

consumidores de energía, o requieren alta temperatura, por tanto, el principio activo puede resultar dañado [7].

Se podría emplear también disolventes orgánicos en procesos con antisolventes o en procesos de emulsión, sin embargo, en estos casos, la toxicidad del producto final puede incrementarse, ya que trazas de disolvente pueden encontrarse en las partículas obtenidas. Es por ello que las características de los disolventes o de los antisolventes empleados en este tipo de procesos deben situarse entre ciertos valores límite de toxicidad, de acuerdo a estándares impuestos por distintas organismos internacionales.

Con el fin de solucionar todos estos problemas, se está investigando actualmente el uso de compuestos no contaminantes que puedan ser utilizados como solventes o como antisolventes para la generación de partículas en la industria farmacéutica. Un ejemplo de ello es el empleo de CO_2 supercrítico (CO_2sc), que está recibiendo una especial atención debido a su carácter no tóxico y no inflamable, además de inerte, barato y medioambientalmente benigno.

1.2 CO_2sc en técnicas de micronización

Durante estos últimos años se ha incrementado notablemente la investigación en el uso de fluidos supercríticos (especialmente el CO_2sc) para la generación de partículas de interés para el sector farmacéutico. Ello ha sido fundamentalmente debido a sus propiedades intermedias de transporte entre los líquidos y los gases. Los fluidos supercríticos pueden ser empleados como solventes o antisolventes en diferentes técnicas no contaminantes con el fin de

producir pequeñas partículas cristalinas en un estrecho intervalo de la curva de distribución de tamaño.

A continuación se va a proceder al estudio de revisión de estas técnicas, explicando sus mecanismos y sus fundamentos relacionados con la termodinámica y la cristalización.

ARTÍCULO

Supercritical fluids for pharmaceutical particle engineering:

Methods, basic fundamentals and modelling,

Chemical engineering and processing: Process intensification

60 (2012) 9-25.

Chemical Engineering and Processing 60 (2012) 9–25

Contents lists available at SciVerse ScienceDirect

Chemical Engineering and Processing: Process Intensification

journal homepage: www.elsevier.com/locate/cep

Review

Supercritical fluids for pharmaceutical particle engineering: Methods, basic fundamentals and modelling

Antonio Tabernero, Eva M. Martín del Valle*, Miguel A. Galán

Department of Chemical Engineering, University of Salamanca, P/Los Caídos S/N, 37008, Spain

ARTICLE INFO

Article history:
Received 3 May 2012
Accepted 18 June 2012
Available online 26 June 2012

ABSTRACT

The interest of the use of supercritical fluids, especially supercritical CO_2, for particle engineering over the last years has received attention from the pharmaceutical industry. Supercritical fluids can be used in different clean technologies to achieve high supersaturation, and consequently small crystalline particles with a narrow particle size distribution can be produced. This article aims to provide a compilation of old and new supercritical fluid as solvent or antisolvent techniques for drug processing and their fundamentals in terms of crystallization, thermodynamics and modelling results.

© 2012 Elsevier B.V. All rights reserved.

Contents

1. Introduction

1.1. Requirements of pharmaceutical industry

Over the last decades, research in advanced drug delivery and targeting have increased drastically due to the requirements of the pharmaceutical industry. As a matter of fact, in mid-90s, several products based on drug delivery had worldwide sales with more than 10 million dollars [1]. Inside the pharmaceutical industry, around 90% are in crystalline form [2].

Particle engineering for drug delivery needs methodologies that can provide control of particle size and polymorphic purity. Particle size affects the delivery route of the drugs, "deciding" what specific organ can be targeted. Particles should be around 0.1–0.3 μm. for intravenous delivery, 1–5 μm. for inhalation delivery, and 0.1–100 μm. for oral delivery [3]. Small size also implies a greater percentage of drug absorbed by the human body and a reduction of the doses number. On the other hand, crystallinity affects the physical and chemical stability, whereas organic and inorganic impurities indicate toxicity [2].

* Corresponding author. Tel.: +34 923 294479; fax: +34 923 294579.
E-mail address: emvalle@usal.es (E.M. Martín del Valle).

0255-2701/$ – see front matter © 2012 Elsevier B.V. All rights reserved.
http://dx.doi.org/10.1016/j.cep.2012.06.004

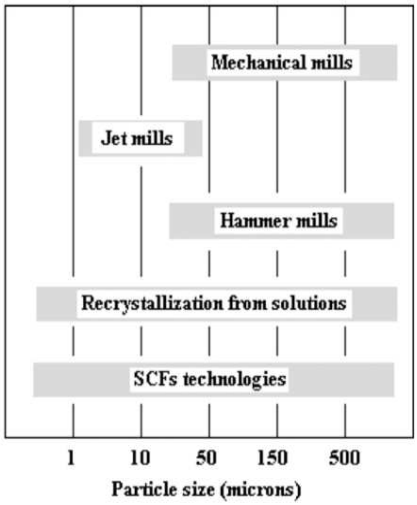

Fig. 1. Different drugs processes for some particle size ranges.

In spite of these facts, conventional micronization techniques for pharmaceutical industry do not give the option to control or modify these previous characteristics.

Specifically, regarding size and distribution, milling and grinding produce a broad particle size distribituion (PSD). Jet milling, a technique that uses impact forces between the particles to break up the products into smaller pieces consumes energy, and in addition does not provide a uniform PSD. Another method like freeze-drying usually requires a subsequent milling due to the broad PSD. Particles with controllable size might be obtained using a spray-drying process, but the required high temperatures to drive the droplets evaporation can damage the pharmaceutical. Finally, if a conventional precipitation process with organic solvents is used, traces of the organic solvent might be remained in the precipitated particles [4–7].

As an example, Fig. 1 shows different techniques and the particle size that can be obtained with them. It can be seen how supercritical fluids (SCFs) technologies can provide a particle size less than 1 μm, offering in addition a clean technology.

1.2. Supercritical fluids and their properties

A SCF can be defined as any fluid which is at conditions above its critical point (Fig. 2). SCFs present gas–liquid transport properties. As it can be observed in Fig. 2, SCFs have liquid-like density, but viscosity and diffusivity remain between liquid-like and gas-like values. In addition, SCFs exhibit almost zero surface tension. Due to these transport properties, SCFs have been introduced in different fields for different applications, such as extractions, chromatography, or particle generation.

Table 1
Critical properties of different compounds [8].

Compound	T_c (K)	P_c (MPa)
Ammonia	405.7	11.3
Benzene	562.2	4.9
Carbon dioxide	304.3	7.4
Chlorotrifluoromethane	384.9	3.9
Ethane	305.6	4.9
Ethylene	282.5	5.1
Methanol	513.7	7.9
n-Propane	367.0	4.3
Water	647.6	22.1
Xenon	562.9	5.84

1.3. Supercritical CO_2

A variety of compounds might be used as SCFs. However, as it can be observed in Table 1, the critical properties are usually extremely high except for a few compounds. These compounds, such as light hydrocarbons, are usually in addition inflammable and toxic products. On the other hand, it seems that carbon dioxide is the only compound that can be used as a "green solvent" with acceptable critical properties. That is the main reason why supercritical CO_2 (sc-CO_2) is the most used SCF.

Furthermore, CO_2 is non-flammable and inert. Its threshold limit value (TLV) is around 5000 ppm. It is as a consequence less toxic than acetone (750 ppm) or pentane (600 ppm). Its TLV and high vapour pressure implies that residual CO_2 is not harmful to human health [9].

Regarding solubility, CO_2 is considered a non-polar solvent, in spite of its quadrupole moment. However, as happens with other supercritical gases, the dielectric constant of the CO_2 increases with pressure. These two opposite effects make difficult to predict the solubility behaviour of different molecules in sc-CO_2. According to Stahl et al. [10], sc-CO_2 is a good solvent for lipophilic compounds with low polarity such as epoxides, ethers or esters at low pressure range.

Nevertheless, molecules constituted by strong polar groups (e.g. –COOH) are less soluble in sc-CO_2. Regarding benzene derivatives, it is important to consider different aspects. It seems that compounds with three phenolic hydroxyls or one carboxyl and two hydroxyl groups can be solubilized in sc-CO_2. The opposite effect, however, has been found for molecules with one carboxyl and three or more hydroxyl groups [10].

Nevertheless, if it is required, the solubility of any polar solid in sc-CO_2 can be enhanced by using different co-solvents. Finally, polar dissolvents like short alcohols and short-chain hydrocarbons (ethanol, acetone) are miscible with sc-CO_2 at relatively moderate pressures. This solubility decreases directly with the number of carbon atoms in the chain. In this context, different works and reviews have been done regarding the solubility of solids in SCF with and without cosolvents [11,12].

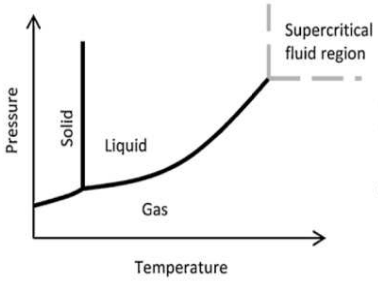

	Density ($kg \cdot m^{-3}$)	Viscosity ($mPa \cdot s$)	Diffusivity ($cm^2 \cdot s^{-1}$)
GAS	0.8-1.3	0.01-0.03	0.1-0.2
LIQUID	800-1200	0.4-1.1	0.00001-0.0001
SCF	300-1000	0.05-0.01	0.0001-0.001

Fig. 2. Phase diagram of a compound and physicochemical properties for liquids, gases and SCFs.

Table 2
Different published reviews and their main subject.

Authors	Main subject
Tom and Debenedetti, 1991 [13]	RESS (fundamentals) for different materials.
Debenedetti et al., 1993 [14]	RESS y GASS. Microencapsulation and proteins formation.
Phillips and Stella, 1993 [15]	RESS for pharmaceutical processes.
Subramanian et al., 1997 [16]	General review. Solubility of solids in SCFs with or without cosolvent.
Subra and Jestin, 1999 [17]	RESS y SAS. Applications and fundamentals of solid formation.
Palakodaty and York, 1999 [18]	Phase behaviour for SCFs as antisolvents.
Reverchon, 1999 [19]	General review and different fundamentals and mechanism of particle formation. Effect of different parameters.
Marr and Gamse, 2000 [20]	General review. SCFs for different applications.
Thiering et al., 2001 [21]	General review. GAS and ASES with scale-up considerations.
Jung and Perrut, 2001 [22]	General review and patents.
Knez and Weidner, 2003 [23]	General review. Design criteria for PGSS.
Reverchon et al., 2003 [24]	RESS, SAS and PGSS based processes for composites production. Foams and membranes formation.
Vemavarapu et al., 2005 [25]	General review and design of processes for particle formation at laboratory scale.
Yeo and Kiran, 2005 [26]	General review and polymer and microencapsulation with SCFs.
Reverchon and Adami, 2006 [27]	SCF techniques for nanomaterials.
Shoyele and Cawthorne, 2006 [7]	General review and comparison with conventional techniques.
Nalawade et al., 2006 [28]	Applications of sc-CO_2 as a processing solvent for polymer applications. Fundamentals.
Tandya et al., 2007 [29]	General review and drug/polymer formulation with different techniques.
Martín and Cocero, 2008 [30]	General review. Fundamentals (mass transfer, phase equilibrium, crystallization) and mechanisms.
Byrappa et al., 2008 [31]	General review and different biomedical applications.
Mishima, 2008 [32]	General review. Microencapsulation, microparticle formation of gene and drug in SCF.
Pasquali et al., 2008 [33]	General review. Control of the solid state of drugs.
Pasquali and Bettini, 2008 [34]	General review and SCFs for pharmaceutical applications.
Cocero et al., 2009 [35]	General review and fundamentals of encapsulation and coprecipitation processes with SCFs.
Reverchon et al., 2009 [36]	General review. SCFs for polymer processing for pharmaceutical applications (scaffolds. microencapsulation).
Kikic, 2009 [37]	Interactions between polymer and SCFs. Modelling solubility of polymers in SCFs.
Kiran, 2009 [38]	Polymer solutions at high pressure. Application areas.
Turk, 2009 [39]	RESS and modifications. Modelling and its fundamentals.
Skerget et al., 2011 [40]	Solubility of solids in SCFs. Modelling.
Beh et al., 2012 [41]	General review. Lipid-based drug carrier systems.

1.4. Particle engineering and sc-CO_2

The use of sc-CO_2 provides therefore several advantages in comparison with the previous conventional techniques. The sc-CO_2 can be used as a solvent, antisolvent, as extracting agent for the organic phase of oil in water emulsions or even to improve the spraying process in different techniques.

These processes and/or their fundamentals have been discussed in different reviews. Table 2 shows reviews for the last two decades with their main innovation. It should be specified that the corresponding acronyms will be explained in section 4. It must be also highlighted the issue 3, volume 60 (2008) of the journal *Advanced Drug Delivery Reviews*. That issue is dedicated to supercritical fluid technologies for drug delivery and pharmaceutical applications (some of them exposed in Table 2).

These previous reviews focus in the use of SCFs for different pharmaceuticals applications, and occasionally for modelling/fundamentals of these types of processes.

Our present review aims to cover a more extended number of SCFs (as solvents or antisolvents mainly) processes for solid particle engineering. Their corresponding modifications and modelling results for the most used processes are also included.

Small crystalline particles with a narrow PSD are obtained because the use of SCFs can provide great and fast supersaturations. Since the supersaturation depends on the phase equilibrium of the system, this review should start therefore with the corresponding fundamentals of the crystallization kinetics and phase equilibria.

2. Relation between crystallization and supersaturation

Get a great and a fast supersaturation is the main objective of the SCFs processes for particle formation. From a thermodynamic point of view, this can be explained due to the difference between the chemical potential of the solute in the fluid (μ_i) and at equilibrium (μ_i^*). This difference is the driving force of the precipitation (Eq. (1)). When the concentration (x_i) is higher than the equilibrium concentration (x^*), the solute will precipitate up to the difference between the corresponding chemical potentials became null, and the equilibrium is achieved [42]. The activity coefficient of the solute (γ_i), and the solute at equilibrium (γ_i^*), the gas constant R and the temperature T are included in Eq. (1).

$$\mu_i - \mu_i^* = RT\,\mathrm{Ln}\left(\frac{\gamma_i x_i}{\gamma_i^* x_i^*}\right) \tag{1}$$

On the other hand, the supersaturation (S) is directly related to the difference between the respective chemical potentials (Eq. (2)):

$$\mathrm{Ln}(S) = \frac{\mu_i - \mu_i^*}{RT} = \mathrm{Ln}\left(\frac{\gamma_i x_i}{\gamma_i^* x_i^*}\right) \tag{2}$$

The previous equation justifies the precipitation of the solid for great values of supersaturation. By using different methodologies, the equilibrium concentration x^* can be reduced drastically, and the solute should precipitate to reach the equilibrium for the system [3].

The supersaturation also establishes the nucleation kinetics. These kinetics can be primary heterogeneous and primary homogeneous. The homogeneous (and the optimal) nucleation occurs without the existence of a solid surface, and it is explained by means of the classical nucleation theory. This theory assumes that clusters or embryos are produced due to a combination process [43]. Eq. (3) shows the embryo free energy for a particle for a given radius r. The term λ is referred to the energy for surface unit ($\mathrm{J\,m^{-2}}$), a is the area of a spherical particle ($\mathrm{m^2}$) with a radius r (m), k_B is the Boltzmann's constant (J K), whereas ν and υ are molecular volume of the precipitated embryo ($\mathrm{m^3}$) and the volume of a spherical particle ($\mathrm{m^3}$) with a radius r.

$$\Delta G = -\left(\frac{\upsilon}{\nu}\right) k_B \cdot T \cdot \mathrm{Ln}(S) + \lambda a \tag{3}$$

According to Eq. (3), nuclei are only formed when the value of the supersaturation is higher than the unit because the free energy is negative. This can be also observed in Fig. 3 which shows the energy change against the radius. For supersaturations greater than the unit, the energy increases until a maximum that corresponds

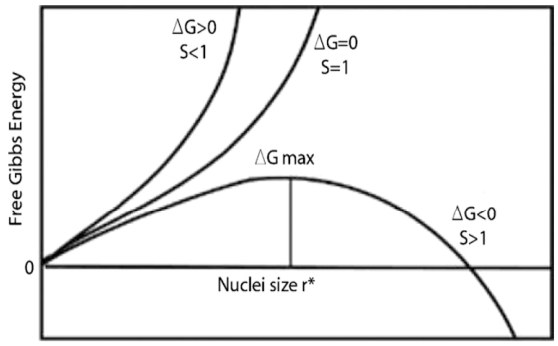

Fig. 3. Free Gibbs energy change against radius [43].

with a specific radius (critical radius r^*). Particles higher than r^* are considered nuclei, but if the particles are smaller than the critical radius, they will redissolve (embryos). Finally, after the maximum, the free energy decreases until the equilibrium is reached. At this value, the nuclei will be stable with their corresponding size [43].

The number of nuclei per volume and time B can be calculated with the knowledge of the supersaturation (Eq. (4)). According to this equation, the term B is strongly non-linear with S. B tends to 0 if the supersaturation is close to 0. However, the number of nuclei increases when the supersaturation is higher than 1:

$$B = A \exp\left[-\frac{16\pi\lambda^3\nu^2}{3k_B^3 T(\mathrm{Ln}\, S)^2}\right] \quad (4)$$

The time to get the supersaturation is important. Fast supersaturation highlights that nucleation is the main phenomenon over crystal growth. On the other hand, there is a competition between both phenomena, with larger crystals and wider PSD for slower supersaturation time.

3. Phase equilibrium

In order to guarantee a proper process design, it is crucial to known the phase behaviour and solubility of the system of interest. In fact, the driving force of any precipitation process is the supersaturation, which is defined as the ratio of the real concentration and the saturation concentration.

Therefore, it would be very important to make a previous theoretical calculation of the saturation concentration. In order to do that, different types of equations can be used to determine concentrations at equilibrium.

Cubic equations of state (EOS), such as Peng–Robinson (PR) for instance (Eq. (5)):

$$P = \frac{R \cdot T}{v - b} - \frac{a}{v^2 + 2bv - b^2} \quad (5)$$

This type of equations establishes a relation between pressure (P), temperature (T) and molar volume (v). In order to take into account the non-ideal behaviour, energetic parameters (a) and covolume (b) must be introduced [44].

These EOS can be used to calculate fugacities. This fact is very important because equilibria are usually calculated based on an iso-fugacity approach for the different phases. This procedure can be used for binary or multicomponent equilibria (liquid–vapour, solid–vapour or solid–liquid–vapour). For solids, the solid phase should be assumed as pure solute, and it would be necessary to use the solid sublimation pressure to calculate the fugacity of the solid. There are few data for sublimation pressure of pharmaceuticals, but this fugacity might be also calculated as a function of a reference sub-cooled liquid state [45].

One of the main limitations of this procedure is the requirement of different properties, such as critical properties or the sublimation pressure of the solid [46]. Although there are different contribution groups or methodologies to estimate these properties [47–52], but the deviation can be increased by the use of these estimations because they have been developed in some occasions for only a specific type of compounds.

Moreover, to get a better fit for the phase equilibria, mixing rules are needed. These mixing rules modify the energetic parameter and the covolume by introducing binary interaction parameters, taking into account deviations due to the interactions. In fact, the "predictive power" of the equation is given by the mixing rules.

The most common mixing rules were established by Van der Waals, and have one or two binary interaction parameters [53,54]. Since then, different works have been published in order to create new mixing rules, even with three interaction parameters, in order to improve the fit [55,56].

Although a proper fit for vapour–liquid equilibria can be obtained using one single binary interaction parameter in the mixing rule, usually two parameters are used [57–59]. However, if there is a solid involved, at least two parameters are needed to get an accurate result with polar solids [56,60,61]. Furthermore, if the system contains a polymer, these equations do not provide a good fit, due to the difficulties for cubic equations to take into account strong interactions.

These parameters should be calculated by regressing experimental data of binary systems against theoretical data. This fact highlights the semiempirical character of the EOS. Moreover, if it would be necessary to estimate a solid–liquid–vapour equilibrium with more than two components (multicomponent and multiphasic equilibria), experimental data for solid–vapour and vapour–liquid equilibria must be previously determined to calculate the corresponding interaction parameters.

Therefore, the EOS might not be a suitable tool for predicting equilibria data at high pressure, given that experimental data are required for obtaining these interaction parameters.

Semiempirical equations are emerging as a good way to fit solubility data of solids in SCFs. These equations do not need solid properties and they include different semiempirical parameters that must be calculated for each solid. These parameters are based on simple error minimization, avoiding therefore the required iterative computational methods for iso-fugacity approaches. One of the first semiempirical equations was published by Chrastil in the 80s (Eq. (6)). This equation [62] is based on the solvato complex formed between solute and SCF at equilibrium, proposing a relation between the solubility (S in $\mathrm{kg\,m^{-3}}$) and the density of the SCF (ρ_1 in $\mathrm{kg\,m^{-3}}$). It can be seen, how three parameters (k is the association factor, A and B) must be determined for this equation by regressing experimental against theoretical data.

$$S = \rho_1^k \exp\left(\frac{A}{T} + B\right) \quad (6)$$

Since then, several modifications of Chrastil's equation and new (and numerous) semiempirical models have been developed, some of them even with 6 adjustable parameters, in order to reduce the deviation [63–70]. Among them, it is possible to find either solubility–density relations or empirical correlations based on the effect of the different experimental parameters (P, T, ρ) in the solubility of the solid. Due to this big number of semiempirical equations, different articles have been published in order to perform a comparison between them (and with cubic EOS) [71–74]. According to some works, semiempirical models usually give a more accurate result in terms of deviation than cubic EOS.

The main drawbacks of these equations are their semiempirical character and their only application for solid–SCFs systems.

However, semiempirical models have been proposed to correlate the solubility of solid–cosolvent-sc-CO_2 and solid–cosolute-sc-CO_2 [75,76].

Molecular-based equations, are non-cubic EOS and can fit properly these solubility data. Lattice-based Sánchez–Lacombe (SL) EOS [77] or off-lattice based theory Perturbed Hard Sphere Chains (PHSC) [78] can be included in this classification. This type of equations needs the use of mixing rules and different molecular properties that should be calculated with different contribution groups [79]. In comparison with other equations, SL-EOS fits successfully the equilibrium with polymers, but fails to predict vapour–liquid equilibria or solid–vapour equilibria (in comparison with PHCT-EOS or PR-EOS). On the other hand, PHCT-EOS fits properly polymeric systems and provides in general a better fit that PR-EOS for vapour–liquid, solid–vapour equilibria and solid–liquid–vapour equilibria, but can fail with high polar molecules [80].

Although it is proved that there are different equations to fit solubility data of binary and multicomponent systems at high pressure, it seems that all the previous methodologies present an important shortcoming.

Solubility data is always required to calculate the interaction parameters for the different equations in order to get a better fit. Therefore, there is not a suitable tool to perform a reasonable and accurate prediction of this type of equilibria without experimental data.

This is the reason why new methodologies to predict these equilibria without experimental data (only with solid properties) are being developed. As an example, De Zordi et al. [81], recently published an article in which solid–vapour equilibria could be estimated by calculating the activity coefficient at infinite dilution of the solute in the dissolution using a linear free energy correlation.

4. Processes with SCFs

There are several processes that use SCFs for particle production. These methods will be explained with more detail after this classification. Depending on the characteristics, these techniques can be divided into different groups:

SCFs as solvents. In this case, the solute must be dissolved in the SCF. Rapid expansion of supercritical solution (RESS), rapid expansion of a supercritical solution into a liquid solvent (RESOLV), rapid expansion of supercritical solution into an aqueous solution (RESSAS) and rapid expansion of supercritical solution with a nonsolvent (RESS-N) are in this group.

SCF as antisolvents. The SCF is put in contact with a solution of the solute. Processes such as gas antisolvent (GAS), supercritical antisolvent (SAS), aerosol solvent extraction system (ASES), solution enhanced dispersion by supercritical fluids (SEDS), particles by compressed antisolvent (PCA) or atomized rapid injection for solvent extraction (ARISE) can be defined in this group.

SCFs as cosolvents or as a compound to reduce the melting point. Techniques in which the solution (or only the solute) is solubilized in the SCF, followed by a rapid depressurization to exploit the Joule–Thomson effect. Particles from gas saturated solutions (PGSS), PGSS-drying, gas assisted melting atomization (GAMA) and depressurization of an expanded liquid organic solution (DELOS) can be included in this group. Similar to DELOS is the process called precipitation by pressure reduction of gas-expanded liquids (PPRGEL).

SCFs as a nebulization compound. The SCF is used to assist the nebulization of the solution, such as carbon dioxide assisted nebulization with a bubble dryer (CAN-BD) and supercritical fluid-assisted atomization (SAA). In SAA, the SCF plays also the role of a cosolvent.

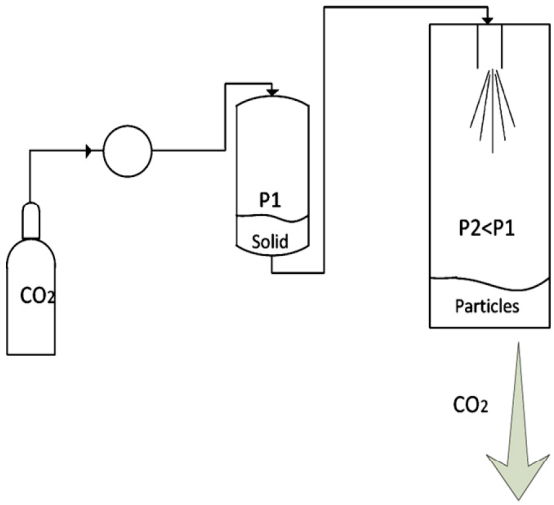

Fig. 4. RESS process.

SCFs as an extracting and antisolvent compound. Supercritical fluid extraction of emulsions (SFEE) combines the extraction and the antisolvent power of the SCFs.

Miscellaneous processes. Techniques to take advantage of different aspects of the SCFs to obtain compounds for pharmaceutical applications.

4.1. RESS and its modifications (RESOLV and RESSAS)

RESS was patented in 1986 [82], and exploits the ability of the sc-CO_2 to solubilize different compounds. The mixture is expanded subsequently to a vessel at atmospheric pressure by using a nozzle. This fast depressurization provides great supersaturation values because the solvent power of the SCF decreases drastically, and the nucleation takes place only in the gas phase. That means good size and distribution. The schematic of the RESS technique can be observed in Fig. 4.

The particle size and morphology might be controlled by changing different parameters [83,84]. The pre-expansion pressure and nozzle design (greater nozzle diameters give higher flow rates) can be controlled to modify the residence time, because the SCF flow rate is strongly dependent on these parameters [85]. Even the structure of the compound might be modified by changing the operation conditions, as occured with the carbamazepine [86].

Formation of liquid droplets should be avoided in this process. It is required to perform a previous thermodynamic study to get a knowledge of the variation of the solid (or polymer) melting temperature with the pressure (knowing the solid–gas equilibrium), and to determine the solubility of the compound in the SCF [86]. The melting point depression should be also considered when a microencapsulation is performed, that is another application for the RESS process [85]. Inclusion complexes with cyclodextrins can be also produced using this technique [87].

Sonic velocities are produced at the exit of the nozzle due to the difference between the pre-expansion pressure and the expansion pressure. As a consequence, the pressure drop at the exit of the nozzle causes a temperature decrease (freezing process). Nozzle design can therefore affect the fluid mechanics of this technique [13,14]. Freezing/condensation is the main reason why the temperature must be kept constant in the nozzle and in the vessel.

RESS process is well-studied and different works regarding their modelling have been published, and many of them have been

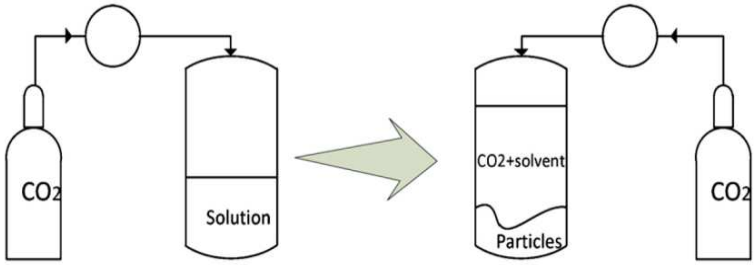

Fig. 5. GAS process.

reviewed by Turk, 2009 [39]. According to different studies, (very well explained in Turk's article), the smallest particles are produced for short residence times and a relative low solubility of the solute in the SCF.

RESS provides a uniform PSD and in addition its application for small scale is relatively simple. Moreover, particles are solvent free and do not require post-processing.

On the other hand, the great SCF/solution rate requirement and the limited solubility (the solubility should be 10^{-4} for a reasonable outcome) of pharmaceuticals in sc-CO_2 due to the difference in polarity are important drawbacks. Another shortcoming is the probability of damaging sensitive high stress products, such as proteins. However, problems concerning solubility might be solved using a liquid [88,89] or even a solid (e.g. menthol) cosolvent [90].

RESS process is not easy to scale-up due to the possibility of nozzle blockage, and in addition, the obtained small particles are difficult to use in proper pharmaceutical form due to the possibility of adhesion/aggregation [39]. Therefore, due to the previous reasons, several modifications have been implemented for the RESS process.

One of these RESS variations is called **RESS-N**. Polymer microparticles or microcapsules of proteins have been produced with this process. The main characteristic of this technique is the use of a cosolvent to enhance the solubility of the solid in the sc-CO_2. This cosolvent must not neither dissolve the polymer in its pure form nor produce the polymer swelling [89]. This process provides in addition the ability to control the thickness and the PSD of the particles by changing the feed composition of the solid. But, liquid cosolvents are usually organic liquids that can produce undesired organic traces.

RESOLV is a simple RESS modification. Although different simulations prove that particles with 10–50 nm diameter range can be obtained with RESS [13,14] as long as there is a subsonic expansion, these particles are usually in the micron-sized due to different collisions mechanisms. RESOLV uses a liquid solvent in the expansion vessel to avoid the growth of the particles in the expansion jet, and therefore, particles less than 100 nm are obtained. However, it is required the use of a stabilization agent [91,92]. The use of the stabilization agent can complicate the understanding of this process, but this fact might be employed to modify the crystallinity and properties of the solute. **RESSAS** is a simple modification of RESOLV, using a water solution with a surfactant as a stabilizing agent [93,94]. For RESSAS and RESOLV, more experimental parameters should be taken into account, such as surfactant properties (surface tension and dynamic interfacial tension) or the solute solubility in the aqueous surfactant solution [39].

4.2. GAS

As it was explained before, one of the main limitations for RESS application is the poor solubility of compounds with high polarity, such as several pharmaceuticals, in sc-CO_2. Therefore, the sc-CO_2 (or another SCF) was started to use as an antisolvent.

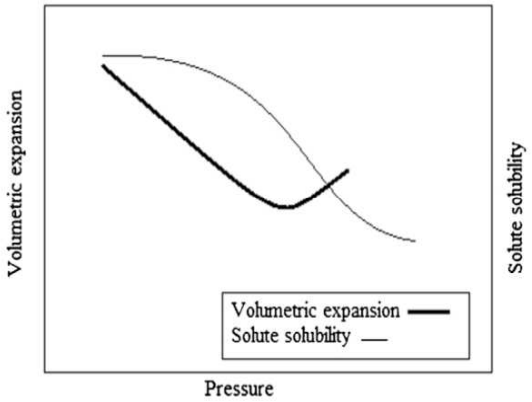

Fig. 6. Suitable conditions to get a succesful micronization with GAS.

GAS consists of the addition of the SCF to a solution. If the SCF is highly soluble in the solvent, and at the same time the solid is not soluble in the SCF, the SCF exerts a high antisolvent effect. Great supersaturations can be therefore achieved.

Fig. 5 illustrates a schematic of a GAS process. GAS is a batch process in which the antisolvent is added to a solution of the targeted compound. Due to the dissolution of the SCF in the solvent, it is produced a volume expansion [59,95], which reduces the solvent density and consequently its "solvent power".

GAS is a well-known process, being the most important parameter the relative volume molar expansion (Eq. (7)) [96]. Although this expansion can be used as the key parameter, different articles established the relative partial molar volume reduction as a better criterion [97,98].

$$\frac{\Delta v}{v} = \frac{v_L(T, P, x_1)}{v_2(T, P_0)} - 1 \tag{7}$$

The knowledge of this expansion provides the ability to manipulate the supersaturation and the PSD. In fact, the minimum relative volume molar expansion corresponds with the maximum attainable supersaturation [96]. The solvent and the thermodynamic conditions are chosen therefore depending on this minimum.

In this process it is very important to take into account how the solubility of the solid decreases. In order to get a proper micronization, the solubility of the solute in the ternary system should decrease sharply to get a fast supersaturation (Fig. 6) [96]. Otherwise it might be produced a cosolvent effect by the use of the SCF. This cosolvent effect has been applied by DELOS to produce microparticles, and it is explained in Section 4.4.

The main advantage of the GAS process is the ability to micronize polar compounds (particles between 0.5 and 500 μm) and to obtain microcapsules [99–101]. However, there is a batch process and an organic solvent is used, and solvent traces can be obtained in the final particles.

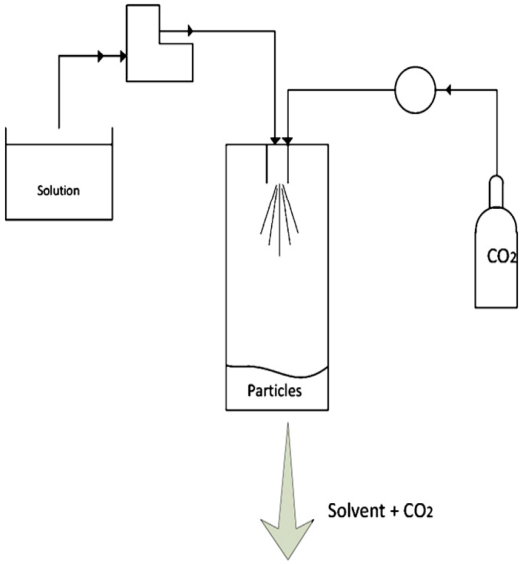

Fig. 7. SAS process.

4.3. SAS, ASES, PCA, SEDS, SAS-EM and ARISE

In order to overcome the previous limitations, new antisolvent processes were applied for particle formation. **SAS**, **PCA** and **ASES** processes are basically identical (Fig. 7), and they are constituted by a vessel in which it is placed a fluid in supercritical state. After that, the solution of the compound is sprayed through a nozzle in that supercritical atmosphere. Due to the solution spraying, the mass transfer is enhanced due to the droplet formation, and consequently small particles with good distribution can be obtained.

Since the solution is sprayed in the vessel, there is the possibility to use different nozzle configurations to achieve different objectives. Hanna and York patented the **SEDS** process in order to micronize proteins or different sugars, avoiding solubility problems [102]. They designed a two (or three) coaxial passages nozzle to provide a simultaneous introduction of the solution/suspension and different solvents in order to overcome solubility drawbacks (Fig. 8A).

However, the most common strategy is to use a coaxial nozzle with two passages, sometimes with a mixing length at the end of the nozzle to provide a premixing between the SCF and the solution (Fig. 8B). The solution is introduced along the inner surface, whereas the SCF is pumped along the outer surface. This allows a closest contact and the mass transfer is enhanced. Particles with a size around 1–5 μm have been obtained with this nozzle configuration [103].

SAS-EM (supercritical antisolvent precipitation with enhanced mass transfer) is another variation of SAS process. It consists of a high-pressure ultrasound precipitation vessel to provide a different methodology to create the jet break-up. This ultrasonic field enhances the mass transfer and turbulence, and another way to tune particle size and morphology by changing the ultrasonic frequency. Although SAS-EM might be classified into enhanced atomization processes, this technique uses the SCF for providing an antisolvent effect [104,105].

However, semicontinous antisolvent processes can provide shortcomings related to nozzle blockage, what may require the use of low flow solution rate. This fact hinders the possibility of scaling-up.

In order to overcome this limitation, **ARISE** was developed to eliminate the capillary nozzle (using a 1 mm of internal diameter), avoiding blockages. In this case, the solution is placed in a pressurized vessel with an inert compound (nitrogen for instance), and then by means of a depressurization the solution is injected into a vessel with a SCF (that should be at lower pressure than the vessel with the inert compound) which will act as antisolvent. The first depressurization improves in addition the subsequent atomization process [106].

SCFs antisolvents (and semicontinous) processes are influenced by different parameters, such as fluid mechanics, thermodynamics, intra-droplet nucleation, crystallization kinetics, and heat and mass transfer.

The most studied antisolvent techniques are SAS and SEDS. Although a lot of works have studied the influence of different experimental parameters on particle size, PSD and morphology, contradictory results have been found in terms of the best conditions to get the smallest particles with a narrow PSD [107–110]. Because of that, we only consider here the influence of the position of the experimental conditions with respect to the mixture critical point (MCP) of the system antisolvent–solvent. The position of the MCP has been introduced as a crucial parameter due to different peculiarities, such as theoretical surface tension vanishing, what affects the mass transfer and the atomization process of the technique.

- The MCP for semicontinous supercritical antisolvent processes

The position of the MCP of the system antisolvent–solvent is very important in supercritical antisolvent processes. When the temperature is above the critical temperature of the SCF, the MCP can be defined as the pressure at which the mixture antisolvent–solvent is in one supercritical phase.

Different works [103,111] have established that the MCP of antisolvent–solvent systems matches with the conditions at which the molar fraction of the solute is the minimum in the ternary systems SCF + solvent + solute (as long as the initial solution is diluted). Therefore, according to these works, pressure and temperature conditions at which the supersaturation is the maximum in the ternary systems might be known using only binary equilibria diagrams antisolvent–solvent. The explanation lies in the antisolvent effect of the SCF. The maximum molar fraction of the CO_2 in the liquid phase (and consequently maximum antisolvent effect) is reached just in the MCP. At these conditions, the maximum attainable supersaturation for the ternary system is reached. Above the MCP, there is only one single supercritical phase, and the solubility of the solid in the ternary system can increase [103–111].

The MCP is usually determined by means of an EOS, neglecting often the effect of the solute because the solutions are diluted. However, several authors have suggested that the effect of the solute should be taken into account. The solute can produce the apparition of immiscibilities liquid–liquid which can hinder the respective mass transfer pathways between the solution and the SCF. The solute can also change the effect of the SCF, acting sometimes this SCF as a cosolvent due to the addition of the solute [112–114].

Surface tension plays an important role in relation with the MCP. Above the MCP, the surface tension reaches a null value, what means that in these semicontinous processes there is no droplet formation existing only one single supercritical phase. However, under the MCP there is droplet formation. Therefore, the precipitation mechanism, particle size and morphologies are different above or under the MCP [108–115].

Several works try to elucidate how the position of the experimental conditions with respect to the MCP can influence the PSD and morphology. However, different results were obtained. The best particle size has been found obtained close to the MCP

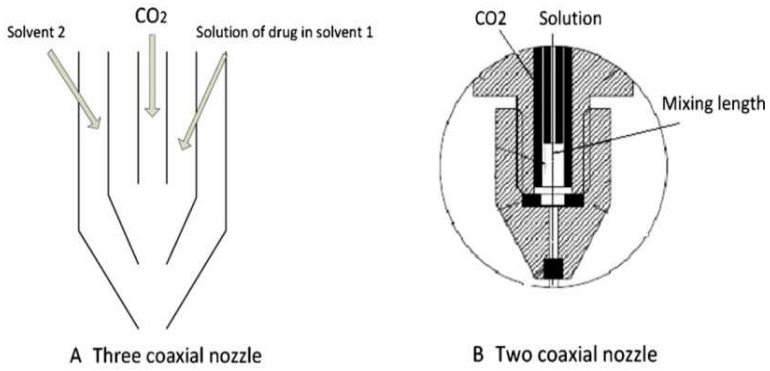

Fig. 8. (A and B) Different SEDS nozzle schematics.

[103,107,111,116], far above the MCP [117–119] and under the MCP [120]. There have also been cases in which the precipitation was not successful under the MCP due to the existence of a liquid phase [121].

In order to get a complete understanding of the precipitation mechanism, more phenomena should be taken into account, mainly hydrodynamic jet conditions and mass transfer. That is the reason why different investigations have been done regarding modelling supercritical antisolvent processes in order to place together all these fundamentals.

- Modelling supercritical antisolvent processes

In order to explain the particle diameter, particle morphology and the precipitation mechanism, many models based on different assumptions have been proposed.

These semicontinous processes start with the atomization of the solution–liquid jet under a high pressure atmosphere. The different disintegration regimes at atmospheric pressure are well-known, and are classified according to empirical correlations, based on Reynolds, Webber and Ohnesorge numbers. These correlations provide a method to identify different breakup regimes depending on the velocity or viscosity of the liquid jet [122].

However, these "classical" definitions are not suitable for atomization regimes at high pressure. Specifically, the influence of the gas atmosphere increases with pressure because the gas might be dissolved in the liquid and in addition the "theoretical" vanishing of the surface tension above the MCP should be considered [123].

In order to overcome the previous anomalies, several studies have investigated the different jet disintregation regimes at high pressure [124,125]. Under the MCP, dripping, axisymmetrical, asymmetrical and atomization regimes are produced [124], and correlations have been proposed in order to distinguish between atomized and non-atomized regimes at high pressure [126].

However, near and above the MCP, although the surface tension is null, there is droplet formation due to the existence of a dynamic surface tension and even an interphase can be observed [115,127]. Nevertheless, once the equilibrium is reached, the droplets disappear. On the other hand, far above the MCP, there is no droplet formation, and the liquid jet behaves like a gas-like jet (composed of gaseous plumes).

Atomization theories were used therefore to establish a relationship between the initial theoretical droplet size (calculated with Jasuja's equation) and the final particle size [120]. The initial droplet size correlated better (although roughly) the particle diameter under the MCP than above the MCP [120]. This is mainly due to the difficulty to estimate the surface tension above the MCP and the existence of a secondary atomization. Those deviations highlight that the mechanism one particle-one droplet cannot be applied for these processes, and more phenomena should be taking into account to explain particle size and morphology, such as mass transfer and jet hydrodynamics.

After the solution is atomized in the supercritical atmosphere, there is a two-way mass transfer between the droplet and the surrounded atmosphere. There is a competitive process between the absorption of the SCF inside the droplet, and the solvent evaporation.

However, two different mechanisms should be considered depending if the conditions are under or above the MCP.

These two mechanisms were mathematically studied considering the two-way mass transfer for a stagnant droplet of toluene under sc-CO_2 atmosphere at isothermal conditions [128,129]. The different interfacial fluxes and the behaviour (swelling/shrinking) of the droplet with the droplet flying time in a high pressure atmosphere were determined using Fick's law and PR-EOS.

Under the MCP the droplet always swells (showing in addition a non-monotonic pressure and temperature dependence) because the flux is inside the droplet. Swelling finishes near the MCP because the diffusion is zero, and consequently the flux becomes also zero. When the droplet is saturated, the droplet shrinks because the mass transfer is out of the droplet [128].

This studio also states that droplets with short lifetimes are not necessarily the fastest to reach supersaturation. Droplet lifetime diverges near the mixture critical point, but far from the critical point the lifetime decreases increasing pressure, showing a non-monotonic temperature dependence.

On the other hand, droplet was defined above the MCP using a "cutoff" value of the density of the system. Droplet can swell (toluene density > CO_2 density) or shrink (CO_2 density > toluene density) depending on the density difference. When the respective densities are similar no droplet was defined [129].

According to these couple of studies, mass transfer under supercritical conditions is faster than under subcritical conditions, but more parameters should be taken into account in this type of processes to confirm this statement, as might be the droplet velocity.

Droplet velocity was considered by Pérez de Diego et al. [130] to perform a mass transfer study with Maxwell-Stefan approach for the system CO_2-DCM (dichloromethane) at subcritical and isothermal conditions. They proved droplet swelling (absorption faster than solvent evaporation) and the strong influence causing by the initial droplet diameter in its lifetime (if the diameter is duplicated, lifetimes increases by four). This fact highlights that pressures just under the MCP are the best to reduce the droplet lifetime because the evaporation process is enhanced with a vapour phase high density.

Tavares-Cardoso et al. [131] added the buoyancy effect to jet hydrodynamics, mass transfer and phase equilibrium for above-MCP conditions. According to their results, at low Reynolds number

(the *k–w* turbulence model was used in its simulation) the fast produced supersaturation prevents to get the real supersaturation and therefore the initial solution concentration does not affect particle size.

The effect of the solute in the evaporation effect was considered by Lora et al. [132], who developed one of the first models at isothermal conditions for SAS process, accounting the previous hydrodynamic, mass transfer (Fick's law) and thermodynamics. They concluded that the supersaturation is reached very fast (50–100 ms) and provides the required strong antisolvent effect to precipitate the solid. However, sometimes antisolvent effect should be coupled with evaporation to get a precipitation. Particle size and morphology can change due to this phenomenon. Therefore, there are cases in which the solid precipitates only due to a strong antisolvent effect (phenanthrene), but for other solids, like naphthalene, an antisolvent-evaporation effect is required.

Heat transfer between droplet-supercritical atmosphere was taken into account by Fadli et al. [133], performing a simulation to study heat and mass transfer with Fick's law and PR-EOS above the MCP. They suggested the possibility of controlling the droplet lifetime by changing the temperature gradient at non-isothermal conditions. According to their results, the injection of cold solvent into warm CO_2 increases the droplet lifetime. On the other hand, warm solvent into colder CO_2 increases the mixing process and decrease the droplet lifetime.

Mukhapadhyay and Valdi [134] studied the temperature changes in SAS process. The temperature variation above the MCP is very small for high flow rates, because of the small droplet size. That indicates a steady temperature profile at these conditions. However, under the MCP there is a 1–3 K variation followed by an stabilization.

The most complete study for SAS was developed by Martín and Cocero [135]. Thermodynamics, hydrodynamics (k–ε turbulence model), mass transfer and crystallization kinetics were simultaneously considered. This work concluded that the supersaturation is the most important parameter to obtain the best particle size, and consequently the experimental parameters should be modified to get the maximum attainable value. Pressure and temperature are the main parameters, but high solution concentrations, high flow rates and high turbulence improves the mixing. Best conditions are near and above the MCP.

All these models are useful to explain the precipitation mechanism and what is happening when a solution is introduced by means of a nozzle in a supercritical atmosphere. However, there are not able to explain the different particle size and morphology, depending on the experimental conditions.

In order to overcome this shortcoming, Reverchon et al. [115] published a complete article based on experimental observations, which conjugated mass transfer, phase equilibria and jet hydrodynamics (observing the gas–liquid boundaries with an optical set-up).

They made a general interpretation to explain particle size and morphology depending on the break-up time (t_b) for breaking the jet and the time for the complete disappearance of the surface tension (t_s). If t_s is less than t_b, there is a gas to solid nucleation (nucleation followed by a size reduction), and nanoparticles are obtained (conditions far above the MCP).

On the other hand, if t_s is greater than t_b (under the MCP), there is a droplet growth due to the solubilization of the CO_2 and then the droplet evaporates. In this case, the obtained microparticles present different morphologies, depending on the mass transfer mechanism of the precipitation inside the droplet.

A mixture between microparticles and nanoparticles can be produced due to a competition between the previous times.

Recently, this theory was numerically explained by calculating t_b and t_s for the system CO_2-dimethyl sulfoxide-yttrium acetate

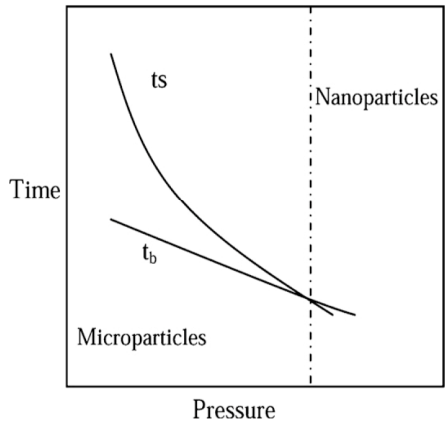

Fig. 9. Two different precipitation mechanisms depending on t_b and t_s [136].

for different concentrations and pressure conditions [136]. t_b and t_s decrease with pressure, and increase with concentration due to the viscosity increase. If both time curves are plotted, a cross point can be observed (Fig. 9). Two different precipitation mechanisms, surface tension vanishing mechanism (nanoparticles), and jet break-up mechanism (microparticles) are distinguished depending on the situation of this point.

Although this last work explains particle size and morphology of the supercritical antisolvent experiments, this work is not able to predict the particle size.

The difficulty to obtain a model to predict the PSD is basically due to aggregation mechanisms, phenomena such as secondary nucleation or particle coalescence or even the different behaviour for each solid. Stratified areas because of mixing problems, and the excess volume due to the behaviour of the antisolvent–solvent mixture should be taken into account, and maybe the change of the entrance of the CO might improve the process [131].

Different phenomena such as vessel design or Brownian motion (modified for the different published works) can be also the reasons why different experimental results have been obtained in literature with respect to the best conditions to obtain the smallest PSD.

4.4. DELOS, PPRGEL, PGSS and PGSS-drying

These processes consist of a previous solution of the solution in the SCFs followed by a depressurization.

DELOS was developed and patented by Ventosa et al. [137]. This process can be used as long as the solution (with the solute to be precipitated) is miscible with the SCF. After this solubilization process, a depressurization at atmospheric pressure is performed. That entails a temperature decrease (Joule–Thomson phenomenon) and uniform supersaturations. The general steps are described in Fig. 10.

The temperature decrease and the supersaturation are enhanced by the capacity of the solution to solubilize CO_2 or another SCF (R-134a has been also used [138]). However, this technique is similar to GAS, and it is important to distinguish the conditions when the SCF is acting as antisolvent or as a cosolvent.

A thermodynamic study of the solubility should be performed to do that. Fig. 11 shows the standard behaviour of a batch process when a SCF is added.

In this figure, *Sr* is the supersaturation ratio of the initial solution, defined as the ratio of the actual concentration and the saturation concentration. It can be seen that the left part of the chart indicates that the SCF acts as cosolvent because the working line lies above the equilibrium curve. However, after the molar fraction x_L is reached, the situation changes, and the equilibrium curve is

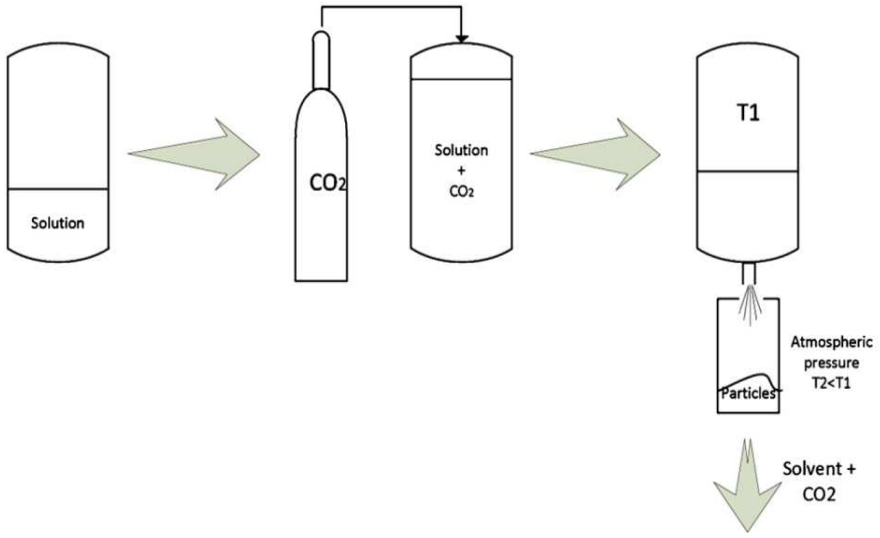

Fig. 10. DELOS process with its corresponding steps.

under the working curve. That means that the SCF is acting as an antisolvent and a GAS process will be produced [139].

That fact can be an advantage, because it would be possible to modify the type of process by changing the initial supersaturation ratio. However, this modification should be performed cautiously, because the precipitation yield decreases when the supersaturation ratio is reduced. According to Ventosa et al. [137], the stirring system is not crucial, and the pressure does not affect the temperature reduction in a great extent. Therefore, lower pressures can be used for an optimum precipitation. Moreover, DELOS has been used to produce polymorphs that cannot be obtained with other crystallization techniques. For instance, polymorph E of the stearic acid has been precipitated with DELOS, whereas with GAS, only polymorph C was produced [140].

Temperature decrease due to the Joule–Thomson effect is exploited by **PPRGEL**. This process use fluids in subcritical state to obtain microparticles. Temperature reduction can be even 70 °C and strongly depends on the SCF (in this case subcritical) released moles from the mixture SCF–solvent [141,142]. Therefore, the key point is to choose a great solvent for the CO_2.

PGSS (Fig. 12) was patented by Weidner et al. [143]. This process is used for micronizing solids that are not miscible in the SCF, but they can swell by the SCF addition, such as esters [144] or fats [145]. This process has been also employed for encapsulating β-carotene in poly-(ε-caprolactone), taking advantage of the low glass transition of the polymer [146].

PGSS entails a melting point depression to create a saturated solution. In this step, viscosity reduction, swelling or plasticization effects by the use of the SCF help the subsequent spraying process. After that, a depressurization is performed at atmospheric pressure to cool-down the solution by the Joule–Thomson effect. Therefore, solid particles are formed. That highlights the importance of controlling the temperature of the spray tower and the hydrodynamic conditions regarding morphology [147].

Since the gas is more soluble in the liquid that vice versa, a less amount of SCF is required to obtain particles, and in addition it is avoided the use of an organic solvent.

It is very important to study previously the solid–liquid–gas equilibria frontiers (and the possibility of the existence of liquid–liquid equilibria) to know the influence of the high pressure on the solid melting temperature [144,148,149]. Furthermore,

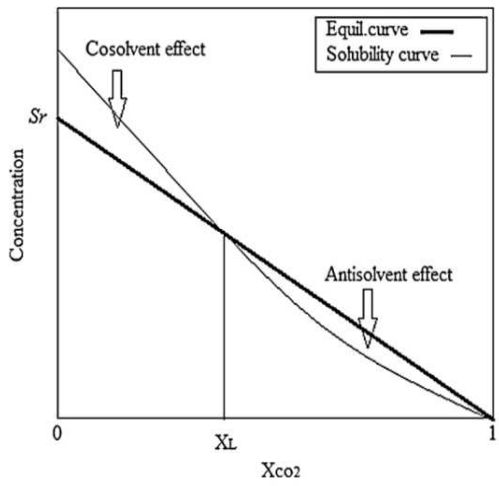

Fig. 11. Chart to distinguish between DELOS and GAS.

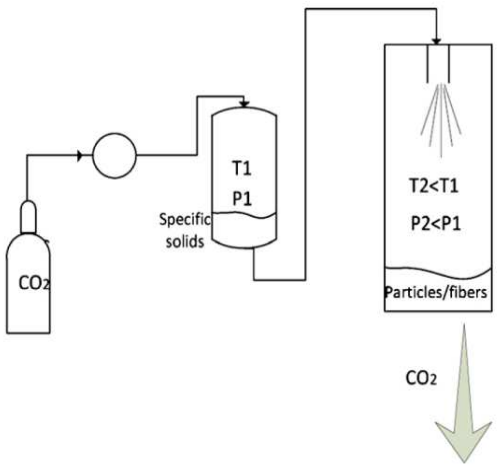

Fig. 12. PGSS process.

differences can be observed between solid–liquid and liquid–solid transitions in this type of processes. That means the existence of hysteresis, and consequently polymorphic transitions should be taken into account [149].

The atomization of the PGSS process can be improved by using a second gas (in this case air) in the atomization and precipitation vessel [150] (**GAMA** process).

However, the most used PGSS variation is called **PGSS-drying**, which was developed by Meterc et al. [151] for drying aqueous compounds (specifically green tea extracts).

Basically, an aqueous solution is contacted with the compressed fluid in a static mixer with several mixing elements. Mass transfer SCF–solution is provided by this mixing. Afterwards, depressurization is performed in a tower at atmospheric pressure and at temperatures above the dew line of the mixture CO_2–water. Knowing the VLE diagram of this mixture, different strategies can be followed for compound drying, such as higher temperatures (although softer than temperatures for conventional extraction processes) with a small amount of CO_2, or lower temperatures and higher mass flow of CO_2 This process provides an inert atmosphere (CO_2 atmosphere without oxygen), avoiding the possibility of the oxidation [151]. Thermal stability of the compound should be taken into account to select a suitable temperature for the spray tower. The ternary equilibrium CO_2 + solid + water should be also considered, given that the knowledge of the solubility of the CO_2 in the liquid phase (and the liquid phase in the CO_2) can be very useful.

Furthermore, the water can be absorbed by the particles surface due to the existence of an atmosphere of carbon dioxide and water [152].

PGSS-drying can be used for micronizing hydrophilic compounds as well as sensitive substances such as essential oils [153]. As an example, a complete study of the micronization of the polyethylene glycol with a PGSS-drying pilot plant was performed by Martín et al. [154]. They found that an increase of the gas/liquid ratio reduces the particle size and the residual moisture because the atomization and the drying process are enhanced. This moisture is given by thermodynamic considerations (mainly the gas–liquid ratio).

The morphology changes with the final humidity, obtaining with high water content a kind of undesireble "paste". On the other hand, low water content produces spherical particles [152,154].

Finally, the obtained particles with PGSS-drying are similar to those obtained with SCF techniques without water. However, regarding microcapsules, the microencapsulation efficiency is lower than the obtained with PGSS process [153,154].

- Modelling PGSS

PGSS was thermodynamically analyzed by Elvassore et al. [155] by calculating the enthalpic changes along the process with the perturbed-hard-sphere-chain-theory EOS. This enthalpic change gives information about the nature of the final product (liquid or solid–liquid). In this way, *P*–*T* charts were depicted to predict if depending on the initial conditions the outcome would be either solid or solid–liquid mixture.

Li et al. [156,157] published two articles for PGSS modelling for the system CO_2 and hydrogenated palm oil (HPO). They considered an annular mist flow at the exit of the nozzle with an existing equilibrium between the CO_2-rich gas phase and the mixed CO_2–HPO liquid phase. They used mass, momentum and energy conservation coupled with crystallization equations and PR-EOS (for fluid properties and phase equilibrium) to calculate different parameters profile inside the nozzle [156]. However, they took the mass conservation for the CO_2-rich phase as a homogeneous model (HPO particles can be found in this phase). Only trends in particle size are predicted by the simulation, giving the model always a smaller particle size (the reason might be that the calculations are only in the nozzle). At the same time, the model cannot explain the mechanism by which bimodal PSD were sometimes experimentally produced.

In the second article and with the same system (CO_2–HPO), they studied independently the governing equations for the CO_2 and the HPO for the CO_2-rich phase. Their results indicated that at the exit of the nozzle the PSD is narrower with a smaller particle size because the particles are formed by melt crystallization, but if the particle formation is due to an atomization process, PSD is larger and wider. A bimodal PSD is explained with this theory [157].

However, both models were only focused on droplet diameter and PSD, without entering in the fluid dynamics of a generated droplet by the PGSS.

In this context, Strumendo et al. [158] studied mass and heat transfer for a saturated and stagnant droplet of tristearin in CO_2 until the particle is generated (solid-liquid equilibrium (SLE is reached). Equilibrium is computed with PHSC-EOS and Stefan equations are used. However, convective motion, gravity and droplet interactions are not taking into account.

Faster heat transfer than mass transfer is obtained according to the results. The time for getting the SLE is calculated for different CO_2 initial mass fractions and initial droplet temperatures. The SLE time goes to zero when the temperature is close to the melting point, and an increase in temperature increases the SLE time. However, the opposite effect was obtained if the initial CO_2 mass fraction is increased. These SLE time results correlate well with the trend of the PSD, which increases with temperature and decreases with initial mass fraction of CO_2. The droplet shrinks for all the investigated conditions, although this shrinking is very small because of the shorter times to reach the equilibrium.

This model does not take into account nozzle hydrodynamics, crystallization or the effect of the drying because bubble formation inside the droplet. However, it highlights the importance of the equipment design in terms of get the correct time to get the particle formation.

- Modelling PGSS-drying

Martín and Weidner [159] published a model for PGSS-drying for the system CO_2–water–PEG. They performed a mass balance and enthalpic balance (with experimental adsorption results water–PEG) to predict the gas–liquid ratio to get a complete evaporation, the moisture concentration in the outcome and the expansion temperature as function of the pre-expansion conditions. They used a PC-SAFT equation to take into account the non-idealities and to calculate the corresponding equilibrium and mass transfer limits in the system.

These mass transfer limits provide information to determine the extracted water to the gas phase in the static mixer as function of the gas–liquid ratio. The authors found out that the water can be totally extracted in the static mixer by changing the gas liquid-ratio and the pre-expansion temperature (first proposed mechanism). Then, by using global mass transfer coefficients, the different profiles of molar flux CO_2–liquid phase were determined as function of the static mixer length [159].

Furthermore, water can be extracted with a second mechanism after the depressurization. In this case, the water should be transported to the CO_2 atmosphere. Therefore, pre-expansion temperature and gas–liquid ratio might be modified to obtain a perfect drying using a mixture between these two mechanisms [152].

Two simultaneous types of atomization for PGSS-drying process were proposed by Martín and Weidner [159]: flash-boiling [160] (a superheated liquid is expanded through a nozzle) and effervescent [161] (a biphasic mixture is expanded through a nozzle, taking advantage of the formed bubbles).

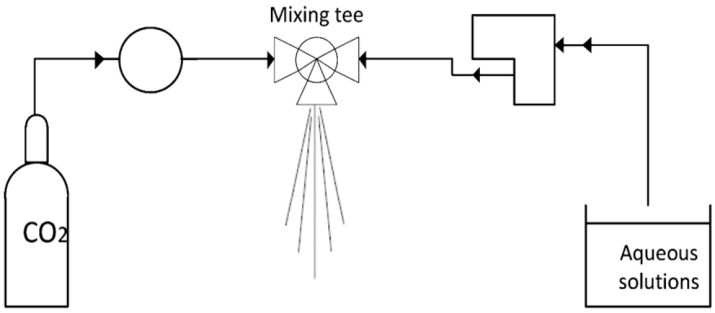

Fig. 13. CAN-BD process.

4.5. CAN-BD and SAA

Both techniques were developed with the aim of using the SCF (mainly sc-CO_2) to improve the atomization process.

CAN-BD (Fig. 13) was used to micronize hydrophilic compounds. Solution and sc-CO_2 are put in contact during short time in a low-dead-volume tee. A quantity of CO_2 is solubilized in water and an emulsion is formed [162]. Subsequently, this emulsion is atomized by using a restrictor to a drying chamber where a N_2 inert flux help the drying process. CO_2 solubilization in water provides an atomization enhancement, differing from the complete saturation occurring in PGSS or PGSS-drying. Droplet diameter might be controlled varying temperature, pressure, flow rates and diameter restrictor. Drawbacks related to the blockage nozzle (Joule–Thomson effect) are avoided because nozzle, tee connection and chamber are heated.

On the other hand, relatively high temperatures to perform the droplets drying process are required, and might damage the active substance.

At our knowledge, a mechanism for this process has not been established yet, but an effervescent atomization might take place.

SAA process was developed by Reverchon [163] in order to avoid the big pressure drop in the tee. A packed tower to mix the CO_2 with the liquid (water or other solvents) at high pressure and temperature was used. Their objective was to saturate the mixture with CO_2 by adding therefore an excess of sc-CO_2 at conditions above the MCP. This saturation is the main difference with PGSS-drying (last technique uses the minimum amount of CO_2). CO_2 acts therefore as a cosolute, improving the atomization at the same time. Subsequently, an atomization of the mixture at atmospheric pressure is performed in a heated precipitator with N_2 to evaporate the droplets.

SAA (like CAN-BD) provides a more efficient atomization because after the primary atomization, the release of CO_2 produces a secondary atomization. Smaller droplets are produced due to this phenomenon.

However, it is important to considerer the limitation of this process with respect to several thermolabile compounds due to the high required temperatures. This can be solved by applying a vaccum in the precipitator [164]. This fact highlights the easy tunability of this process to produce particles and/or microcapsules [165].

As occurs with other techniques with SCFs, the previous thermodynamic study can play an important role regarding morphology or PSD. In this case, the experiments should lie in a single liquid-phase (with respect to the antisovent–solvent diagram) to produce the same morphology, avoiding biphasic areas. The temperature should be enough to produce the solvent evaporation, and at the same time the glass transition temperature must not be reached (if the solid is a polymer) [166].

SAA has not been modelling yet and the mechanism is complicated, because the antisolvent effect of the sc-CO_2 should be considered. Rodrigues et al. [167] precipitated lysozyme with SAA, obtaining two different morphologies, what indicated that antisolvent and atomization crystallizations might be produced at the same time. Same authors precipitated the same compound using high nitrogen-solution ratios, obtaining a one single morphology with a similar PSD. Therefore, it seems that a strong and intensive mixing could be enough to precipitate particles [167].

The main mechanism of particle nucleation in this process was clarified by using a population balance. It was shown that SAA process produces mainly a primary nucleation [168].

4.6. SFEE

One of the main limitations for the previous techniques is the particle size. Except for a few occasions (mainly with RESS or RESOLV), particles are usually in a micrometric range. Nevertheless, sub-micron particles can be required for different applications. In this context, methodologies using *w–o* emulsions can be very useful. **SFEE** mixes the efficiency of the SFE and the ability of the emulsion processes to obtain nanoparticles. Basically, the SCF is put in contact with water in oil emulsions (w/o) or oil in water emulsions (o/w), and the SCF extracts oil-organic phase in which it is solubilized the water-insoluble drug. The drug remains therefore in a suspension that should be established by using a surfactant that at the same time avoids aggregation phenomena. In addition, this technique provides "clean" particles with low concentration (ppm) of the solvent [169].

Different compounds were successfully processed with SFEE [170]. Those compounds can have similar structure to the backbone of many steroids, can presented mechanical micronization difficulties or they can be even water-insoluble.

Polymers can be also processed with SFEE. In this case, it is very important to take into consideration the equilibrium CO_2–water–polymer. This fact can decrease the glass transition to form plasticized polymer beads, although this phenomenon can be even beneficial for the emulsion stabilization and solvent removal [171].

The use of emulsions and SCF can be used together for w/o emulsion reaction assisted by sc-CO_2. This technique has been employed to produce metal oxides [172]. In this case, the sc-CO_2 extracts the organic phase and at the same time it is produced a reaction in the aqueous phase with the CO_2 as a reactant to produce nanoparticles.

Pharmaceutical compounds can be encapsulated with SFEE process by creating an emulsion of a drug–polymer mixture. Capsules are formed inside the emulsion droplet [171].

At the beginning, this process was considered only as a discontinuous process. However, high pressures with large time increase the surface tension, and the emulsion might be destabilized. A packed tower was used therefore to perform a continuous process. Although these towers might be blocked if solids are involved, this blockage can be avoided due to existence of a suspension

with low residence time and a surfactant. A continuous process provides greater drug/polymer recovering (with similar particle distribution) and less residuals (better contact between the different phases). Moreover, the extraction is six times faster [173].

Therefore, the main limitation for the SFEE is the control of the emulsion. The emulsion should be stable, avoiding coalescence phenomenon (more possible with double emulsions). A phase equilibria study of the complete system should be performed to know the proper operation conditions. Experiments should be carried out in the biphasic zone, to create a stable emulsion (in the one-phase area the emulsion is not stable and the particles are aggregates) [174].

As long as the droplet corresponds to a stable emulsion, it is assumed droplet-particle theory. However, the results not always agree with this theory, and particle size larger than droplet size have been obtained, due to the existence of interactions.

For instance, higher concentration of the drug/polymer solutions increases the viscosity in the oily phase, getting emulsion droplets bigger [175].

The mechanism for the SFEE is explained taking into account the mass transfer routes. It is assumed that there is a direct extraction between the SCF and the organic phase inside the droplet. At the same time, due to the equilibrium between the solvent-aqueous phases there is a diffusion of the organic solvent in water following for its extraction from the aqueous phase [173]. The first step is known as direct supercritical extraction whereas the second step is known as indirectal supercritical extraction.

- Modelling SFEE

In order to get a complete understanding of this process, it would be necessary to see the evolution of a single droplet during the precipitation process. That was illustrated by Mattea et al. [176,177]. They studied in a high pressure visual cell the evolution of a single droplet of the organic solvent for the system CO_2–DCM–water taking into account the volume and surface tension changes, and calculating the concentration profiles of the droplet. It was showed (using a sessile drop and taking advantage of the change of the refractive index) that droplet undergoes a swelling/shrinking process depending on the experimental conditions. Under the MCP, the droplet swells up to a maximum value, followed by a droplet shrinking. Equilibrium CO_2–DCM and the solubility of CO_2 in water explain this phenomenon. Based on these considerations, under the MCP there is a point in which the DCM diffusion out of the droplet turns out faster than the diffusion towards the droplet. This theory can explain the swelling phenomenon over the shrinking process that occurs above the MCP, conditions at which the equilibrium does not establish a barrier for the diffusion [176].

On the other hand, applying a pendant droplet methodology, it was observed an increase of the surface tension of the organic phase, meaning that the emulsion becomes unstable with time. That is one limitation of a batch process (greater times are required).

It was shown that the CO_2 addition does not affect the surfactant properties, as long as the surfactant concentration is not very high (higher concentrations can involve the precipitation of the surfactant). Finally, by adding beta-carotene it was shown that each droplet behaves as a single GAS process, theory that applied to calculate the different molar flux inside/out of the droplet [177].

4.7. Miscellaneous

The previous processes usually employ sc-CO_2. However, more fluids in supercritical or subcritical state can be employed for drug processing.

Water, for instance, can be used in subcritical state to produce particles of hydrophobic compounds [178,179]. This process consists of heating the water up to 200 °C at high pressure to maintain the water in liquid state. At this temperature, the dielectric constant of the water decreases, and therefore the water can solubilize hydrophobic compounds. However, cosolvents should be used to reduce the dielectric constant and get a complete solubilization. The use of cosolvents also offers the possibility of controlling particles morphology [178]. Then, as happens with the rest of SCFs techniques, a fast supersaturation can be achieved if the solution is cooling down, and the solid precipitates. It is required a subsequent drying process because the particles are suspended in an aqueous medium.

A carrier/excipient can be used in the precipitation chamber [178]. Drug agglomeration can be avoided by the use of this carrier, as it was appointed by Sanganwar et al. [180], to design the SAS-DEM process (supercritical antisolvent–drug excipient mixing). This is a typical SAS process, but with lactose as a suspended excipient in the vessel, inducing the co-mixing.

Different (antisolvent and solvent) techniques can be employed at the same time. RESS and SEDS were used together for the crystallization of a triblock polymer PLA–PEG–PLA. This polymer is partial soluble in sc-CO_2, what indicates that it could not be processed with RESS or SEDS. In order to overcome this drawback, a SEDS process of the polymer solution was performed, and after that the resulting mixture was sprayed in a vessel at atmospheric pressure (RESS). The polymer was then precipitated using two techniques simultaneously [181].

A variation of the PGSS can be applied to produce powder coatings [182]. Coatings are formed by two components (binder and hardener). Continuous powder coating spraying process (CPCSP) melts the components in two different vessels, and subsequently those components are mixed in a static mixer with compressed CO_2. The mixture is subsequently sprayed in a tower, and the gas is removed by using a cyclon. This process provides a control of morphology and particle size depending on the viscosity of the mixture.

The use of SCFs can produce valuable techniques to obtain different complex formations or to impregnate polymers with pharmaceuticals. Controlled particle deposition (CPD) can provide complex formations of a soluble drug in sc-CO_2 in a porous solid carrier. The carrier is non-soluble in sc-CO_2. This drug is dissolved in the SCF, and by a subsequent permeation of the supercritical solution into the carrier, the drug is precipitated into the porous, forming a complex [183].

On the other hand, supercritical solvent impregnation (SSI) requires the dissolution of the drug in the SCF. The solution is subsequently put in contact with a polymer. If the polymer swells due to the addition of the SCF, it is possible (after a subsequent depressurization) to impregnate the polymer with the drug, obtaining therefore a drug release system [184]. As happens with other techniques that use sc-CO_2, the key point of this process is the solubility of the different compounds in the SCF and the polymer swelling. This technique has been even applied to impregnate intraocular [185] or contact lens with drugs [186,187] and different starches with essential oils [188,189].

5. Conclusions

Supercritical fluids techniques are a good alternative for conventional methods for drug processing. They can be employed (specifically sc-CO_2) as “green” technologies to obtain crystalline pharmaceuticals with a narrow particle size distribution. In this context, an extensive research has been performed over these last 20 years to increase the possibilities of these techniques.

Nowadays, it is possible to process different compounds in spite of their characteristics, by only changing the methodology, or the used supercritical fluid (the use of water for instance has been proposed). Moreover, the supersaturation, and consequently the particle size, can be controlled by modifying the experimental conditions.

However, prior to the use of these techniques, it is usually required to perform a thermodynamic study in order to know the solubility behaviour of the system and the corresponding phase frontiers. Nevertheless, at present time, there is not a general equation to provide a proper estimation of this solubility and/or equilibria data.

Same occurs with the particle size and the morphology of the final product. A general model to predict the particle characteristics has not been developed yet. Nevertheless, many of the mechanism for the most employed processes have been established. Based on these works, it is possible to get a qualitative prediction of the effect of the parameters in particle size, and have a previous knowledge of the general characteristics of the produced particles.

Acknowledgment

This research was supported by funds from the Ministerio de Ciencia e Innovación (Spain), project CTQ2009-08222 (PPQ Subprogram).

References

[1] D.D. Breimer, Future changes for drug delivery research, Advanced Drug Delivery Reviews 33 (1998) 265–268.
[2] B.Y. Shekunov, P. York, Crystallization processes in pharmaceutical technology and drug delivery design, Journal of Crystal Growth 211 (2000) 122–136.
[3] P. York, U.B. Kompella, B.Y. Shekunov, Supercritical Fluid Technology for Drug Product Development, Marcel-Dekker, New York, 2004.
[4] S. Miranda, S. Yaeger, Homing in on the best size reduction method, Chemical Engineering 105 (1998) 102–110.
[5] M.D. Louet, M. Van Oort, A.J. Hickey, Aerosol dispersion of respirable particles in narrow size distributions produced by jet-milling and spray drying techniques, Pharmaceutical Research 21 (2004) 1200–1206.
[6] T.L. Rogers, K.P. Johston, R.O. Williams, Solution based particle formation of pharmaceutical powders by supercritical or compressed fluid CO_2 and cryogenic spray-freezing technologies, Drug Development and Industrial Pharmacy 27 (2001) 1003–1015.
[7] S.A. Shoyele, S. Cawthorne, Particle engineering techniques for inhaled biopharmaceuticals, Advanced Drug Delivery Reviews 58 (2006) 1009–1029.
[8] M. McHugh, V. Krukonis, Supercritical Fluid Extraction, Butterworth-Heinemann, Boston, 1994.
[9] E.J. Beckman, Supercritical and near-critical CO_2 in green chemical synthesis and processing, Journal of Supercritical Fluids 28 (2004) 121–191.
[10] E. Stahl, W. Schilz, W. Schutz, E. Willing, Extraction with Supercritical Gases, Verlag Chemie, Weinheim, 1980.
[11] S.S. Ting, D.L. Tomasko, S.J. Macnaughton, N.R. Foster, Chemical-physical interpretation of cosolvent effects in supercritical fluids, Industrial and Engineering Chemistry Research 32 (1993) 1482–1487.
[12] N.R. Foster, H. Singh, S.L.J. Yun, D.L. Tomasko, S.J. Macnaughton, Polar and nonpolar cosolvent effects on the solubility of cholesterol in supercritical fluids, Industrial and Engineering Chemistry Research 32 (1993) 2849–2853.
[13] J.W. Tom, P.G. Debenedetti, Particle formation with supercritical fluids—a review, Journal of Aerosol Science 5 (1991) 555–584.
[14] P.G. Debenedetti, J.W. Tom, S.-Y. Yeo, G.-B. Lim, Application of supercritical fluids for the production of sustained delivery devices, Journal of Controlled Release 24 (1993) 27–44.
[15] E.M. Phillips, V.J. Stella, Rapid expansion from supercritical solutions: application for pharmaceutical processes, International Journal of Pharmaceutics 94 (1993) 1–10.
[16] B. Subramaniam, R.A. Rajewski, K. Snavely, Pharmaceutical processing with supercritical carbon dioxide, Journal of Pharmaceutical Sciences 8 (1997) 885–890.
[17] P. Subra, P. Jestin, Powders elaboration in supercritical media: comparison with conventional routes, Powder Technology 103 (1999) 2–9.
[18] S. Palakodaty, P. York, Phase behavioral effects on particle formation processes using supercritical fluids, Pharmaceutical Research 7 (1999) 976–985.
[19] E. Reverchon, Supercritical antisolvent precipitation of micro- and nanoparticles, Journal of Supercritical Fluids 15 (1999) 1–21.
[20] R. Marr, T. Gamse, Use of supercritical fluids for different processes including new developments—a review, Chemical Engineering and Processing 39 (2000) 19–28.
[21] R. Thiering, F. Dehghani, N.R. Foster, Current issues relating to anti-solvent micronisation techniques and their extension to industrial scales, Journal of Supercritical Fluids 21 (2001) 159–177.
[22] J. Jung, M. Perrut, Particle design using supercritical fluids: literature and patent survey, Journal of Supercritical Fluids 20 (2001) 179–219.
[23] Z. Knez, E. Weidner, Particles formation and particle design using supercritical fluids, Current Opinion in Solid State & Materials Science 7 (2003) 353–361.
[24] E. Reverchon, M.C. Volpe, G. Caputo, Supercritical fluid processing of polymers: composite particles and porous material elaboration, Current Opinion in Solid State & Materials Science 7 (2003) 391–397.
[25] C. Vemavarapu, M.J. Mollan, M. Lodaya, T.E. Needham, Design and process aspects of laboratory scale SCF particle formation systems, International Journal of Pharmaceutics 292 (2005) 1–16.
[26] S.-D. Yeo, E. Kiran, Formation of polymer particles with supercritical fluids: a review, Journal of Supercritical Fluids 34 (2005) 287–308.
[27] E. Reverchon, R. Adami, Nanomaterials and supercritical fluids, Journal of Supercritical Fluids 37 (2006) 1–22.
[28] S. Nalawade, F. Picchioni, L.P.B.M. Janssen, Supercritical carbon dioxide as green solvent for processing polymer melts: processing aspects and applications, Progress in Polymer Science 31 (2006) 19–43.
[29] A. Tandya, R. Mammucari, F. Dehghani, N.R. Foster, Dense gas processing of polymeric controlled, International Journal of Pharmaceutics 328 (2007) 1–11.
[30] A. Martín, M.J. Cocero, Micronization processes with supercritical fluids: fundamentals and mechanisms, Advanced Drug Delivery Reviews 60 (2008) 339–350.
[31] K. Byrappa, S. Ohara, T. Adschiri, Nanoparticles synthesis using supercritical fluid technology—towards biomedical applications, Advanced Drug Delivery Reviews 60 (2008) 299–327.
[32] K. Mishima, Biodegradable particle formation for drug and gene delivery using supercritical fluid and dense gas, Advanced Drug Delivery Reviews 60 (2008) 411–432.
[33] I. Pasquali, R. Bettini, F. Giordano, Supercritical fluid technologies: an innovative approach for manipulating the solid-state of pharmaceuticals, Advanced Drug Delivery Reviews 60 (2008) 399–410.
[34] I. Pasquali, R. Bettini, Are pharmaceuticals really going supercritical? International Journal of Pharmaceutics 364 (2008) 176–187.
[35] M.J. Cocero, A. Martín, F. Mattea, S. Varona, Encapsulation and co-precipitation processes with supercritical fluids: fundamentals and applications, Journal of Supercritical Fluids 47 (2009) 545–555.
[36] E. Reverchon, R. Adami, S. Cardea, G. Della Porta, Supercritical fluids processing of polymers for pharmaceutical and medical applications, Journal of Supercritical Fluids 47 (2009) 484–492.
[37] I. Kikic, Polymer–supercritical fluid interactions, Journal of Supercritical Fluids 47 (2009) 458–465.
[38] E. Kiran, Polymer miscibility, phase separation, morphological modifications and polymorphic transformations in dense fluids, Journal of Supercritical Fluids 47 (2009) 466–483.
[39] M. Turk, Manufacture of submicron drug particles with enhanced dissolution behaviour by rapid expansion processes, Journal of Supercritical Fluids 47 (2009) 537–545.
[40] M. Skerget, Z. Knez, M. Knez-Hrncic, Solubility of solids in sub- and supercritical fluids: a review, Journal of Chemical and Engineering Data 56 (2011) 694–719.
[41] C.C. Beh, R. Mammucari, N.R. Foster, Lipids-based drug carrier systems by dense gas technology: a review, Chemical Engineering Journal 188 (2012) 1–14.
[42] I.V. Markov, Crystal Growth for Beginners: Fundamentals of Nucleation, Crystal Growth and Epitaxy, World Scientific, Singapore, 2003.
[43] J.A. Dirksen, T.A. Ring, Fundamentals of crystallization: kinetic effects on particle size distributions and morphology, Chemical Engineering Science 10 (1991) 2389–2427.
[44] D.Y. Peng, D.B. Robinson, A new two constant equation of state, Industrial & Engineering Chemistry Fundamentals 15 (1976) 59–64.
[45] I. Kikic, M. Lora, A. Bertucco, A thermodynamic analysis of three-phase equilibria in binary and ternary systems for applications in rapid expansion of supercritical solutions (RESS), particles from gas-saturated solutions (PGSS) and supercritical antisolvent (SAS), Industrial and Engineering Chemistry Research 36 (1997) 5507–5515.
[46] P. Coimbra, D. Fernandez, P. Ferreira, M.H. Gil, H.C. De Sousa, Solubility of irgacure® 2959 photoinitiator in supercritical carbon dioxide: experimental determination and correlation, Journal of Supercritical Fluids 45 (2008) 272–281.
[47] L. Constantinou, R. Gani, New group contribution method for estimating properties of pure compounds, AIChE Journal 10 (1994) 1697–1710.
[48] P. Coutsikos, E. Voutsas, K. Magoulas, D.P. Tassios, Prediction of vapor pressures of solid organic compounds with a group-contribution method, Fluid Phase Equilibria 207 (2003) 263–281.
[49] J. Marrero, R. Gani, Group-contribution based estimation of pure component properties, Fluid Phase Equilibria 183–184 (2001) 183–208.
[50] E. Neau, S. Garnier, A. Avaullée, A consistent estimation of sublimation pressures using a cubic equation of state and fusion properties, Fluid Phase Equilibria 164 (1999) 173–186.
[51] A. Tabernero, E.M. Martín del Valle, M.A. Galán, Estimation of sublimation enthalpies of solids constituted by aromatic and/or polycyclic aliphatic rings by using a group contribution method, AIChE Journal, in press.

[52] A. Tabernero, E.M. Martín del Valle, M.A. Galán, On the use of semiempirical models of (solid + supercritical fluid) systems to determine solid sublimation properties, Journal of Chemical Thermodynamics 43 (2011) 711–718.
[53] A.C. Caballero, L.N. Hernandez, L.A. Estevez, Calculation of interaction parameters for binary solid–SCF equilibria using several EOS and mixing rules, Journal of Supercritical Fluids 5 (1992) 283–295.
[54] P. Coutsikos, K. Magoulas, G.M. Kontogeorgis, Prediction of solid–gas equilibria with the Peng–Robinson equation of state, Journal of Supercritical Fluids 25 (2003) 197–212.
[55] Y. Adachi, H. Sugie, A new mixing rule—modified conventional mixing rule, Fluid Phase Equilibria 28 (1986) 103–118.
[56] M.R. Housaindokht, M.R. Bozorgmehr, Calculation of solubility of methimazole, phenazopyridine and propanolol in supercritical carbon dioxide, Journal of Supercritical Fluids 43 (2008) 390–397.
[57] C.J. Chang, C.-Y. Day, C.-M. Ko, K.-L. Chiu, Densities and *P–x–y* diagrams for carbon dioxide dissolution in methanol, ethanol, and acetone mixtures, Fluid Phase Equilibria 131 (1997) 243–258.
[58] Z. Knez, M. Skerge, L. Ilic, C. Lutge, Vapor–liquid equilibrium of binary CO_2–organic solvent systems (ethanol, tetrahydrofuran, *ortho*-xylene, *meta*-xylene, *para*-xylene), Journal of Supercritical Fluids 43 (2008) 383–389.
[59] A. Kordikowski, A.P. Schenk, R.M. Van Nielen, C.J. Peters, Volume expansions and vapour–liquid equilibria of binary mixtures of a variety of polar solvents and certain near-critical solvents, Journal of Supercritical Fluids 8 (1995) 205–216.
[60] I. Ashour, R. Almehaideb, S.-E. Fateen, G. Aly, Representation of solid–supercritical fluid phase equilibria using cubic equations of state, Fluid Phase Equilibria 167 (2000) 41–61.
[61] H.C. De Sousa, M. Sousa Costa, P. Coimbra, A.A. Matias, C.M.M. Duarte, Experimental datermination and correlation of meloxicam sodium salt solubility in supercritical carbón dioxide, Journal of Supercritical Fluids 63 (2012) 40–45.
[62] J. Chrastil, Solubility of solids and liquids in supercritical gases, Journal of Physical Chemistry 86 (1982) 3016–3021.
[63] Y. Adachi, B.C.-Y. Lu, Supercritical fluid extraction with carbon dioxide and ethylene, Fluid Phase Equilibria 14 (1983) 147–156.
[64] R. Ch, G. Madras, An association model for the solubilities of pharmaceuticals in supercritical carbon dioxide, Thermochimica Acta 507–508 (2010) 99–105.
[65] J.M. Del Valle, J.M. Aguilera, An improved equation for predicting the solubility of vegetable oils in supercritical carbon CO_2, Industrial and Engineering Chemistry Research 27 (1988) 1551–1553.
[66] M.D. Gordillo, M.A. Blanco, A. Molero, E. Martinez de la Ossa, Solubility of the antibiotic penicillin G in supercritical carbon dioxide, Journal of Supercritical Fluids 15 (1999) 183–190.
[67] K.S. Kumar, K.P. Johnston, Modelling the solubility of solids in supercritical fluids with density as the independent variable, Journal of Supercritical Fluids 1 (1988) 15–22.
[68] J. Mendez-Santiago, A.S. Teja, The solubility of solids in supercritical fluids, Fluid Phase Equilibria 158–160 (1999) 501–510.
[69] D.L. Sparks, R. Hernandez, L.A. Estevez, Evaluation of density-based models for the solubility of solids in supercritical carbon dioxide and formulation of a new model, Chemical Engineering Science 63 (2008) 4292–4301.
[70] Z.-R. Yu, B. Singh, S.S.H. Rizvi, J. Zollweg, Solubility of fatty acids, fatty acid esters, triglycerides, and fats and oils in supercritical carbon dioxide, Journal of Supercritical Fluids 7 (1994) 51–59.
[71] X. Bian, Z. Du, Y. Tang, An improved density-based model for the solubility of some compounds in supercritical carbon dioxide, Thermochimica Acta 519 (2011) 16–21.
[72] A. Jouyban, H.-K. Chan, N.R. Foster, Mathematical representation of solute solubility in supercritical carbon dioxide using empirical expressions, Journal of Supercritical Fluids 24 (2002) 19–35.
[73] C.-S. Su, Y.-P. Chen, Correlation for the solubilities of pharmaceutical compounds in supercritical carbon dioxide, Fluid Phase Equilibria 254 (2007) 167–173.
[74] A. Tabernero, E.M. Martín del Valle, M.A. Galán, A comparison between semiempirical equations to predict the solubility of solids in supercritical carbón dioxide, Journal of Supercritical Fluids 52 (2010) 161–174.
[75] S.N. Reddy, G. Madras, Modeling of ternary solubilities of solids in supercritical carbon dioxide in the presence of cosolvents or cosolutes, Journal of Supercritical Fluids 63 (2012) 105–114.
[76] M. Sauceau, J.-J. Letourneau, D. Richon, J. Fages, Enhanced density-based models for solid compound solubilities in supercritical carbon dioxide with cosolvents, Fluid Phase Equilibria 208 (2003) 99–113.
[77] I.C. Sánchez, R.H. Lacombe, An elementary molecular theory of classical fluids, Journal of Physical Chemistry 80 (1976) 2352–2362.
[78] Y. Song, T. Hino, S.M. Lambert, J.M. Prausnitz, A perturbed hard-sphere-chain equation of state for normal fluids and polymers, Industrial and Engineering Chemistry Research 33 (1994) 1047–1057.
[79] N. Elvassore, A. Bertucco, M. Fermeglia, Phase-equilibria calculation by group-contribution perturbed-hard-sphere-chain equation of state, AIChE Journal 48 (2002) 359–368.
[80] S. Colussi, N. Elvassore, I. Kikic, A comparison between semi-empirical and molecular-based equations of state for describing the thermodynamic of supercritical micronization processes, Journal of Supercritical Fluids 39 (2006) 118–126.
[81] N. De Zordi, I. Kikic, M. Moneghini, D. Solinas, Solubility of pharmaceutical compounds in supercritical carbon dioxide, Journal of Supercritical Fluids 66 (2012) 16–22.
[82] R.D. Smith, R. Wash, US Patent 4582731, April 15, 1986.
[83] C.-S. Su, M. Tang, Y.-P. Chen, Micronization of nabumetone using the rapid expansion of supercritical solutions (RESS) process, Journal of Supercritical Fluids 50 (2009) 69–76.
[84] C. Domingo, E. Berends, G.M. Van Rosmales, Precipitation of ultrafine organic crystals from the rapid expansion of supercritical solutions over a capillary and a frit nozzle, Journal of Supercritical Fluids 10 (1997) 39–55.
[85] M. Turk, G. Upper, P. Hils, Formation of composite drug–polymer particles by co-precipitation during the rapid expansion of supercritical fluids, Journal of Supercritical Fluids 39 (2006) 253–263.
[86] D. Bolten, M. Turk, Micronisation of carbamazepine through rapid expansion of supercritical solutions (RESS), Journal of Supercritical Fluids 62 (2012) 32–40.
[87] M. Charoenchaitrakool, F. Dehghani, N.R. Foster, Utilization of supercritical carbon dioxide for complex formation of ibuprofen and methyl-β-cyclodextrin, International Journal of Pharmaceutics 239 (2002) 103–112.
[88] B. Kongsombut, A. Tsutsumi, N. Suankaew, T. Charinpanitkul, Encapsulation of SiO_2 and TiO_2 fine powders with poly(DL-lactic-co-glycolic acid) by rapid expansion of supercritical CO_2 incorporated with ethanol cosolvent, Industrial and Engineering Chemistry Research 48 (2009) 11230–11235.
[89] K. Mishima, K. Matsuyama, D. Tanabe, S. Yamauchi, T.J. Young, K.P. Johnston, Microencapsulation of proteins by rapid expansion of supercritical solution with a nonsolvent, AIChE Journal 46 (2000) 857–865.
[90] R. Thakur, R.B. Gupta, Rapid expansion of supercritical solution with solid cosolvent (RESS-SC) process: formation of Griseofulvin nanoparticles, Industrial and Engineering Chemistry Research 44 (2005) 7380–7387.
[91] P. Pathak, M.J. Meziane, T. Desai, Y.-P. Sun, Formation and stabilization of ibuprofen nanoparticles in supercritical fluid processing, Journal of Supercritical Fluids 37 (2006) 279–286.
[92] A. Sane, J. Limtrakul, Formation of retinyl palmitate-loaded poly(L-lactide) nanoparticles using rapid expansion of supercritical solutions into liquid solvents (RESOLV), Journal of Supercritical Fluids 51 (2009) 230–237.
[93] M. Turk, D. Bolten, Formation of submicron poorly water-soluble drugs by rapid expansion of supercritical solution (RESS): results for naproxen, Journal of Supercritical Fluids 55 (2010) 778–785.
[94] T.J. Young, S. Mawson, K.P. Johnston, I.B. Henriksen, G.W. Pace, A.K. Mishra, Rapid expansion from supercritical to aqueous solution to produce submicron suspensions of water-insoluble drugs, Biotechnology Progress 16 (2000) 402–407.
[95] C.Y. Tai, C.-S. Chen, Effect of CO_2 on expansion and supersaturation of saturated solutions, AIChE Journal 44 (1998) 989–992.
[96] J.C. De la Fuente Badilla, C.J. Peters, J. de Swaan Arons, Volume expansion in relation to the gas-antisolvent process, Journal of Supercritical Fluids 17 (2000) 13–23.
[97] M. Mukhopadhyay, Partial molar volume reduction of solvent for solute crystallization using carbon dioxide as antisolvent, Journal of Supercritical Fluids 25 (2003) 213–223.
[98] M. Mukhopadhyay, S.V. Dalvi, Partial molar volume molar fraction of solvent in binary (CO_2-solvent) solution for solid solubility predictions, Journal of Supercritical Fluids 29 (2004) 221–230.
[99] Y. Bakhbakhi, P.A. Charpentier, S. Rohani, Experimental study of GAS process for producing microparticles of beclomethasone-17,21-dipropionate suitable for pulmonary delivery, International Journal of Pharmaceutics 309 (2006) 71–80.
[100] M.J. Cocero, S. Ferrero, Crystallization of β-carotene by a GAS process in batch. Effect of operating conditions, Journal of Supercritical Fluids 22 (2002) 237–245.
[101] N. Elvassore, A. Bertucco, P. Caliceti, Production of insulin-loaded poly(ethylene glycol)/poly(L-lactide) (PEG/PLA) nanoparticles by gas antisolvent techniques, Journal of Pharmaceutical Sciences 90 (2001) 1628–1636.
[102] M. Hanna, P. York, WO Patent 95/01221, 1994.
[103] A. Tabernero, E.M. Martín del Valle, M.A. Galán, Precipitation and tretinoin and acetaminophen with solution enhanced dispersion by supercritical fluids (SEDS), role of phase equilibria to optimize particle diameter, Powder Technology 217 (2012) 177–188.
[104] P. Chattopadhyay, R.B. Gupta, Production of griseofulvin nanoparticles using supercritical CO_2 antisolvent with enhanced mass transfer, International Journal of Pharmaceutics 228 (2001) 19–31.
[105] P. Chattopadhyay, R.B. Gupta, Protein nanoparticles formation by supercritical antisolvent with enhanced mass transfer, AIChE Journal 48 (2002) 235–244.
[106] K.W. Hutchenson, A.M. Scurto, B. Subramaniam, Gas-Expanded Liquid and Near-Critical Media, American Chemical Society, USA, 2009.
[107] F. Miguel, A. Martín, T. Gamse, M.J. Cocero, Supercritical antisolvent precipitation of lycopene. Effect of the operating parameters, Journal of Supercritical Fluids 36 (2007) 225–235.
[108] E. Reverchon, I. De Marco, E. Torino, Nanoparticles production by supercritical antisolvent precipitation: a general interpretation, Journal of Supercritical Fluids 43 (2007) 126–138.
[109] M.A. Tavares-Cardoso, S. Antunes, F. Van Keulen, B.S. Ferreira, A. Geraldes, J.M.S. Cabral, A.F. Palavra, Supercritical antisolvent micronisation of synthetic all-trans-β-carotene with tetrahydrofuran as solvent and carbon dioxide as antisolvent, Journal of Chemical Technology and Biotechnology 84 (2009) 115–122.
[110] A. Tenorio, M.D. Gordillo, C. Pereyra, E. Martinez de la Ossa, Controlled submicro particle formation of ampicillin by supercritical antisolvent precipitation, Journal of Supercritical Fluids 40 (2007) 308–316.

[111] F. Miguel, A. Martín, F. Mattea, M.J. Cocero, Precipitation of lutein and co-precipitation of lutein and poly-lactic acid with the supercritical anti-solvent process, Chemical Engineering and Processing 47 (2008) 1594–1602.

[112] B. De Gioannis, A. Vega-González, P. Subra, Anti-solvent and co-solvent effect of CO_2 in the solubility of griseofulvin in acetone and ethanol solutions, Journal of Supercritical Fluids 29 (2004) 49–57.

[113] E. Reverchon, I. De Marco, Supercritical antisolvent precipitation of cefonicid: thermodynamic interpretation of results, Journal of Supercritical Fluids 31 (2004) 207–215.

[114] A. Weber, L.V. Yelash, T. Kraska, Effect of the phase behaviour of the solvent-antisolvent systems on the gas-antisolvent-crystallisation of paracetamol, Journal of Supercritical Fluids 33 (2005) 107–113.

[115] E. Reverchon, E. Torino, S. Dowy, A. Brauer, A. Leipertz, Interactions of phase equilibria, jet fluid dynamics and mass transfer during supercritical antisolvent micronization, Chemical Engineering Journal 156 (2010) 446–458.

[116] P. Subra, C.-G. Laudani, A. Vega-González, E. Reverchon, Precipitation and phase behavior of theophylline in solvent–supercritical CO_2 mixtures, Journal of Supercritical Fluids 35 (2005) 95–105.

[117] I. De Marco, E. Reverchon, Supercritical antisolvent micronization of cyclodextrins, Powder Technology 183 (2008) 239–246.

[118] E. Reverchon, R. Adami, G. Caputo, I. De Marco, Spherical microparticles production by supercritical antisolvent precipitation: interpretation of results, Journal of Supercritical Fluids 47 (2008) 70–84.

[119] E. Reverchon, G. Della Porta, Production of antibiotic micro- and nanoparticles by supercritical antisolvent precipitation, Powder Technology 106 (1999) 23–99.

[120] M. Rantakylä, M. Jäntti, O. Aaltonen, M. Hurme, The effect of initial drop size on particle size in the supercritical antisolvent precipitation (SAS) technique, Journal of Supercritical Fluids 24 (2002) 251–263.

[121] M.A. Tavares-Cardoso, G.A. Monteiro, G.A. Cardoso, T.J.V. Prazeres, J.M.F. Figuereido, J.M.G. Martinho, J.M.S. Cabral, A.M.F. Palavra, Supercritical anti-solvent micronization of minocycline hydrochloride, Journal of Supercritical Fluids 44 (2008) 238–244.

[122] A. Lefebvre, Atomization and Sprays, Taylor and Francis, United States, 1989.

[123] Y. Sun, B. Shekunov, Surface tension of etanol in supercritical CO_2, Journal of Supercritical Fluids 27 (2003) 73–83.

[124] E. Badens, O. Boutin, G. Charbit, Laminar jet dispersion and jet atomization in pressurized carbon dioxide, Journal of Supercritical Fluids 36 (2005) 81–90.

[125] T. Petit-Gas, O. Boutin, E. Badens, Role of hydrodynamics in supercritical anti-solvent processes, Journal of Supercritical Fluids 51 (2009) 248–255.

[126] N. Czerwonatis, R. Eggers, Disintigration of liquid jets and drop drag coefficients in pressurized nitrogen and carbon dioxide, Chemical Engineering & Technology 24 (2001) 619–624.

[127] S.S. Dukhin, C. Zhu, R. Dave, R. Pfeffer, J.J. Luo, F. Chavez, Y. Shen, Dynamic interfacial tension near critical point of a solvent–antisolvent mixture and laminar jet stabilization, Colloids and Surfaces A: Physicochemical and Engineering Aspects 229 (2003) 181, 199.

[128] J.O. Werling, P. Debenedetti, Numerical modelling of mass transfer in the supercritical antisolvent process: miscible conditions, Journal of Supercritical Fluids 18 (1999) 11–24.

[129] J.O. Werling, P. Debenedetti, Numerical modelling of mass transfer in the supercritical antisolvent process, Journal of Supercritical Fluids 16 (2000) 167–181.

[130] Y. Perez de Diego, F.E. Wubbolts, P.J. Jansens, Modelling mass transfer in the PCA process using the Maxwell–Stefan approach, Journal of Supercritical Fluids 37 (2006) 53–62.

[131] M.A. Tavares-Cardoso, J.M.S. Cabral, A.M.F. Palavra, V. Geraldes, CFD analysis of supercritical antisolvent (SAS) micronization of minocycline hydrochloride, Journal of Supercritical Fluids 47 (2008) 247–258.

[132] M. Lora, A. Bertucco, I. Kikic, Simulation of the semicontinous supercritical antisolvent recrystallization process, Industrial and Engineering Chemistry Research 39 (2000) 1487–1496.

[133] T. Fadli, A. Erriguible, S. Laugier, P. Subra-Paternault, Simulation of heat and mass transfer of CO_2–solvent mixtures in miscible conditions: isothermal and non-isothermal mixing, Journal of Supercritical Fluids 52 (2010) 193–202.

[134] M. Mukhopadhyay, S.V. Dalvi, Mass and heat transfer analysis of SAS: effects of thermodynamic states and flow rates on droplet size, Journal of Supercritical Fluids 30 (2004) 333–348.

[135] A. Martín, M.J. Cocero, Numerical modeling of jet hydrodynamics, mass transfer, and crystallization kinetics in the supercritical antisolvent (SAS) process, Journal of Supercritical Fluids 32 (2004) 203–219.

[136] F. Marra, I. De Marco, E. Reverchon, Numerical analysis of the characteristic times controlling supercritical antisolvent micronization, Chemical Engineering Science 71 (2012) 39–45.

[137] N. Ventosa, S. Sala, J. Veciana, J. Torres, J. Llibre, Depressurization of en expanded liquid organic solution (DELOS): a new procedure for obtaining submicron- or micron-sized crystalline particles, Crystal Growth and Design 1 (2001) 299–303.

[138] M. Gimeno, N. Ventosa, S. Sala, J. Veciana, Use of 1,1,1,2-tetrafluoroethane (R-134a)-expanded liquids as solvent media for ecoefficient particle design with the DELOS crystallization process, Crystal Growth and Design 6 (2006) 23–25.

[139] N. Ventosa, S. Sala, J. Veciana, DELOS process: a crystallization technique using compressed fluids. 1. Comparison to the GAS crystallization method, Journal of Supercritical Fluids 26 (2003) 33–45.

[140] S. Sala, E. Elizondo, E. Moreno, T. Calvet, M.A. Cuevas-Diarte, N. Ventosa, J. Veciana, Kinetically driven crystallization of a pure polymorphic phase of stearic acid from CO_2-expanded solutions, Crystal Growth and Design 10 (2010) 1226–1232.

[141] S.V. Dalvi, M. Mukhopadhyay, Large and rapid temperature reduction of organic solutions with supercritical CO_2, AIChE Journal 53 (2007) 2814–2823.

[142] S.V. Dalvi, M. Mukhopadhyay, A novel process for precipitation of ultra-fine particles using sub-critical CO_2, Powder Technology 195 (2009) 190–195.

[143] E. Weidner, Z. Knez, Z. Novak, EP 0744992 or WO 95/21688.

[144] Z. Mandzuka, Z. Knez, Influence of temperature and pressure during PGSS micronization and storage time on degree of crystallization and crystal forms of monostearate and tristearate, Journal of Supercritical Fluids 45 (2008) 102–111.

[145] M. Lubary, T.W. de Loos, J.H. ter Horst, G.W. Hofland, Production of microparticles from milk products using the supercritical solvent melt micronization (SCMM) process, Journal of Supercritical Fluids 55 (2011) 1079–1088.

[146] E. De Paz, A. Martín, C.M.M. Duarte, M.J. Cocero, Formulation of β-carotene with poly-(ε-caprolactones) by PGSS process, Powder Technology 217 (2012) 77–83.

[147] S. Pollak, M. Petermann, S. Kareth, A. Kilzer, Manufacturing of pulverised nanocomposites—dosing and dispersion of additives by the use of the supercritical carbon dioxide, Journal of Supercritical Fluids 53 (2010) 137–141.

[148] E. De Paz, A. Martín, S. Rodriguez-Rojo, J. Herreras, M.J. Cocero, Determination of phase equilibrium (solid–liquid–gas) ion poly-(ε-caprolactone)–carbon dioxide systems, Journal of Chemical and Engineering Data 55 (2010) 2781–2785.

[149] S. Spilimbergo, G. Luca, N. Elvassore, A. Bertucco, Effect of high-pressure gases on phase behaviour of solids lipids, Journal of Supercritical Fluids 38 (2006) 289–294.

[150] S. Salmaso, N. Elvassore, A. Bertucco, P. Caliceti, Production of solid lipid submicron particles for protein delivery using a novel supercritical gas-assisted melting atomization process, Journal of Pharmaceutical Sciences 98 (2009) 640–650.

[151] D. Meterc, M. Petermann, E. Weidner, Drying of aqueous green tea extracts using a supercritical fluid spray process, Journal of Supercritical Fluids 45 (2008) 253–259.

[152] M. Pham, S. Pollak, M. Petermann, Micronisation of poly(ethylene oxide) solutions and separation of water by PGSS-Drying, Journal of Supercritical Fluids 64 (2012) 19–24.

[153] S. Varona, S. Kareth, A. Martín, M.J. Cocero, Formulation of lavandin essential oil with biopolymers by PGSS for application as biocide in ecological agriculture, Journal of Supercritical Fluids 54 (2010) 369–377.

[154] A. Martín, H. Minh Pham, A. Kilzer, S. Kareth, E. Weidner, Micronization of polyethylene glicol by PGSS (particles from gas saturated solutions)-drying of aqueous solutions, Chemical Engineering and Processing 49 (2010) 1259–1266.

[155] N. Elvassore, M. Flaibani, A. Bertucco, P. Caliceti, Thermodynamic analysis of micronization processes from gas-saturated solutions, Industrial and Engineering Chemistry Research 42 (2003) 5924–5930.

[156] J. Li, H.A. Matos, E. Gomes de Azevedo, Two-phase homogeneous model for particle formation from gas-saturated solution processes, Journal of Supercritical Fluids 32 (2004) 275–286.

[157] J. Li, M. Rodrigues, A. Paiva, H.A. Matos, E. Gomes de Azevedo, Modeling of the PGSS process by crystallization and atomization, AIChE Journal 51 (2005) 2343–2357.

[158] M. Strumendo, A. Bertucco, N. Elvassore, Modeling of particle formation processes using gas saturated solutions atomization, Journal of Supercritical Fluids 41 (2007) 115–125.

[159] A. Martín, E. Weidner, PGSS-drying: mechanism and modeling, Journal of Supercritical Fluids 55 (2010) 271–281.

[160] E. Sher, T. Bar-Kohany, A. Rashkovan, Flash-boiling atomization, Progress in Energy and Combustion Science 34 (2008) 417–439.

[161] S. Sovani, P.E. Sojka, A. Lefebvre, Effervescent atomization, Progress in Energy and Combustion Science 27 (2001) 483–521.

[162] R.E. Sievers, U. Karst, P.D. Milewski, S.P. Sellers, B.A. Miles, J.D. Schaefer, C.R. Stoldt, C.Y. Xu, Formation of aqueous small droplet aerosols assisted by supercritical carbon dioxide, Aerosol Science and Technology 30 (1999) 3–15.

[163] E. Reverchon, Supercritical-assisted atomization to produce micro- and/or nanoparticles of controlled size and distribution, Industrial and Engineering Chemistry Research 41 (2002) 2405–2411.

[164] R. Adami, S. Liparoti, E. Reverchon, A new supercritical assisted atomization configuration, for the micronization of thermolabile compounds, Chemical Engineering Journal 173 (2011) 55–61.

[165] E. Reverchon, G. Lamberti, A. Antonacci, Supercritical fluid assisted production of HPMC composite microparticles, Journal of Supercritical Fluids 46 (2008) 185–196.

[166] E. Reverchon, A. Antonacci, Polymer microparticles production by supercritical assisted atomization, Journal of Supercritical Fluids 39 (2007) 444–452.

[167] M.A. Rodrigues, J. Li, L. Padrela, A. Almeida, H.A. Matos, E. Gomes de Azevedo, Anti-solvent effect in the production of lysozyme nanoparticles by supercritical-fluid assisted atomization processes, Journal of Supercritical Fluids 48 (2009) 253–260.

[168] H.-T. Wu, M.-W. Yang, Precipitation kinetics of PMMA sub-micrometric particles with a supercritical assisted-atomization process, Journal of Supercritical Fluids 59 (2011) 98–107.

[169] P. Chattopadhyay, B.Y. Shekunov, D. Yim, D. Cipolla, B. Boyd, S. Farr, Production of solid lipid nanoparticle suspensions using supercritical fluid extraction emulsions (SFEE) for pulmonary delivery using the AERx system, Advanced Drug Delivery Reviews 59 (2007) 444–453.
[170] B.Y. Shekunov, P. Chattopadhyay, J. Seitzinger, R. Huff, Nanoparticles of poorly water-soluble drugs prepared by supercritical fluid extraction of emulsions, Pharmaceutical Research 23 (2006) 196–204.
[171] P. Chattopadhyay, R. Huff, B.Y. Shekunov, Drug encapsulation using supercritical fluids extraction of emulsions, Journal of Pharmaceutical Sciences 95 (2006) 667–679.
[172] P. Chattopadhyay, R.B. Gupta, Supercritical CO_2-based formation of silica nanoparticles using water-in-oil microemulsions, Industrial and Engineering Chemistry Research 42 (2003) 465–472.
[173] G. Della Porta, N. Falco, E. Reverchon, Continous supercritical emulsions extractions: a new technology for biopolymer microparticles production, Biotechnology & Bioengineering 108 (2011) 676–686.
[174] G. Della Porta, R. Campardelli, N. Falco, E. Reverchon, PLGA microdevices for retinoids sustained release produced by supercritical emulsion extraction: continous vs batch operation layouts, Journal of Pharmaceutical Sciences 100 (2011) 4357–4367.
[175] G. Della Porta, E. Reverchon, Nanostructured microspheres producd by supercritical fluid extraction of emulsions, Biotechnology & Bioengineering 100 (2008) 1020–1033.
[176] F. Mattea, A. Martín, C. Schulz, P. Jaeger, R. Eggers, M.J. Cocero, Behaviour of an organic solvent drop during the supercritical extraction of emulsions, AIChE Journal 56 (2010) 1184–1195.
[177] F. Mattea, A. Martín, A. Matias-Gago, M.J. Cocero, Supercritical antisolvent precipitation from an emulsion: β-carotene nanoparticle formation, Journal of Supercritical Fluids 51 (2009) 238–247.
[178] A. Carr, R. Mammucari, N.R. Foster, Particle formation of budesonide from alcohol-modified subcritical water solutions, International Journal of Pharmaceutics 405 (2010) 169–180.
[179] A. Carr, R. Mammucari, N.R. Foster, The solubility and micronization of griseofulvin using subcritical water, Industrial and Engineering Chemistry Research 49 (2010) 3403–3410.
[180] G.P. Sanganwar, S. Sathigari, R.J. Babu, R.B. Gupta, Simultaneous production and co-mixing of microparticles of nevirapine with excipients by supercritical antisolvent method for dissolution enhancement, European Journal of Pharmaceutical Sciences 39 (2010) 169–174.
[181] A.-Z. Chen, Z. Zhao, S.-B. Wang, Y. Li, C. Zhao, Y.-G. Liu, A continous RESS process to prepare PLA-PEG-PLA microparticles, Journal of Supercritical Fluids 59 (2011) 92–97.
[182] E. Weidner, M. Petermann, K. Blatter, V. Rekowski, Manufacture of powder coatings by spraying of gas-enriched melts, Chemical Engineering and Technology 24 (2001) 529–533.
[183] M. Turk, G. Upper, M. Steurenthaler, Kh. Hussein, M.A. Wahl, Complex formation of ibuprofen and β-cyclodextrin by controlled particle deposition (CPD) using sc-CO_2, Journal of Supercritical Fluids 39 (2007) 435–443.
[184] P. Alessi, I. Kikic, A. Cortesi, A. Fogar, M. Moneghini, Polydimethylsiloxanes in supercritical solvent impregnation (SSI) of polymers, Journal of Supercritical Fluids 27 (2003) 309–315.
[185] Y. Masmouda, L.B. Azzouk, O. Forzano, J.-M. Andre, E. Badens, Supercritical impregnation of intraocular lenses, Journal of Supercritical Fluids 60 (2011) 98–105.
[186] V.P. Costa, M.E.M. Braga, C.M.M. Duarte, C. Alvarez-Lorenzo, A. Concheiro, M.H. Gil, H.C. De Sousa, Anti-glaucoma drug-loaded contact lenses prepared using supercritical solvent impregnation, Journal of Supercritical Fluids 53 (2010) 165–173.
[187] V.P. Costa, M.E.M. Braga, J.P. Guerra, A.R.C. Duarte, C.M.M. Duarte, E.O.B. Leite, M.H. Gil, H.C. De Sousa, Development of therapeutic contact lenses using a supercritical solvent impregnation method, Journal of Supercritical Fluids 52 (2010) 306–316.
[188] S. Varona, S. Rodriguez-Rojo, A. Martín, M.J. Cocero, C.M.M. Duarte, Supercritical impregnation of lavandin (*Lavandula hybrida*) essential oil in modified starch, Journal of Supercritical Fluids 58 (2011) 313–319.
[189] L.N. Comin, F. Temelli, M.D.A. Saldana, Impregnation of flax oil in pregelatinized corn starch using supercritical CO_2, Journal of Supercritical Fluids 61 (2012) 221–228.

1.3. Conclusiones

Debido a las propiedades de transporte intermedias entre líquidos y gases de los fluidos supercríticos, estos pueden ser utilizados en diferentes técnicas para la precipitación de sólidos.

Estas técnicas se presentan como una buena alternativa a los métodos convencionales para la generación de partículas de la industria farmacéutica ya que producen partículas con una estrecha distribución de tamaño, a la vez que permiten el control de esta distribución mediante la variación de las condiciones experimentales. Además, en el caso de usar CO_2sc se evita el empleo de compuestos tóxicos para el ser humano o el medio ambiente.

Sin embargo, se debe realizar un estudio termodinámico previo a la utilización de estas técnicas para determinar su posible viabilidad. En este aspecto, lo más complejo es la determinación de la solubilidad del sólido en el fluido supercrítico, ya que actualmente no existe ningún modelo fiable que pueda predecir estos datos experimentales.

Algo similar ocurre con la distribución de tamaño de partícula obtenida. No existe ningún modelo o ecuación general que pueda predecir este parámetro. Sin embargo, los mecanismos de formación de partículas en los procesos más comunes han sido definidos, por lo que es posible realizar una aproximación cualitativa del efecto de las diferentes variables experimentales en la distribución final de tamaño de partícula así como en la morfología resultante.

● Referencias también citadas

[1] M. V. Gunchenko; N. V. Dekhtiarenko, N. V.; O. Yu Galkin, World pharmaceutical market trends analysis.

[2] International Federation of Pharmaceutical Manufacturers and Associations (IFPMA), The pharmaceutical industry and global health. Facts and figures, 2012.

[3] Eva M. Martín del Valle; Miguel A. Galán; Ruben G. Carbonell, Drug delivery Technologies: The way forward in the new decade. Ind. Eng. Chem. Res. 48 (2009) 2475-2486.

[4] P. York; U. B. Kompella; B. Y. Shekunov, Supercritical fluid technology for drug product development. 1º Ed.-New York: Ed. Marcel-Dekker, 2004.

[5] B. Subramaniam; R. A. Rajewski; K. Snavely, Pharmaceutical processing with supercritical carbon dioxide. J. Pharm. Sci. 86 (1997) 885-890.

[6] B. Shekunov; P. York; Crystallization processes in pharmaceutical technology and drug delivery design. J. Crystal Growth 211 (2000) 122-136

[7] S. A. Shoyele; S. Cawthorne, Particle engineering techniques for inhaled biopharmaceuticals. Adv. Drug. Del. Rev. 58 (2006) 1009-1029.

CAPÍTULO 2.

Objetivos y justificación

Esta tesis se encuadra dentro una de las líneas de investigación del grupo al que pertenezco, referida a procesos de producción de sistemas de liberación controlada de productos farmacéuticos.

En este sentido, el grupo de investigación está trabajando en diferentes líneas con el fin de la obtención de partículas y microcápsulas en un amplio intervalo de tamaño que se indican a continuación:

• Producción de nanocápsulas desde 200 a 400 nm. mediante gelificación iónica y complejación electrostática. De esta manera se han obtenido nanopartículas con un bajo índice de polidispersión y diferentes características superficiales

• Producción de microcápsulas desde 20 a 100 micras mediante el uso de una boquilla tipo "fan jet" para producir la rotura de un chorro laminar con una corriente de aire.

• Producción de micropartículas desde 300 a 600 micras mediante el uso de una técnica con una boquilla vibratoria.

• Producción de micropartículas desde 1 a 5 micras mediante el uso de un proceso de atomización a alta presión usando CO_2sc como antisolvente. Este método será detallado a continuación, ya que es el estudiado en la presente tesis.

La técnica escogida con CO_2sc como antisolvente fue la técnica SEDS ya que se ha diseñado la geometría de la boquilla de atomización que permite mejorar el mecanismo de transferencia de materia y obtener así una mejor distribución final de tamaño.

El dispositivo SEDS se empleó para la micronización de dos sólidos: acetaminofén y tretinoína (ácido all-trans-retinoico) usando etanol como disolvente para ambos fármacos.

Acetaminofén fue usado como fármaco modelo ya que son numerosos los estudios recogidos en bibliografía en los cuáles este sólido es micronizado mediante el uso de técnicas con fluidos supercríticos.

Por otro lado, la tretinoína (compuesto derivado del ácido retinoico) está siendo actualmente estudiada para tratar el enfisema pulmonar por los grupos de cirugía torácica y de anatomía patológica de la Universidad de Salamanca con los que se colabora en distintas investigaciones. Dado que esta patología requiere el uso de inhaladores para la administración de su tratamiento, las partículas empleadas deben tener tamaño entre 1-5 micras para que este compuesto pueda llegar a los alveolos pulmonares.

Finalmente, etanol se usó como disolvente en ambos sistemas porque cumple todos los requisitos requeridos para usar una técnica con CO_2sc como antisolvente: Tanto los sólidos (tretinoína como acetaminofén) como el CO_2sc son solubles en etanol en las condiciones de operación estudiadas.

En la técnica SEDS, como se ha visto en el apartado anterior, campos como la termodinámica, hidrodinámica, transferencia de materia y cristalización desempeñan un papel sumamente importante en la precipitación del fármaco, por ello estos factores serán estudiados en el desarrollo de esta tesis.

El estudio termodinámico es fundamental en este tipo de procesos. Así, la solubilidad del sólido en el fluido supercrítico condiciona su uso como solvente o antisolvente, mientras que el mecanismo de precipitación en un proceso con antisolventes depende de los equilibrios de fases correspondientes.

Por tanto, este trabajo pretende estudiar la termodinámica involucrada en este tipo de precipitación en condiciones supercríticas. Para ello se hará un énfasis especial en el efecto del equilibrio de fases sobre la distribución de tamaño de partícula obtenida así como la solubilidad de fármacos en CO_2sc. Posteriormente se realizará el estudio de la transferencia de materia y regímenes de atomización en un proceso SEDS.

Teniendo en cuenta lo anteriormente descrito, los objetivos específicos del trabajo pueden enumerarse como a continuación se describe:

● Estudio de los equilibrios de fase (líquido-vapor, sólido-vapor y sólido-líquido-vapor) de los sistemas CO_2sc-etanol-acetaminofén y CO_2sc-etanol-tretinoína. Determinación visual del punto crítico de mezcla antisolvente-disolvente mediante el uso de una celda de equilibrio a alta presión.

● Comparación de ecuaciones semiempíricas descritas en bibliografía para determinar el modelo óptimo para modelar sistemas constituidos por CO_2sc y fármacos con y sin cosolventes dependiendo de las condiciones experimentales.

● Mejora de los modelos semiempíricos descritos en bibliografía mediante el uso de la mecánica estadística no extensiva.

● Desarrollo de procedimientos para la determinación de las propiedades de sublimación de fármacos.

● Desarrollo de un test de consistencia para la de evaluación de la solubilidad de compuestos farmacéuticos en CO_2sc.

● Obtención de partículas de acetaminofén y tretinoína mediante un proceso de atomización en condiciones supercríticas (SEDS) .Relación de los equilibrios de fase con tamaño de partícula y morfología de las partículas obtenidas.

- Estudio de la relación de los diferentes regímenes de atomización a alta presión, transferencia de materia gota-medio supercrítico y tamaño inicial de gota.

- Determinación de las condiciones óptimas para operar en nuestro sistema SEDS.

- Y por último obtener unas conclusiones generales que determinarán un trabajo futuro.

CAPÍTULO 3.

Procedimiento experimental

Como ya se indicó en los objetivos, es necesaria la determinación experimental del punto crítico de mezcla y hacer el estudio de los equilibrios con el fin de conocer el proceso y justificar los resultados obtenidos en cuestión de distribución de tamaño y morfología de las partículas obtenidas.

Para ello se utilizaron dos dispositivos experimentales:

Una celda de equilibrio para estudiar el equilibrio de fases y la posible aparición de inmiscibilidades en los sistemas estudiados, y por otra parte un equipo SEDS para la generación de partículas.

Los reactivos utilizados y la descripción de los equipos experimentales, junto con sus correspondientes procedimientos experimentales, se indican a continuación.

3.1. Reactivos

Los reactivos utilizados en este trabajo han sido los siguientes:

3.1.1. Acetominofén (paracetamol) (CAS 103-90-2):

Dicho fármaco fue suministrado con una pureza del 99% por Sigma-Aldrich. Su estructura molecular se representa en la fig. 3.1.

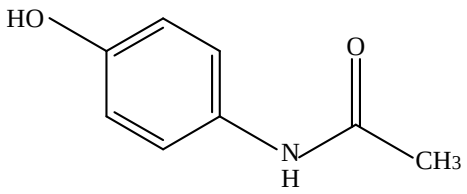

Fig.3.1 Estructura molecular del acetominofén.

3.1.2. Ácido all-trans-retinoico o tretinoína (CAS 116-31-4):

La tretinoína es el otro fármaco que se ha utilizado. Fue suministrada con una riqueza del 100,8% por Fagron. Su estructura molecular se muestra en la fig. 3.2.

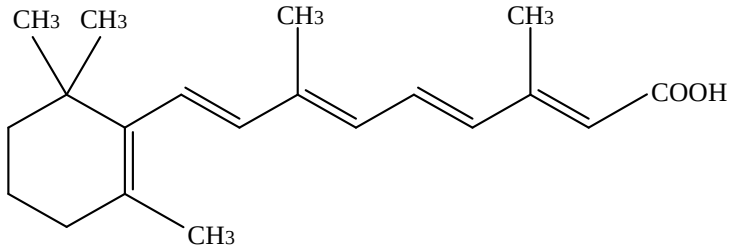

Fig.3.2 Estructura molecular de la tretinoina.

3.1.3. Etanol (CAS 64-17-5):

El etanol fue usado como disolvente tanto para el acetominofén como para la tretinoína. Fue suministrado con un 99,50% de pureza procedente de Panreac. Su estructura molecular se representa en la fig. 3.3.

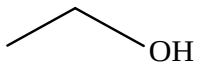

Fig. 3.3. Estructura molecular del etanol.

3.1.4. Dióxido de carbono (CAS 124-38-9):

El CO_2 fue elegido como antisolvente en ambos sistemas por sus características, descritas en la introducción de este trabajo. Dicho compuesto fue suministrado por Air Liquide. Su estructura molécular se describe en la fig. 3.4.

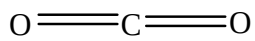

Fig.3.4. Estructura molecular del CO_2.

Otro compuesto utilizado, aunque no como reactivo, fue el nitrógeno (99,995%). Se usó con la finalidad de controlar el volumen disponible en la celda de alta presión. Este nitrógeno fue suministrado (al igual que el CO_2) por Air Liquide.

3.2. Celda de equilibrio

3.2.1. Descripción

Una celda de equilibrio fue utilizada como ya se ha indicado con el fin de observar las fases existentes en los sistemas estudiados (CO_2-etanol-acetaminofén y CO_2-etanol-tretinoína), la posible aparición de inmiscibilidades así como para la observación de la posible precipitación del sólido, determinando el porcentaje de precipitación de forma aproximada.

De modo esquemático, este proceso consiste en la adición de CO_2 a una disolución para llevar posteriormente el sistema a condiciones de equilibrio en las cuáles se obtenga CO_2sc. Durante ese proceso se podrán observar las distintas fases e inmiscibilidades que pueden aparecer.

Además, esta instalación puede utilizarse para determinar de forma aproximada el porcentaje de sólido precipitado en condiciones discontinuas por la adición a la celda de un tubo para tomar muestras. Una vez alcanzado el

equilibrio se puede recoger una muestra del líquido y determinar la cantidad de fármaco existente en él.

Por tanto, conociendo la cantidad inicial de fármaco introducido en el dispositivo junto a la cantidad de fármaco que queda en el líquido, se puede determinar el porcentaje de precipitación a unas condiciones definidas. Sin embargo, debido a las características del dispositivo experimental (indicadas en la sección 3.2.2.) este valor será una aproximación al porcentaje de precipitación real.

El diagrama de este equipo puede observarse en la figura 3.5.

El principal componente de este dispositivo es una celda (Sitec) de volumen variable (8-17 ml). Este volumen puede ser controlado mediante un sistema auxiliar de nitrógeno que desplaza un pistón, que sirve para modificar la altura del pistón en la celda, de forma que al controlar la altura, se controla al volumen y la presión.

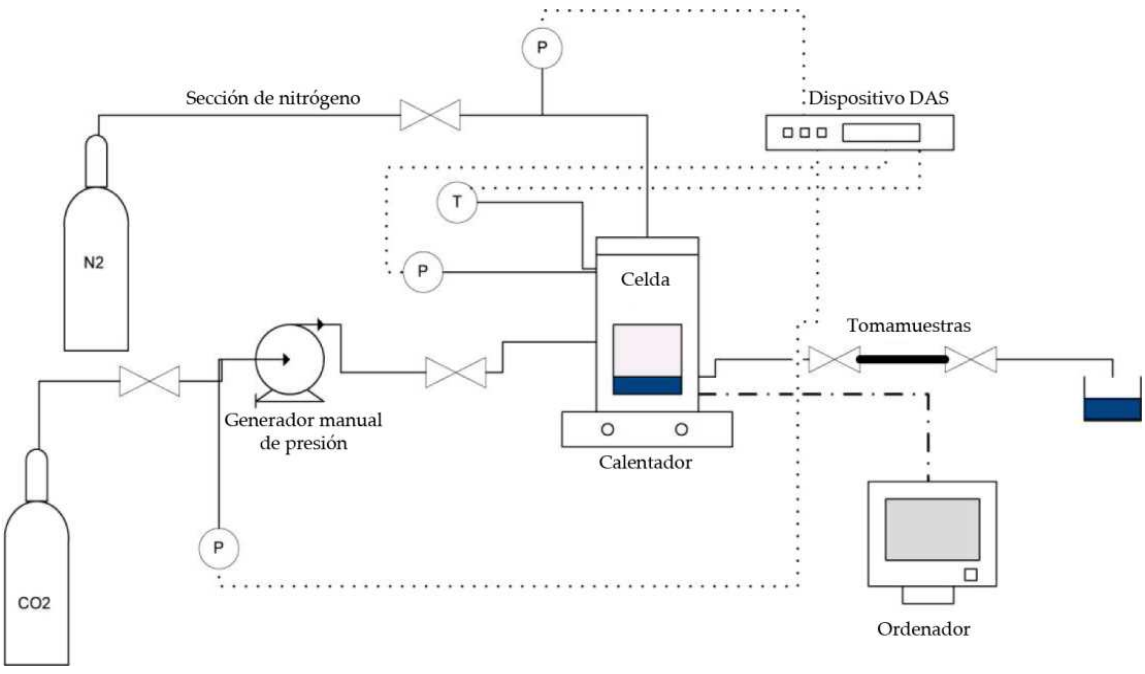

Figura 3.5. Esquema de la celda de equilibrio.

El CO_2 en estado supercrítico es obtenido con un generador de presión manual (Sitec 750.1030). Una camisa calefactora y un agitador magnético (Velp Scientific) están conectados a la celda para calentar y agitar la mezcla situada en su interior. A su vez, existen controladores para la temperatura y presión en el interior de la celda, el generador manual de presión, y la altura del pistón en la sección del nitrógeno.

Asimismo, es posible observar lo que sucede en el interior de la celda con el uso de una cámara (Santec). Todos los controladores y la cámara están conectados a un dispositivo DAS-8000. Finalmente, este dispositivo está conectado a un ordenador, con el que es posible monitorizar todos los parámetros durante el experimento.

Una fotografía de algunos componentes de la instalación que forman parte de la figura 3.5 (celda abierta sin pistón (a), celda cerrada con pistón (b), generador manual de presión (c) y la cámara (d)) pueden observarse en la figura 3.6.

a)

b)

c)

d)

Figura 3.6. Celda abierta (a); celda cerrada con pistón (b); generador manual de presión (c); cámara (d)

3.2.2. Procedimiento

Cada experimento comienza con la introducción de 1 ml de la disolución objeto de estudio en la celda. Esta cantidad fue determinada por medidas de seguridad, teniendo en cuenta que la expansión de volumen del etanol debido a la adición de CO_2sc puede llegar a ser entre 300-400%. Estas disoluciones deben ser diluidas para intentar evitar en la mayor medida posible una influencia negativa del sólido en el equilibrio de fases. En este sentido, la concentración de

la disolución de acetaminofén en etanol fue de 5 mg/ml, mientras que la concentración de la disolución tretinoína-etanol fue de 1 mg/ml. Ambas concentraciones fueron elegidas porque están en el intervalo óptimo de concentraciones para este tipo de técnicas dado por bibliografía [1]. Además con estas concentraciones no existe la necesidad de ningún proceso adicional para favorecer la disolución de cualquiera de los fármacos en etanol.

Posteriormente, por medio del generador de presión manual se inyecta CO_2 a la celda hasta alcanzar la presión deseada. Si fuera necesaria una presión más elevada, se utilizará la línea de nitrógeno para desplazar el pistón (reducción de volumen) y por tanto incrementar la presión.

A continuación, la celda es calentada lentamente hasta alcanzar las condiciones deseadas de presión y temperatura, y estas son mantenidas durante al menos 1 h. para asegurarse que se alcanza el estado de equilibrio.

Durante este proceso de calentamiento todos los fenómenos que ocurren en el interior de la celda son observados a través del ordenador debido a la conexión entre la cámara y el ordenador. De esta forma se pueden identificar las diferentes fases del sistema a las condiciones deseadas. Como ejemplo, el punto crítico de mezcla se identifica cuándo se observa una única fase.

Al acabar el experimento la celda se descomprime lentamente por la tubería de salida de la celda, y posteriormente, el sólido precipitado es recogido del interior de la celda mediante la adición del disolvente. Debido a este proceso de recolección de partículas, éstas no pueden ser analizadas posteriormente.

Como se ha indicado, este equipo se puede utilizar como un precipitador discontinuo que permitiría la determinación aproximada del porcentaje precipitado de sólido en el sistema objeto de estudio.

Para ello, se instaló una toma de muestra en la salida de la celda. Una vez alcanzado el equilibrio a las condiciones deseadas, todo el líquido se recoge en la toma de muestra, que consiste en un tubo conectado a la celda. Posteriormente, por espectrofotometría, se determina la cantidad de soluto que queda disuelto en la muestra. La cantidad de sólido precipitada se determina entonces por diferencia de masa entre la cantidad inicial y la cantidad que se mantiene disuelta en la disolución. Sin embargo, debido al necesario proceso de descompresión, una cantidad del sólido precipitado puede salir por el tomamuestras, produciéndose su redisolución en el disolvente. Debido a este hecho, el porcentaje de precipitación siempre será aproximado.

En este aspecto, es necesario indicar que el acetaminofén y la tretinoína presentan un máximo a la longitud de onda de 250 nm. y 350 nm. respectivamente.

3.3. Equipo SEDS

3.3.1. Descripción

En el equipo SEDS se lleva a cabo la precipitación de los distintos sólidos (acetaminofén y tretinoína). Este equipo consiste básicamente en un recipiente en el que se consigue un ambiente constituido por un fluido supercrítico (en nuestro caso CO_2sc). La disolución con el sólido a micronizar es atomizada en este recipiente por medio de una boquilla. El CO_2sc actúa entonces como antisolvente, se consigue un elevado y rápido grado de supersaturación y el sólido precipita.

La principal diferencia entre el equipo SEDS y otros procesos de atomización en un medio supercrítico es el diseño de la boquilla, la cuál debe tener geometría coaxial. Además, en este caso existe una longitud de mezcla para favorecer el proceso de solubilización del fluido supercrítico en el disolvente.

La boquilla tiene un diámetro de 80 μm., un diámetro externo de tubo de $1.5 \cdot 10^{-3}$ m. y un diámetro interno de $1 \cdot 10^{-3}$ m. Por otro lado, la longitud de la zona de premezcla 0.75 mm.

En la figura 3.7 pueden observarse los esquemas de la boquilla y del equipo SEDS utilizado en esta tesis.

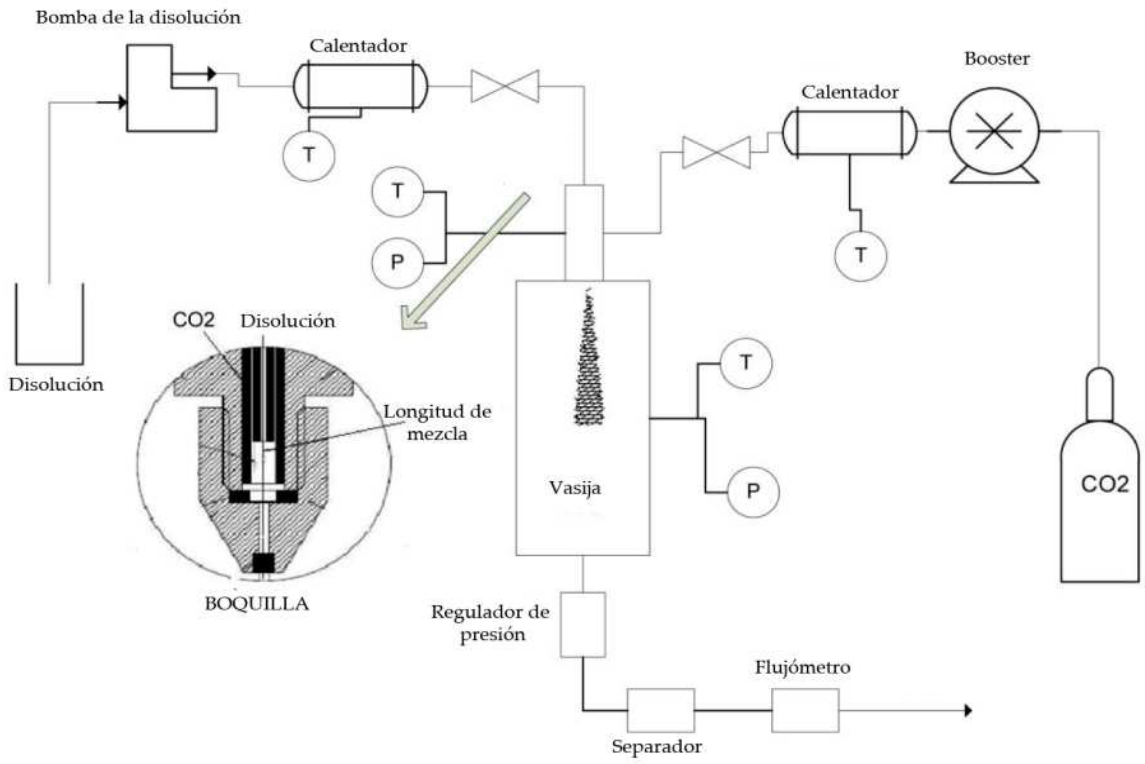

Figura 3.7. Esquema del equipo SEDS y su correspondiente boquilla.

El SEDS contiene una vasija encamisada de 500 ml dónde tiene lugar la precipitación. Un alimentador (booster PowerStar 4B) que emplea aire se utiliza para introducir CO_2 y conseguir la presión deseada en el interior de la vasija.

Por otro lado, una bomba de diafragma (Sera, modelo RK411.1) se usa para impulsar la disolución a la vasija. Esta bomba dispone de un sistema para controlar el caudal del fluido introducido. La presión en el interior de la vasija se controla mediante un regulador de presión (Tescom, model 26-1700).

Hay calentadores distribuidos a lo largo del equipo para calentar la disolución y el CO_2, además de mantener constante la temperatura en el interior de la vasija y en la boquilla. Todos estos parámetros (presión y temperatura) se monitorizan desde un cuadro de control (RFL Electricite tableautier).

Al final de la vasija se sitúa un filtro de policarbonato con 0,1 μm de tamaño de poro (Millipore). Asimismo, el caudal de CO_2 se controla con un flujómetro de masas (Bronckhorst), situado después de una vasija que tiene el objetivo de recuperar el disolvente y un regulador de presión.

En la figura 3.8, puede observarse una fotografía de alguno de los componentes del equipo SEDS (parte superior de la vasija (a), bomba de diafragama (b), booster (c) y caja de control (d)).

a)

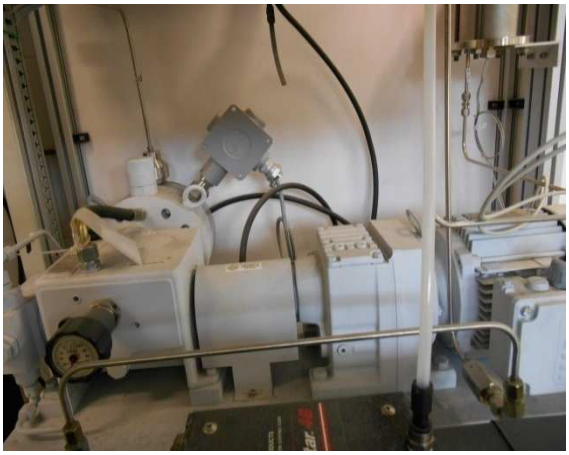

b)

c)

d)

Figura 3.8.Parte superior de la vasija (a); bomba diafragma (b); booster (c); caja de control (d)

3.3.2. Procedimiento

El procedimiento seguido con el equipo SEDS para la generación de partículas se describe a continuación.

El experimento comienza con la adición de CO_2 a la vasija, fijando el flujo con el flujómetro junto con el regulador de presión. A la vez se confiere presión a la vasija por medio del booster, usando la línea auxiliar de aire a la que está

conectado. La temperatura en la vasija, en la boquilla y en las tuberías por las que circula el fluido es ajustada desde el cuadro de control.

Posteriormente, se ajusta el caudal de la disolución en la bomba de diafragma, y se bombea la disolución hacia la vasija. Ambos CO_2 y disolución entran a la vasija por medio de una boquilla con geometría coaxial y con una longitud de premezcla.

Después de la atomización de la disolución, la atmósfera constituida por CO_2sc ejerce un efecto antisolvente. Este fenómeno fuerza la precipitación del fármaco, que queda depositado en el filtro al final de la vasija.

Al finalizar cada experimento, se deja pasar una corriente de CO_2 durante varios minutos para secar las partículas y para arrastrar restos de disolvente que pueda quedar en el interior de la vasija.

3.4. Determinación del tamaño de partícula.

El tamaño de partícula y su distribución se determinó mediante análisis de imagen, usando el programa ImageJ.

Para ello, primeramente se realizaron fotos a los filtros que contenían partículas sólidas con un microscopio electrónico de barrido (SEM), modelo ZEISS DSM 940.

Sobre estas fotos se realiza el análisis de imagen. Este análisis se basa en el conteo de los pixeles que componen una partícula después de realizar un modelado del umbral del color.

Posteriormente, fijando un calibrado del tamaño de cada pixel, se obtiene como resultado el número de partículas y su diámetro correspondiente. Con el fin de contar un mayor número de partículas, este proceso se realiza dos veces sobre tres distintas áreas del filtro.

3.5. Análisis por difracción de rayos X.

La cristalinidad del sólido obtenido se estudió con un difractómetro Bruker D8 Advanced con radiación generada a 30 mA y 40 kV. Las muestras de acetaminofén fueron medidas en un rango de 2θ entre 10° -60° con una amplitud de paso de 0.04° y con un tiempo de cada paso de 3.0 s. [2].

Por otro lado, las muestras de tretinoína fueron medidas en un rango de 2θ entre 2°-30° con una amplitud de paso de 0.025° y con un tiempo de paso de 3.0 s. [3].

● Referencias

[1] M. Mukhopadhyay; S. Dalvi, Mass and heat transfer analysis of SAS: effect of thermodynamic states and flow rates on droplet size. The J. Supercrit. Fluids 30 (2004) 333-348.

[2] M. Khanmohammadi; A. B. Garmarudi; N. Moazzen; K. Ghasemi, Qualitative discrimination between paracetamol tables made by near infrared spectroscopy and chemometrics with regard to polymorphism. J. Structural Chem. 4 (2010) 663-669.

[3] X. Zhang; Q. Xia; N. Gu, Preparation of all-trans retinoic acid nanosuspensions using a modified precipitation method. Drug. Dev. Ind. Pharm. 32 (2006) 857-863.

CAPÍTULO 4.

Equilibrios de fases en procesos de generación de partículas con fluidos supercríticos

4.1. Importancia de los equilibrios de fases.

En la precipitación de sólidos, de acuerdo con la teoría de nucleación, la monodispersión y la morfología de las partículas obtenidas están directamente relacionadas con el grado de supersaturación así como la velocidad a la que se alcanza éste.

Para lograr el grado de supersaturación definido anteriormente (capítulo 1) en los procesos que emplean fluidos supercríticos como antisolventes, la solubilidad del sólido en el fluido supercrítico tiene que ser baja, a la vez que el disolvente debe ser soluble en el fluido supercrítico.

Por tanto, previo a la aplicación de la técnica con fluidos supercríticos como antisolventes, debe hacerse un estudio termodinámico de los sistemas binarios pertenecientes al sistema total a fin de determinar la viabilidad de este proceso de precipitación.

Además, mediante este estudio se puede adquirir más información. En concreto, sobre el mecanismo de precipitación, que depende directamente de las condiciones a las cuáles la fase líquida y vapor pasan a formar una única fase supercrítica (punto crítico de mezcla).

Asimismo, la morfología de las partículas obtenidas puede variar dependiendo de la aparición de inmiscibilidades líquido-líquido en los sistemas de interés.

En los sistemas estudiados en esta tesis intervienen equilibrios líquido-vapor (disolvente-antisolvente), sólido-vapor (sólido-antisolvente), sólido-líquido (sólido-disolvente) y sólido-líquido-vapor (sólido-disolvente-antisolvente). Sin embargo, no es necesario el estudio de los equilibrios sólido-líquido que

intervienen en los distintos sistemas debido que la presión no ejerce una influencia significativa sobre ellos.

A continuación se describirán las características de los equilibrios de fases estudiados, así como el efecto la importancia del punto crítico de mezcla y de la expansión de volumen

4.2. Equilibrio líquido-vapor (disolv.-antisolvente)

El equilibrio de fases liquido-vapor en los procesos donde el fluido supercrítico actúa como antisolvente, se define como el existente entre el fluido supercrítico y el disolvente. Específicamente existen 6 tipos de equilibrios líquido-vapor, descritos por Van Konynenburg y Scott [1], dependiendo de las inmiscibilidades líquido-líquido que se presentan. Dichas inmiscibilidades no son deseables en los procesos de generación de partículas con fluidos supercríticos, ya que la aparición de fases líquidas adicionales implica una mayor dificultad en la precipitación del sólido, por la existencia de barreras a la transferencia de materia.

La determinación del equilibrio líquido-vapor es fundamental ya que establece la solubilidad del disolvente en el fluido supercrítico así como las condiciones a las que aparece el punto crítico de mezcla (MCP) antisolvente-disolvente.

Este punto se puede definir como la presión a la que (siempre y cuando la temperatura de operación sea mayor que la temperatura crítica del antisolvente) las fases líquida y vapor se transforman en una única fase. En este sentido, las distintas fases a varias temperaturas para sistemas binarios de este

tipo pueden analizarse en la figura 4.1, que representa el diagrama de equilibrio CO_2-etanol [2].

Como puede observarse en la figura 4.1, cuando la temperatura es menor que la temperatura crítica del CO_2 (condiciones subcríticas), la región de coexistencia está compuesta por una fase líquida y por otra fase vapor entre las presiones de saturación de ambos componentes. Fuera de la región de coexistencia, existe únicamente una única fase (líquido o vapor) dependiendo de la fracción molar del CO_2.

Por otro lado, a una temperatura mayor que la temperatura crítica del CO_2 (condiciones supercríticas), no existe presión de saturación del CO_2. Debido a este fenómeno, la curva de líquido desaparece en el llamado punto crítico de mezcla (MCP). Por encima de estas condiciones, existe una única fase líquida a la izquierda (gas-líquido expandido) o una única fase supercrítica a la derecha dependiendo de la fracción molar del CO_2 en la mezcla.

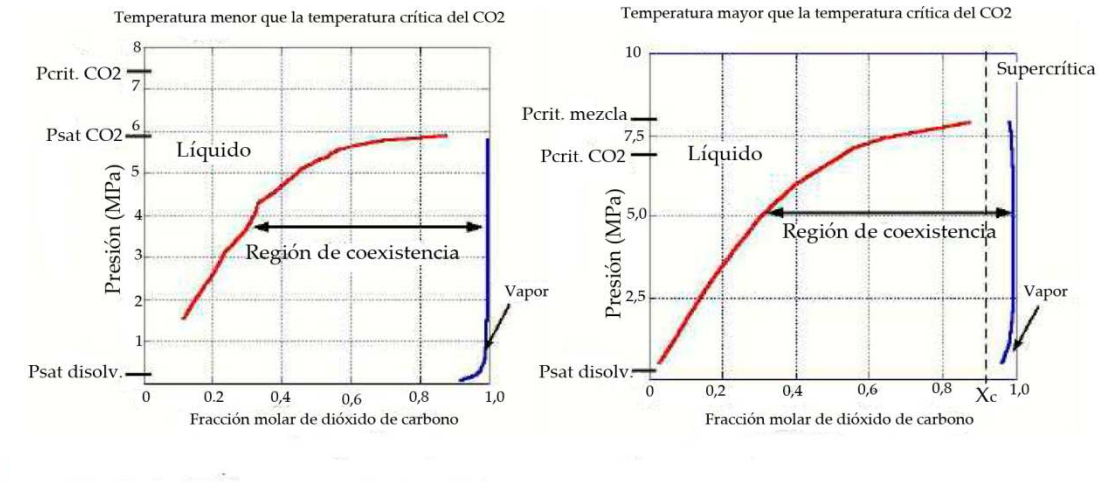

Figura 4.1. Diagramas de equilibrio líquido-vapor CO_2-etanol [2].

Teniendo en cuenta lo descrito, y además que la tensión superficial alcanza un valor nulo en las condiciones del MCP puede deducirse su importancia en este tipo de procesos. Así, el mecanismo de precipitación dependerá directamente de las condiciones experimentales respecto al MCP.

Por debajo del punto crítico de mezcla tiene lugar la formación de gotas debido a la existencia de tensión superficial. A continuación se produce la transferencia de materia y de energía entre la gota y el fluido supercrítico que la rodea. Se consigue entonces un efecto antisolvente, y el sólido precipita.

Por encima del punto crítico de mezcla, al ser nulo el valor de la tensión superficial no se produce la formación de gotas porque no existe interfase. A estas condiciones se produce la formación de una "pluma" y el mecanismo de transferencia de materia es diferente.

Trabajos recientes indican que en condiciones por encima del punto crítico de mezcla la interfase no desaparece instantáneamente, sino que su valor decrece progresivamente hasta su total desaparición [3-4]. Esta velocidad de desaparición de la tensión superficial varía dependiendo si las condiciones son ligeramente por encima o muy encima del MCP. A condiciones ligeramente superiores la interfase desaparece a una velocidad más lenta que a condiciones muy por encima del punto crítico de mezcla.

De los anteriores párrafos se puede concluir que existen tres importantes condiciones experimentales con respecto al MCP: Condiciones inferiores, ligeramente encima y muy encima del MCP.

Por tanto, basándose en lo anteriormente descrito, la determinación del MCP debe obtenerse previamente a la utilización de esta técnica, que emplea fluidos supercríticos como antisolventes, ya que estas condiciones determinarán el mecanismo de precipitación.

4.2.1. Determinación del punto crítico de mezcla.

El punto crítico de mezcla puede determinarse de dos maneras diferentes, experimental de manera visual y teóricamente mediante el diagrama de fases.

• Experimentalmente: Este proceso requiere la utilización de una celda de equilibrio visual (una celda con ventana) que permita observar la evolución de las distintas fases. En este caso, el MCP se observa cuando una fase líquida y otra fase vapor dan lugar a en una única fase, supercrítica.

• Teóricamente: Mediante una ecuación de estado para describir el equilibrio líquido-vapor del sistema estudiado a la temperatura objetivo. El MCP puede ser observado sobre el diagrama de equilibrio líquido-vapor obtenido (ver figura 4.1).

4.3. Equilibrio sólido-vapor (soluto-antisolvente)

Como se describió en la sección 4.1, otro de los factores fundamentales para conseguir la precipitación del sólido en estos procesos, es la solubilidad de este sólido en el fluido supercrítico. Este hecho justifica la importancia de estudiar el equilibrio sólido-vapor (soluto-fluido supercrítico) mediante los correspondientes diagramas de fases.

El diagrama de fases de una mezcla binaria altamente asimétrica (típico sistema binario entre CO_2 y un sólido) se muestra en la figura 4.2. Esta mezcla está caracterizada por la existencia de una gran diferencia entre el tamaño molecular y estructura de los dos componentes. El sólido suele estar en exceso en la mezcla, y además la baja solubilidad de este sólido resulta en una reducción del punto de fusión del sólido [5].

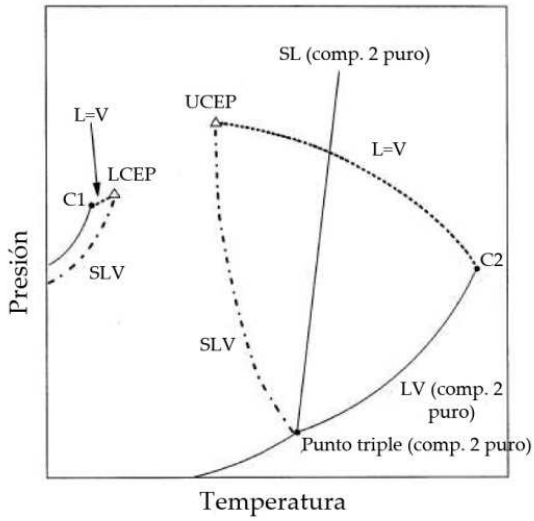

Figura 4.2. Diagrama de fases de una mezcla binaria asimétrica [5]

En la figura 4.2 se pueden identificar las temperaturas conocidas como UCEP (*"upper critical end point"* o punto crítico final superior) y LCEP (*"lower critical end point"* o punto crítico final inferior). Entre estos dos puntos sólo existe equilibrio sólido-fluido supercrítico porque el UCEP y LCEP representan las temperaturas a las cuáles la curva sólido-líquido-fluido supercrítico corta a la curva líquido-vapor del compuesto correspondiente.

En el UCEP se cortan la curva del equilibrio líquido-vapor del compuesto más pesado con la curva sólido-líquido-vapor procedente de la fusión de ese mismo sólido a presiones elevadas (*"melting point depresión"*)

Mientras, en el LCEP se cortan las curvas del equilibrio líquido-vapor del fluido supercrítico con la curva del equilibrio sólido-líquido-vapor debido a la presencia del sólido en exceso.

Como consecuencia de esta fusión de fases, a esas temperaturas se produce un aumento brusco de la solubilidad del sólido en el fluido supercrítico (en mayor medida en el UCEP). Este hecho es importante para extracciones supercríticas, ya que esas condiciones pueden resultar las óptimas para operar en ese proceso.

Esta temperatura se determina comúnmente de manera experimental mediante el estudio de la solubilidad del sólido en el fluido supercrítico en función de la temperatura y la presión. Así, el UCEP sería la temperatura a la cuál se produce un aumento elevado de solubilidad. Este hecho se puede observar en la figura 4.3 [6], que representa la solubilidad del naftaleno en CO_2sc (el UCEP estaría situado en torno a 60 °C).

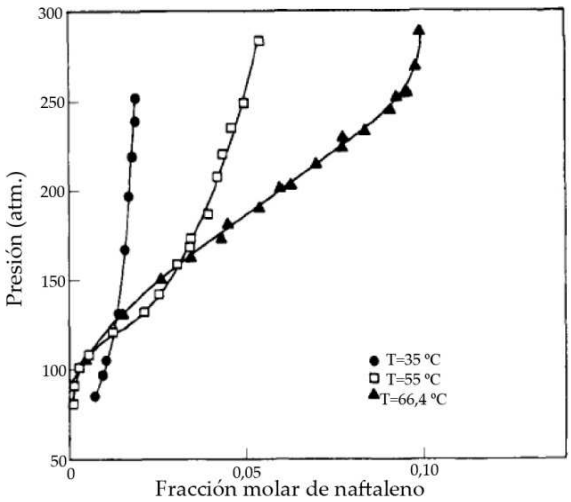

Figura 4.3. Solubilidad de naftaleno en CO_2sc [6].

La reducción del punto de fusión del sólido a alta presión es otro aspecto a tratar en este tipo de sistemas binarios compuestos por sólidos con alejados puntos triples. Esta aparición de una fase líquida a temperaturas menores puede afectar la viabilidad de diferentes procesos con fluidos supercríticos.

La reducción del punto de fusión del sólido se puede observar nuevamente en el diagrama de la figura 4.2, en el cuál la línea sólido-líquido-vapor cae a temperaturas más bajas que la curva de coexistencia sólido-líquido o el punto de fusión del sólido puro. Eso indica que el sólido funde a temperaturas más bajas en presencia de un fluido supercrítico, pudiendo ser afectada la composición de la fase vapor [5].

4.4. Equilibrio soluto-disolvente-antisolvente

En las secciones anteriores se ha justificado la importancia del equilibrio líquido-vapor para determinar las condiciones del punto crítico de mezcla. Estas condiciones diferencian los distintos mecanismos de precipitación en las técnicas que usan fluidos supercríticos como antisolventes.

Sin embargo, la presencia del sólido (incluso en baja composición) puede producir la modificación de ese punto crítico de mezcla. De hecho, en algunos casos, como consecuencia de la adición de sólido un diagrama de equilibrio líquido-vapor de tipo I puede transformarse a otro tipo, presentándose inmiscibilidades las cuáles no existirían en el equilibrio líquido-vapor sin sólido [7].

Esta aparición de inmiscibilidades en un sistema ternario pueden observarse visualmente mediante el uso de una celda de equilibrio, o teóricamente por medio de una ecuación de estado para determinar el diagrama de equilibrio de este sistema multicomponente.

Además, el equilibrio soluto-disolvente-antisolvente puede proporcionar información muy importante relativa a las condiciones a las cuáles la solubilidad del sólido en el sistema ternario es la mínima. Por tanto, este equilibrio indica las condiciones a las que se alcanza el máximo grado de supersaturación en el sistema.

Para la estimación de un equilibrio sólido-líquido-vapor de un sistema ternario con una ecuación de estado cúbica (en este caso Peng-Robinson [8] porque es la ecuación más empleada en estos casos), se necesita disponer previamente de datos de equilibrio de los sistemas binarios individuales. Con estos datos de equilibrio se calcularán los distintos coeficientes de interacción

de los sistemas binarios individuales, los cuáles son necesarios para la descripción del diagrama de un sistema ternario a las condiciones investigadas de presión y temperatura.

4.5. Expansión de volumen.

Como se explicaba en el capítulo 1 (artículo 1), la expansión de volumen es el parámetro fundamental que condiciona la precipitación de un sólido con la técnica discontinua GAS. En este proceso, cabe recordar que el CO_2 se añade a la disolución con el sólido. Como consecuencia de esta adición se producía una expansión de volumen del disolvente. Esta expansión es el parámetro clave para lograr la precipitación porque se reduce la densidad del disolvente y el sólido precipita.

Por tanto, en este tipo de proceso discontinuo se buscan las condiciones a las cuáles este volumen de expansión sea el máximo posible, ya que un elevado grado de supersaturación se alcanzaría a estas condiciones.

Debido a la importancia de este parámetro, diversos estudios han sido dedicados a la definición de ecuaciones de cálculo para distintas expansiones de volumen.

Primeramente se definió la expansión de volumen total. Sin embargo, este parámetro presentaba siempre los mismos valores independientemente del disolvente (figura 4.4.), por lo que no era apto para realizar un buen *"screening"* del disolvente [9].

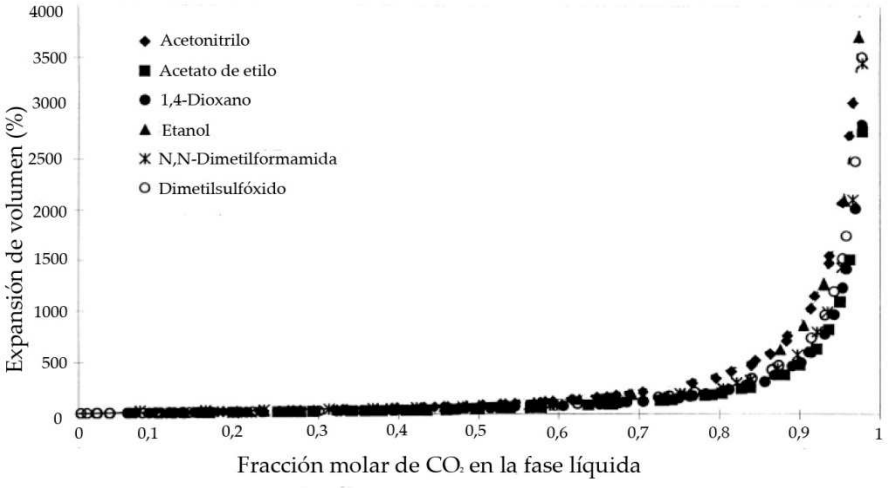

Figura 4.4. Expansión de volumen de la fase líquida para varios sistemas CO_2-disolventes [9].

Se modificó entonces la expansión de volumen total mediante la definición de la expansión relativa del volumen molar (figura 4.5). Para este parámetro, el grado de supersaturación máximo se obtiene a las condiciones a las cuáles la expansión relativa del volumen molar es la mínima. En este caso, este mínimo difiere para cada sistema, por lo que esta expansión de volumen posibilita la elección del disolvente más adecuado [9-10].

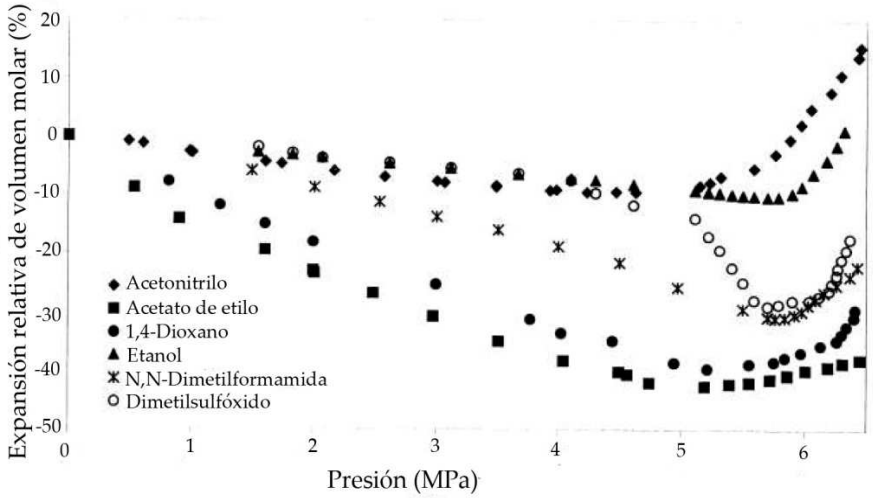

Figura 4.5. Expansión relativa del volumen molar para varios sistemas CO_2-disolvente[9].

4.6. Resultados y discusión.

En el artículo a continuación se procede a la precipitación de acetaminofén y tretinoína mediante la técnica SEDS usando CO_2sc y etanol como antisolvente y disolvente respectivamente, así como el efecto de la presión, temperatura y concentración en este proceso.

Con el fin de determinar las condiciones a las cuáles se alcanza el máximo grado de supersaturación, la aparición de inmiscibilidades se realiza un estudio de los equilibrios de fase de los sistemas binarios y ternarios con la ecuación de estado de Peng-Robinson. Los diagramas ternarios obtenidos demuestran que el máximo grado de supersaturación alcanzado coincide con el punto crítico de mezcla del equilibrio líquido-vapor fluido supercrítico-antisolvente. Los diagramas ternarios prueban también la no aparición de inmiscibilidades y el efecto antisolvente del CO_2sc a las condiciones experimentales investigadas. Esos resultados fueron confirmados mediante el uso de una celda de equilibrio visual.

Las diferentes distribuciones de tamaño de partícula obtenidas con la técnica SEDS fueron explicadas teniendo en cuenta la posición de las condiciones experimentales con respecto al punto crítico de mezcla. El mejor resultado obtenido, partículas esféricas de tamaño 0,5-0,75 micras sin agregados, fue obtenido a unas condiciones ligeramente por encima del punto crítico de mezcla del sistema antisolvente-disolvente.

ARTÍCULO

Precipitation of tretinoin and acetaminophen with solution enhanced dispersion by supercritical fluids (SEDS). Role of phase equilibria to optimize particle diameter.

Powder technology 217 (2012) 177-188.

Powder Technology 217 (2012) 177–188

Contents lists available at SciVerse ScienceDirect

Powder Technology

journal homepage: www.elsevier.com/locate/powtec

Precipitation of tretinoin and acetaminophen with solution enhanced dispersion by supercritical fluids (SEDS). Role of phase equilibria to optimize particle diameter

Antonio Tabernero, Eva M. Martín del Valle *, Miguel A. Galán

Department of Chemical Engineering, University of Salamanca, P/Los Caídos S/N, 37008, Spain

ARTICLE INFO

Article history:
Received 27 May 2011
Received in revised form 6 October 2011
Accepted 15 October 2011
Available online 21 October 2011

Keywords:
SEDS
Acetaminophen
Tretinoin
Phase equilibria

ABSTRACT

Precipitation of acetaminophen and tretinoin is performed using supercritical enhanced dispersion by supercritical fluids (SEDS), using carbon dioxide and ethanol as antisolvent and solvent respectively. In order to assure the no existence of immiscibilities and to determine the conditions at which the maximum attainable supersaturation is produced, it is performed a phase equilibria study of the ternary and binary systems with Peng–Robinson equation of state. The ternary equilibrium diagrams show that the maximum supersaturation matches with the mixture critical point given by the vapor–liquid diagram and also show information about the cosolvent effect of both antisolvent and solvent, proving in addition the no existence of immiscibilities at all the investigated conditions. These results are confirmed using a windowed cell. The effect of pressure, temperature and solution concentration in the precipitation process is discussed. The different particle diameters of the precipitated particles are explained with the aid of the phase equilibria diagrams, taking into account the position of experimental conditions with respect to the mixture critical point. The best results for both solids, spherical microparticles without aggregates and with a size around 0.5–0.75 μm, are obtained just above the mixture critical point of the mixture antisolvent–solvent.

© 2011 Elsevier B.V. All rights reserved.

1. Introduction

Very small drug particles have attracted interest in current drug delivery technology since they can travel faster to the targeted organ and distribute in a more evenly way in the body. Depending on the type of delivery routes, controlling the size scale of drugs is a key step. Particles should be around 0.1–0.3 μm for intravenous delivery, 1–5 μm for inhalation delivery and 0.1–100 μm for oral delivery [1].

Conventional methods like milling, spray drying, recrystallization, or emulsion techniques do not provide crystalline particles with a suitable particle size distribution (PSD). Furthermore, they can degrade the drug or even toxic solvent traces can be obtained in the outcome [2].

The use of supercritical fluids (SCFs) as antisolvents has been proposed in order to overcome these drawbacks. Processes such as gas antisolvent (GAS), supercritical antisolvent (SAS) or solution enhanced dispersion by supercritical fluids (SEDS) have been successfully used to obtain pharmaceuticals and different nanomaterials [3–5]. In these antisolvent processes, the SCF must be miscible with the solvent, but the solute must be sparingly soluble in the SCF. The addition of SCFs reduces the solvent power of the solvent, thus achieving a great and fast supersaturation, which according to the nucleation theory is the most important requirement to obtain small particles with a suitable PSD [6]. Several reviews discuss these precipitation processes, explaining their advantages or disadvantages [3–5, 7, 8].

One of these processes (developed by Hanna and York [9]) is known as solution enhanced dispersion by supercritical fluids (SEDS). This semicontinous process is similar to SAS process, which consists in spraying a solution into condensed gas in a pressurized vessel. However, the nozzle design of both processes is different. SEDS nozzle presents a coaxial design with a mixing length, in order to enhance the mass transfer and get a simultaneous delivery of the solution and the antisolvent [9].

In this process, it is important to take into account different experimental and theoretical aspects, such as phase equilibria, nucleation kinetics, hydrodynamics or mass transfer [10, 11].

It is crucial to study the phase behavior of the solid–solvent–antisolvent system in order to determine the conditions at which this mixture is whether in one single phase (supercritical phase) or in a binary liquid–vapor region. In this context, the mixture critical point (MCP) can be defined as the pressure and temperature conditions at which the liquid–vapor mixture merges in one single supercritical phase [12, 13].

The location of the MCP has a big influence in processes in which a solution is sprayed into a supercritical atmosphere. Above the MCP, the surface tension reaches a zero value. As a consequence, there is no

* Corresponding author. Tel.: +34 923 294479; fax: +34 923 294579.
E-mail address: emvalle@usal.es (E.M. Martín del Valle).

0032-5910/$ – see front matter © 2011 Elsevier B.V. All rights reserved.
doi:10.1016/j.powtec.2011.10.025

droplet formation and only one supercritical phase exists after the jet breakup. In this case, the nucleation is similar to a gas-to-particle nucleation [10].

On the other hand, under the MCP, there is droplet formation because the surface tension does not reach a null value, and consequently there is a multiphase mixing after the jet breakup.

Therefore, the knowledge of the phase behavior is very important in order to understand the subsequent precipitation mechanism, in which phemomena such as jet breakup, mass transfer, and nucleation kinetics are involved [14–16].

Usually, the equilibria studies only deal with the equilibrium of the antisolvent–solvent system, assuming that the MCP of this binary system matches with the MCP of the ternary system, and without taking into account the role of the solute. As a matter of fact, several studies have shown that the role of the solute might be neglected, supposing that the solid precipitates whatever the composition is [15, 16].

This last approach does not consider the possibility of a cosolvent effect of the SCF, or the appearance of immiscibilities in the ternary systems when a solid is introduced in the multicomponent system.

In fact, several authors suggest [14, 16] conducting fundamental phase behavior studies considering all three components, as some solutes may significantly change the shape of the P-xy phase envelopes. For instance, De Gioannis et al. [14] studied the solubility of griseofulvin in CO_2-acetone and CO_2-ethanol mixtures, showing that the solubility of the solid always decreases in the system with acetone. Nevertheless, the solubility of griseofulvin in CO_2-ethanol mixtures is higher than its solubility in the pure solvents, and therefore the CO_2 acts as a cosolvent. This last phenomenon has been observed in other systems [13]. Another study shows that CO_2 acts as a cosolvent at low CO_2 concentrations in CO_2-1-propanol-salicylic acid systems. However, if its concentration is increased, CO_2 provides an antisolvent effect [17].

Alternatively, Weber et al. [18] explained the appearance of an immiscibility region at certain conditions in the CO_2-ethanol-acetaminophen system. However, immiscibilities may also be caused due to the melting point depression [19], as can occur with polymeric systems [20].

These evidences may explain why unsuccessful precipitations have been occasionally reported [21], highlighting that the ternary equilibrium should be determined previously. Indeed several studies have been done in order to explain the different particle characteristics depending on whether the different experiments were performed above or under the MCP [10, 22, 23].

In general, spherical nanoparticles can be obtained operating at conditions far above the MCP [10]. Alternatively, under the MCP hollow particles or spherical microparticles with aggregates are produced depending on the mass transfer and nucleation mechanisms [10].

Different results can be found in the literature regarding the PSD. The best result can be obtained above [24, 25], near the MCP (above or under) [16, 23, 26, 27], or even at conditions near the critical point of the SCF [28].

Nevertheless, these studies have been performed mainly with a SAS process, whereas only a few studies have been carried out with a SEDS process [12, 29]. Indeed it is possible to find in the literature investigations in which a phase equilibria study is performed together with a precipitation process using SEDS. However, these studies usually focus on the effect of a single parameter (such as pressure, temperature, antisolvent flow, solvent flow, concentration …) on the particles characteristics. They do not specifically focus on establishing a relation between the location of the MCP and the particle diameter of the particles since several parameters usually change simultaneously.

The aim of our investigation is to determine what role the phase equilibria is playing during the precipitation of tretinoin and acetaminophen from ethanol solutions, using supercritical CO_2 as antisolvent in a SEDS process. The phase equilibria of the respective ternary systems have been depicted using the Peng Robinson equation of state (PR-EOS). This study provides information about the existence of immiscibilities, the location of the MCP, and the cosolvent effect of both solvent and antisolvent. The position of the MCP and the existence of immiscibilities are confirmed by means of a study with a windowed cell.

The relation between the particle diameter of the precipitated solids and the location of the operating conditions (above or under the MCP) were studied performing a thermodynamic interpretation, taking the phase equilibria diagrams as a reference.

Acetaminophen is a drug which has already been precipitated by Wubbolts et al. [30] using CO_2 as an antisolvent (SAS process) and ethanol as a solvent. However, this compound was only processed at conditions under the MCP (6.2 MPa and 298 K), obtaining elongated crystals with a PSD of about 200 μm [30]. Recently, this drug was precipitated again from acetone solutions using SAS, although this was only at certain conditions (11.0 MPa and 308 K) [31]. In this case, elongated particles were produced with connected elements on the particle surface [31].

Tretinoin or retinoic acid (RA) is the acid form of vitamin A and has beneficial properties to treat several illnesses or even cancer. Although several vitamin A-derivatives (lycopene [27], lutein [16], beta-carotene [32] or astaxanthina [33]) have already been obtained using SCFs as antisolvents, RA has not been precipitated yet.

Specifically, lycopene was obtained in the form of needle-like particles with a length between 80 and 5 μm [27]. The same morphology was obtained with the precipitation of lutein (with a length between 5 and 150 μm) [16]. Beta-carotene was also processed with SEDS, obtaining different morphologies (plate-like or leaf-like) and PSDs (between 3 and 100 μm) [32]. Finally, nubbly particles of astaxanthin between 0.5 and 6 μm were obtained when this solid was precipitated with SEDS [32].

2. Experimental section

2.1. Materials

Acetaminophen with a purity of 99.0% was purchased from Sigma-Aldrich, whereas tretinoin with a richness of 100.8% was supplied by Fagron Ibérica. Ethanol (purity of 99.9%) was obtained from BDH Prolabo. Carbon dioxide at 99.5% was purchased from Air Liquide.

2.2. Precipitation apparatus and procedure

A schematic diagram of the experimental apparatus for precipitating the solutes is shown in Fig. 1. This apparatus consists of a jacketed cylindrical vessel (500 mL) where the precipitation takes place. An air operated gas booster (SPRAGUE products, model PowerStar4B S080P4BS080) with a maximum outlet pressure of 8000 psi is used to feed CO_2 to the precipitation vessel. A diaphragm pump (SERA, model RK411.1 with a nominal capacity of 0–12 l/h at 50 Hz) is employed to pump the organic solution. The pressure inside the vessel is controlled by means of a back pressure regulator (TESCOM model 26–1700).

There are different heating systems employed for heating the CO_2 and the organic solution, as well as for keeping the temperature inside the vessel and nozzle constant. All these parameters are controlled and modified using a control box (RFL Electricite tableautier).

The experiment starts by adding CO_2 to the vessel, and subsequently heating the vessel and CO_2 line. The pressure is controlled with the back pressure regulator, whereas the temperature inside the nozzle, vessel, and heating tubes is controlled with the control box. When the targeted temperature and pressure are reached, the solution is pumped through the nozzle where it is mixed with the CO_2. The solution is pumped through the inside tube, whereas the CO_2 is pumped through the outside tube. Finally, the mixture is

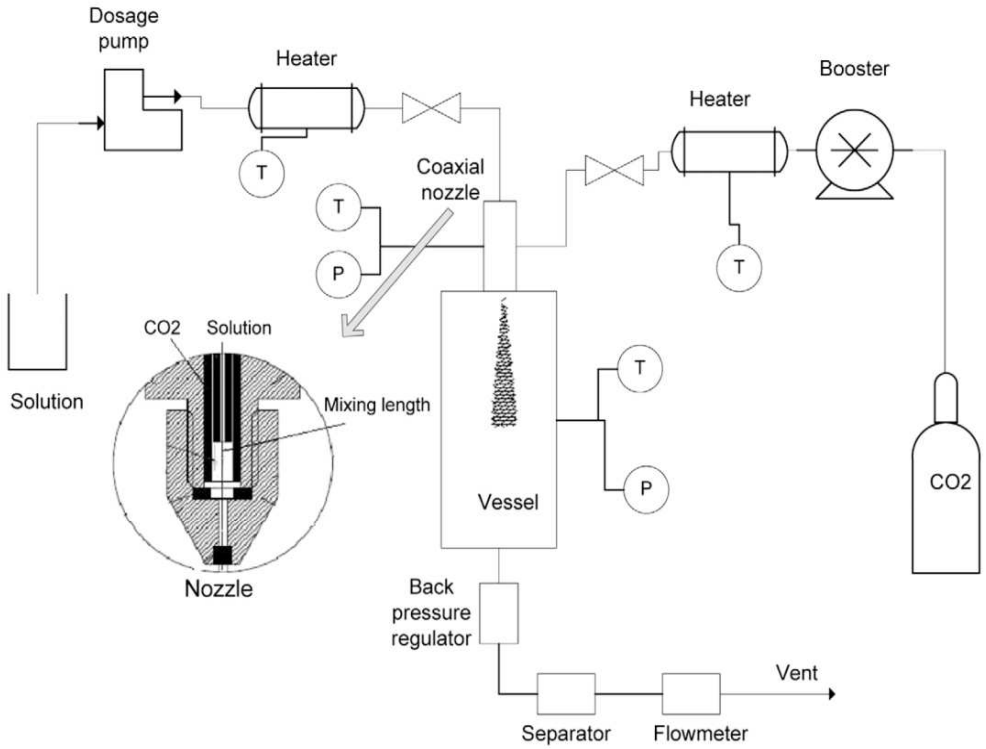

Fig. 1. Schematics of the SEDS plant.

sprayed inside the pressurized vessel through the nozzle. The experiment ends when the solution is completely pumped, maintaining a stream of CO_2 in order to drag the particles that have been precipitated on the walls of the vessel.

The antisolvent flow is measured with a mass flow meter (BRONKHORST, model F113AC with a nominal range of 0.6–30 kg/h), which is positioned after a vessel to separate the mixture antisolvent–solvent. On the other hand, the dissolution flow can be modified by varying the dosage pump's frecuency.

The particles are collected in a 0.1 μm isopore membrane polycarbonate filter (MILLIPORE, model VCTP02500) that is placed at the end of the vessel.

2.3. Windowed cell

The visual estimation of the MCP is performed in a windowed cell (Fig. 2). The main component is an optic cell (SITEC) with a variable volume between 8 and 17 ml, which is controlled by a displaceable

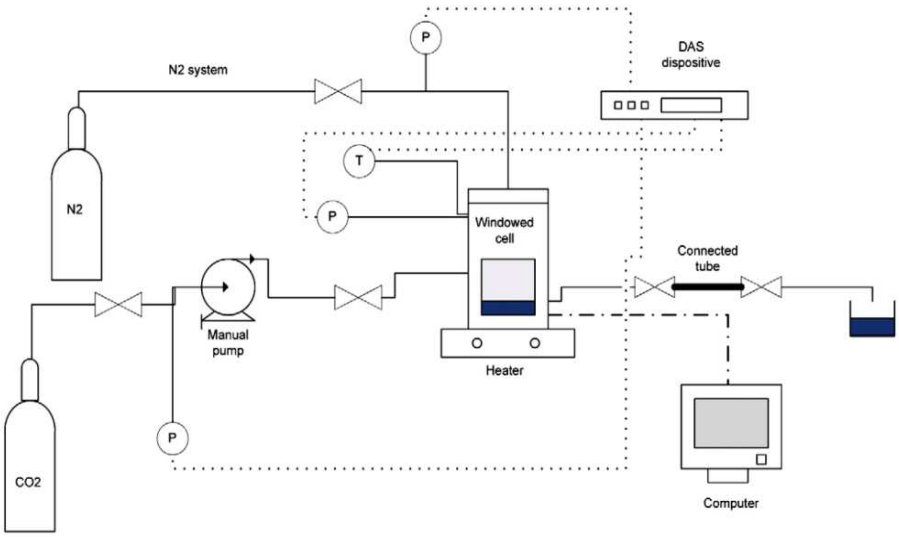

Fig. 2. Schematic of the windowed plant.

piston. This displacement (and consequently the cell volume) is manipulated by means of a N_2 system. The sc-CO_2 is obtained with a manual pressure generator (SITEC 750.1030). A heater jacket and a magnetic stirrer (Velp Scientific) are connected to the cell to heat and shake the dissolution inside. The temperature is controlled with a controller (SITEC 772.5011). The pressure inside the cell, in the manual pressure generator, and in the N_2 section is also controlled with the controller (SITEC 14 TPR/HP). The position of the piston (which defines the cell volume depending on the pressure of the N_2 section) is controlled by a height controller (SITEC 772.9002). It is possible to follow the process inside the optic cell by means of a camera (SANTEC). The controllers and camera are connected to a DAS-8000 dispositive. This dispositive is connected to a computer where it is possible to track every parameter during the experiment.

The experiment begins by adding a known amount of a solution containing a certain drug in the cell. Afterwards, the optic cell is given pressure by injecting CO_2 through the pressure generator. If the pressure is not enough, it is possible to manipulate the piston with the N_2 section, reducing the cell volume and consequently increasing the pressure. Then, the cell is slowly heated until the desirable conditions are achieved. During the heating process, the phenomena occurring inside the cell are observable with the camera. The MCP will be observed on the computer when a single supercritical phase fills the cell.

This device is also employed to experimentally determine the amount of precipitated solid at certain conditions in a batch process. Once the equilibrium is reached, a liquid sample is collected using a tube that is connected to the cell, until all the liquid with the remaining solubilized solid is recovered. In this context, it is necessary to collect the sample carefully to minimize the pressure drop, avoiding at the same time the particles' redissolution. Subsequently, the solubilized solid in the sample is determined by UV/vis.

The next step is to depressurize the cell and recover the precipitated solid (which is stuck and strongly agglomerated on the walls or at the bottom of the optic cell) by means of adding the adequate dissolvent repeatedly.

The previous fact (it is necessary to add solvent to recover the particles at the bottom of the cell) prevents collecting the particles in a suitable way. Therefore, no attempts have been made in order to recover the particles. This equipment is only used to determine the MCP and the conditions at which the precipitation yield is near its maximum.

Finally, the lines are cleaned passing a stream of fresh CO_2 during 10 min. The experiments are performed three times to obtain an averaged outcome.

2.4. Scanning electron microscope (SEM) and particle distribution analysis

Pictures of the particles on the filter are taken using a scanning electron microscope (SEM), model ZEISS DSM 940, equipped with a microanalysis system EDX (Z II of Tracor Northern).

The particle size distribution is analyzed using imageJ (image programming and analysis in Java) [34]. The program counts the pixels that make up a particle after increasing the image contrast between the background and the particles. The major and minor axis lengths for the particle are adjusted based on a distance calibration performed by the user before the image analysis.

In order to count more particles and assure that the particle distribution is homogeneous along the whole filter, this process is performed two times with three different images of different regions of the filter

On the images, black holes with a diameter of 0.1 μm can be observed. These holes correspond to the filter.

2.5. X-ray diffractometry (XRD) analysis

Powder X-ray diffraction measurements were performed on a Bruker D8 Advance difractometer with Cu Kα radiation generated at 30 mA and 40 kV. Acetaminophen samples were measured in 2θ range from 10° to 60° with a step size of 0.04° and a step time of 3.0 s. On the other hand, RA samples were measured in 2θ range from 2° to 30° with a step size of 0.025° and a step time of 3.0 s.

3. Phase equilibrium model

In order to get a better understanding of the precipitation process, phase equilibria of the ternary systems CO_2-ethanol-acetaminophen and CO_2-ethanol-RA should be determined. By describing these systems with an equation of state (EOS), it is possible to know the cosolvent effect for both the solvent and antisolvent, as well as if the system presents immiscibilities at certain conditions [18].

To do this, the Peng–Robinson equation of state (PR-EOS) (Eq. (1)) [35] was used to depict these diagrams following an isofugacity approach.

$$P = \frac{RT}{v-b} - \frac{a(T)}{v^2 + 2bv - b^2} \tag{1}$$

In Eq. (1), v is the molar volume, R the gas constant and P and T the pressure and temperature of the system respectively. For a pure component, the attractive parameter a and the repulsive term b are defined in function of its critical properties T_C and P_C:

$$a = 0.45724\frac{R^2T_C^2}{P_C^2}\alpha(T_R) \tag{2}$$

$$b = 0.07780\frac{RT_C}{P_C} \tag{3}$$

The temperature dependency for the attractive parameter a is treated with a corrector term α (Eq. (4)), in which the acentric factor w takes into account the no sphericity of the molecule:

$$\alpha(T_R) = \left[1 + \left(0.374 + 1.542w + -0.269w^2\right)\left(1-T_R\right)^{0.5}\right]^2 \tag{4}$$

In multicomponent systems, it is necessary to use a mixing rule to consider the interactions between the different components. In this study, Van der Waals mixing rules with one single interaction parameter k_{ij} are used (considering l_{ij} as a null value). This parameter should be determined for each binary system:

$$a_m = \sum_i \sum_j x_i x_j \sqrt{a_i a_j}\left(1-k_{ij}\right) \tag{5}$$

$$b_m = \sum_i \sum_j x_i x_j \left(\frac{b_i + b_j}{2}\right)\left(1-l_{ij}\right) \tag{6}$$

In Eqs. (5) and (6) a_i, a_j, b_i, b_j are the pure component parameters, x_i and x_j are the mole fraction, and k_{ij} is the binary interaction parameter.

PR-EOS is not able to reproduce the solid behavior. Therefore, the fugacity coefficient is calculated from the fugacity coefficient of the solid in a sub-cooled state, which is corrected by means of a simplified Clapeyron-type approach (Eq. (7)) [36].

$$Ln\varphi_3^S = Ln\varphi_3^L + \frac{\Delta H_{tp}}{R}\left(\frac{1}{T_{tp}} - \frac{1}{T}\right) \tag{7}$$

In Eq. (7) $\varphi_3^S$and φ_3^L are the fugacity coefficient of the solid and the fugacity coefficient of the solid in a sub-cooled liquid state respectively.

Table 1
Objective functions used in this work.

Parameter	Equilibrium type	Objective function
k_{12}	VLE antisolvent–solvent	$\sum_{i=1}^{N} 1 \Big/ N \cdot \left(x_{expi} - x_{calci}\right)^2 + \left(y_{expi} - y_{calci}\right)^2$
k_{13}	SVE antisolvent–solute	$\sum_{i=1}^{N} 1 \Big/ N \cdot \left(y_{expi} - y_{calci}\right)^2$

The T_{tp} is the triple point temperature and ΔH_{tp} is the fusion enthalpy in the triple point. Accepting a small deviation, T_{tp} and ΔH_{tp} can be replaced by the normal melting temperature T_M and heat of fusion ΔH_M.

It is required to determine the k_{ij} for each binary system if a ternary system is modeled with PR-EOS. These parameters are obtained by minimizing an objective function and can be considered temperature independent because according to other works, their variation with temperature is minimal [37, 38].

Table 1 shows the respective objective functions to calculate the interaction parameters for the vapor–liquid equilibrium (VLE) and the solid–vapor equilibrium (SVE). Subscripts 1, 2 and 3 denote respectively the antisolvent (CO_2), the solvent, and the solid. The liquid molar fraction is x and y is the vapor molar fraction.

The parameter k_{23} corresponds to the solid–liquid equilibrium. However, this parameter is not calculated and can be neglected given that at high pressure the main interactions come from solute–antisolvent and solvent–antisolvent equilibria [39]. More information about how to describe different ternary multiphasic systems with cubic EOS can be found elsewhere [17, 40–42].

4. Results

4.1. Phase equilibrium model

The properties of the different compounds are required if it is desired to depict the equilibrium diagram of a ternary system.

Table 2 shows the critical parameters and the acentric factors for each component, as well as the triple point temperature and the fusion enthalpy for each solid.

The properties of the CO_2, ethanol, and acetaminophen are well-known [18], whereas the properties of the RA are determined with the group contribution method of Lydersen modified by Joback [43]. This is except for the fusion enthalpy of the RA, which is taken as the value of the same property of the beta-carotene (a compound with a similar molecular structure) [27].

Secondly, the interaction binary parameters k_{ij} should be calculated. The parameter from the CO_2-ethanol system is correlated from experimental VLE data [44], whereas the parameter from the CO_2-acetaminophen system is correlated from experimental SVE data [45]. The parameter for the CO_2-RA system is taken as 0.400, given that there is no experimental solubility data in literature for this compound. This value is obtained by fitting experimental solubility data of different terpenoids (e.g. cholesterol and its esters) in CO_2 with PR-EOS and using Van der Waals mixing rules with one single parameter [37]. Table 3 summarizes these results.

Table 2
Properties of the components.

Property	CO_2	Ethanol	Acetaminophen	RA
MW	44.01	46.07	151.16	284
Tc (K)	304	514	766	977
Pc (bar)	73.83	61.37	41.8	15.70
W	0.225	0.644	0.729	0.648
Ttp (K)	–	–	443	460
ΔH_{fus} (J/mol)	–	–	27,100	27,500

Table 3
Binary interaction parameters k_{ij}.

	Ethanol	RA	Acetaminophen
CO_2	0.080 refitted from [44]	0.400 refitted from [37]	0.221 refitted from [45]

Knowing these parameters, it is possible to depict the different equilibrium diagrams. Fig. 3 describes the CO_2-ethanol VLE for 313 and 318 K. These temperatures are chosen because they are higher than the CO_2 critical temperature. It is also important to take into account that higher temperatures could degrade a biodegradable polymer (thinking in a posterior microencapsulation), as happens with poly-ethylene glycol [20]. The MCP for both temperatures can be also determined on this diagram. Specifically, the MCP is located close to 75 bar at 313 K, and close to 80 bar at 318 K.

Figs. 4 and 5 describe the evolution of the solubility of the acetaminophen and RA in their respective ternary systems. In this context, the evolution of the molar fraction of acetaminophen was already calculated in a previous article using the sublimation pressure of acetaminophen [46].

For both systems, there are not bumps in the diagrams at the investigated conditions. This fact points out that the presence of the solute does not produce the appearance of immiscibilities [18].

It can be observed how the solubility of the solid decreases with pressure until a minimum is achieved. The maximum attainable supersaturation will be achieved at this point. The MCP of the antisolvent–solvent equilibrium is located at these conditions and therefore matches with the conditions at which the maximum supersaturation for the ternary system is reached. After the minimum, there is a little increase in the solubility as a consequence of the transition from a biphasic phase to a single supercritical phase. This phenomenon can be found in other systems [16].

Furthermore, the fact that the solubility decreases significantly with pressure until the MCP points out that there is not a cosolvent effect of the CO_2 as occurs with other systems [14], highlighting that the CO_2 acts as an antisolvent.

However, it is important to notice that in the CO_2-ethanol-acetaminophen system, a cosolvent effect is produced due to the ethanol given that the solubility of acetaminophen in CO_2 is around 10^{-5}, whereas in the ternary system this value increases up to 10^{-2}. Nevertheless, at the vicinities of the MCP this solubility becomes again around 10^{-5}.

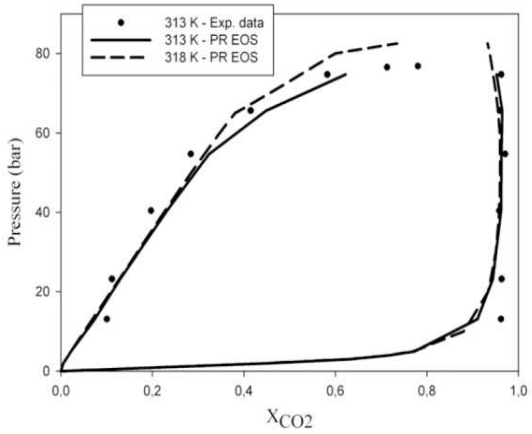

Fig. 3. VLE CO_2-ethanol.
Experimental data from [44]).

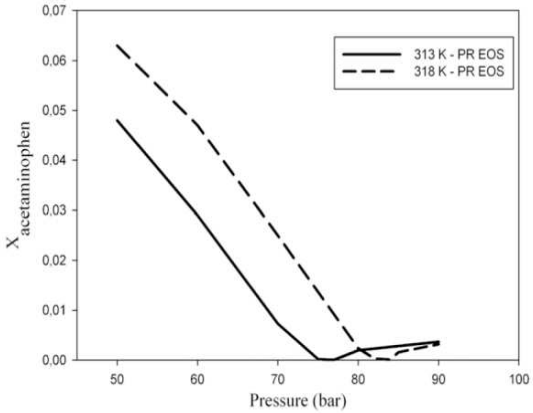

Fig. 4. Evolution of the acetaminophen molar fraction as function of pressure in the system CO_2-ethanol-acetaminophen.

The temperature effect in the solubility can be also observed in the equilibria diagrams (Figs. 4 and 5). If the pressure remains constant, the molar fraction increases with the temperature. This occurs because the CO_2 becomes less soluble in ethanol when temperature increases, as can be seen in the VLE diagram (Fig. 3).

Since the process of the windowed cell is a batch process, it is important to take into account the relative molar volume expansion of the ethanol when CO_2 is added [40, 47, 48]. This parameter (Eq. (8)) can be calculated by means of PR-EOS.

$$\frac{\Delta v}{v} = \frac{v_L(T,P,x_1)}{v_2(T,P_0)} - 1 \tag{8}$$

This last expression was defined by several authors replacing the conventional definition of the relative total volume expansion. This definition was considered inadequate because for a given antisolvent, the relative total volume expansion does not distinguish the behavior of different solvents [40, 47, 48].

The relative molar volume expansion plays the most important role in a batch process because the maximum attainable supersaturation is achieved when its value is at its minimum [48].

Fig. 6 depicts the relative molar volume expansion of ethanol in CO_2 as a function of pressure. At both temperatures, the molar volume expansion decreases with increasing pressure.

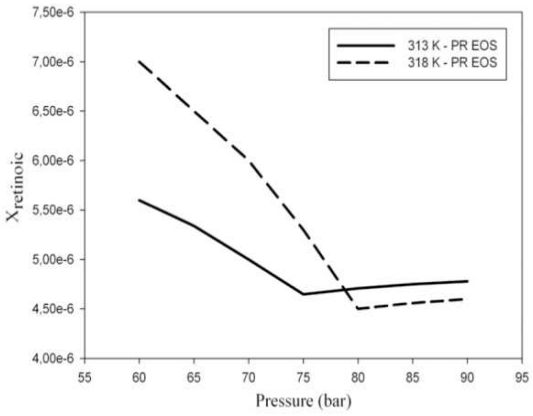

Fig. 5. Evolution of the RA molar fraction as function of pressure in the system CO_2-ethanol-RA.

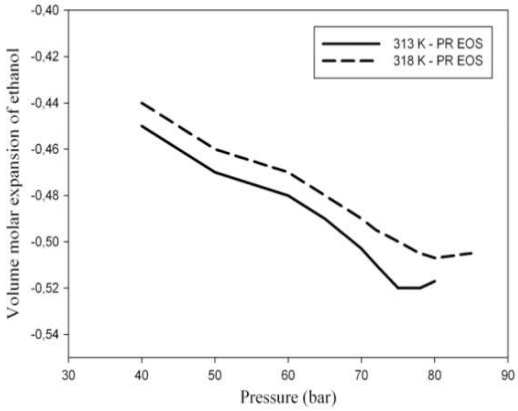

Fig. 6. Relative molar volume expansion of the ethanol with CO_2 at 313 K and 318 K.

The effect of temperature is also observable. The molar volume expansion decreases with temperature as a consequence of the lesser solubility of CO_2 in ethanol, as can be seen in the VLE figure (Fig. 3).

The minimum molar volume expansion matches with the MCP given by Fig. 3. Therefore, from a theoretical point of view it can be concluded based on PR-EOS that, the optimal conditions for a batch process for both systems are close to the MCP given by the VLE (where the maximum attainable supersaturation is produced).

4.2. Windowed cell results

Diluted dissolutions of 5 mg/ml of acetaminophen and 1 mg/ml of RA are introduced in the cell. The dissolutions should be diluted because concentrations higher than 10 mg/ml can produce the displacement of the MCP towards higher pressures [13].

A known amount of dissolution (around 3 ml) is introduced into the cell. This quantity is defined according to the minimum volume of the cell (8 ml) and the total volume expansion of the ethanol due to the addition of CO_2. At high pressure, this expansion can even be greater than 300% [49]. If the expansion of the solution is greater than the cell volume, a drastic increase in pressure (and consequently also in temperature) might be produced, making it difficult to control the experiment's parameters.

For both systems, two phases are observed until the pressure is around 77 bar at 313 K. At these conditions one single phase fills the cell. On the other hand, if the temperature is 318 K, one single phase appears at 81 bar. These conditions match with the conditions

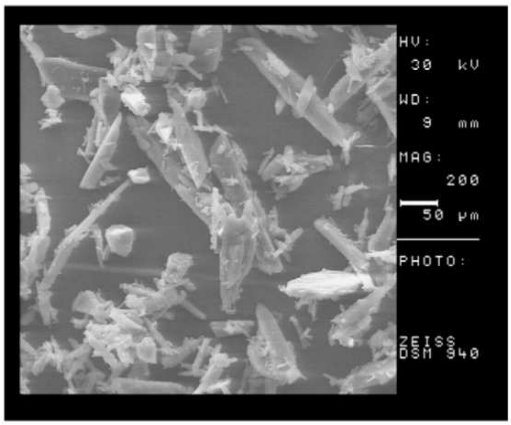

Fig. 7. SEM image of unprocessed acetaminophen.

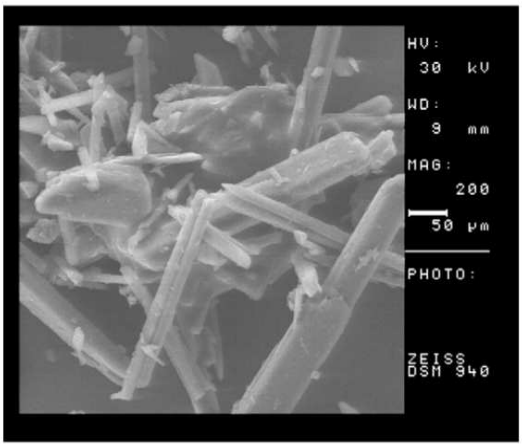

Fig. 8. SEM image of unprocessed RA.

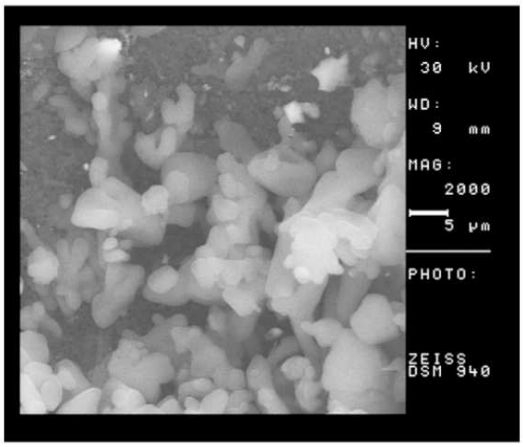

Fig. 9. SEM image of experiment 2 (acetaminophen particles at 70 bar and 318 K).

given by the VLE (Fig. 3) and the Figs. 4 and 5. No immiscibilities are observed for both temperatures between 60 and 100 bars.

The precipitation yield was determined for each solute at 313 K and 318 K. The precipitation yield for the acetaminophen ranges (from 60 to 100 bars) from a value around 70% to a value around 82% at both temperatures. This interval of yield is similar at both temperatures.

However, the maximums yields are found at different conditions. At 313 K, the maximum is obtained at 76 bars, whereas at 318 K the maximum is displaced to 82 bars. At pressures greater than the MCP, the yield decreases slightly until a value of around 78–80%, keeping this value almost constant at higher pressures. This increase is due to the slight increase of the solubility of the solid (Fig. 4), which occurs because of the transition from a biphasic phase to a one single supercritical phase.

On the other hand, the precipitation yield for the RA varies (from 60 to 100 bars) from 75% to 88% at both temperatures. As occurs with acetaminophen, this interval is almost identical at 313 K and 318 K. The maximums are obtained at 76 bars (313 K) and 81 bar (318 K). For higher pressures than the MCP, the yield decreases until a value of around 85%. This value does not undergo a significant variation at greater pressures. The explanation is in Fig. 5, where it can be seen how a slight increase in the solubility of the RA in the system is produced at pressures greater than the MCP.

Table 4
Experimental conditions and precipitation results with SEDS process.

Exp.	Solute	P (bar)	T (K)	d_m (µm)	SEM image	Position with respect to the MCP
1	Acet	70	313	1.39	–	Under
2	Acet	70	318	2.12	Fig. 9	Under
3	Acet	75	313	0.75	–	Near
4	Acet	75	318	0.91	–	Under
5	Acet	80	313	0.55	–	Near and above (*)
6	Acet	80	318	0.61	Fig. 13	In the MCP (*)
7	Acet	90	313	0.97	–	Above
8	Acet	90	318	1.08	–	Above
9	Acet	100	313	1.42	–	Above
10	Acet	100	318	1.33	–	Above
11	RA	70	313	0.79	–	Under
12	RA	70	318	0.89	Fig. 10	Under
13	RA	75	313	0.67	–	Near and above
14	RA	75	318	0.71	–	Under
15	RA	80	313	0.52	–	Near and above (*)
16	RA	80	318	0.54	–	In the MCP (*)
17	RA	90	313	1.44	Fig. 14	Above
18	RA	90	318	1.72	–	Above
19	RA	100	313	1.66	–	Above
20	RA	100	318	1.98	–	Above

It is important to notice that these maximums are obtained at conditions that match with the minimum molar volume expansion produced when CO_2 is added to ethanol (Fig. 6). A minimum molar volume expansion highlights that the maximum attainable supersaturation has been reached. As a result, the precipitation yield is near its maximum at these conditions. However, at greater pressures the value of the volume molar expansion increases, which involves a lesser supersaturation, therefore reducing the precipitation yield.

4.3. Precipitation results with SEDS process

In this work, it is studied how particle diameter and the existence of aggregates are affected if the experiments are performed above or under the MCP. According to our previous results with the windowed cell and the calculated phase equilibria with PR-EOS, the experiments are performed between 70 and 100 bar, given that the maximum supersaturation is achieved within this interval of pressure for 313–318 K.

The ratio between the CO_2 flow rate and the solution flow rate is kept constant with a value of 6:1. A flow rate ratio between 5:1 and 10:1 is usually employed in this type of process. The concentrations values are 5 mg/ml for the acetaminophen solutions and 1 mg/ml for RA.

According to our previous results, neither solute has an influence on the antisolvent–solvent P-xy diagram at the previous concentrations, pressure and temperature conditions, assuring a complete miscibility.

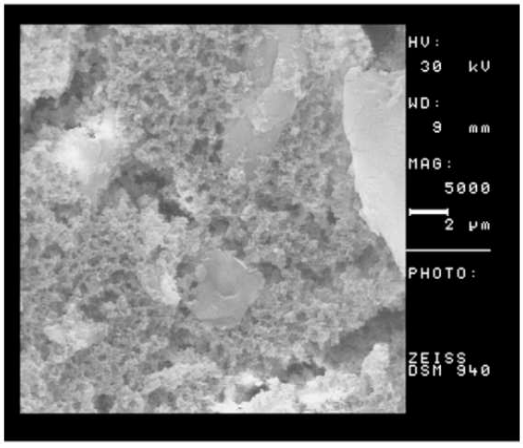

Fig. 10. SEM image of experiment 12 (RA particles at 70 bar and 318 K).

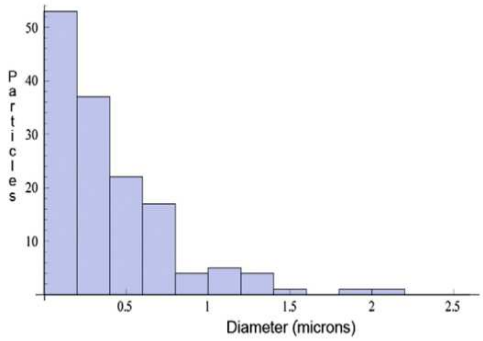

Fig. 11. Histogram of experiment 5 (acetaminophen at 80 bar and 313 K).

Figs. 7 and 8 illustrate unprocessed particles of acetaminophen and RA respectively. Both unprocessed solids have the shape of needle-like particles of 150 μm.

Table 4 gives the results of the different experiments for both solids. The PSD is given as the mean diameter (d_m). The symbol * marks the conditions at which the PSD is at its minimum for both temperatures.

4.3.1. Under the MCP

Under the MCP, both solids are mainly precipitated in the form of aggregates with microparticles. This can be observed in Figs. 9 and 10. The spherical particles are formed inside the droplet, and the solidification takes place condensing on the internal particle surface [10]. The appearance of aggregates can be explained in view of two different theories. The first states that several nuclei can be formed inside the droplet and a connection can be established between the nuclei [10]. That might force that several particles grow as one single particle. Another theory is that the brownian motion can induce droplet or particle collisions, producing a coalescence phenomenon and the formation of aggregates [6].

In these type of experiments (under the MCP), the SCF might rarely produce a predominant dryer effect over the antisolvent effect. In semicontinous processes with SCFs as antisolvents, droplets are formed under the MCP due to the existence of surface tension. These droplets undergo through a shrinking or swelling process depending on the mass and heat transfer paths [50], and eventually the droplet disappears, producing particle formation. However, sometimes a single droplet (coming perhaps from a secondary atomization) can collide with the filter because its flying time is too short to produce the required heat and mass transfer paths. In these cases it seems that the SCF produces a predominant drying effect on the remaining droplet, and as a consequence particles (which can act as new nuclei for secondary nucleation) are formed on the filter, consequently creating larger, irregular and aggregated particles.

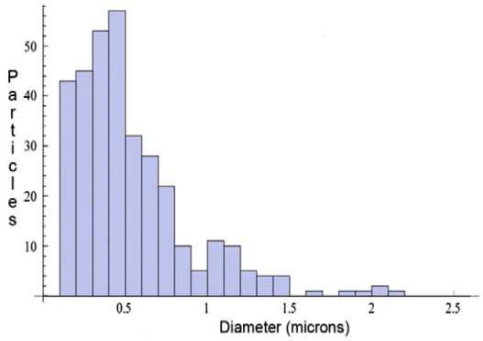

Fig. 12. Histogram of experiment 16 (RA at 80 bar and 318 K).

4.3.2. Near and near above the MCP

The effect of the pressure is the same for both compounds. An increase in pressure is accompanied by a reduction of the PSD until the conditions are close the MCP (approx. 80 bar at 318 K and 75 bar at 313 K).

Specifically, the PSD of the acetaminophen ranges from 1.39 μm to 0.55 μm at 313 K, whereas at 318 K the size varies between 2.12 and 0.61 μm. The best PSD is achieved at 80 bar for both temperatures. After that, an increase in pressure at constant temperature yields a larger PSD.

On the other hand, the PSD of the RA varies between 0.79–0.52 μm at 313 K and from 0.89 μm to 0.54 μm at 318 K. In this case, the best result is also found at 80 bar at both temperatures. As occurs with acetaminophen, if pressure increases after the MCP the PSD also becomes larger.

Therefore, for both solids, the PSD decreases inversely with the pressure until the MCP, and after that, the PSD increases proportionally. This fact has been already reported by other authors with SAS process [16, 27], and highlights that the supersaturation is the main parameter in the SEDS process to control the size of the particles.

Figs. 11 and 12 show the histograms of experiment 5 (acetaminophen at 80 bar and 313 K) and experiment 16 (RA at 80 bar and 318 K). At these conditions, the mixture is respectively near above the MCP and just in the MCP, existing only a single supercritical phase for both experiments. Under these conditions, precipitates of acetaminophen and RA tend to be spherical microparticles with a few aggregates. Fig. 13 illustrates this for the acetaminophen.

It is possible to produce these aggregates at conditions near the MCP due to the exothermic effect of the mixing enthalpy. It was demonstrated that in a SAS process, the mixing enthalpy can play an important role in the morphology of the particles if conditions are close to the MCP [51]. For instance, the mixing enthalpy could even increase the temperature almost 5.5 K in the CO_2-DMSO system at supercritical conditions [51]. This heating process might produce a displacement from a single supercritical phase to a biphasic phase, which can involve a coalescence phenomenon forming aggregates. In our experiments an increase in temperature (between 1 and 3 K) was observed in the mixing length of the nozzle. This slight temperature increase occurs because although the CO_2-ethanol system can be as exothermic as the CO_2-DMSO system [52, 53], the increase of temperature is produced inside the nozzle (SEDS) and not in the vessel as

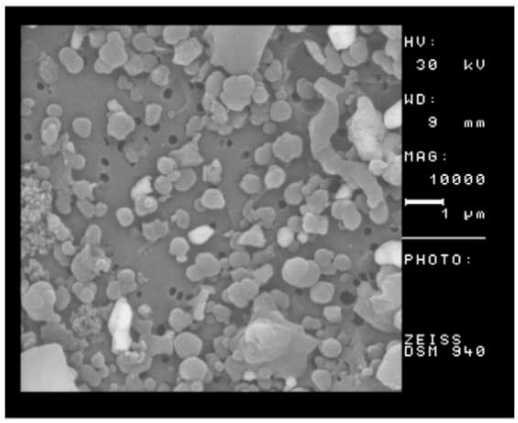

Fig. 13. SEM image of experiment 6 (acetaminophen particles at 80 bar and 318 K).

happens in SAS. Therefore, the mixing heat can be partially (but not totally) compensated with the temperature controller of the vessel.

4.3.3. Above the MCP

As long as the pressure is increased above the MCP the agglomerates start to disappear because the effect of the mixing enthalpy becomes neglectable and the particles are more spherical. These particle characteristics are typical for a gas-to-solid nucleation, and are kept for all the experiments performed above the MCP. Fig. 14 illustrates these characteristics for RA when the experiment is performed above the MCP (90 bar and 313 K). Although this fact is always the same for all performed experiments in one single supercritical phase, the PSD is larger above the MCP. This is due to the small increase in the solid's solubility (Figs. 4 and 5), which implies a lesser supersaturation, making the PSD larger according to the crystallization theory.

In order to explain the larger PSD, it is very important to take into account the mass transfer. Mass transfer in this type of processes can be due to different mechanisms such as molecular diffusion resulting from a concentration gradient, the nucleation process inside the droplet, or to a convective mechanism (inside and outside the droplet) as a consequence of the transport of material between a boundary surface and a moving fluid. The diffusion and nucleation (inside the droplet) are only taken into account if there is droplet formation, whereas the convective mechanism is always present because it is related to the fluid's velocity. Although the convective mechanism is not considered in different studies, this effect can be relevant in this type of processes [10]. Therefore, if there is no droplet formation, the mass transfer might be reduced given that there is no diffusion along the droplet interface. This might be another reason accounting for why the PSD is slightly larger if the conditions are in one single supercritical phase.

4.3.4. Temperature effect

The effect of temperature can also be observed. At the same pressure, if temperature is increased, the PSD is larger. The reason is illustrated in the VLE diagram (Fig. 3). The solubility of the CO_2 in ethanol decreases inversely with the temperature. Therefore, the supersaturation is lesser and the PDS is larger. This temperature effect has been observed previously in different experiments involving either the SAS or SEDS processes [12, 23, 27].

4.3.5. Solution concentration effect

Finally, the effect of the concentration in the PSD is studied for both solids at 80 bars and 318 K. The effect of the initial concentration is checked in this work by increasing the concentrations of acetaminophen

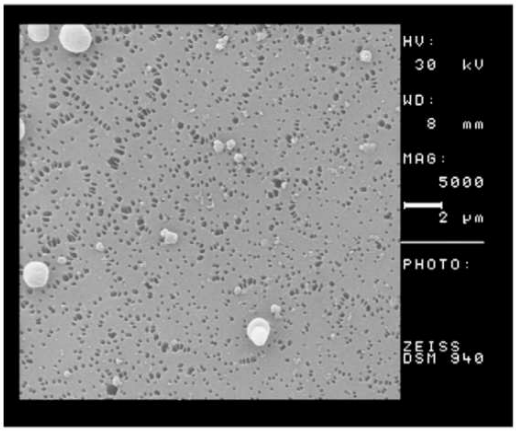

Fig. 14. SEM image of experiment 17 (RA particles at 313 K and 90 bar).

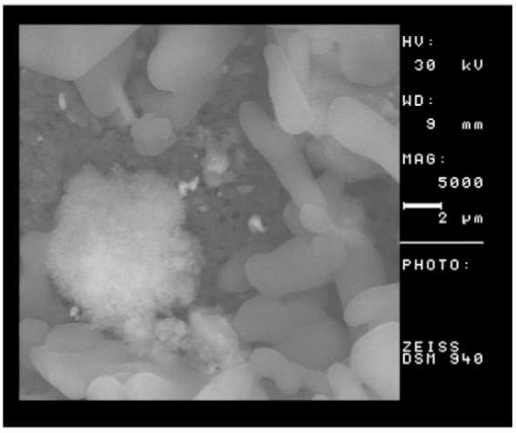

Fig. 15. SEM image of acetaminophen particles at 80 bars and 318 K with an initial concentration of 20 mg/ml.

and RA up to a value of 20 mg/ml. Upon these conditions, the acetaminophen particles are obtained in the form of aggregates or particles larger than 5 µm (Fig. 15) without a spherical form. On the other hand, RA particles are not produced, obtaining instead a homogeneous layer of the compound that covers the filter with single and large particles. In this case, the filter holes are not observed because they are covered by this layer. Therefore, at concentrations of 20 mg/ml both precipitations were unsuccessful. Although several studies have shown that higher concentrations involve a decrease in particle size (because higher concentrations can produce a greater supersaturation that can make smaller particles [27, 12]), the opposite behavior was also found by other authors [13, 55]. They stated that the solid affects the phase equilibria, producing a displacement of the MCP due to the presence of the solid.

In order to check this phenomenon, the concentration of the solutions (for both drugs) was modified up to 20 mg/ml, observing in the windowed cell if there was a displacement in the MCP. The MCP did not undergo a displacement, discarding therefore the previous theory for our systems.

In our case, this size increase can be due to a brownian motion. Higher concentrations can produce a greater supersaturation, which can make smaller particles precipitate. However, if more nuclei are formed, more collisions can be produced between the nuclei, giving as a result agglomerates or single particles with a larger size.

4.3.6. Which conditions are the optimal to obtain a good PSD without aggregates?

According to the previous results, it can be concluded that the best conditions to obtain spherical microparticles without aggregates in a SEDS process are above the MCP, in one single supercritical phase in order to get a gas-to-solid nucleation. In this context, it is important to take into account the effect of the mixing enthalpy, and perform the experiments at least between 5 and 10 bars above the MCP.

However, the narrowest PSD is obtained at conditions near and near above the MCP. Although in the MCP and near above the MCP the surface tension should disappear, droplet formation occurs due to a gradient of density and/or temperature [54]. This droplet is fast and progressively reduced until the equilibrium is reached, when the droplet disappears. In this case, all mass transfer mechanisms might occur and, in addition, the supersaturation will be the maximum.

A few particles with a larger size, in comparison with the mean PSD, can be observed in the histograms and in the respective images for all experiments. They are produced due to a phenomenon of secondary contact nucleation. This type of nucleation produces larger

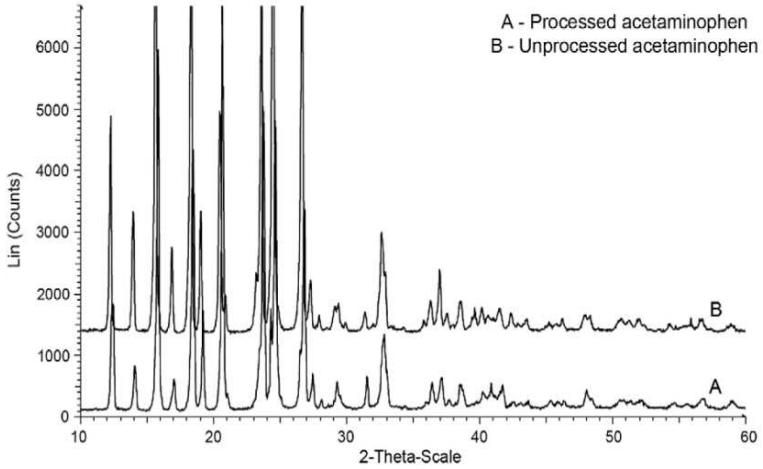

Fig. 16. XRD patterns of unprocessed and processed acetaminophen (experiment 1).

crystals than homogeneous nucleation [6]. After particle formation, these particles can collide with the wall of the vessel, leaving behind residual particles. New particles will be formed from these nuclei by means of secondary nucleation kinetics. Therefore, the growth of these particles takes place on the walls of the vessel, and subsequently the vent process with CO_2 drags them towards the filter.

4.3.7. X-ray diffractometry (XRD) of the precipitated particles

Figs. 16 and 17 describe the XRD patterns for (processed and unprocessed) acetaminophen and RA respectively. It can be observed that the unprocessed materials are crystalline. However, the XRD patterns of the processed pharmaceuticals are distinct if they are compared with the unprocessed materials. The diffraction peaks for both processed solids present usually lower intensities or are displaced. Therefore, the precipitated solids present a reduced crystallinity.

These phenomena are usually found in processed solids at high pressure, and the explanation can be the disordered growth of the particles during the precipitation process [12]. In fact, amorphous solids [21], semicrystalline solids or high crystalline solids can be obtained using SCFs as antisolvents [56].

5. Conclusions

In this work, the role of the phase behavior in the SEDS process has been studied precipitating successfully acetaminophen and tretinoin. The optimal conditions to perform the experiments were determined in a theoretical way by modeling the binary and ternary equilibria with PR-EOS, and in an experimental way by using a windowed cell. Both results confirm the non existence of immiscibilities at all the investigated conditions and the position of the MCP (approx. 75 bar for 313 K and 80 bar for 318 K). For a fixed temperature, the particle diameter decreases with pressure until the MCP, where the narrowest PSD is achieved. However, above the MCP, the PSD is larger. The main reason for this behavior is the increase of solubility of the solid in the ternary system above the MCP, due to the transition from a biphasic phase to a one single supercritical phase. Regarding size, it is important to take into account possible secondary nucleation due to particles–wall or particle–particle collisions. These phenomena can produce aggregates and/or larger particles with respect to the mean size.

In contrast, the particles under the MCP are mainly aggregates with microparticles, the larger aggregates dissapearing above the MCP. Above the MCP, a gas-to-solid nucleation is produced favoring the

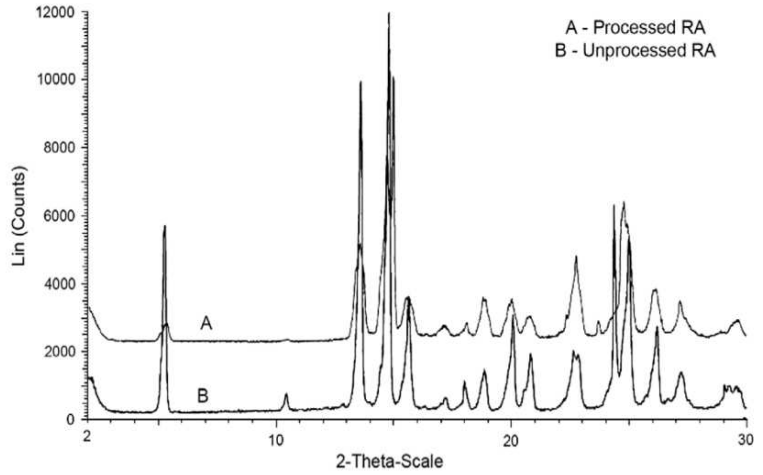

Fig. 17. XRD patterns of unprocessed and processed RA (experiment 14).

production of spherical microparticles. Considering the aggregation mechanism, it is important to take into account phenomena such as mixing enthalpy or brownian motion. The first one involves heat, producing a transition from a one phase to a biphasic phase, and the second directly favors the formation of aggregates.

The effect of temperature and concentration has also been discussed. An increase in temperature for a fixed pressure favors a larger PSD as a consequence of the reduction of the supersaturation. This can be because the solubility of the antisolvent in the solvent decreases with temperature.

Although greater supersaturations can be achieved for higher concentrations, phenomena such as particle collisions can be increased. As a result, at higher concentrations the precipitations were unsuccessful.

Overall, it seems that in the SEDS process experiments should be performed near above the MCP in order to obtain the narrowest PSD without aggregates.

Acknowledgments

Financed by the Ministerio de Ciencia e Innovación (Spain), project CTQ 2009–08222 (PPQ subprogram). Mr. Antonio Tabernero also appreciates the Ministerio de Ciencia e Innovación (Spain) for the grant provided to him.

References

[1] P. York, U.B. Kompella, B.Y. Shekunov, in: J. Swarbrick (Ed.), Supercritical Fluid Technology for Drug Product Development, Marcel Dekker, Inc., New York, NY, 2004.
[2] S.A. Shoyele, S. Cawthorne, Particle engineering techniques for inhaled biopharmaceuticals, Advanced Drug Delivery Reviews 58 (2006) 1009–1029.
[3] L. Sze Tu, F. Dehghani, N.R. Foster, Micronisation and microencapsulation of pharmaceuticals using a carbon dioxide antisolvent, Powder Technology 126 (2002) 134–149.
[4] Z. Knez, E. Weidner, Particles formation and particle design using supercritical fluids, Current Opinion in Solid State and Materials Science 7 (2003) 353–361.
[5] E. Reverchon, R. Adami, Nanomaterials and supercritical fluids, Journal of Supercritical Fluids 37 (2006) 1–22.
[6] J.A. Dirksen, T.A. Ring, Fundamentals of crystallization: kinetic effects on particle size distributions and morphology, Chemical Engineering Science 10 (1991) 2389–2427.
[7] A. Martín, M.J. Cocero, Micronization processes with supercritical fluids: fundamentals and mechanism, Advanced Drug Delivery Reviews 60 (2008) 339–350.
[8] J. Jung, M. Perrut, Particle design using supercritical fluids: literature and patent survey, Journal of Supercritical Fluids 20 (2001) 179–219.
[9] M. Hanna, P. York, Method and Apparatus for the Formation of Particles, WO95/01221, 1994.
[10] E. Reverchon, E. Torino, S. Dowy, A. Brauer, A. Leipertz, Interactions of phase equilibria, jet fluid dynamics and mass transfer durins supercritical antisolvent micronization, Chemical Engineering Journal 156 (2010) 446–458.
[11] A. Martín, M.J. Cocero, Numerical modelling of jet hydrodynamics, mass transfer and crystallization kinetics in the supercritical antisolvent (SAS) process, Journal of Supercritical Fluids 32 (2004) 203–219.
[12] E. Franceschi, M.H. Kunita, M.V. Tres, A.F. Rubira, E.C. Muniz, M.L. Corazza, c. Dariva, S.R.S. Ferreira, J.V. Oliveira, Phase behaviour and process parameters effects on the characteristics of precipitated theophyllina using carbon dioxide as antisolvent, Journal of Supercritical Fluids 44 (2008) 8–20.
[13] E. Reverchon, I. De Marco, Supercritical antisolvent micronization of Cefonicid: thermodynamic interpretation of results, Journal of Supercritical Fluids 31 (2004) 207–215.
[14] B. De Gioannis, A.V. González, P. Subra, Anti-solvent and co-solvent effect of CO_2 on the solubility of griseofulvin in acetone and ethanol solutions, Journal of Supercritical Fluids 29 (2004) 49–57.
[15] Y. Pérez de Diego, H.C. Pellikaan, F.E. Wubbolts, G.J. Witkamp, P.J. Jansens, Operating regimes and mechanism of particle formation during the precipitation of polymers using the PCA process, Journal of Supercritical Fluids 35 (2005) 147–156.
[16] F. Miguel, A. Martín, F. Mattea, M.J. Cocero, Precipitation of lutein and co-precipitation of lutein and poly-lactic acid with the supercritical-antisolvent process, Chemical Engineering and Processing 47 (2008) 1594–1602.
[17] A. Shariati, C.J. Peters, Measurements and modeling of the phase behavior of ternary systems of interest for the GAS process. I. The system carbon dioxide + 1-propanol + salicylic acid, Journal of Supercritical Fluids 23 (2002) 195–208.
[18] A. Weber, L.V. Yelash, T. Kraska, Effect of phase behaviour of the solvent–antisolvent systems on the gas–antisolvent-crystallization of paracetamol, Journal of Supercritical Fluids 33 (2005) 107–113.
[19] F.P. Lucien, N.R. Foster, Solubilities of solid mixtures in supercritical carbon dioxide: a review, Journal of Supercritical Fluids 17 (2000) 111–134.
[20] A. Martín, F. Mattea, L. Gutiérrez, F. Miguel, M.J. Cocero, Co-precipitation of carotenoids and bio-polymers with the supercritical antisolvent process, Journal of Supercritical Fluids 41 (2007) 138–147.
[21] E. Reverchon, G. Della Porta, Production of antibiotic micro-and nano-particles by supercritical antisolvent precipitation, Powder Technology 106 (1999) 23–29.
[22] I. De Marco, E. Reverchon, Supercritical antisolvent micronization of cyclodextrinas, Powder Technology 183 (2008) 239–246.
[23] P. Subra, C.-G. Laudani, A.-V. González, E. Reverchon, Precipitation and phase behaviour of theophylline in solvent-supercritical CO_2 mixtures, Journal of Supercritical Fluids 35 (2005) 95–105.
[24] E. Reverchon, I. De Marco, Supercritical antisolvent precipitation of cephalosporins, Powder Technology 164 (2006) 139–146.
[25] E. Reverchon, I. De Marco, E. Torino, Nanoparticles production by supercritical antisolvent precipitation: a general interpretation, Journal of Supercritical Fluids 43 (2007) 126–138.
[26] A. Tenorio, M.D. Gordillo, C.M. Pereyra, E.J. Martínez de la Ossa, Screening design of experiment applied to supercritical antisolvent precipitation of amoxicillin, Journal of Supercritical Fluids 44 (2008) 230–237.
[27] F. Miguel, A. Martín, T. Gamse, M.J. Cocero, Supercritical antisolvent precipitation of lycopene. Effect of the operating parameters, Journal of Supercritical Fluids 36 (2006) 225–235.
[28] M. Rantakylä, M. Jäntti, O. Aaltonen, M. Hurme, The effect of initial drop size on particle size in the supercritical antisolvent precipitation (SAS) technique, Journal of Supercritical Fluids 24 (2002) 251–263.
[29] E. Franceschi, A.M. De Cesaro, M. Feiten, S.R.S. Ferreira, C. Dáriva, M.H. Kunita, A.F. Rubira, E.C. Muniz, M.L. Corazza, J.V. Oliveira, Precipitation of β-carotene and PHVB and co-precipitation from SEDS technique using supercritical CO_2, Journal of Supercritical Fluids 47 (2008) 259–269.
[30] F.E. Wubbolts, O.S.L. Bruinsma, G.M. Van Rosmalen, Dry-spraying of ascorbic acid or acetaminophen solutions with supercritical carbon dioxide, Journal of Crystal Growth 198–199 (1999) 767–772.
[31] G.H. Chong, R. Yanus, T.S.Y. Choong, N. Abdullah, S.Y. Spotar, Simple guidelines for a self-built laboratory-scale supercritical anti-solvent system, Journal of Supercritical Fluids (in press), doi:10.1016/j.supflu.2011.04.020.
[32] E. Franceschi, A.M. De Césaro, S.R.S. Ferreira, J. Vladimir Oliveira, Precipitation of β-carotene microparticles from SEDS technique using supercritical CO_2, Journal of Food Engineering 95 (2009) 656–663.
[33] Hai Long Hong, Quang Lin Suo, Li Min Han, Chung Pin Li, Study on precipitation of astaxanthin in supercritical fluid, Powder Technology 191 (2009) 294–298.
[34] W.S. Rasband, ImageJ, U. S. National Institutes of Health, Bethesda, Maryland, USA, 1997–2011http://imagej.nih.gov/ij/.
[35] D.Y. Peng, D.B. Robinson, A new two constant equation of state, Industrial and Engineering Chemistry Fundamentals 15 (1976) 59–64.
[36] J.M. Prausnitz, R.N. Lichtenthaler, E.G. De Azevedo, Molecular Thermodynamics of Fluid-Phase Equilibria, 2ª ed. Prentice-Hall, New Jersey, 1986.
[37] Z. Huang, S. Kawi, Y.C. Chiew, Solubility of cholesterol and its esters in supercritical carbon dioxide with and without cosolvents, Journal of Supercritical Fluids 30 (2004) 25–39.
[38] K.-W. Cheng, S.-J. Kuo, M. Tang, Y.-P. Cheng, Vapor–liquid equilibria at elevated pressures of binary mixtures of carbon dioxide with methyl salicylate, eugenol, and diethyl phthalate, Journal of Supercritical Fluids 18 (2000) 87–99.
[39] D. Dixon, K.P. Johnston, Mollecular thermodynamics of solubilities in gas–antisolvent crystallization, AICHE Journal 37 (1991) 1441–1449.
[40] J.C. De la Fuente Badilla, C.J. Peters, J. de Swaan Aarons, Volume expansion in relation to the gas–antisolvent process, Journal of Supercritical Fluids 17 (2000) 13–23.
[41] S. Garnier, E. Neau, P. Alessi, A. Cortesi, I. Kikic, Modelling solubility of solids in supercritical fluids using fusion properties, Fluid Phase Equilibria 158–160 (1999) 491–500.
[42] I. Kikic, M. Lora, A. Bertucco, A thermodynamic analysis of three-phase equilibria in binary and ternary systems for applications in rapid expansion of a supercritical solution (RESS), particles from gas-saturated solutions (PGSS), and supercritical antisolvent (SAS), Industrial and Engineering Chemistry Research 36 (1997) 5507–5515.
[43] B.E. Poling, J. Prausnitz, J.P. O'Connell, The Properties of Gases and Liquids, 5th edition McGraw-Hill, New York, 2001.
[44] Z. Knez, M. Skerget, L. Ilic, C. Lütge, Vapor–liquid equilibrium of binary CO_2-organic solvent systems (ethanol, tetrahydrofuran, *orto*-xylene, *meta*-xylene, *para*-xylene), Journal of Supercritical Fluids 43 (2008) 383–389.
[45] S. Bristow, B. Shekunov, P. York, Solubility analysis of drug compounds in supercritical carbon dioxide using static and dynamic extraction systems, Industrial and Engineering Chemistry Research 40 (2001) 1732–1739.
[46] A. Tabernero, E.M.M. Martín del Valle, M.A. Galán, On the use of semiempirical models of (solid+supercritical fluids) systems to determine solid sublimation properties, The Journal of Chemical Thermodynamics 43 (2011) 711–718.
[47] J.C. De La Fuente, A. Shariati, C.J. Peters, On the selection of optimum thermodynamic conditions for GAS process, Journal of Supercritical Fluids 32 (2004) 55–61.
[48] M. Mukhopadhyay, Partial molar volume reduction of solvent for solute crystallization using carbon dioxide as antisolvent, Journal of Supercritical Fluids 25 (2003) 213–223.
[49] A. Kordikowski, A.P. Schenk, R.M. Van Nielen, C.J. Peters, Volume expansions and vapor–liquid equilibria of binary mixtures of a variety of polar solvents and certain near-critical solvents, Journal of Supercritical Fluids 8 (1995) 205–216.
[50] M. Mukhopadhyay, S.V. Dalvi, Mass and heat transfer analysis of SAS: effects of thermodynamic states and flow rates on droplet size, Journal of Supercritical Fluids 30 (2004) 333–348.
[51] F. Zahran, J. Morére, A. Cabañas, J.A.R. Renuncio, C. Pando, Role of excess molar enthalpies in supercritical antisolvent micronizations using dimethylsulfoxide as the polar solvents, Journal of Supercritical Fluids (in press), doi:10.1016/j.supflu.2011.02.015.
[52] D.R. Cordray, R.M. Izatt, J.J. Christiansen, J.L. Oscarson, The excess enthalpies of (carbon dioxide+ethanol) at 308.15, 325.15, 373.15, 413.15, and 473.15 K from 5.00 to 14.91 MPa, The Journal of Chemical Thermodynamics 20 (1988) 655–663.

[53] W. Dai, K. Ochi, K. Kojima, Excess enthalpy data in binary systems containing a supercritical fluid and their correlation, Journal of Chemical and Engineering Data 43 (1998) 687–694.
[54] A. Tenorio, P. Jaeger, M.D. Gordillo, C.M. Pereyra, E. Martínez de la Ossa, On the selection of limiting hydrodynamic conditions for the supercritical antisolvent (SAS) process, Industrial and Engineering Chemistry Research 48 (2009) 9224–9232.
[55] E. Reverchon, G. Della Porta, P. Pallado, Supercritical antisolvent precipitation of salbutamol microparticles, Powder Technology 114 (2001) 17–22.
[56] M. Rehman, B.Y. Shekunov, P. York, D. Lechuga-Ballesteros, D.P. Miller, T. Tan, P. Colthorpe, Optimisation of powders for pulmonary delivery using supercritical fluid technology, European Journal of Pharmaceutical Sciences 22 (2004) 1–17.

4.7. Conclusiones

En el artículo previo se ha estudiado el papel de los equilibrios de fases en la precipitación de acetaminofén y tretinoína con un equipo SEDS.

Primeramente, se determinaron el punto crítico de mezcla y la aparición de inmiscibilidades mediante un estudio teórico-experimental de los equilibrios de fase con la ecuación de Peng-Robinson y una celda de equilibrio con ventanas. Tanto el estudio teórico como el experimental indicaron la no existencia de inmiscibilidades, así como la posición del punto crítico de mezcla del sistema CO_2-etanol (75 bares a 313 K y 80 bares a 318 K).

En cuanto a los resultados del proceso de precipitación, a una temperatura fija, el tamaño de partícula disminuye con la presión hasta alcanzar el punto crítico de mezcla. Sin embargo, por encima del punto crítico, el tamaño aumenta con la presión. Esto es debido al incremento de la fracción molar del sólido en el sistema ternario a condiciones por encima del punto crítico de mezcla debido a la transición de una región bifásica a una monofásica.

Además, partículas agregadas se obtienen principalmente a condiciones por debajo del punto crítico de mezcla por la existencia de una nucleación en una región bifásica. Sin embargo, por encima del punto crítico de mezcla las partículas son más esféricas, y los agregados desaparecen debido a la posibilidad de la existencia de una nucleación gas-sólido. En este aspecto, es importante tener en cuenta el efecto de la entalpía de mezcla y del movimiento browniano.

Finalmente, se estudió el efecto de la temperatura y de la concentración de la disolución inicial de fármaco en la distribución de tamaño de partícula. A una presión definida, el incremento de temperatura produce un incremento de

tamaño como consecuencia de la disminución de la solubilidad del antisolvente en el disolvente. Por otro lado, no se pudo lograr la precipitación de los sólidos a concentraciones muy elevadas, debido probablemente a efectos de la colisión entre partículas.

En general, se puede concluir que desde el punto de vista de los equilibrios de fases, la distribución de tamaño óptima con menor cantidad de agregados fue obtenida a condiciones ligeramente por encima del punto crítico de mezcla.

• Referencias también citadas

[1] P. H. Van Konynenburg; R. L. Scott, Critical lines and phase equilibria in binary Van der Waals mixtures. Philos. Trans. Roy. Soc. 29 (1980) 495-540.

[2] K. Suzuki; H. Sue; M. Itou; R. L. Smith; H. Inomata; K. Arai; S. Saito, Isothermal vapor-liquid equilibrium data for binary systems at high pressures: carbon dioxide-methanol, carbon dioxide-ethanol, carbon dioxide-1-propanol, ethane-ethanol, and ethane-1-propanol systems. J. Chem. Eng. Data 35 (1990) 63-66.

[3] E. Reverchon; E. Torino; S. Dowy; A. Brauer; A. Leipertz, Interactions of phase equilibria, jet fluid dynamics and mass transfer during supercritical antisolvent micronization. Chem. Eng. J. 156 (2010) 446-458.

[4] S. S. Dukhin; C. Zhu; R. Dave; R. Pfeffer; J. J. Luo; F. Chavez; Y. Shen, Dynamic interfacial tension near critical point of a solvent-antisolvent mixture and jet estabilization, Colloid: Surf. A: Physicochem. Eng. Asp. 229 (2003) 181-199.

[5] F. P. Lucien; N. R. Foster, Solubilities of solid mixtures in supercritical carbon dioxide: A review. J. Supercrit. Fluids 17 (2000) 111-134.

[6] M. McHugh; M. E. Paulaitis, Solid solubilities of naphthalene and biphenyl in supercritical carbon dioxide. J. Chem. Eng. Data 25 (1980) 326-329.

[7] E. Reverchon; I. De Marco, Supercritical antisolvent micronization of cefonicid: thermodynamic interpretation of results. J. Supercrit. Fluids 31 (2004) 207-215.

[8] D. Y. Peng; D. B. Robinson, A new two constant equation of state. Ind. Eng. Chem. Fund. 15 (1976) 59-64.

[9] J. C. De la Fuente Badilla; C. J. Peters; J. de Swans Arons. J. Supercrit. Fluids 17 (2000) 13-23.

[10] P. York; U. B. Kompella; B. Y. Shekunov, Supercritical fluid technology for drug product development. 1º Ed.-New York: Ed. Marcel-Dekker, 2004.

CAPÍTULO 5.

Estudio comparativo de ecuaciones semiempíricas empleadas en equilibrios sólido-vapor

5.1. Ecuaciones semiempíricas

Como se ha observado, es importante el realizar un estudio previo de los equilibrios de fase antes de emplear una técnica con fluidos supercríticos como antisolventes.

Este estudio se realizó en el capítulo 4, dónde se detallaron los equilibrios de fase de los sistemas binarios y ternarios objeto de estudio. Estos equilibrios fueron ajustados mediante el uso de la ecuación de estado cúbica de Peng-Robinson.

Sin embargo, al estudiar los equilibrios sólido-fluido supercrítico se observó que las ecuaciones de estado cúbicas (como la ecuación de Peng-Robinson) presentaban varios inconvenientes a la hora de ajustar este tipo de equilibrios. Estos inconvenientes se describen a continuación.

En primer lugar, para el empleo de ecuaciones cúbicas se requiere conocer el valor de ciertas propiedades del sólido, como son sus propiedades críticas y sus propiedades de sublimación. Esto puede ser un problema si estas propiedades no han sido determinadas previamente de forma experimental, lo cuál es común para muchos sólidos complejos como los farmacéuticos. Ello conlleva a que se empleen diferentes modelos de contribución de grupos para su estimación teórica [1-2]. Sin embargo, estos modelos pueden producir errores muy elevados en la predicción de propiedades de moléculas complejas, o algunas veces, como ocurre en el caso de la presión de sublimación, no existe ningún modelo para estimar esta propiedad para todas las familias de sólidos.

El segundo inconveniente es que las ecuaciones de estado cúbicas producen un error elevado cuando son empleadas para ajustar equilibrios sólido-vapor

con moléculas de polaridad elevada. En este caso, para disminuir el error se añade una serie de coeficientes de interacción en las reglas de mezcla correspondientes, dándose en caso de que en ocasiones se necesitan más de dos de estos coeficientes para lograr un error aceptable en el ajuste [3-4]. Esto anterior, unido al algoritmo de cálculo que debe implementarse, hace aún más tedioso el procedimiento de ajuste de este tipo de equilibrios con ecuaciones de estado cúbicas.

Con el fin de evitar los problemas anteriormente descritos, se han propuesto en bibliografía diferentes ecuaciones para ajustar la solubilidad de sólido en fluidos supercríticos. Entre esas propuestas, en estos últimos años ha crecido el interés en el uso de ecuaciones semiempíricas [5-13].

Estas ecuaciones no requieren propiedades del sólido ni métodos computacionales complejos. Su única desventaja es su carácter semiempírico ya que necesitan datos experimentales para la determinación de parámetros ajustables (la cantidad de estos parámetros depende de la ecuación) mediante la regresión de datos experimentales frente a datos teóricos [5-13].

Algunas de estas ecuaciones están basadas en teorías como la formación de un complejo de solvatación entre el soluto y el fluido supercrítico o la relación entre el factor de mejora y la densidad del fluido supercrítico. Mientras, otras ecuaciones están basadas en observaciones experimentales.

A continuación se describirán las ecuaciones semiempíricas más utilizadas para realizar un ajuste de la solubilidad de un sólido en fluidos supercríticos. Estas ecuaciones han sido comparadas con la finalidad de obtener un criterio de selección en función del error de ajuste a distintas condiciones experimentales. Dicho estudio comparativo se recoge en el trabajo siguiente.

5.2. Resultados y discusión

El objetivo de este artículo es la determinación de la óptima ecuación semiempírica para ajustar la solubilidad de fármacos en CO_2sc dependiendo de las condiciones experimentales. Para ello se recopilaron datos experimentales de solubilidad de 27 compuestos farmacéuticos en CO_2sc, los cuáles fueron modelados con 9 ecuaciones semiempíricas (Chrastil, Adachi-Lu, Del Valle-Aguilera, Sparks, Kumar-Johnston, Bartle, Méndez Santiago-Teja, Yu, Gordillo). De acuerdo a los resultados obtenidos, la ecuación de Sparks es la que generalmente proporciona el mejor ajuste de este tipo de datos de solubilidad. Sin embargo, a unas condiciones experimentales determinadas, la ecuación de Gordillo proporcionó el mejor ajuste. Se compararon además las ecuaciones semiempíricas con la ecuación cúbica de Peng-Robinson en términos de error, demostrando que las ecuaciones semiempíricas ajustan mejor la solubilidad de sólidos complejos en CO_2sc.

ARTÍCULO

A comparison between semiempirical equations to predict the solubility of pharmaceutical compounds in supercritical carbon dioxide

The Journal of Supercritical Fluids 52 (2010) 161-174.

J. of Supercritical Fluids 52 (2010) 161–174

Contents lists available at ScienceDirect

The Journal of Supercritical Fluids

journal homepage: www.elsevier.com/locate/supflu

A comparison between semiempirical equations to predict the solubility of pharmaceutical compounds in supercritical carbon dioxide

Antonio Tabernero, Eva M. Martín del Valle*, Miguel Á. Galán

Department of Chemical Engineering, University of Salamanca, P/Los Caídos S/N, 37008, Spain

ARTICLE INFO

Article history:
Received 4 November 2009
Received in revised form 7 January 2010
Accepted 19 January 2010

Keywords:
Supercritical fluids
Pharmaceutical
Solubility
Semi-empirical equations
Carbon dioxide

ABSTRACT

The aim of this work is to determine, depending on the operation conditions, which semiempirical equation provides the best fit to solubility data of pharmaceutical compounds in supercritical CO_2. Solubility data from 27 different pharmaceutical solutes were collected from literature and the different density-based models (Chrastil, Adachi-Lu, del Valle-Aguilera, Sparks, Kumar-Johnston, Bartle, Méndez Santiago-Teja) together with the Yu's model and Gordillo's model were employed. The results showed that, in general, Sparks' equation provides the best fit to the solubility data for this kind of solids in supercritical CO_2. However, at certain specific conditions, the best correlation is obtained using Gordillo's equation. By means of a brief comparison with Peng-Robinson equation of state, semiempirical equations present a more accuracy prediction compared to cubic equations of state, and present no drawbacks such as properties estimation and computational difficulties.

© 2010 Elsevier B.V. All rights reserved.

1. Introduction

Nowadays, the requirements of the medical and pharmaceutical industries are focused in the development of technologies to obtain ultra-purity products. In this context, during the last decades, supercritical fluids (SCFs) have been widely employed in different processes. This is due to the solvent power, high diffusivity and low viscosity, very adequate for these applications. Supercritical carbon dioxide (sc-CO_2) is the most commonly used molecule because of their light critical properties (P_c = 73.8 bar and T_c = 304 K) and their environmental benefits [1].

One of these processes is the extraction of medical compounds from natural sources. Supercritical fluid extraction (SFE) presents several advantages in relation with conventional techniques, like the improvement in mass transfer, better extraction time and the possibility to change the solvation power with a simple depressurization [2]. With SFE, cholesterol [3], carotenoids [4–6] and other pharmaceutical products [7–9] have been extracted with high purity.

More recently, new techniques which employ SCFs have been used in drug processing, reducing the particle size distribution and controlling the morphology without contaminating the active [10–13]. The feasability of the devices RESS, SAS or SEDS, amongst others, has been proved repeated times to obtain particles or microcapsules of pharmaceutical products [14–16].

In each of these processes (extraction and drug processing) is crucial to know the solubility of the solid in the SCF in order to determine the conditions to achieve the best outcome.

Different models have been used to predict the solubility of solids in SCFs, such as theoretical equations of state or semiempirical equations. Theoretical models like cubic equation of state or perturbed equations need large and complicated computational methods and the knowledge of the solid properties (macroscopic critical properties and sublimation pressure are needed for cubic equations of state and molecular parameters for perturbed equations). These properties can be determined by contributional groups methods or experimentally [17–19], but in both cases, due to several drawbacks, an error is produced in their estimations.

On the other hand, semiempirical equations, like density based models, do not need solid properties. They are based on simple error minimization and they use only available independent variables like pressure, temperature and density of pure sc-CO_2. The only drawback is the semiempirical character, which means that solubility data are needed. However, in the last years the number of articles on this subject have been significantly increased [20–23]. Several equations have been presented by different authors, covering from three to six parameters, which are necessary to determine for each solid.

Numerous studies were performed to investigate and predict the solubility of the systems sc-CO_2-medical compounds with semiempirical equations. Hojjati et al. [21] used six different equations to correlationate the solubility data of three aromatase inhibitors finding the best fit with K-J's model and Gordillo's model. The same research group determined the solubility of five statin

* Corresponding author. Tel.: +34 923 294479; fax: +34 923 294579.
E-mail address: emvalle@usal.es (E.M.M. del Valle).

0896-8446/$ – see front matter © 2010 Elsevier B.V. All rights reserved.
doi:10.1016/j.supflu.2010.01.009

Nomenclature

Symbols

a	attractive parameter (pure component).
a_m	attractive parameter (Van der Waals mixing rule).
A	parameter.
AARD	average absolute relative deviation (eq. (13)).
ΔH_{tp}	entalphy of fusion at the triple point.
b	repulsive term (pure component).
b_m	repulsive term (Van der Waals mixing rule).
B	parameter.
C	parameter.
D	parameter.
e_0	parameter.
e_1	parameter
e_2	parameter.
E	parameter and enhancement factor (eq. (9)).
F	parameter.
k_{ij}	mixing rule parameter.
k	association parameter.
P	pressure.
P_{ref}	reference pressure (1 bar).
P^{sub}	sublimation pressure.
S	solubility of the solid in supercritical carbon dioxide.
T	temperature.
UCEP	upper critical end point.
v	molar volume.
y_1	minimum molar fraction of the system.
y_2	molar fraction and maximum molar fraction of the system.

Greek letters

ρ_1	density of carbon dioxide.
ρ_{ref}	critical density of the carbon dioxide (700 kg/m^3).
φ	fugacity coefficient.

compounds and correlationated the experimental data with four semiempirical equations [24] obtaining the maximum accuracy with MST and Bartle models. Sparks et al. [25] evaluated five density-based models with six solids and developed a new model where the prediction of the solubility data is improved compared to other equations. Méndez-Santiago and Teja [26] described a new density-based model and presented the solubility data of 90 compounds (not only pharmaceuticals). The experimental data were fitted with two equations, the MST model in 47 solids and for the rest of solids (43), an equation described by Harvey that requires the sublimation pressures. Finally, Jouyban et al. [27] fitted five semiempirical equations to 106 published solubility data (again, not only pharmaceuticals) obtaining the minimum error with a new correlation, but since 2002 when the article was published, new semiempirical equations have been presented.

Therefore, it is still uncertain which is the best equation to predict more accurately the solubility of pharmaceutical solids in SCFs. In this work, a comparison between the 9 most used semiempirical equations of state have been done (Chrastil's model, VA model, AL model, Sparks's model, MST model, KJ model, Bartle's model, Gordillo's model and Yu's model), presenting also the parameters for each equation. The model developed by Jouyban et al. [27] was not used here because of his low use. Sets of solubility data from 27 pharmaceutical solutes were taken from the literature in order to determine what is the most suitable equation for this kind of compounds or depending on the conditions, what equation should be used. Finally, a brief comparison with Peng-Robinson equation of state was performed indicating some of the main advantages of using semiempirical equations with respect to cubic equations.

2. Review of semiempirical models

Chrastil [28] described one of the first density-based model, based on the solvato complex formed between the solute and solvent molecules at equilibrium (eq. (1))

$$S = \rho_1^k \exp\left(\frac{A}{T} + B\right) \tag{1}$$

Eq. (1) establish a relationship between the solubility of the solute (S in kg m^{-3}) and the pure density of the SCF (ρ_1 in kg m^{-3}).The parameter k is the association number which describes the number of SCF molecules in the solvated complex, A is a function of the entalphy of solvation and enthalpy of vaporization, B depends on the molecular weight of the solute and T is the temperature (K).

Chrastil's equation has some limitations. It is not valid over a wide range of temperatures and for a solubility higher than 100–200 kg m^{-3} [25]. Therefore, the model described by Chrastil underwent several modifications, deriving in different equations.

Adachi and Lu [29] made the parameter k density dependent, achieving a lower error in the prediction of the solubility of different solutes. The AL model is shown in eq. (2):

$$S = \rho_1^{(e_0+e_1\cdot\rho_1+e_2\cdot\rho_1^2)} \exp\left(\frac{A}{T} + B\right) \tag{2}$$

A different modification was proposed by del Valle and Aguilera [30], improving the fit obtained with Chrastil's model in the prediction of the solubility of vegetable oils in sc-CO_2. They took into account the change of the enthalpy of vaporization with the temperature, considering the association number k independent of density. The del Valle and Aguilera's equation (VA) can be expressed as follows:

$$S = \rho_1^k \exp\left(\frac{A}{T} + B + \frac{C}{T^2}\right) \tag{3}$$

The last Chrastil's modification was done by Sparks et al. [25], because there were cases in which AL's equation was better than VA and viceversa. They combinated eq. (2) and eq. (3), considering the effect of the density in the association number k and the change of the enthalpy of vaporization with the temperature. The result was Sparks model (Sparks), described in eq. (4), which improves the results obtained with AL and VA models.

$$S = \rho_1^{(e_0+e_1\cdot\rho_1+e_2\cdot\rho_1^2)} \exp\left(\frac{A}{T} + B + \frac{C}{T^2}\right) \tag{4}$$

Kumar and Johnston [31] proposed a new density-based model (KJ) with a linear relationship between $\ln(y_2)$ and $\ln(\rho_1)$ (eq. (5)). Nevertheless, they showed that their previous relationship or Chrastil's ($\mathrm{Ln}(y_2)$ vs. ρ_1) cannot be generalized and depend on the system.

$$\ln(y_2) = A + B\cdot\rho_1 + \frac{C}{T} \tag{5}$$

In eq. (5), y_2 is the solubility of the solute in the SCF. Is important to realize that, again, the enthalpies of vaporization and solvation are relationed with the parameter C. Appart from the relationships established by Chrastil (and their modifications) or Kumar and Johnston, more density-based models were presented.

Bartle et al. [32] relationed the enhancement factor (ratio of the actual solubility to the ideal solubility) of the solute and the density of the solvent (eq. (6))

$$\ln\left(y_2\cdot\frac{P}{P_2^{sub}}\right) = a + C\cdot\rho_1 \tag{6}$$

Term C is related to the solvation of the solute and a comes from the vapor pressure of the solute, thus [25]:

$$a = A + \frac{B}{T} \tag{7}$$

To solve some of the inconveniences that involve the estimation of the sublimation pressure, Bartle et al. [32] changed the sublimation pressure by a reference pressure. In addition, a corrective term with a reference density should be introduced. Therefore, considering these latest constraints and eq. (7), is possible to describe Bartle's equation as follows:

$$\ln\left(y_2 \cdot \frac{P}{P_{ref}}\right) = A + \frac{B}{T} + C \cdot (\rho_1 - \rho_{ref}) \tag{8}$$

In eq. (8), ρ_{ref} is a reference density, (a value of 700 kg m^{-3} was chosen), and P_{ref} is the reference pressure, typically taken as 1 bar.

Another density-based model was proposed by Méndez-Santiago and Teja [26]. This model comes from the linear relationship between $T\ln(E)$ and ρ_1 (eq. (9)),which was derived from the theory of dilute solutions.

$$T \cdot \ln(E) = A' + B' \cdot \rho_1 \tag{9}$$

E is the enhancement factor and ρ_1 is the density of the solvent. Méndez-Santiago and Teja [26] tested the validity of this expression. However, it is necessary to determine previously the sublimation pressures. Its value is substituted by a Clausius–Clapeyron type expression. Therefore, Méndez-Santiago and Teja's (MST) model results in eq. (10):

$$T \cdot \ln(y_2) = A + B \cdot \rho_1 + C \cdot T \tag{10}$$

Eqs. (1)–(5), (8) and (10) are all density-based models. However, these models do not take into account the pressure in an individual term, and consequently the best results are expected only at isobaric conditions. In this context, according to Yu et al. [33], the solubility shows a curvilinear behaviour with pressure at a constant temperature and with temperature at a constante pressure. In addittion, the solubility is affected by the interaction between pressure and temperature. Hence, these authors proposed by the first time, a model in which pressure and temperature appear as individual terms (Yu). This model can be expressed as follows (eq. (11)):

$$y_2 = A + B \cdot P + C \cdot P^2 + D \cdot P \cdot T \cdot (1 - y_2) + E \cdot T + F \cdot T^2 \tag{11}$$

Gordillo et al. [34] made a modification upon the previous equation to improve the fit in the solubility of Penicillin G in sc-CO_2. Eq. (12) symbolizes the Gordillo's equation:

$$\ln(y_2) = A + B \cdot P + C \cdot P^2 + D \cdot P \cdot T + E \cdot T + F \cdot T^2 \tag{12}$$

3. Methods

To establish which is the best model to predict the solubility of pharmaceutical solids in sc-CO_2, solubility data from 27 compounds of interest were collected from literature. Among these solids, we included anticarcinogenic, antioxidants, different vitamines, aromatase inhibitors and even anti-inflammatories. The details and references are listed in Table 1. It is important to realize that none of the experimental data from the articles were excluded and all published data were considered correct. In order to compare the parameters and the error, we specify the following units: bar (pressure), kg m^{-3} (density and solubility) and Kelvin (temperature). The Newton's method was used to determine the parameters of each equation. Mathematica 6.1 was employed to perform the nonlinear regression analysis between experimental and theoretical data.

4. Results and discussion

Tables 2–10 resume the parameters obtained for each compound with each equation, and their corresponding average absolute relative deviation AARD (eq. (13)). In these tables is possible to observe that the parameter k from Chrastil and VA equations are almost identical. We assumed that the tiny differences are due to limitations in the numerical mathematical tool.

$$\text{AARD}(\%) = \frac{100}{n} \cdot \sum \frac{y_2^{\text{calculated}} - y_2^{\text{experimental}}}{y_2^{\text{experimental}}} \tag{13}$$

Table 1
Details and reference of the solubility of pharmaceutical compounds in sc-CO_2.

No.	Compuesto	N	Pressure (bar)	Temperature (K)	$-\log(y_2)-(-\log(y_1))$	Reference
1	Astaxanthin	26	100–400	313–333	2.08	[35]
2	β-Carotene	23	200–350	313–353	1.55	[36]
3	Cyproterone acetate	40	120–350	308–348	1.29	[37]
4	Exemestane	45	120–350	308–348	2.18	[21]
5	Fluvastatin	45	120–350	308–348	2.08	[24]
6	Letrozole	45	120–350	308–348	1.92	[21]
7	Licopene	20	200–400	323–353	0.42	[38]
8	Lovastatin	45	120–350	308–348	1.02	[24]
9	Medroxyprogesterone Acetate	40	120–350	308–348	1.41	[37]
10	Methimazole	40	120–350	308–348	1.54	[39]
11	2-Methylbenzoic acid	18	110–245	313–333	1.38	[40]
12	3-Methylbenzoic acid	18	110–245	313–333	1.46	[40]
13	4-Methylbenzoic acid	18	110–245	313–333	1.22	[40]
14	Naproxen	18	90–195	313–333	1.22	[41]
15	Nimesulide	8	130–220	312–331	1.07	[42]
16	Nitrendipine	42	100–300	333–373	1.90	[43]
17	Paclitaxel	12	140–345	312–329	0.76	[44]
18	Penicillin G	18	100–350	313–333	1.18	[34]
19	Penicillin V	24	80–280	314–334	1.02	[45]
20	Phenazopyridine	45	120–350	308–348	1.66	[39]
21	Propanolol	45	120–350	308–348	1.83	[39]
22	Retinol	20	200–350	313–353	0.49	[36]
23	Simvastatin	45	120–350	308–348	1.43	[24]
24	Taxol	12	205–475	308–318	0.85	[46]
25	α-Tocopherol	24	200–350	313–353	0.74	[36]
26	Vitamin D-3	14	100–300	313–353	0.80	[47]
27	Vitamin K-1	24	200–350	313–353	1.11	[36]

Table 2
Parameters from Chastil's equation.

No.	k	A	B	AARD (%)
1	4.98	−9531.26	−9.41	52.98
2	9.59	−10209.00	−33.97	26.69
3	10.29	−3949.55	−57.05	24.74
4	7.93	−10058.60	−21.86	30.58
5	9.47	−9160.84	−35.58	14.73
6	7.68	−9791.41	−24.09	38.47
7	1.18	−3314.94	−2.53	5.72
8	3.44	−3767.69	−12.41	5.90
9	8.52	−5716.24	−39.61	18.91
10	6.80	−5619.27	−30.31	12.69
11	5.24	−6642.15	−12.41	2.34
12	5.49	−6263.50	−15.27	3.50
13	4.89	−5609.86	−15.23	2.67
14	4.84	−4750.16	−19.63	9.77
15	7.79	−5338.16	−36.17	14.08
16	4.99	−5489.24	−18.34	15.35
17	1.45	−4064.92	0.30	30.46
18	6.89	−7590.54	−24.60	25.43
19	3.07	−3283.03	−9.42	18.17
20	6.27	−5735.97	−25.76	15.46
21	13.27	−13143.80	−48.82	22.43
22	6.81	−3295.34	−32.93	7.96
23	9.31	−7241.67	−40.18	13.06
24	12.74	−5446.28	−75.18	4.34
25	7.09	−3358.65	−34.48	3.82
26	6.70	−5907.31	−25.36	34.11
27	9.68	−3810.53	−50.59	6.68

Table 11 shows the AARD produced by each equation when is correlated with the different compounds. The lowest error fit is marked with (*). The average AARD for each equation (having in account all the AARD for the different compounds) and their corresponding standard desviation values can be observed in Fig. 1. The first conclusion is that Yu's equation produced the highest error and standar deviation, in line with previous works [21,27]. This error might be due to the fact that this equation is not valid for certain conditions. The model was improved with Gordillo et al. [34], who reduced the AARD from 25.05 to 15.83 and the standar deviation from 26.99 to 11.11.

The other equations provided (in terms of error and standar deviation) similar results. The fits using Chrastil's equation with 3 parameters were improved with its subsequent derivations and the increase in the parameters number, decreasing the AARD from 17.07 to 12.26. It is important to realize that with some compounds like β-carotene or exemestane, the VA's equation with 4 parameters provided a better fit than AL's equation with 5 parameters. This is because the effect of the temperature was not compensated. Trying to solve this problem, Sparks et al. [25] merged AL and VA equations, removing inconvenients related to the temperature and decreasing the AARD in the prediction. Also, it must be noticed that

Table 3
Parameters from del Valle and Aguilera's equation.

No.	k	A	B	C	AARD (%)
1	5.02	−67486.40	79.49	9.41×10^6	55.67
2	9.51	36783.70	−102.67	-7.96×10^6	12.24
3	10.37	−16060.80	−38.91	1.96×10^6	24.73
4	7.89	24573.60	−73.21	-5.80×10^6	18.60
5	9.48	−14347.50	−27.89	862149.00	14.59
6	7.65	8557.82	−51.26	-3.07×10^6	38.99
7	1.18	−29737.60	36.37	4.48×10^6	4.42
8	3.43	411.15	−18.72	−687045.00	5.78
9	8.95	−26613.10	−8.28	3.43×10^6	17.10
10	6.81	−13879.50	−17.89	1.36×10^6	12.34
11	5.25	−24269.60	14.76	2.85×10^6	2.26
12	5.50	−23429.90	11.20	2.78×10^6	3.20
13	4.89	−17560.80	3.20	1.93×10^6	2.49
14	4.83	101.16	−27.09	−781925.00	9.74
15	7.79	−654873.00	972.00	1.04×10^8	14.06
16	5.09	−27402.10	12.10	3.85×10^6	14.13
17	1.41	−97332.00	146.14	1.49×10^7	29.37
18	6.91	81318.20	−161.79	-1.44×10^7	26.00
19	3.07	−3446.39	−9.17	26524.90	18.13
20	6.30	−12625.50	−15.45	1.13×10^6	15.71
21	13.43	−50306.20	5.57	6.22×10^6	18.14
22	6.92	3495.31	−43.84	-1.14×10^6	7.97
23	9.35	−15671.20	−27.69	1.39×10^6	12.74
24	12.75	−116992.00	102.92	1.75×10^7	3.58
25	7.09	−4086.76	−33.40	120118.00	3.78
26	6.75	−10202.30	−19.24	711598.00	34.30
27	9.74	−12497.10	−37.84	1.43×10^6	5.98

Table 4
Parameters from Adachi-Lu's equation.

No.	e_0	e_1	e_2	A	B	AARD (%)
1	189.74	−0.07	2.57×10^{-5}	−10914.40	−982.21	41.33
2	−115.21	0.46	-1.74×10^{-5}	−9789.61	625.62	25.85
3	−10.98	4.71×10^{-3}	-9.04×10^{-7}	−4140.42	64.37	15.57
4	−16.37	9.05×10^{-3}	-3.40×10^{-6}	−9953.07	106.42	36.43
5	−8.74	6.00×10^{-3}	-2.03×10^{-6}	−9224.62	62.81	9.31
6	156.42	−0.05	1.50×10^{-5}	−8756.60	−834.29	28.79
7	22.44	-8.72×10^{-3}	3.54×10^{-6}	−3527.40	−112.61	4.50
8	−0.39	1.99×10^{-3}	-9.31×10^{-7}	−3601.68	6.05	4.38
9	−2.19	1.85×10^{-3}	6.62×10^{-8}	−6010.22	23.25	11.12
10	−5.02	3.58×10^{-3}	-1.09×10^{-6}	−5734.22	34.48	10.43
11	1.34	1.57×10^{-3}	-6.30×10^{-7}	−6617.89	7.91	3.02
12	−2.50	3.28×10^{-3}	-1.33×10^{-6}	−6198.49	26.17	5.53
13	2.69	7.76×10^{-4}	-2.76×10^{-7}	−5626.69	−3.48	1.53
14	11.59	-3.64×10^{-3}	1.81×10^{-6}	−5026.36	−52.17	8.93
15	106.38	−0.04	1.91×10^{-5}	−6212.88	−539.20	6.35
16	8.25	2.52×10^{-3}	1.54×10^{-6}	−5879.12	−32.00	14.01
17	105.93	-4.17×10^{-3}	1.65×10^{-5}	−5365.57	−541.87	18.97
18	−21.54	0.01	-4.34×10^{-6}	−7314.54	123.35	21.17
19	7.75	-3.39×10^{-3}	1.88×10^{-6}	−3883.37	−28.79	5.99
20	50.86	-1.48×10^{-3}	4.99×10^{-6}	−5547.62	−266.57	21.40
21	−9.66	3.05×10^{-3}	5.16×10^{-7}	−14163.30	88.87	19.68
22	−30.74	0.01	-4.02×10^{-6}	−3514.26	170.60	6.66
23	25.19	-5.60×10^{-3}	2.01×10^{-6}	−7273.29	−124.87	14.80
24	−146.57	0.05	-1.49×10^{-5}	−5262.65	796.75	4.36
25	−18.26	8.36×10^{-3}	-2.80×10^{-6}	−3467.30	102.53	3.39
26	−5.60	3.19×10^{-3}	-6.92×10^{-7}	−6373.97	44.13	27.39
27	48.73	−0.02	5.88×10^{-6}	−3908.68	−254.95	3.69

with several compounds (cyproterone acetate, letrozole or methimazole amongst others) AL equation provided a slightly better fit than the obtained with Sparks' equation. These can be explained in part because of the mathematica tool numerical error and the lower effect of the temperature in the studied range of these compounds.

In some compounds (taxol and 2-methylbenzoic acid), Chrastil's equation correlationated slightly better with the experimental data than some of its derivatives. In this case, a good fit was also obtained with all Chrastil's derivatives. The effect of adding more parameters did not significantly improved the AARD.

MST and Bartle equations provided similar results in terms of AARD and standard deviations. They improved Chrastil's equation with the same number of parameters, but the fit was worse compared to AL and Sparks equations and similar to VA. According to Méndez-Santiago and Teja [26], the error produced with his equation is due to limitations at lower densities. Bartle's equation with only two parameters was applied only with isotherms. Actually, the author did not take into account the effect of the temperature [32]. Nevertheless, in this article, the proposed equation had one more parameter to solve this problem, but the results are worse than AL, Sparks and KJ equations.

Table 5
Parameters from Sparks' equation.

No.	e_0	e_1	e_2	A	B	C	AARD (%)
1	184.38	-6.70×10^{-3}	2.51×10^{-5}	−65557.4	−869.45	8.87×10^{6}	43.07
2	−47.66	0.02	-7.61×10^{-6}	30261.00	210.83	-6.84×10^{6}	13.08
3	−13.24	5.74×10^{-3}	-1.33×10^{-6}	−9025.10	83.31	796058.00	16.21
4	4.15	4.78×10^{-4}	1.13×10^{-7}	27275.20	−54.99	-6.29×10^{6}	14.88
5	−17.49	9.50×10^{-3}	-3.40×10^{-6}	−17366.60	120.65	1.37×10^{6}	10.64
6	208.24	−0.07	2.19×10^{-5}	8770.28	−1135.97	-2.96×10^{6}	29.37
7	17.29	-6.63×10^{-3}	2.70×10^{-6}	−24936.40	−54.24	3.64×10^{6}	3.60
8	0.086	1.78×10^{-3}	-8.45×10^{-7}	−1842.49	0.93	−290441.00	4.27
9	−11.82	5.97×10^{-3}	-1.76×10^{-6}	−24831.30	100.61	3.03×10^{6}	10.57
10	−8.44	5.06×10^{-3}	-1.71×10^{-6}	−14072.80	64.68	1.38×10^{6}	10.95
11	−1.38	2.75×10^{-3}	-1.12×10^{-6}	−26971.60	53.27	3.30×10^{6}	3.74
12	−5.39	4.54×10^{-3}	-1.86×10^{-6}	−28055.90	74.71	3.54×10^{6}	5.85
13	1.09	1.47×10^{-3}	-5.67×10^{-7}	−18481.20	24.60	2.08×10^{6}	1.78
14	14.76	-5.07×10^{-3}	2.44×10^{-6}	10738.30	−92.78	-2.54×10^{6}	8.58
15	106.38	−0.04	1.91×10^{-5}	−330517.0	356.07	1.09×10^{6}	5.63
16	2.91	1.64×10^{-4}	2.54×10^{-7}	−24182.50	20.60	3.23×10^{6}	12.58
17	106.41	−0.04	1.64×10^{-5}	−57059.70	−464.02	8.28×10^{6}	18.90
18	−17.67	9.23×10^{-3}	-3.47×10^{-6}	75897.20	−23.90	-1.35×10^{7}	20.47
19	7.93	-3.48×10^{-3}	1.93×10^{-6}	6640.22	−45.87	-1.71×10^{6}	6.24
20	30.09	-7.33×10^{-3}	2.27×10^{-6}	−13788.00	−143.68	1.37×10^{6}	20.92
21	−29.81	0.01	-3.93×10^{-6}	−47108.60	237.81	5.63×10^{6}	18.17
22	−51.95	0.02	-6.46×10^{-6}	17568.5	253.03	-3.54×10^{6}	5.32
23	−5.85	5.63×10^{-3}	-2.10×10^{-6}	−18444.30	56.88	1.86×10^{6}	8.93
24	−205.39	0.06	-2.03×10^{-5}	−122602.0	1307.27	1.84×10^{7}	3.13
25	−17.90	8.22×10^{-3}	-2.75×10^{-6}	−3249.66	100.33	−36022.8	3.37
26	−4.90	2.76×10^{-3}	-4.74×10^{-7}	−2439.93	35.01	−662116.00	27.08
27	53.95	−0.02	6.60×10^{-6}	−1104.78	−286.78	−462088.00	3.64

Table 6
Parameters from MST's equation.

No.	A	B	C	AARD (%)
1	−14235.80	2.95	27.27	52.72
2	−16552.90	5.14	28.59	34.63
3	−10478.20	5.14	15.64	22.91
4	−15639.50	4.33	34.45	32.68
5	−15489.20	5.02	31.27	14.30
6	−14765.20	3.96	29.71	20.49
7	−6272.55	1.27	7.57	7.84
8	−7613.82	2.32	13.23	5.37
9	−11721.90	4.54	21.17	16.23
10	−10899.00	3.82	19.71	10.99
11	−11333.40	3.02	27.00	4.35
12	−11058.10	3.13	26.05	5.04
13	−10124.70	2.83	21.93	3.78
14	−8802.68	2.64	15.72	10.41
15	−10222.30	4.11	17.65	12.59
16	−9755.48	3.26	11.88	14.91
17	−8219.08	1.58	14.64	31.23
18	−12995.70	3.82	25.35	25.22
19	−6671.97	1.80	13.75	16.59
20	−11857.10	4.03	22.08	9.21
21	−20684.90	6.57	43.88	21.69
22	−8537.03	3.82	16.11	8.30
23	−13566.80	4.93	25.82	10.95
24	−13095.40	5.87	14.92	3.53
25	−8911.22	4.04	16.46	3.91
26	−9207.14	2.79	18.69	29.84
27	−10374.5	5.12	18.06	5.05

The last density model, the equation developed by Kumar and Johnston provided the best fit compared to the other equations with also three parameters. It showed that in general, the linear relationship established by Kumar and Johnston is more adecquate in this kind of compounds than the proposed by Chrastil [28], but the AARD obtained with VA, AL and Sparks equations was not reduced using KJ's model.

The main conclusion obtained from Table 11 and Fig. 1 is that the best semiempirical model is the equation developed by Sparks. This equation is the only one that considers the effect of the temperature in the enthalpy of vaporization and the change of the association number k with the density.

It is important to notice that in Table 1, for 9 of the 27 compounds, Gordillo's model provides the best fit, so that at certain conditions, this equation should be employed instead of Sparks' equation. To define the conditions in which Gordillo's model provides the best fit, a division criterion was established. The experimental data was separated according to the values of $-\log(y_2)-(-\log(y_1))$, taking arbitrarily 1.41 as a reference value. This parameter has been chosen because changes in pressure and

Table 7
Parameters from KJ's equation.

No.	A	B	C	AARD (%)
1	11.57	4.79×10^{-3}	−9793.90	49.56
2	8.23	0.01	−10529.40	29.57
3	−5.82	0.01	−3950.25	19.77
4	15.94	9.04×10^{-3}	−10289.50	30.22
5	10.92	0.01	−9469.27	11.81
6	12.17	8.13×10^{-3}	−9784.36	21.98
7	−3.72	2.36×10^{-4}	−3426.10	5.84
8	−0.66	3.60×10^{-3}	−3962.64	9.80
9	1.56	9.37×10^{-3}	−5904.33	14.63
10	2.01	7.46×10^{-3}	−5796.55	9.56
11	10.83	6.00×10^{-3}	−6908.56	8.02
12	9.36	6.28×10^{-3}	−6511.01	9.72
13	5.96	5.46×10^{-3}	−5837.64	6.55
14	0.78	5.85×10^{-3}	−5085.12	11.36
15	0.46	9.25×10^{-3}	−5522.70	8.59
16	2.27	6.52×10^{-3}	−5883.62	18.51
17	0.81	9.66×10^{-4}	−4481.08	26.60
18	7.29	7.28×10^{-3}	−7725.95	24.36
19	0.68	2.96×10^{-3}	−3517.06	11.49
20	3.99	8.10×10^{-3}	−6622.55	8.14
21	19.80	0.02	−13297.30	21.08
22	−1.48	7.37×10^{-3}	−3433.39	7.18
23	5.48	0.01	−7544.12	13.68
24	−9.36	0.01	−5523.55	3.81
25	−1.71	7.92×10^{-3}	−3586.69	3.38
26	3.67	5.92×10^{-3}	−5186.53	29.85
27	−2.97	0.01	−4021.79	5.23

Table 8
Parameters from Bartle's equation.

No.	A	B	C	AARD (%)
1	25.73	−11665.50	8.91×10^{-3}	56.29
2	26.37	−12175.70	0.01	31.03
3	13.21	−6081.47	0.02	23.40
4	32.54	−11947.00	0.01	32.06
5	28.89	−11165.20	0.02	11.42
6	27.97	−11394.10	0.01	17.38
7	7.14	−5230.80	3.64×10^{-3}	8.61
8	12.29	−5676.49	6.89×10^{-3}	4.19
9	19.02	−7814.86	0.01	17.24
10	18.00	−7646.63	0.011	12.43
11	26.24	−8903.79	9.22×10^{-3}	4.44
12	25.04	−8533.78	9.59×10^{-3}	4.81
13	21.05	−7855.41	8.66×10^{-3}	4.20
14	15.47	−6866.06	8.13×10^{-3}	11.80
15	16.66	−7021.02	0.01	14.58
16	16.68	−7394.01	8.96×10^{-3}	15.11
17	14.01	−6904.57	4.81×10^{-3}	31.92
18	23.34	−9662.91	0.01	25.90
19	13.32	−5270.04	5.48×10^{-3}	16.17
20	20.21	−8395.76	0.01	10.94
21	30.78	−11317.20	0.01	20.75
22	14.70	−5374.74	0.01	8.95
23	23.42	−9299.93	0.014	9.15
24	9.93	−7426.40	0.02	4.71
25	14.76	−5500.98	0.01	4.46
26	17.59	−6684.34	7.94×10^{-3}	30.15
27	15.83	−6035.3	0.02	6.54

temperature affect the molar fraction. Using a plot of the solubility of naphthalene in sc-CO_2 at several temperatures (Fig. 2), McHugh and Paulaitis [48] illustrated the solubility behaviour of a solid in sc-CO_2. At temperatures near the critical temperature of CO_2, an increase in pressure involves an increase in the solubility until a certain value is reached (this curve follows Chrastil's relationship log solubility vs pressure). This value remains almost constant with additional pressure changes. If the temperature increases, the change in solubility with pressure becomes more drastic, but it seems that a constant solubility value is systematically achieved, even with an increase in pressure (vertical asymptote). Finally, at a certain temperature (closer to the melting point), the solubility increases significantly, suggesting the existence of an upper critical end point (UCEP). Therefore, Chrastil's relationship is not valid and a modification is needed. Considering the differences in the molar fraction, it was possible to take into account pressure as well as temperature, distinguishing different situations.

In Table 12 and Fig. 3 are showed, respectively, the values of AARD for each equation for each compound and the average values of AARD for each equation when $-\log(y_2)-(-\log(y_1)) \leq 1.41$. On the other hand, Table 13 and Fig. 4 represents, respectively, the values of AARD for each equation for each compound and the average values of AARD for each equation when the parameter is >1.41.

Table 9
Parameters from Yu's equation.

No.	A	B	C	D	E	F	AARD (%)
1	1.26×10^{-4}	-3.70×10^{-8}	-1.79×10^{-13}	1.22×10^{-10}	-7.81×10^{-7}	1.21×10^{-9}	33.06
2	4.58×10^{-5}	-1.50×10^{-7}	1.95×10^{-11}	4.43×10^{-10}	-1.90×10^{-7}	1.55×10^{-10}	21.19
3	2.28×10^{-3}	1.78×10^{-8}	4.32×10^{-9}	-3.69×10^{-9}	-1.31×10^{-5}	1.98×10^{-8}	22.92
4	0.04	-6.75×10^{-5}	6.52×10^{-9}	2.07×10^{-7}	-2.17×10^{-4}	2.84×10^{-7}	98.55
5	9.73×10^{-4}	-2.02×10^{-5}	3.66×10^{-9}	6.01×10^{-8}	-4.94×10^{-5}	6.01×10^{-8}	56.86
6	1.52×10^{-3}	-2.79×10^{-6}	1.52×10^{-10}	8.69×10^{-9}	-8.14×10^{-6}	1.06×10^{-8}	54.27
7	7.46×10^{-3}	1.73×10^{-8}	-5.89×10^{-12}	-3.91×10^{-11}	-4.84×10^{-7}	7.82×10^{-10}	3.12
8	1.18×10^{-4}	-2.58×10^{-6}	-7.13×10^{-10}	9.57×10^{-9}	4.89×10^{-7}	-2.93×10^{-9}	8.55
9	3.87×10^{-3}	-9.51×10^{-6}	2.79×10^{-9}	2.85×10^{-8}	-1.84×10^{-5}	2.01×10^{-8}	15.70
10	1.06×10^{-3}	-5.05×10^{-6}	5.26×10^{-10}	1.61×10^{-8}	-3.87×10^{-6}	1.75×10^{-9}	15.29
11	0.14	-4.74×10^{-4}	-5.48×10^{-8}	1.62×10^{-6}	-7.01×10^{-4}	7.44×10^{-7}	11.36
12	0.21	-3.00×10^{-4}	2.04×10^{-8}	9.85×10^{-7}	-1.20×10^{-3}	1.68×10^{-6}	17.09
13	0.01	-4.72×10^{-5}	-9.62×10^{-9}	1.67×10^{-7}	-5.31×10^{-5}	4.56×10^{-8}	3.30
14	-8.39×10^{-4}	-2.50×10^{-6}	-7.13×10^{-10}	9.31×10^{-9}	6.36×10^{-6}	-1.20×10^{-8}	6.27
15	4.49×10^{-4}	-6.25×10^{-6}	1.17×10^{-9}	2.07×10^{-8}	-6.35×10^{-8}	-4.70×10^{-9}	4.72
16	1.75×10^{-3}	-2.92×10^{-6}	1.07×10^{-9}	8.10×10^{-9}	-8.68×10^{-6}	1.05×10^{-8}	21.53
17	3.88×10^{-4}	3.70×10^{-7}	-1.96×10^{-11}	-1.10×10^{-9}	-2.86×10^{-6}	5.16×10^{-9}	4.66
18	-2.64×10^{-4}	-2.83×10^{-6}	5.54×10^{-11}	9.20×10^{-9}	2.72×10^{-6}	-6.01×10^{-9}	23.43
19	2.35×10^{-3}	-9.15×10^{-6}	-5.97×10^{-9}	4.14×10^{-8}	-1.30×10^{-5}	1.56×10^{-8}	6.68
20	2.35×10^{-3}	-5.97×10^{-6}	5.82×10^{-10}	1.89×10^{-8}	-1.14×10^{-5}	1.26×10^{-8}	17.97
21	0.05	-7.36×10^{-5}	1.88×10^{-8}	2.08×10^{-7}	-2.96×10^{-4}	3.99×10^{-7}	71.02
22	−0.05	-3.03×10^{-5}	-2.32×10^{-8}	1.87×10^{-7}	3.53×10^{-4}	-6.12×10^{-7}	6.73
23	4.00×10^{-3}	-1.61×10^{-5}	3.32×10^{-9}	4.84×10^{-8}	-1.57×10^{-5}	1.07×10^{-8}	95.20
24	3.17×10^{-5}	-1.00×10^{-8}	1.34×10^{-11}	3.36×10^{-11}	-1.96×10^{-7}	3.00×10^{-10}	3.12
25	0.04	3.97×10^{-5}	1.62×10^{-7}	-3.64×10^{-7}	-2.63×10^{-4}	5.60×10^{-7}	29.33
26	−0.04	-5.81×10^{-5}	2.72×10^{-8}	1.51×10^{-7}	2.48×10^{-4}	-4.10×10^{-7}	20.31
27	-5.22×10^{-3}	-2.11×10^{-5}	3.23×10^{-8}	6.28×10^{-8}	6.58×10^{-5}	-1.54×10^{-7}	3.75

Table 10
Parameters from Gordillo's equation.

No.	A	B	C	D	E	F	AARD (%)
1	20.57	0.083	-1.89×10^{-5}	-2.04×10^{-4}	−0.41	8.45×10^{-4}	25.45
2	−136.68	−0.13	1.40×10^{-5}	3.83×10^{-3}	0.78	-1.24×10^{-3}	22.55
3	−4.08	−0.04	-5.21×10^{-6}	1.49×10^{-4}	$5.79 \cdot 10^{-3}$	-9.04×10^{-5}	5.52
4	−108.36	−0.02	-4.16×10^{-5}	1.50×10^{-4}	0.56	-8.22×10^{-4}	35.99
5	−41.24	−0.04	-3.91×10^{-5}	2.08×10^{-4}	0.18	-3.15×10^{-4}	20.47
6	−89.49	−0.06	-5.12×10^{-5}	2.79×10^{-4}	0.47	-7.45×10^{-4}	27.11
7	5.63	0.02	-4.94×10^{-6}	-5.07×10^{-4}	−0.16	3.01×10^{-4}	2.46
8	−33.20	−0.03	-2.51×10^{-5}	1.33×10^{-4}	0.14	-2.45×10^{-4}	12.53
9	−1.94	−0.02	-2.94×10^{-5}	1.41×10^{-4}	−0.04	1.97×10^{-5}	6.90
10	−22.31	−0.03	-2.90×10^{-5}	1.53×10^{-4}	0.08	-1.55×10^{-4}	11.90
11	−12.42	−0.08	-9.11×10^{-5}	3.81×10^{-4}	0.06	-1.67×10^{-4}	17.08
12	−20.12	−0.08	-9.18×10^{-5}	4.04×10^{-4}	0.11	-2.71×10^{-4}	19.16
13	−15.51	−0.07	-8.33×10^{-5}	3.42×10^{-4}	0.07	-1.78×10^{-4}	14.50
14	−50.61	−0.08	-2.00×10^{-4}	4.92×10^{-4}	0.28	-5.53×10^{-4}	15.63
15	1848.47	0.02	-1.49×10^{-4}	1.66×10^{-4}	−11.58	0.018	14.51
16	5.79	−0.01	-4.46×10^{-5}	1.26×10^{-4}	−0.10	1.18×10^{-4}	25.20
17	−28.01	0.12	-7.67×10^{-6}	-3.62×10^{-4}	$-4.42 \cdot 10^{-3}$	2.79×10^{-4}	7.04
18	−178.36	−0.02	-3.73×10^{-5}	1.44×10^{-4}	1.01	-1.56×10^{-3}	13.39
19	−20.25	0.02	-4.22×10^{-5}	1.19×10^{-5}	0.05	-5.04×10^{-5}	16.10
20	−24.32	−0.02	-3.72×10^{-5}	1.43×10^{-4}	0.08	-1.44×10^{-4}	13.09
21	−8.24	−0.09	1.16×10^{-6}	$2.89 \cdot \times 10^{-4}$	0.02	-8.25×10^{-5}	12.99
22	−40.34	$-2.83 \cdot 10^{-4}$	-3.81×10^{-5}	9.38×10^{-5}	0.21	-3.53×10^{-4}	3.90
23	−27.91	−0.04	-3.35×10^{-5}	2.16×10^{-4}	0.13	-2.57×10^{-4}	52.79
24	107.50	$-6.08 \cdot 10^{-3}$	-1.51×10^{-5}	7.36×10^{-5}	−0.79	1.24×10^{-3}	1.50
25	−18.54	−0.02	-2.74×10^{-5}	1.24×10^{-4}	0.09	-1.90×10^{-4}	3.49
26	−82.60	−0.09	2.77×10^{-5}	2.41×10^{-4}	0.49	-8.06×10^{-4}	17.64
27	−9.18	0.02	-2.37×10^{-5}	1.17×10^{-4}	0.03	-1.19×10^{-4}	8.56

Fig. 4 proves that when the parameter is >1.41 Sparks' equation provides the best fit (the one with the AARD lower than 20%) because the higher temperature is close to an UCEP. A large increase in the solubility is produced, so that it was important to consider the changes in the enthalpy of vaporization with temperature. Because of that, a more accuracy correlation is obtained with VA's equation in comparison with AL's equation. The worst fit was clearly with Yu's equation (with a value of AARD of 45%), showing that this model is not valid at these conditions because it was not able to take into account the great increase in the solubility.

When the parameter is ≤1.41 (Table 12 and Fig. 3) all equations provided better results than >1.41 (Table 13 and Fig. 4). This situation suggested that the main problems were when the UCEP or its proximities are reached. Four equations provided an AARD around 10% (AL with 8.39%, Sparks with 8.14%, Gordillo with 9.82% and Yu with 10.03%). Again, Sparks' model gave the more accurate prediction, although the AARD is very similar to the obtained with AL's

Table 11
AARD (%) of each equation with each pharmaceutical compound.

N	Chrastil	VA	AL	Sparks	MST	KJ	Bartle	Yu	Gordillo
1	52.98	55.67	41.33	43.07	52.72	49.56	56.29	33.06	25.45*
2	26.69	12.24*	25.85	13.08	34.63	29.57	31.03	21.29	22.55
3	24.74	24.73	15.57	16.21	22.91	19.77	23.40	22.92	5.52*
4	30.58	18.60	36.43	14.88*	32.68	30.22	32.06	98.55	35.99
5	14.73	14.59	9.31*	10.64	14.30	11.81	11.42	56.85	20.47
6	38.47	38.99	28.79	29.37	20.49	21.98	17.38*	54.27	27.11
7	5.72	4.42	4.50	3.60	7.84	5.84	8.61	3.12	2.46*
8	5.90	5.78	4.38	4.27	5.37	9.80	4.19*	8.55	12.53
9	18.91	17.10	11.12	10.57	16.23	14.63	17.24	15.70	6.90*
10	12.69	12.34	10.43	10.95	10.99	9.56*	12.43	15.29	11.90
11	2.34	2.26*	3.02	3.74	4.35	8.02	4.44	11.36	17.08
12	3.50	3.20*	5.53	5.85	5.04	9.72	4.81	17.09	19.16
13	2.67	2.49	1.53*	1.78	3.78	6.55	4.20	3.30	14.50
14	9.77	9.74	8.93	8.58	10.41	11.36	11.80	6.27*	15.63
15	14.08	14.06	6.35	5.63	12.59	8.59	14.58	4.72*	14.51
16	15.35	14.13	14.01	12.58*	14.91	18.51	15.11	21.53	25.20
17	30.46	29.37	18.97	18.90	31.23	26.60	31.92	4.66*	7.04
18	25.43	26.00	21.17	20.47	25.22	24.36	25.90	23.43	13.39*
19	18.17	18.13	5.99*	6.24	16.59	11.49	16.17	6.68	16.10
20	15.46	15.71	21.40	20.92	9.21	8.14*	10.94	17.97	13.09
21	22.43	18.14	19.68	18.17	21.69	21.08	20.75	71.02	12.99*
22	7.96	7.97	6.66	5.32	8.30	7.18	8.95	6.73	3.90*
23	13.06	12.74	14.80	8.93*	10.95	13.68	9.15	95.20	52.79
24	4.34	3.58	4.36	3.13	3.53	3.81	4.71	3.12	1.50*
25	3.82	3.78	3.39	3.37*	3.91	3.38	4.46	29.33	3.49
26	34.11	34.30	27.39	27.08	29.84	29.85	30.15	20.31	17.64*
27	6.68	5.98	3.69	3.64*	5.05	5.23	6.54	3.75	8.56
$\bar{X}$	17.08	15.78	13.87	12.26*	16.10	15.56	16.24	25.04	15.83
S.D.	12.64	12.61	10.82	10.82*	12.08	10.78	12.18	26.99	11.11

Table 12
AARD (%) of each equation with each pharmaceutical compound with $-\log(y_2)-(-\log(y_1))\leq 1.41$.

N	Chrastil	VA	AL	Sparks	MST	KJ	Bartle	Yu	Gordillo
3	24.74	24.73	15.57	16.21	22.91	19.77	23.40	22.92	5.52*
7	5.72	4.42	4.50	3.60	7.84	5.84	8.61	3.12	2.46*
8	5.90	5.78	4.38	4.27	5.37	9.80	4.19*	8.55	12.53
9	18.91	17.10	11.12	10.57	16.23	14.63	17.24	15.70	6.90*
11	2.34	2.26*	3.02	3.74	4.35	8.02	4.44	11.36	17.08
13	2.67	2.49	1.53*	1.78	3.78	6.55	4.20	3.30	14.50
14	9.77	9.74	8.93	8.58	10.41	11.36	11.80	6.27*	15.63
15	14.08	14.06	6.35	5.63	12.59	8.59	14.58	4.72*	14.51
17	30.46	29.37	18.97	18.90	31.23	26.60	31.92	4.66*	7.04
18	25.43	26.00	21.17	20.47	25.22	24.36	25.90	23.43	13.39*
19	18.17	18.13	5.99*	6.24	16.59	11.49	16.17	6.68	16.10
22	7.96	7.97	6.66	5.32	8.30	7.18	8.95	6.73	3.90*
24	4.34	3.58	4.36	3.13	3.53	3.81	4.71	3.12	1.50*
25	3.82	3.78	3.39	3.37*	3.91	3.38	4.46	29.33	3.49
26	34.11	34.30	27.39	27.08	29.84	29.85	30.15	20.31	17.64*
27	6.68	5.98	3.69	3.64*	5.05	5.23	6.54	3.75	8.56
$\bar{X}$	12.64	12.25	8.39	8.14*	12.13	11.47	12.76	10.03	9.82
S.D.	10.52	10.59	7.61	7.61	9.64	8.41	9.66	8.65	5.69*

Table 13
AARD (%) of each equation with each pharmaceutical compound with $-\log(y_2)-(-\log(y_1))>1.41$.

N	Chrastil	VA	AL	Sparks	MST	KJ	Bartle	Yu	Gordillo
1	52.98	55.67	41.33	43.07	52.72	49.56	56.29	33.06	25.45*
2	26.69	12.24*	25.85	13.08	34.63	29.57	31.03	21.19	22.55
4	30.58	18.60	36.43	14.88*	32.68	30.22	32.06	98.55	35.99
5	14.73	14.59	9.31*	10.64	14.30	11.81	11.42	56.85	20.47
6	38.47	38.99	28.79	29.37	20.49	21.98	17.38*	54.27	27.11
10	12.69	12.34	10.43	10.95	10.99	9.56*	12.43	15.29	11.90
12	3.50	3.20*	5.53	5.85	5.04	9.72	4.81	17.09	19.16
16	15.35	14.13	14.01	12.58*	14.91	18.51	15.11	21.53	25.20
20	15.46	15.71	21.40	20.92	9.21	8.14*	10.94	17.97	13.09
21	22.43	18.14	19.68	18.17	21.69	21.08	20.75	71.02	12.99*
23	13.06	12.74	14.80	8.93*	10.95	13.68	9.15	95.20	52.79
$\bar{X}$	22.36	19.67	20.69	17.13*	20.69	20.34	20.12	45.64	24.25
S.D.	14.05	14.74	11.45	10.75	14.16	12.40	14.75	31.52	11.87*

model. In this case, the most important effect is the change in the parameter *k*. Nevertheless, it should be notice that in 7 of the 16 pharmaceutical compounds the best fit is obtained with Gordillo's model, which requires a new sub-division.

The new criterion (classifiying the data shown in Table 12) was to consider the temperature range and the final temperature whithin the fits are more adecquate. A final temperature value around 350 K was established. This is explained because in several occasions the vicinities of the UCEP were not reached, but depending on the temperature, the shape of the solubility curve is in between the UCEP and the Chrastil's shapes (curve at 328 K in Fig. 2). According to Table 14 and Fig. 5, when a wide temperature range is presented (with a final temperature higher than 348 K), all equations produce an AARD higher than 10% except the Gordillo's model where the AARD is reduced to 7.54%. Also, it is observed how Sparks's and AL's model provided again a similar AARD (11.02% and 10.60%) reducing considerably the values obtained with Chrastil and VA (15.28% and 14.62%). Consequently, the change in the

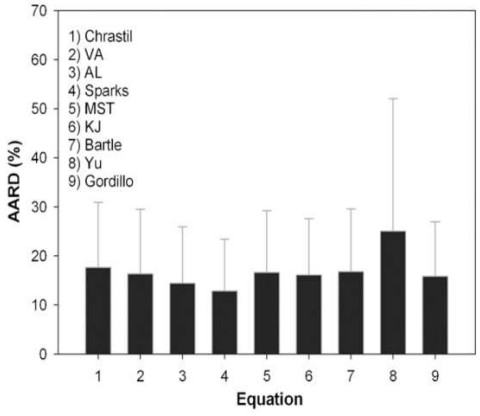

Fig. 1. Mean AARD with their corresponding standard deviations.

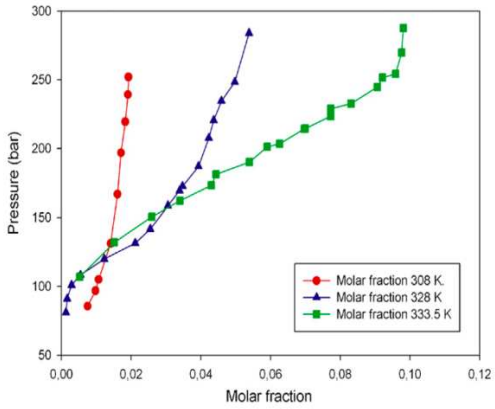

Fig. 2. Solubility of naphtalene in sc-CO_2 at different temperatures (experimental data from McHugh and Paulaitis [48]).

Table 14
Mean AARD and standard deviations with $-\log(y_2)-(-\log(y_1)) \leq 1.41$ (wide ΔT or wide ΔP with high initial P).

N	Chrastil	VA	AL	Sparks	MST	KJ	Bartle	Yu	Gordillo
3	24.74	24.73	15.57	16.21	22.91	19.77	23.40	22.92	5.52*
7	5.72	4.42	4.50	3.60	7.84	5.84	8.61	3.12	2.46*
8	5.90	5.78	4.38	4.27	5.37	9.80	4.19*	8.55	12.53
9	18.91	17.10	11.12	10.57	16.23	14.63	17.24	15.70	6.90*
17	30.46	29.37	18.97	18.90	31.23	26.60	31.92	4.66*	7.04
18	25.43	26.00	21.17	20.47	25.22	24.36	25.90	23.43	13.39*
22	7.96	7.97	6.66	5.32	8.30	7.18	8.95	6.73	3.90*
24	4.34	3.58	4.36	3.13	3.53	3.81	4.71	3.12	1.50*
25	3.82	3.78	3.39	3.37*	3.91	3.38	4.46	29.33	3.49
26	34.11	34.30	27.39	27.08	29.84	29.85	30.15	20.31	17.64*
27	6.68	5.98	3.69	3.64*	5.05	5.23	6.54	3.75	8.56
$\bar{X}$	15.28	14.82	11.02	10.60	14.49	13.68	15.10	12.87	7.54*
S.D.	11.76	11.76	8.47	8.62	10.92	9.87	10.92	9.71	5.09*

parameter k should be considered. It can be observed that Table 14 includes the compounds 17, 18 and 24. For these compounds, the data were in a narrow temperature range, being the final temperature around 330 K. These solids were included in this category because the pressure range and final pressure are very high (475 bar for 24, 350 bar for 18 and 345 bar for 17). These large values correspond to those conditions where Gordillo's equation fitted better to the experimental data.

However, for $-\log(y_2)-(-\log(y_1)) \leq 1.41$, with small temperature range and a final temperature lower than 348 K, the best equations were Sparks' and AL's model (AARD 5.03% and 5.04% respectively). It seems obvious that in these cases, the most important issue is to consider the change in the parameter k instead of temperature (Table 15 and Fig. 6). The worst results are obtained with Gordillo's equation, showing that this model is only suitable at certain specific conditions.

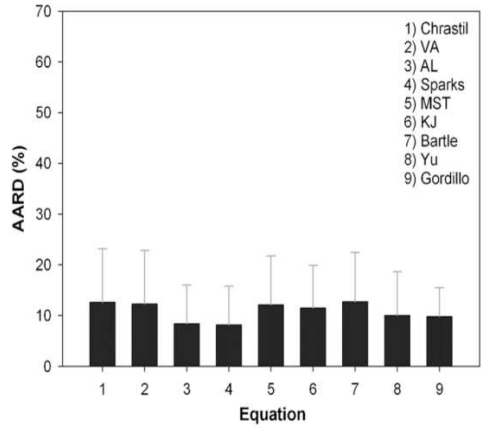

Fig. 3. Mean AARD with their corresponding standard deviations for $-\log(y_2)-(-\log(y_1)) \leq 1.41$.

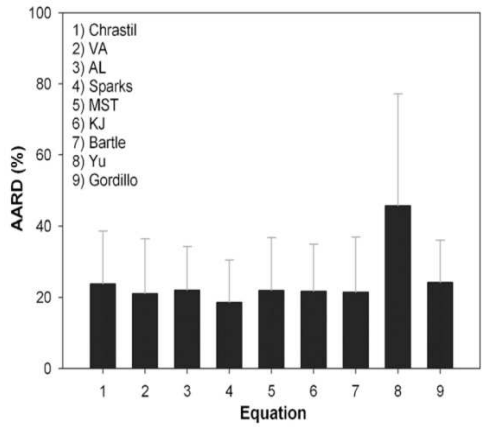

Fig. 4. Mean AARD with their corresponding standard deviations for $-\log(y_2)-(-\log(y_1)) > 1.41$.

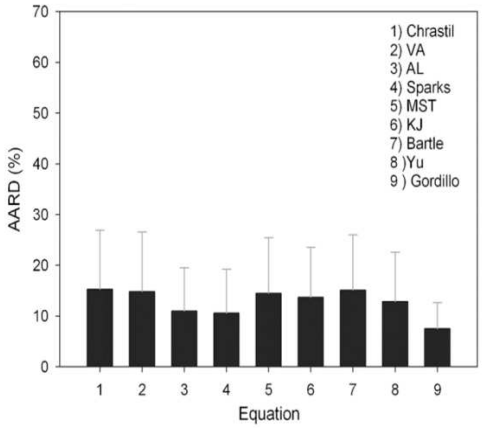

Fig. 5. Mean AARD with their corresponding standard deviations when $-\log(y_2)-(-\log(y_1)) \leq 1.41$ for wide ΔT or ΔP with high initial P.

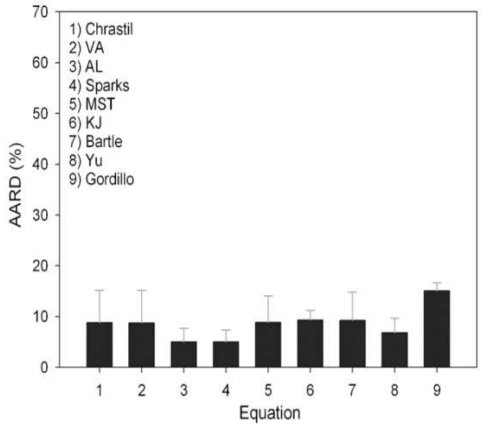

Fig. 6. Mean AARD with their corresponding standard deviations when $-\log(y_2)-(-\log(y_1)) \leq 1.41$ for low ΔT and ΔP.

Table 15
Mean AARD and standard deviations with $-\log(y_2)-(-\log(y_1))\leq 1.41$ (low ΔT and ΔP).

N	Chrastil	VA	AL	Sparks	MST	KJ	Bartle	Yu	Gordillo
11	2.34	2.26*	3.02	3.74	4.35	8.02	4.44	11.36	17.08
13	2.67	2.49	1.53*	1.78	3.78	6.55	4.20	3.30	14.50
14	9.77	9.74	8.93	8.58	10.41	11.36	11.80	6.27*	15.63
15	14.08	14.06	6.35	5.63	12.59	8.59	14.58	4.72*	14.51
19	18.17	18.13	5.99*	6.24	16.59	11.49	16.17	6.68	16.10
$\bar{X}$	8.82	8.74	5.04	5.03*	8.85	9.30	9.23	6.81	15.06
S.D.	6.39	6.43	2.63	2.33	5.18	1.95	5.60	2.85	1.58*

The previous situations are shown in Figs. 7–10. Fig. 7 describes the solubility of cyproterone acetate in sc-CO_2 with a wide temperature range and $-\log(y_2)-(-\log(y_1))\leq 1.41$. It is possible to observe how Gordillo's equation fits the curve better than other models, like Sparks'. Nevertheless, for higher values of $-\log(y_2)-(-\log(y_1))$ both equations present more similar results, although Gordillo's model always approaches the experimental data with a better fit. On the other hand, in Fig. 8 (solubility of exemestane in sc-CO_2), the opposite phenomenon occurs, Sparks' equation gives a better correlation due to the high value of $-\log(y_2)-(-\log(y_1))$, since the vicinities of the UCEP have been reached. Fig. 9 describes the solubility of the taxol in sc-CO_2. In this case, (high initial pressure together with a high pressure range), the experimental data were fitted properly by all equations (always with an AARD below 5%), although Gordillo's model provides the best correlation (AARD of 1.50%) at these conditions. Fig. 10 (solubility of penicillin V in sc-CO_2) describes the last case, when $-\log(y_2)-(-\log(y_1))\leq 1.41$ without a wide pressure or temperature ranges. According to the previous discussion, at these conditions, AL's and Sparks' model correlate almost identically with the experimental data, and the most important issue is to modify the association number *k*. In Fig. 10, it is possible to observe how at these conditions, AL's equation fits experimental data better than Gordillo's model.

All results can be summarized as follows. If the solubility data of a pharmaceutical compound is available, the best equation to pre-

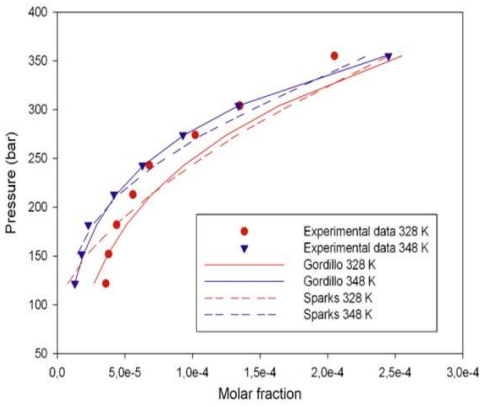

Fig. 7. Solubility of cyproterone acetate in sc-CO_2: $-\log(y_2)-(-\log(y_1))\leq 1.41$. Wide temperature range (308-348 K) (experimental data from Yamini et al. [37]).

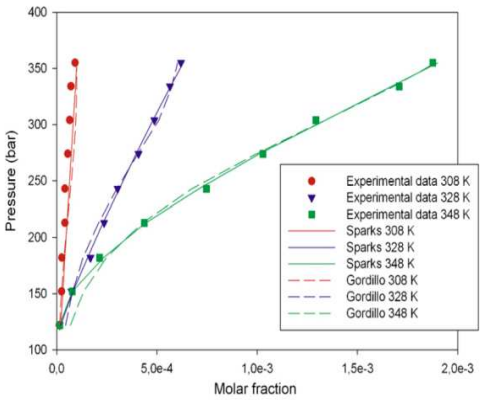

Fig. 8. Solubility of exemestane in sc-CO_2: $-\log(y_2)-(-\log(y_1))>1.41$ (experimental data from Hojjati et al. [21]).

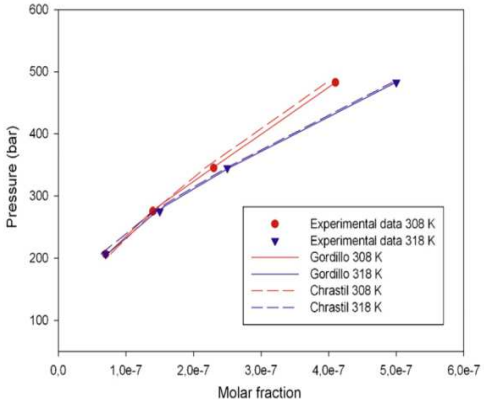

Fig. 9. Solubility of taxol in sc-CO_2: $-\log(y_2)-(-\log(y_1))\leq 1.41$. Wide pressure range (275 bar) with a initial pressure of 200 bar (experimental data from Nalesnik et al. [46]).

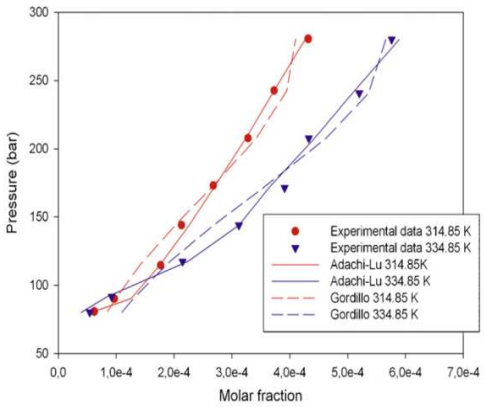

Fig. 10. Solubility of penicillin V in sc-CO_2: $-\log(y_2)-(-\log(y_1))\leq 1.41$ without wide pressure or temperature range (experimental data from Ko et al. [45]).

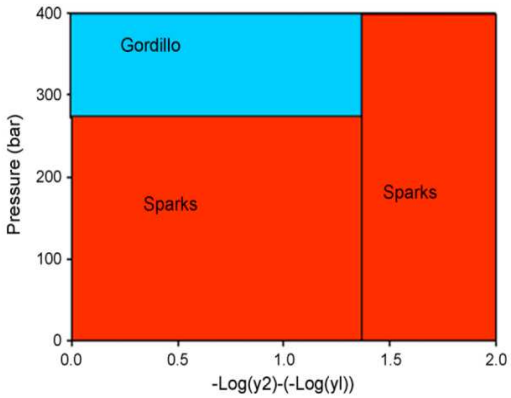

Fig. 11. Semiempirical equation most suitable depending on the solubility data conditions.

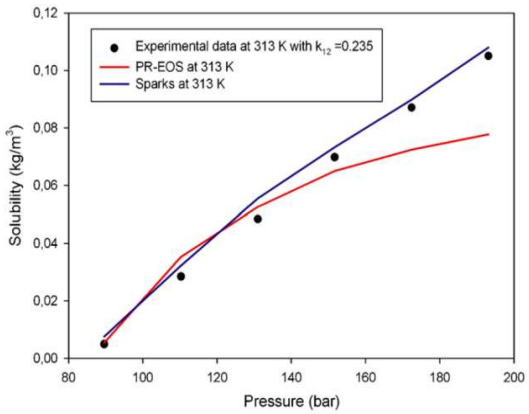

Fig. 12. Solubility of naproxen in sc-CO_2 fitted with PR-EOS and Sparks' equation (experimental data from Ting et al. [41]).

dict its behaviour is the model developed by Sparks. However, in several occasions, Gordillo's model produces the best fit. To find out when this situation happens, a division criterion should be established.

If the value of the expression $-\log(y_2)-(-\log(y_1))$ is higher than an arbitrary value of 1.41 (the conditions are closed to the UCEP) the best equation is Sparks' equation (Fig. 8). But, if $-\log(y_2)-(-\log(y_1))$ is lower than 1.41, a new division is required. With a wide temperature range (Fig. 7) or a wide pressure range with a high initial pressure (Fig. 9), Gordillo's equation is more suitable. Otherwise, if the previous range conditions are not wide, Sparks' model is again the best (Fig. 10). Finally, Fig. 11 shows which semiempirical equation produces the best fit in the solubility data depending on the different operation conditions.

5. A comparison of semi-empirical equations with Peng-Robinson equation of state

A brief comparison between the results obtained with the semiempirical equations and the most used cubic equation of state are performed in this section. Peng-Robinson equation of state (eq. (14)) with classical Van der Waals mixing rules (with one parameter) was employed because is a well-established and well-known equation to predict the solubility of solids in SCFs [49].

$$P = \frac{RT}{v-b} - \frac{a(T)}{v^2+2bv-b^2} \tag{14}$$

Where v is the molar volume and R the gas constant. For a pure component, the attractive parameter a and the repulsive term b are defined as a function of its critical properties T_C and P_C. On the other hand, the dependence of the temperature of the attractive parameter a is treated with a corrector term α (eq. (15)) where the acentric factor w takes into account the no esfericity of the molecule. To consider the interactions between the compounds, Van der Waals mixing rules are used (eq. (16) and eq. (17)).

$$\alpha(T_R) = \left[1+\left(0.374+1.542w+-0.269w^2\right)(1-T_R)^{0.5}\right]^2 \tag{15}$$

$$a_m = \sum_i \sum_j y_i y_j \sqrt{a_i a_j}\left(1-k_{ij}\right) \tag{16}$$

$$b_m = \sum_i y_i b_i \tag{17}$$

The equilibrium CO_2-solid has been modelled with iso-fugacity criteria, assuming the solid phase in the system as a pure solute, with the equations described by de la Fuente et al. [50]. The fugacity coefficient value of the solid is calculated from the fugacity coefficient of the solid in a sub-cooled state corrected by means of a simplified Clapeyron-type approach [50–51], avoiding sublimation pressure calculations (eq. (17)).

$$\ln\varphi_3^S = \ln\varphi_3^L + \frac{\Delta H_{tp}}{R}\left(\frac{1}{T_{tp}}-\frac{1}{T}\right) \tag{17}$$

The solubility data of naproxen and penicillin V were fitted with PR-EOS. The solid properties were taken from literature [41,45,52]. To correct deviations in the mixing rule, the adjustable interaction parameter k_{12} (considered temperature independent) was obtained by means of a regression from experimental data in front of theoretical data with the following objective function:

$$\sum_{i=1}^{N} \frac{1}{N}\cdot\left(y_{exp\,i}-y_{calci}\right)^2 \tag{18}$$

Fig. 12 shows a comparison between PR-EOS and Sparks' equation (the best semiempirical equation according to the conditions) for solubility data of naproxen at 313 K. It is possible to observe the AARD reduction obtained with the semiempirical equation (from 15% to 7%).

Fig. 13 shows a comparison between PR-EOS and Sparks' equation (again, the best semiempirical equation according to the experimental conditions) for solubility data of penicillin V at 314 K. In this case, the error with PR-EOS is around 35%, being drastically reduced to 6% using a semiempirical equation.

It is important to notice how the error with PR-EOS increases with a higher solid molecular weight and higher pressure (although the tendency is still present). In addition, the polarity is also a property that makes the fit worse. This AARD might be reduced taking the sublimation pressure or the critical properties as adjustable parameters, or using directly more parameters in the mixing rule. Nevertheless, the incorporation of additional parameters does not yield sufficient improvement in prediction [53]. Housaindokht and Bozorghmehr [54] employed different mixing rules with PR-EOS trying to reduce the AARD in the correlation of the solubility of methimazole, phenazopyridine and propanolol in sc-CO_2 at different temperatures. With PR-EOS, they obtained the best average AARD around, respectively, 16%, 18% and 22% using a mixing rule with 3 parameters. In this work, the accuracy was improved using the corresponding semiempirical equation, to 9%, 8% and 13%, and in addition without estimation of critical properties.

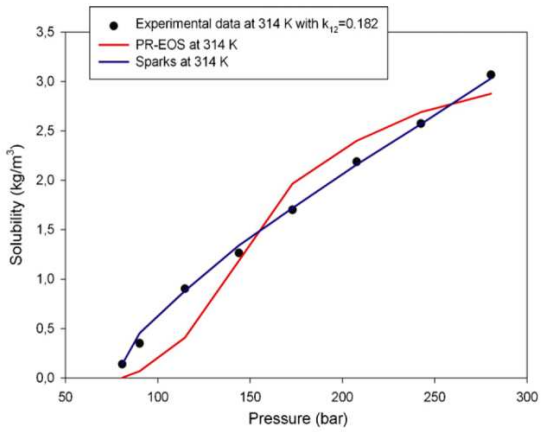

Fig. 13. Solubility of penicillin V in sc-CO_2 fitted with PR-EOS and Sparks' equation (experimental data from Ko et al. [45]).

Similar results were obtained studying the solubility of a photochromic dye in sc-CO_2. Several density-based models (Chrastil, Bartle and MST models) and cubic equation of state (PR-EOS and Soave-Redlich-Kwong (SRK) EOS) with Van der Waals mixing rule with 2 parameters were employed. The best fit was obtained with the semiempirical models, reducing the average AARD from 12% (PR-EOS) and 13% (SRK-EOS) to 6% (MST's model) [55].

These results highlight that for pharmaceuticals compounds (solids with high polarity and high molecular weight), semiempirical equations are more suitable to predict their solubility in sc-CO_2. Although a big number of parameters must be determined in certain semiempirical equations, it is important to realize that the accuracy in the prediction is improved with respect to cubic equations of state and without the need to estimate the properties of the solids, avoiding in addition computational complexity.

6. Conclusions

The 9 most used semiempirical equations have been applied to fit the solubility data of 27 pharmaceutical compounds in sc-CO_2. In general, Sparks' model provides the lowest mean AARD, but in 9 compounds, Gordillo's model produces the lowest individual AARD. To explain this phenomenon, an arbitrary value of 1.41 in the difference between the negative logarithms of the highest and the lowest molar fraction was chosen in order to discriminate two zones depending on the appearance of the UCEP or its vicinities. When the previous value is exceed, Sparks' equation provides again the best fit, but if the value is lower than the arbitrary threshold, a new division must be done attending to the high or low values of the pressure range and temperature range. If any of these parameters have a high value, Gordillo's model should be used, but otherwise, Sparks' model is again the best equation. Finally, from a comparison with Peng-Robinson equation of state, it can be concluded that semiempirical equations provide a better fit in these systems with respect to cubic equations of state.

References

[1] M. Kemmere, T. Meyer, Supercritical Carbon Dioxide, first ed., Wiley-Vch, Germany, 2005, pp. 37–48.
[2] F. Sahena, I.S.M. Zaidul, S. Jinap, A.A. Karim, K.A. Abbas, N.A.N. Norulaini, A.K.M. Omar, Application of supercritical CO_2 in lipid extraction—A review, Journal of Food Engineering (2009), doi:10.1016/j.jfoodeng.2009.06.026.
[3] N. Vedaraman, C. Srinavasakannan, G. Brunner, B.V. Ramabrakmam, P.G. Brao, Experimental and modeling studies on extraction of cholesterol from cow brain using supercritical carbon dioxide, The Journal of Supercritical Fluids 34 (2005) 27–34.
[4] J. Shi, C. Yi, S. Xue, Y. Jiang, Y. Ma, Effects of supercritical CO_2 fluid parameters on chemical composition and yield of carotenoids extraction extracted from pumpkin, LWT-Food Science and Technology (2009), doi:10.1016/j.lwt.2009.07.003.
[5] G.L. Filho, V.V. De Rosso, M.A.A. Meireles, P.T.V. Rosa, A.L. Oliveira, A.Z. Mercadante, F.A. Cabral, Supercritical CO_2 extraction of carotenoids from pitanga fruits (*Eugenia uniflora* L.), The Journal of Supercritical Fluids 46 (2008) 33–39.
[6] M.S. Gómez-Prieto, M.L. Ruiz del Castillo, G. Flores, G. Santa-María, G.P. Blanch, Application of Chrastil's model to the extraction in sc-CO_2 of β-carotene and lutein in *Mentha Spicata* L., The Journal of Supercritical Fluids 43 (2007) 32–36.
[7] L. Karlsson, A. Torstensson, L.T. Taylor, The use of supercritical fluid extraction for sample preparation of pharmaceutical formulations, Journal of Pharmaceutical and Biomedical Analysis 15 (1997) 601–611.
[8] C.R. Piantino, F.W.B. Aquino, L.A. Follegatti-Romero, F.A. Cabral, Supercritical CO_2 extraction of phenolic compounds from *Baccharis dracunculifolia*, The Journal of Supercritical Fluids 47 (2008) 209–214.
[9] N. Bahramifar, Y. Yamini, M. Shamsipur, Investigation on the supercritical carbon dioxide extraction of some polar drugs from spiked matrices and tablets, The Journal of Supercritical Fluids 35 (2005) 205–211.
[10] J. Jung, M. Perrut, Particle design using supercritical fluids: Literature and patent survey, The Journal of Supercritical Fluids 20 (2001) 179–219.
[11] A. Martín, M.J. Cocero, Micronization processes with supercritical fluids: Fundamentals and mechanisms, Advanced Drug Delivery Reviews 60 (2008) 339–350.
[12] E. Reverchon, Supercritical antisolvent precipitation of micro and nanoparticles, The Journal of Supercritical Fluids 15 (1999) 1–21.
[13] E.M. Martín del Valle, M.A. Galán, R.G. Carbonell, Drug deliveries technologies: The way forward in the new decade, Industrial and Engineering Chemical Research 48 (2009) 2475–2486.
[14] M.J. Cocero, A. Martín, F. Mattea, S. Varona, Encapsulation and co-precipitation processes with supercritical fluids: Fundamentals and applications, The Journal of Supercritical Fluids 47 (2009) 545–555.
[15] I. Pasquali, R. Bettini, Are pharmaceuticals really going supercritical? International Journal of Pharmaceutics 364 (2008) 176–187.
[16] E. Reverchon, R. Adami, S. Cardea, G. Della Porta, Supercritical fluids processing of polymers for pharmaceutical and medical applications, The Journal of Supercritical Fluids 47 (2009) 484–492.
[17] B.E. Poling, J. Prausnitz, J.P. OïConnell, The Properties of Gases and Liquids, fifth ed., McGraw-Hill, New York, 2001, pp. 2.3–2.34.
[18] S. Garnier, E. Neau, P. Alessi, A. Cortesi, I. Kikic, Modelling solubility of solids in supercritical fluids using fusion properties, Fluid Phase Equilibria 158 (1999) 491–500.
[19] E. Neau, S. Garnier, L. Avaullée, A consistent estimation of sublimation pressures using a cubic equation of state and fusion properties, Fluid Phase Equilibria 164 (1999) 173–186.
[20] Y.-M. Chen, Y.-P. Chen, Measurements for the solid solubilities of antipyrine, 4-aminoantipyrine and 4-dimethylaminoantipyrine in supercritical carbon dioxide, Fluid Phase Equilibria 282 (2009) 82–87.
[21] M. Hojjati, A. Vatanara, Y. Yamini, M. Moradi, A.R. Najafabadi, Supercritical CO_2 and highly selective aromatase inhibitors: Experimental solubility and empirical correlation, The Journal of Supercritical Fluids (2009), doi:10.1016/j.supflu.2009.06.015.
[22] G.I. Burgos-Solórzano, J.F. Brennecke, M.A. Stadtherr, Solubility measurements and modeling of molecules of biological and pharmaceutical interest with supercritical CO_2, Fluid Phase Equilibria 220 (2004) 57–69.
[23] E.S. Choi, M.J. Noh, K.P. Yoo, Solubilities of o-,m- and p-coumaric acid isomers in carbon dioxide at 308.15-323.15 K and 8.5-25 Mpa, Journal of Chemical and Engineering Data 43 (1998) 6–8.
[24] M. Hojjati, Y. Yamini, M. Khajeh, A. Vatanara, Solubility of some statin drugs in supercritical carbon dioxide and representing the solute solubility data with several density-based correlations, The Journal of Supercritical Fluids 41 (2007) 187–194.
[25] D.L. Sparks, R. Hernández, L.A. Estévez, Evaluation of density-based models for the solubility of solids in supercritical carbon dioxide and formulation a new model, Chemical Engineering Science 63 (2008) 4292–4301.
[26] J. Méndez-Santiago, A.S. Teja, The solubility of solids in supercritical fluids, Fluid Phase Equilibria 158 (1999) 501–510.
[27] A. Jouyban, H.K. Chan, N.R. Foster, Mathematical representation of solute solubility in supercritical carbon dioxide using empirical expressions, The Journal of Supercritical Fluids 24 (2002) 19–35.
[28] J. Chrastil, Solubility of solids and liquids in supercritical gases, Journal of Physical Chemistry 86 (1982) 3016–3021.
[29] Y. Adachi, B.C.Y. Lu, Supercritical fluid extraction with carbon dioxide and ethylene, Fluid Phase Equilibria 14 (1983) 147–156.
[30] J.M. del Valle, J.M. Aguilera, An improved equation for predecting the solubility of vegetable oils in supercritical CO_2, Industrial and Engineering Chemistry Research 27 (1988) 1551–1553.
[31] S. Kumar, K.P. Johnston, Modelling the solubility of solids in supercritical fluids with density as independent variable, The Journal of Supercritical Fluids 1 (1988) 15–22.
[32] K.D. Bartle, A.A. Clifford, S.A. Jafar, G.F. Shilstone, Solubilities of solids and liquids of low volatility in supercritical carbon dioxide, Journal of Physical and Chemical Reference Data 20 (1991) 201–219.
[33] Z. Yu, B. Singh, S.S.H. Rizvi, J.A. Zollewg, Solubilities of fatty acids, fatty acid esters, and fats and oils in supercritical CO_2, The Journal of Supercritical Fluids 7 (1994) 51–59.

[34] M.D Gordillo, M.A. Blanco, A. Molero, E. Martínez de la Ossa, Solubility of the antibiotic penicillin G in supercritical carbon dioxide, The Journal of Supercritical Fluids 15 (1999) 183–190.
[35] J.C. de la Fuente, B. Oyarzún, N. Quezada, J.M. del Valle, Solubility of carotenoid pigments (lycopene and astaxanthin) in supercritical carbon dioxide, Fluid Phase Equilibria 247 (2006) 90–95.
[36] M. Johannsen, G. Brunner, Solubilities of the fat-soluble vitamins A,D,E and K in supercritical carbon dioxide, Journal of Chemical and Engineering Data 42 (1997) 106–111.
[37] M. Asghari-Khiavi, Y. Yamini, M.A. Farajzadeh, Solubilities of two steroids drugs and their mixtures in supercritical carbon dioxide, The Journal of Supercritical Fluids 30 (2004) 111–117.
[38] J. Shi, M. Khatri, S.J. Xue, g.S. Mittal, Y. Ma, D. Li, Solubility of lycopene in supercritical CO_2 fluid as affected by temperature and pressure, Separation and Purification Technology 66 (2009) 322–328.
[39] Y. Yamini, J. Arab, M. Asghari-Khiavi, Solubilities of phenazopyridine, propanolol, and methimazole in supercritical carbon dioxide, Journal of Pharmaceutical and Biomedical Analysis 32 (2003) 181–187.
[40] Kuen-Long Tsai, Fuan-Nan Tsai, Solubilities of methylbenzoic acid isomers in supercritical carbon dioxide, Journal of Chemical and Engineering Data 40 (1995) 264–266.
[41] S.S.T. Ting, S.J. Macnaughton, D.L. Tomasko, N.R. Foster, Solubility of naproxen in supercritical carbon dioxide with and without cosolvents, Industrial Engineering Chemistry Research 32 (1993) 1471–1481.
[42] S.J. Macnaughton, I. Kikic, N.R. Foster, P. Alessi, A. Cortesi, I. Colombo, Solubility of anti-inflammatory drugs in supercritical carbon dioxide, Journal of Chemical and Engineering Data 41 (1996) 1083–1086.
[43] Z. Knez, M. Skerget, P. Sencar-Bozic, A. Rizner, Solubility of nifedipine and nitrendipine in supercritical CO_2, Journal of Chemical and Engineering Data 40 (1995) 216–220.
[44] V. Vandana, A.S. Teja, The solubility of paclitaxel in supercritical CO_2 and N_2O, Fluid Phase Equilibria 135 (1997) 83–87.
[45] M. Ko, V. Shah, P.R. Bienkowski, H.D. Cochran, Solubility of the antibiotic penicillin V in supercritical CO_2, The Journal of Supercritical Fluids 4 (1991) 32–39.
[46] C.A. Nalesnik, B.N. Hansen, J.T. Hsu, Solubility of pure taxol in supercritical carbon dioxide, Fluid Phase Equilibria 146 (1998) 315–323.
[47] Z. Knez, M. Skerget, Phase equilibria of the vitamins D_2, D_3 and K_3 in binary systems with CO_2 and propane, The Journal of Supercritical Fluids 20 (2001) 131–144.
[48] M. McHugh, M.E. Paulaitis, Solid solubilities of naphtalene and biphenyl in supercritical carbon dioxide, Journal of Chemical and Engineering Data 25 (1980) 326–338.
[49] D.Y. Peng, D.B. Robinson, A new two constant equation of state, Industrial and Engineering Chemistry Fundamentals 15 (1976) 59–64.
[50] J.C. De la Fuente Badilla, A. Shariati, C.J. Peters, On the selection of optimum thermodynamic conditions for the GAS process, The Journal of Supercritical Fluids 32 (2004) 55–61.
[51] F. Miguel, A. Martín, T. Gamse, M.J. Cocero, Supercritical anti solvent precipitation of lycopene. Effect of the operating parameters, The Journal of Supercritical Fluids 36 (2006) 225–235.
[52] D.M. Aragón, D.P. Pacheco, M.A. Ruidíaz, A.D. Sosnik, F. Martínez, Extended Hildebrand solubility approach for naproxen solubility estimation in ethanol+water cosolvent mixtures, Revista de la Facultad de Química Farmacéutica 1 (2008) 113–122.
[53] I. Ashour, R. Almehaideb, S.-E. Fateen, G. Aly, Representation of solid-supercritical fluid phase equilibria using cubic equations of state, Fluid Phase Equilibria 167 (2000) 41–61.
[54] M.R. Housaindokht, M.R. Bozorgmehr, Calculation of solubility of methimazole, phenazopyridine and propanolol in supercritical carbon dioxide, The Journal of Supercritical Fluids 43 (2008) 390–397.
[55] P. Coimbra, M.H. Gil, C.M.M. Duarte, B.M. Heron, H.C. de Sousa, Solubility of a spiroindolinonaphthoxazine photochromic dye in supercritical carbon dioxide: Experimental datermination and correlation, Fluid Phase Equilibria 238 (2005) 120–128.

5.3. Conclusiones

En el artículo anterior se han utilizado 9 ecuaciones semiempíricas para ajustar la solubilidad de 27 fármacos en CO_2sc. Se ha observado que la ecuación de Sparks es la que produce el menor promedio de error de ajuste, aunque para 9 sólidos la ecuación de Gordillo proporcionaba un ajuste mejor que el obtenido con el modelo de Sparks.

Con el fin de explicar el fenómeno anterior, se realizó una división en las condiciones experimentales para deducir a que temperatura se sitúa el UCEP. Esta división se estableció dependiendo del incremento de solubilidad en términos logarítmicos. Asimismo, por debajo del UCEP, se realizó otra división dependiendo del intervalo de presión y de temperatura.

A condiciones superiores al UCEP, todas las ecuaciones proporcionaban un error superior al obtenido por debajo de ese mismo punto debido a la dificultad de captar el elevado incremento de solubilidad. A una temperatura superior al UCEP la ecuación de Sparks es la óptima para realizar el ajuste.

A condiciones inferiores al UCEP la ecuación de Sparks proporcionaba nuevamente el menor error, aunque para intervalos elevados de presión o de temperatura, la ecuación de Gordillo ajustaba con un error inferior.

Finalmente, se ha realizado una comparación entre ecuaciones semiempíricas y la ecuación de estado cúbica de Peng-Robinson, concluyendo que las ecuaciones semiempíricas producían un error inferior que las ecuaciones cúbicas.

● Referencias también citadas

[1] L. Constantinou; R. Gani, New group contribution method for estimating properties of pure compounds, AIChE J. 40 (1994) 1697-1710.

[2] J. Marrero; R. Gani, Group-contribution based estimation of pure component properties, Fluid Phase Equilib. 183-184 (2001) 183-208.

[3] I. Ashour; R. Almehaideb; S.-E. Fateen; G. Aly, Representation of solid-supercritical fluid phase equilibria using cubic equations of state, Fluid Phase Equilib. 167 (2000) 41-61.

[4] P. Coutsikos; K. Magoulas; G. M. Kontogeorgis, Prediction of solid-gas equilibria with the Peng-Robinson equation of state, J. Supercrit. Fluids 25 (2003) 197-212.

[5] J. Chrastil, Solubility of solids and liquids in supercritical gases, J. Phys. Chem. 86 (1982) 3016-3021.

[6] Y. Adachi; B. C. Y. Lu, Supercritical fluid extraction with carbon dioxide and ethylene, Fluid Phase Equilib. 14 (1983) 147-156.

[7] J. M. del Valle; J. M. Aguilera, An improved equation for predicting the solubility of vegetable oils in supercritical CO_2, Ind. Eng. Chem. Res. 27 (1988) 1551-1553.

[8] D. L. Sparks; R. Hernández; L. A. Estévez, Evaluation of density-basedmodels for the solubility of solids in supercritical carbon dioxide and formulation a new model, Chem. Eng. Sci. 63 (2008) 4292-4301.

[9] S. Kumar; K. P. Johnston, Modelling the solubility of solids in supercritical fluids with density as independent variable, J. Supercritical Fluids 1 (1988) 15-22.

[10] K. D. Bartle; A. A. Clifford; S. A. Jafar; G. F. Shilstone, Solubilities of solids and liquids of low volatility in supercritical carbon dioxide, J. Phys. Chem. Ref. Data 20 (1991) 201-219.

[11] J. Méndez-Santiago; A. S. Teja, The solubility of solids in supercritical fluids, Fluid Phase Equilib. 158 (1999) 501-510.

[12] Z. Yu; B. Singh; S. S. H. Rizvi; J. A. Zollweg, Solubilities of fatty acids, fatty acid esters, and fats and oils in supercritical CO_2, J. Supercrit. Fluids 7 (1994) 51-59.

[13] M. D. Gordillo; M. A. Blanco; A. Molero; E. Martínez de la Ossa, Solubility of the antibiotic penicillin G in supercritical carbon dioxide, J. Supercrit. Fluids 15 (1999) 183-190.

CAPÍTULO 6.

Estudio comparativo de ecuaciones semiempíricas empleadas en equilibrios sólido-vapor con cosolventes. Aplicación de modelos q

6.1. Ecuaciones semiempíricas para el ajuste de equilibrios sólido-vapor con cosolventes

Como se ha comentado en el capítulo 1, la determinación de la solubilidad de sólidos en fluidos supercríticos es un factor determinante para poder conocer previamente la viabilidad de los procesos que emplean fluidos supercríticos.

Asimismo, en el capítulo 4 se han observado una serie de problemas como el error obtenido y la obtención de propiedades del sólido para ajustar los equilibrios sólido-fluido supercrítico.

Con el fin de evitar esos problemas, se emplearon ecuaciones semiempíricas como modelos alternativos a las ecuaciones cúbicas. Estas ecuaciones fueron descritas y comparadas en el capítulo 5.

Sin embargo, estos modelos fueron definidos únicamente para sistemas binarios sólido-fluido supercrítico, por lo que no pueden ser usados para ajustar equilibrios de sistemas constituidos por un sólido, un fluido supercrítico y un cosolvente. Esta limitación puede ser considerada como una desventaja, ya que en algunas ocasiones, procesos que emplean CO_2sc en la industria farmacéutica necesitan del empleo de cosolventes para incrementar la solubilidad del fármaco en dicho CO_2sc [1-2].

Por ello, se han desarrollado durante estos últimos años una serie de ecuaciones a fin de modelar la solubilidad de sólidos en fluidos supercríticos en presencia de cosolventes [3-8].

6.1.1. Inconsistencia teórica en las ecuaciones semiempíricas.

En el estudio descrito en el cap. 5 sobre las ecuaciones semiempíricas se observó que en todos los modelos basados en la formación de un complejo de solvatación (Chrastil y sus derivadas), el término exponencial tomaba la forma del argumento de Boltzmann, *exp(-E/RT)* dónde *E* es la energía, variable dependiente de la temperatura.

Sin embargo, si en estos modelos la temperatura tiende a infinito, el término exponencial se transforma en *exp(constante),* que difiere del valor que se obtendría con el argumento de Boltzmann (que sería la unidad). Esto ocurre también para sistemas con cosolventes (como se describirá en el artículo siguiente), indicando la existencia de una inconsistencia teórica de estos modelos con la temperatura.

Con el objeto de intentar solventar esta inconsistencia teórica y de reducir el error producido en el ajuste mediante ecuaciones semiempíricas, en esta tesis se procedió a la transformación de estos modelos usando la teoría de la entropía de Tsallis y la función exponencial *q*. Esta función se considera un algebra de deformación, siendo *q* el parámetro de deformación.

Esta teoría ha sido aplicada previamente en muchos campos de la ciencia y se basa en una generalización del concepto de entropía de Boltzmann usando la distribución dada por la mecánica estadística no extensiva [9-11].

A continuación, se describirán las ecuaciones semiempíricas más utilizadas para realizar un ajuste de la solubilidad de un sólido en fluidos supercríticos en presencia de cosolventes, así como la definición de las ecuaciones generalizadas por el uso de la función exponencial *q*. Todos estos modelos han sido comparados con dos objetivos:

• La obtención de un criterio de selección de ecuación semiempírica más adecuada para los equilibrios sólido-fluido supercrítico-cosolvente, en función del error de ajuste dependiendo de diferentes parámetros experimentales.

• Estudiar si los nuevos modelos *q* disminuyen el error de ajuste de estos datos experimentales en comparación con los modelos antiguos.

6.2. Resultados y discusión

El objetivo de este trabajo es el empleo de distintas ecuaciones semiempíricas para modelar la solubilidad de fármacos en CO_2sc con y sin cosolventes. Así, se realizará una comparación de 8 modelos diferentes basándose en el error producido, número de parámetros, rango de aplicación (proximidad al punto crítico de mezcla) e interacciones soluto-cosolvente.

Se propone también la modificación de los modelos originales a través de la introducción en ellos de la función exponencial *q* con el fin de estudiar la aplicación de la teoría de entropía de Tsallis en este tipo de ecuaciones.

Todas las ecuaciones estudiadas ajustaron el equilibrio sólido-CO_2sc-cosolvente con un error aproximado del 10%. La ecuación de González (con 4 parámetros) y la de Reddy-Madras (5 parámetros) parecen ser las más convenientes debido a que pueden aplicarse sobre un rango de concentraciones amplio de cosolvente y además no necesitan de una gran cantidad de parámetros. Sin embargo, el error de ajuste se incrementaba con todas las ecuaciones cuando las condiciones experimentales se acercaban al punto crítico de mezcla.

Por otro lado, con los modelos modificados con la función exponencial *q* se obtuvo el mismo error que con los originales. Sin embargo, estos modelos no

presentaban inconsistencias teóricas con la temperatura y se pudo observar una relación entre el parámetro q y la estructura molecular del fármaco, que puede ser de utilidad para un futuro desarrollo de un test de consistencia.

ARTÍCULO

Modelling solubility of solid active principle ingredients in sc-CO_2 with and without cosolvents: A comparative assessment of semiempirical models based on Chrastil´s equation and its modifications.

The Journal of Supercritical Fluids, in press (2013)

G Model
SUPFLU-2862; No. of Pages 12
ARTICLE IN PRESS

J. of Supercritical Fluids xxx (2013) xxx–xxx

Contents lists available at ScienceDirect

The Journal of Supercritical Fluids

journal homepage: www.elsevier.com/locate/supflu

Modelling solubility of solid active principle ingredients in sc-CO_2 with and without cosolvents: A comparative assessment of semiempirical models based on Chrastil's equation and its modifications

A. Tabernero[a], S.A.B. Vieira de Melo[b,*], R. Mammucari[c], E.M. Martín del Valle[a], N.R. Foster[c]

[a] *Departamento de Ingeniería Química, Universidad de Salamanca, P/Los Caídos s/n, 37008 Salamanca, Spain*
[b] *Programa de Engenharia Industrial, Escola Politécnica, Universidade Federal da Bahia, Rua Prof. Aristides Novis, 2, Federação, 40210-630 Salvador, BA, Brazil*
[c] *School of Chemical Engineering, The University of New South Wales, Sydney, NSW 2052, Australia*

ARTICLE INFO

Article history:
Received 5 August 2013
Received in revised form
18 November 2013
Accepted 22 November 2013

Keywords:
Solubility
Cosolvents
Semiempirical models
q-Exponential function

ABSTRACT

Predicting solubility of solids in supercritical solvents with and without cosolvents is a key step supporting the application of supercritical fluids to processes as the extraction of natural compounds and particle engineering. The aim of this work is modelling the solubility of solid therapeutic compounds in supercritical carbon dioxide with and without cosolvents using semiempirical models. A comparative assessment of eight models is presented based on deviations, number of parameters, range of applicability (concentration of cosolvents and proximity to the mixture critical point) and cosolvent–solute interactions.

All equations provide an average deviation on solubility around 10%. The use of the González (with four parameters) and Reddy and Madras equation (with five parameters) is judged the most convenient as they have the smaller number of parameters and are applicable over a suitable range of cosolvent concentrations. In all cases it has been possible to relate the solubility behaviour to the cosolvent–solute interaction and the concentration of cosolvent. However, deviations increase when conditions are slightly close to the mixture critical point.

A modification is proposed through the introduction of a "*q* exponential function". The modified *q*-models can be regarded as generalized models based on the Tsallis's statistical non-extensive entropy theory. In fact, the original Chrastil and González equation can be seen as a particular case of the *q*-Chrastil and *q*-González models. They have deviations similar to the other model and show potential for further studies.

© 2013 Elsevier B.V. All rights reserved.

1. Introduction

The use of supercritical fluids (SCFs) for the extraction of high-value compounds from natural sources and for particle production of active pharmaceutical ingredients (API) has been extensively studied in last decades [1–3]. These processes exploit the particular gas–liquid properties of a SCF, such as liquid-like density and gas-like diffusivity and viscosity. Moreover, the product obtained is often free of residual organic solvent and if a non-flammable and non-hazardous SCF is used, these techniques can be considered as "green" processes. Due to its mild critical properties, non-toxicity and environmental friendliness, carbon dioxide is the most commonly applied SCF [4].

Processes such as supercritical fluid extraction (SFE) take advantage of the peculiar properties of SCFs. Supercritical fluid extraction consists on establishing a contact between a solid raw material and a SCF. The SCF diffuses in the raw material, solubilises certain components and diffuses to the bulk supercritical solvent. The solubilised material can be recovered by depressurization. The process can be applied to the extraction of high-value products free from residual solvent. Mass transfer properties have a key role on the kinetics of this process, however the first criteria to evaluate the practicability of a SFE is the solubility of the compounds of interest in SCF which determine the theoretical limit of the process output [5–7].

* Corresponding author. Tel.: +55 71 32039802; fax: +55 71 32039801.
E-mail address: sabvm@ufba.br (S.A.B. Vieira de Melo).

0896-8446/$ – see front matter © 2013 Elsevier B.V. All rights reserved.
http://dx.doi.org/10.1016/j.supflu.2013.11.017

Please cite this article in press as: A. Tabernero, et al., Modelling solubility of solid active principle ingredients in sc-CO_2 with and without cosolvents: A comparative assessment of semiempirical models based on Chrastil's equation and its modifications, J. Supercrit. Fluids (2013), http://dx.doi.org/10.1016/j.supflu.2013.11.017

G Model
SUPFLU-2862; No. of Pages 12
ARTICLE IN PRESS

Supercritical fluid technologies are also used for particle formation through rapid expansion of a supercritical solution (RESS). The RESS process can generate micro- or nanoparticles devoid of residual organic solvent [8–10]. As in SFE, high density of SCF is used for their solvent power towards the compounds of interest, thus the importance of evaluating the solubility of complex molecules in SCFs.

In both SFE and RESS processes, knowing the solubility of the compounds of interest in the SCF allows evaluating the feasibility of the process. When the SCF used is CO_2, the processing of polar molecules – like those often found in pharmaceuticals or natural products – suffers the shortcoming of the low polarity of the SCF solvent [4]. To overcome this drawback, cosolvents are used to improve process yields [1,11–13]. As cosolvents are organic solvents their use should be as limited as possible to mitigate related problems like possible toxic residues in the final product. Further, biphasic regions should be avoided due to additional mass transfer resistance that can hinder processing. Therefore, the solubility of solid compounds in pure sc-CO_2 and in CO_2 + cosolvent mixtures is worth of investigation.

Experimental determination of solubility in sc-CO_2 can be a time consuming and costly task. For this reason models able to correlate and predict solubility of solids in sc-CO_2 are very desirable. Cubic equations of state and non-cubic equations of state (EOS) have been used to model solubility of solids in sc-CO_2 with and without cosolvents [14–16]. However, these equations require robust computational methods and the knowledge of several properties such as sublimation pressure, molar volume, critical temperature and pressure, and sometimes also molecular parameters. These properties for pharmaceuticals are scarce in the literature and group contribution methods are usually applied leading to additional uncertainties with the use of these equations [17,18].

Semiempirical models can be applied as alternative to cubic and non-cubic EOS to correlate and predict solubility of solid API in sc-CO_2. These models correlate the experimental solubility data to the density of the supercritical solvent and the temperature of the binary system, and thus do not require pure solid properties. Although these models have been initially developed for systems without cosolvents, recently new models and modifications of previous models have been proposed that incorporate additional parameters and are applicable to systems with cosolvents. Most of them are modifications of the Chrastil's equation with an increasing number of parameters [19–24]. However, an increase in the number of parameters does not correspond to a better performance and often the models become much more empirical. Moreover, these models usually do not take in account cosolvent–solute interactions or the concentration of cosolvent and their performance near the mixture critical point has not been evaluated.

The present work contributes to understanding modelling solubility of solid APIs in sc-CO_2 using semiempirical models and assesses several models considering the effect of pressure, mixture critical point, cosolvent concentration and the relationship between the corresponding solubility parameters. Extensions of Chrastil and Méndez-Santiago and Teja models, González, Tang, Reddy and Madras models are considered, and a new model is proposed based on the Tsallis's [25] statistical non-extensive entropy theory.

The new model uses the q-exponential function to generalize Chrastil's equation for calculating the solubility of solid in binary systems, and to modify the González's model for ternary systems.

Although the new q-Chrastil and q-González models proposed have shown deviations similar to the other models, they have potential for further investigations mainly because their parameters have a physical meaning and because, being generalizations, they can perform better for some systems at high temperature.

2. Modelling solubility of solids in pure SCF

Chrastil [19] published one of the first models to fit experimental data of solubility of solids in pure SCFs (Eq. (1)). The model assumes that there is equilibrium between the solid and the SCF, forming a solvate complex constituted by molecules of solute and surrounding molecules of SCF. A relationship between the solubility and the density of the SCF was established, using three adjustable parameters (k, A and B). The parameters values are determined minimizing the deviations between experimental and calculated solubility data. S is the solubility of the solid in the SCF, T is the temperature, ρ is the density of the pure SCF and k is the association number of the solvate-complex.

$$S = \rho^k \times \exp\left(\frac{A}{T} + B\right) \tag{1}$$

Modifications have been proposed either on the solvent density term or the temperature exponential term to improve correlation and prediction ability of Chrastil's equations applied to SCF systems. A review of these modifications is in Tabernero et al. [24]. The common consequence of these modifications is an increase in the number of parameters used. These parameters have no physical meaning and weaken the usefulness of the model for predictive calculations. The challenge is to improve the predictive capacity of semiempirical models without addition of new parameters. Particularly, in the present paper, we investigate a modification of the exponential term of Chrastil's equation that does not increase the number of parameters.

In Chrastil's equation, the exponential term comes from the Boltzmann's weight argument in the form of $\exp(-E/RT)$ where E is the energy that is a mechanical, non temperature dependent variable [25,26]. However, often empirical modifications are introduced in this kind of exponential term considering that energy depends on temperature. The most common relationship considered between energy and temperature is the linear one. In this case, the following equation is used:

$$E = E_0 + E_1 T \tag{2}$$

Using Eq. (2), the Boltzmann's weight argument becomes

$$\frac{E}{RT} = \frac{E_0}{Rt} + \frac{E_1}{R} \tag{3}$$

Expressing $E_0/R = A$ and $E_1/R = B$, the exponential term of the Chrastil's equation is obtained.

However, several works indicate that the correct way to express the energy exponential term is based on the Tsallis's weight argument instead of Boltzmann's one, leading to an energy term independent of temperature [25,27]. It should be noted that using Boltzmann's weight argument there is an inconsistency when T rises to infinity. In this case, the exponential term should be equal to unity but with Chrastil's equation this terms becomes a constant $\exp(B)$. The same inconsistency occurs with the equations proposed by Adachi and Lu [28], del Valle and Aguilera [29], Sparks [22] – as described in Tabernero et al. [24] – and for what else equation that expresses the exponential term based on Boltzmann's argument. Although it is not usual to perform solubility studies of solids in SCFs at high temperature, such inconsistency might hinder the modelling process of solubility data with semiempirical equations. Moreover, as discussed in [24], the Chrastil's model and its derivatives perform worse at higher temperatures (close to the upper critical end point of the corresponding system). Trying to overcome this problem, we are proposing a generalised Chrastil's equation for calculation of solubility of solid in binary systems based on the Tsallis's statistical non-extensive entropy theory [30]. Tsallis's theory has been applied in different areas of science, such as in the application of q-Weibull distribution to model hazard rate in

Please cite this article in press as: A. Tabernero, et al., Modelling solubility of solid active principle ingredients in sc-CO_2 with and without cosolvents: A comparative assessment of semiempirical models based on Chrastil's equation and its modifications, J. Supercrit. Fluids (2013), http://dx.doi.org/10.1016/j.supflu.2013.11.017

G Model
SUPFLU-2862; No. of Pages 12
ARTICLE IN PRESS
A. Tabernero et al. / J. of Supercritical Fluids xxx (2013) xxx–xxx

problems of reliability engineering [31] or in the investigation of deviations from Arrhenius law in kinetics of chemical and biophysical processes [32]. Other interdisciplinary applications can be found elsewhere [33].

The new q-Chrastil's equation uses the definition of the q-exponential function expressed as follows [26]:

$$\exp_q x = [1+(1-q)x]^{1/1-q}, \quad \text{if} \quad [1+(1-q)x] > 0 \tag{4}$$

or

$$\exp_q x = 0, \quad \text{if} \quad [1+(1-q)x] \leq 0 \tag{5}$$

Applying the q-exponential function it is possible to express q-Chrastil's equation as

$$S = \rho^k \times \exp_q\left(\frac{A_q}{T}\right) \tag{6}$$

where k, Aq and q are the only adjustable parameters. So, the q-Chrastil's equation has the same three adjustable parameters as the original Chrastil's equation, but without the theoretical inconsistency in the exponential term described above. As happened with the Chrastil's equation, parameter k is the number of molecules of the SCF surrounding the solute, whereas the parameter A is related to the solvation energy.

3. Modelling solubility of solids in SCF with cosolvents

Recently, several attempts have been made to extend the applicability of Chrastil's equation to solid/SCF systems including cosolvents as indicated below. Sauceau et al. [34] proposed the following equation based on the Chrastil's equation by adding a new parameter k_3 to take in account the molecules of cosolvent surrounding the solute (Eq. (7)). In this equation, parameter k_1 is the original parameter k of Chrastil's equation that refers to the molecules of SCF surrounding the solute.

$$S = \rho^{(k_1+k_3)} \times \exp\left(\frac{A}{T}+B\right) \tag{7}$$

In Eq. (7), ρ is the mixture (SCF + cosolvent) density, and there are four adjustable parameters: A, B, k_1 and k_3. Once parameters k_1 and k_3 are simultaneously fitted to the same experimental data, we proposed to consider them as a single constant ks. We propose as well to consider ρ as the density of the pure SCF to circumvent the requirement of data that might not be available in literature. The resulting equation (Eq. (8)) resembles the original Chrastil's equation; however, it should be fitted to experimental data from ternary systems.

$$S = \rho^k \times \exp\left(\frac{A}{T}+B\right) \tag{8}$$

where $ks = k_1 + k_3$. This equation is referred to here as Chrastil3 model and the adjustable parameters are A, B and ks.

However, with our modifications, Eq. (8) can only be applied for a fixed concentration of cosolvent, a drawback that does not affect other semiempirical models. González et al. [35] proposed the following modification of the Chrastil's equation for ternary systems (Eq. (9)), in which there is an additional term related to the concentration of cosolvent (m) in the mixture.

$$S = \rho_{SCF}^k \times m^\gamma \times \exp\left(\frac{A}{T}+B\right) \tag{9}$$

where ρ_{SCF} is the density of the pure SCF, k is the association number of the SCF, m is the cosolvent concentration (molar fraction) in the binary mixture SCF-cosolvent and γ is the association number for the cosolvent. With this equation, it is possible to take into account the cosolvent concentrations without performing additional calculations concerning the density of the fluid phase, however there are four adjustable parameters to be fitted: A, B, k and γ.

Sovova [36] proposed a model based on an increase of the solubility of the solid in the SCF + cosolvent mixture with respect to the solubility of the same solid in the pure SCF. Tang et al. [37] modified Sovova's model by adding a temperature dependent term. The following equation resulted (Eq. (10)):

$$S_2 - S_1 = k \times y_3^m \times S_1^n \times \exp\left(\frac{A}{T}\right) \tag{10}$$

In Eq. (10), S_2 is the solubility (molar fraction) of the solid in the mixture SCF + cosolvent, S_1 is the solubility of the solid in the pure SCF (molar fraction), y_3 is the concentration of cosolvent (molar fraction) in the binary mixture SCF + cosolvent, and T is the temperature (K). There are four adjustable parameters: A, k, m and n.

Méndez-Santiago and Teja [38] developed an equation applicable to the solubility of solids in pure SCFs. By combining the theory of dilute solutions and the definition of the effective Henry's constant, the authors proposed a linear relationship between the enhancement factor ($y_2 \times P/P_{ref}$) and the density of the pure SCF. Sauceau et al. [34] used an extended equation for systems with cosolvents by including a term with the molar fraction of the cosolvent and a new semiempirical parameter D, giving Eq. (11) as follows

$$T \times \mathrm{Ln}\left(\frac{S_2 \times P}{P_{ref}}\right) = A + B \times \rho_{SCF} + C \times T + D \times y_3 \tag{11}$$

where P_{ref} is a standard reference pressure (1 bar), P is the pressure of the system (bar), ρ_{SCF} is the density of the pure SCF and y_3 is the concentration of cosolvent in the mixture SCF + cosolvent (molar fraction), A, B, C and D are the adjustable parameters.

Reddy and Madras [39,40] proposed Eqs. (12) and (13) to fit solubility of solids in SCF with cosolvents. Both are based on the formation of a solvato-complex between the solute and the SCF with the cosolvent, although with different theoretical basis in their development.

Specifically, the fugacity coefficients of the cosolvent and solute in the supercritical phase in Eq. (12) are expressed in terms of the activity coefficients at infinite dilution, which are calculated with NRTL (non-random two-liquid) equation. On the other hand, the fugacity coefficients of Eq. (13) are calculated in terms of Henry's constant at infinite dilution.

$$\mathrm{Ln}(S_2) = \mathrm{Ln}(y_3) + (k-1) \times \mathrm{Ln}\left(\frac{P}{P_{ref}}\right) + \frac{A + B \times y_3}{T} + C \times \rho_{SCF} + D \tag{12}$$

$$\mathrm{Ln}(S_2) = (k+\gamma-1) \times \mathrm{Ln}\left(\frac{P}{P_{ref}}\right) + \gamma \times \mathrm{Ln}(y_3) + \frac{(A + B \times \rho_{SCF} + C \times y_3)}{T} + D \times \rho_{SCF} + E \tag{13}$$

For both equations, the standard reference pressure P_{ref} is 1 bar, S_2 is the solubility of the solid in the SCF + cosolvent mixture, y_3 the molar fraction of the cosolvent in the binary mixture SCF + cosolvent and ρ_{SCF} is the density of the pure SCF. For Eq. (12), named here as RedMa5 model, five parameters should be regressed (A, B, C, D, and k) and for Eq. (13), named here as RedMa7 model, seven parameters are needed (A, B, C, D, E, k and γ).

Following the same procedure adopted to develop the new q-Chrastil's equation from the original Chrastil's equation using the q-exponential function, we propose a new model to correlate and predict the solubility of solids in SCF with cosolvent based on the González's equation. We modify González's equation (Eq. (9)) because it expresses the exponential term based on Boltzmann's

Please cite this article in press as: A. Tabernero, et al., Modelling solubility of solid active principle ingredients in sc-CO_2 with and without cosolvents: A comparative assessment of semiempirical models based on Chrastil's equation and its modifications, J. Supercrit. Fluids (2013), http://dx.doi.org/10.1016/j.supflu.2013.11.017

G Model
SUPFLU-2862; No. of Pages 12
ARTICLE IN PRESS

Table 1
The models tested and the number of adjustable parameters (NAP).

Model	Chrastil3	González	Tang	MST	RedMa5	RedMa7	q-Chrastil	q-González
Equation number	8	9	10	11	12	13	6	14
NAP	3	4	4	4	5	7	3	4

argument. Applying the q-exponential function in Eq. (9) it is possible to express q-González's equation as

$$S = \rho_{SCF}^{k} \times m^{\gamma} \times \exp_q\left(\frac{A_q}{T}\right) \quad (14)$$

where ρ_{SCF} is the density of the pure SCF, k is the association number of the SCF, m is the cosolvent concentration in the mixture SCF + cosolvent (molar fraction) and γ is the association number for the cosolvent. With this equation, it is possible to take into account the cosolvent concentrations without performing additional calculations concerning density of binary mixtures. The number of adjustable parameters (Aq, q, k and γ) is the same as in González's equation.

It is important noticing that with our modifications in Sauceau's equation for systems with cosolvents (Eq. (8)), the original Chrastil's equation for binary systems (without cosolvents) is recovered (Eq. (1)). Applying the q-exponential function to Eq. (1), leads to obtaining the q-Chrastil's equation (Eq. (6)). For this reason we apply the q-Chrastil model (Eq. (6)) to systems with cosolvents.

Table 1 shows a summary of the models tested in this work with the corresponding number of adjustable parameters.

4. Procedure for calculation and comparison of the models

In a previous work, an extensive comparison of nine semiempirical models to fit experimental data of solubility of 27 solid API systems in pure $scCO_2$ was conducted [24]. However, the results showed that semiempirical equations provide higher deviations for a wide temperature range (as long as the final temperature is close to the upper critical end point). To overcome this limitation, q-Chrastil equation is being proposed in the present work. Taking that into account, the comparison between Chrastil's equation (Eq. (1)) and q-Chrastil's equation (Eq. (6)) applied to a wider range of molecules is presented: experimental data on solubility of APIs in sc-CO_2 for 58 binary systems have been used. The number of data points (N) and the temperature and pressure range for each system are presented in Table 2. Density data was taken from NIST webbook [41]. It is important to say that all isotherm data were used together in the minimization procedure of the objective function in terms of the sum of relative deviation in solubility to estimate the parameters of the models, i.e., all parameters are considered to be roughly independent of temperature. This is the best way to estimate the parameters of the model because it allows predicting solubility in the range of temperature considered by interpolation. The average relative deviation in solubility was calculated by the following expression (Eq. (15)):

$$\mathrm{AARD} = \left(\frac{100}{N}\right) \times \sum_{i=1}^{N} \frac{|y_{cal} - y_{exp}|}{y_{exp}} \quad (15)$$

Experimental data on solubility of solid APIs in $scCO_2$ with cosolvents for 27 ternary systems were chosen from the literature. To the best of our knowledge, the solubilities of acetazolimide and m-HBA in pure $scCO_2$ are not available in literature. The solubilities of all the other compounds studied in systems with cosolvents were modelled with Chrastil and q-Chrastil equations in pure $scCO_2$ (see Table 2).

Table 3 shows the ternary systems selected with the corresponding experimental conditions and indicates if the operating conditions where less than 10 bar above the mixture critical point (MCP) of the binary CO_2 + cosolvent mixture at any temperature. References from vapour–liquid equilibria studies were used to get the MCP experimental data for these systems are included in Table 3.

Table 2
Binary systems API-$scCO_2$ used to compare Chrastil's and q-Chrastil's equations.

Solute	Temperature range (K)	Pressure range (bar)	N	Ref.
2-Methylbenzoic acid	313–333	110–245	18	[42]
3-Methylbenzoic acid	313–333	110–245	18	[42]
3,5-Dinitrobenzoic acid	308–328	100–210	15	[37]
4-Aminoantipyrine	308–328	100–220	21	[43]
4-Methylbenzoic acid	313–333	110–245	18	[42]
Acetaminophen	313–353	80–300	10	[44]
Alpha-tocopherol	313–353	200–350	24	[45]
Aspirine	318–328	120–200	8	[46]
Astaxanthin	313–333	100–400	26	[47]
Atorvastatin	308–348	120–350	45	[48]
Beta-carotene	313–353	200–350	23	[45]
Budesonide	338–358	215–285	21	[49]
Caffeic acid	313–333	150–500	24	[50]
Caffeine	313–353	200–350	24	[51]
Cholesterol	313–333	100–250	22	[52]
Cholesterolbenzoate	308–328	120–270	20	[52]
Clofibric acid	308–328	100–220	21	[53]
Clozapine	318–348	120–355	27	[54]
Cyproterone acetate	308–348	120–350	40	[55]
Diflunisal	308–328	90–250	21	[56]
Exemestane	308–348	120–350	45	[57]
Fenofibrate	308–328	100–220	21	[53]
Flurbiprofen	303–323	80–250	27	[58]
Fluvastatin	308–348	120–350	45	[48]
Gemfibrozil	308–328	100–220	21	[53]
Hexadecanoic acid	308–318	130–225	10	[59]
Irgacure2959	308–328	100–260	21	[60]
Ketoprofen	312–331	100–220	10	[61]
Lamotrigine	308–348	120–355	45	[54]
Letrozole	308–348	120–350	45	[57]
Lycopene	313–333	200–400	19	[62]
Lidocaine	298–318	70–250	33	[63]
Lovastatin	308–348	120–350	45	[48]
Medroxyprogesterone acetate	308–348	120–350	40	[55]
Methimazole	308–328	120–350	40	[64]
Nabumetone	308–328	100–220	21	[65]
Naproxen	313–333	90–195	18	[66]
Nimesulide	313–333	130–220	8	[61]
Nitrendipine	333–373	100–300	42	[67]
Octadecanoic acid	308–318	130–225	10	[59]
Ortho-hydroxybenzoic acid	308–328	80–200	49	[68]
Penicillin G	313–333	100–350	18	[69]
Penicillin V	315–335	80–280	24	[70]
Phenazopyridine	308–348	120–350	45	[64]
Procaine	298–318	70–250	28	[63]
Progesterone	308–328	105–240	40	[71]
Propanolol	308–348	120–350	45	[64]
Propyl p-hydroxybenzoate	308–328	80–230	18	[72]
p-toluenesulfonamide	308–328	80–210	15	[73]
Rosuvastatin	308–348	120–350	45	[48]
Simvastatin	308–348	120–350	45	[48]
Taxol	308–318	205–475	12	[74]
Testosterone	308–328	85–240	39	[71]
Tetradecanoic acid	308–318	100–225	11	[75]
Theobromine	313–353	210–345	23	[51]
Theophylline	313–353	200–350	22	[51]
Vitamine D2	313–353	200–320	19	[45]
Vitamine D3	313–353	200–350	23	[45]

N: number of data points.

Please cite this article in press as: A. Tabernero, et al., Modelling solubility of solid active principle ingredients in sc-CO_2 with and without cosolvents: A comparative assessment of semiempirical models based on Chrastil's equation and its modifications, J. Supercrit. Fluids (2013), http://dx.doi.org/10.1016/j.supflu.2013.11.017

Table 3
Ternary systems API-scCO_2-cosolvent used to compare the models.

(Number) System	Temp. (K)	Press. (bar)	% Cosolvent	MCP	R	N	Ref.
(1) 1-Propanol-naproxen	333	110–180	1.75–5.25	[79]	1.04	15	[66]
(2) 2-propanol-naproxen	323–333	110–180	1.75–5.25	[80]	1.04	22	[66]
(3) Acetone-cholesterol	318–328	100–240	3.0	[81]	1.05	13	[52]
(4) Acetone-cholesterolbenzoate	318–328	130–270	3.0	[81]	1.02	12	[52]
(5) Acetone-mHBA	318–328	91–201	3.5	[81]	0.65	22	[77]
(6) Acetone-naproxen	318–333	90–190	1.75–5.25	<10 [81]	0.84	33	[66]
(7) Acetone-oHBA	318–328	86–201	3.5	<10 [81]	0.65	22	[77]
(8) Acetone-propyl *p*-hydroxybenzoate	308	80–230	3.5	[81]	0.78	6	[72]
(9) Cyclohexane-propyl *p*-hydroxybenzoate	308	80–230	3.5	<10 [82]	0.64	6	[72]
(10) Ethanol-acetazolimide	313–323	150–200	5.0	[83]	0.79	16	[78]
(11) Ethanol-aspirine	318–328	100–200	3.0	[83]	0.94	10	[46]
(12) Ethanol-hexadecanoic acid	308–318	125–225	0.73–4.16	[83]	1.19	20	[59]
(13) Ethanol-naproxen	323–333	110–180	1.75–5.25	<10 [83]	1.13	24	[66]
(14) Ethanol-octadecanoic acid	308–318	125–225	0.73–4.16	[83]	1.02	20	[59]
(15) Ethanol-*p*-toluenesulfonamide	308–328	80–210	3.5	<10 [83]	0.95	15	[73]
(16) Ethanol-tetradecanoic acid	308–318	100–225	0.73–4.16	[83]	1.18	21	[75]
(17) Ethyl acetate-3,5-Dinitrobenzoicacid	308–328	80–210	1.5–5.5	<10 [84]	0.60	25	[37]
(18) Ethyl acetate-naproxen	333	110–180	1.75–5.25	[84]	0.77	18	[66]
(19) Methanol-aspirine	318–328	100–200	3.0	[85]	1.17	10	[46]
(20) Methanol-cholesterol	318–328	100–240	3.0	[85]	1.45	13	[52]
(21) Methanol-cholesterolbenzoate	318–328	130–270	3.0	[85]	1.40	12	[52]
(22) Methanol-mHBA	318–328	91–201	3.5	<10 [85]	0.90	19	[77]
(23) Methanol-naproxen	323–333	110–190	1.75–5.25	<10 [85]	1.26	26	[66]
(24) Methanol-oHBA	318–328	96–201	3.5	[85]	0.90	21	[77]
(25) 3-Methyl-1-butanol-hexadecanoic acid	308–318	125–225	0.73–1.98	[86]	1.16	15	[59]
(26) 3-Methyl-1-butanol-octadecanoic acid	308–318	125–225	0.73–1.98	[86]	1.00	15	[59]
(27) 3-Methyl-1-butanol-tetradecanoic acid	308–318	100–225	0.73–1.98	<10 [86]	1.14	16	[75]

R: ratio between the Hildebrand solubility parameters of the cosolvent and the solute.

Taking into account the interactions between cosolvent and solute, the ratio *R* between the Hildebrand solubility parameters of the cosolvent and the solute was calculated by Eq. (16). Hildebrand's parameter provides an estimation of the interactions between compounds. Solvent power can be quantified by using *R*: when a stronger solvent effect is present the Hildebrand parameters for the cosolvent and the solute are similar (*R* is close to 1). Therefore, the parameter *R* was used to observe the effect of the cosolvent–solute interactions on the deviation of each of the models. Fedors' group contribution method [76] was used to calculate the solubility parameter of the pure cosolvent and of the pure solute. The ratio *R* between the solubility parameters is also given in Table 3.

$$R = \frac{\delta_{cosolv}}{\delta_{solute}} \quad (16)$$

In this modelling study of solubility of APIs in ternary systems, the effect of pressure range, vicinity to the mixture critical point, concentration of cosolvent and the value of parameter *R* on the performance of the models was investigated.

For both binary and ternary systems, Newton's method was used to perform data regressions and estimation of the corresponding parameter for all the systems and models.

5. Results and discussion

5.1. Calculation of solubility of solid APIs in pure scCO_2

In this section, *q*-Chrastil (Eq. (6)) and original Chrastil (Eq. (1)) models were used for fitting experimental solubility data of 58 APIs in pure scCO_2 (see Table 2). Table 4 shows the AARD calculated for each binary system with Chrastil3 and *q*-Chrastil models and the value of the parameter *q*. All other estimated parameters are given in Appendices A and B.

According to the results, Chrastil3 and *q*-Chrastil fit the solubility data of solid APIs in scCO_2 with roughly the same deviation and the same standard deviation. Moreover, both equations reproduce experimental data in the same way, as it can be observed in Fig. 1, where both the experimental and the calculate data of solubility

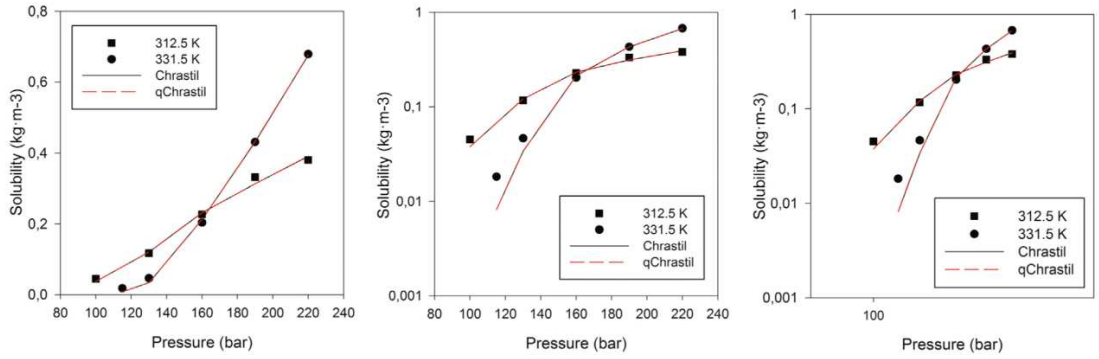

Fig. 1. Prediction of the solubility of ketoprofen in sc-CO_2 with *q*-Chrastil and Chrastil3 with linear–linear, linear–log and log–log scales. Experimental data from [61].

Please cite this article in press as: A. Tabernero, et al., Modelling solubility of solid active principle ingredients in sc-CO_2 with and without cosolvents: A comparative assessment of semiempirical models based on Chrastil's equation and its modifications, J. Supercrit. Fluids (2013), http://dx.doi.org/10.1016/j.supflu.2013.11.017

Table 4
AARD calculated for the binary systems with Chrastil3 and *q*-Chrastil models.

Solute	Chrastil3	*q*-Chrastil	*q* Value
2-Methylbenzoic acid	2.34	2.31	1.032
3-Methylbenzoic acid	3.49	3.37	1.037
3,5-Dinitrobenzoic acid	4.87	4.95	1.025
4-Methylbenzoic acid	2.67	2.59	1.043
4-aminoantipyrine	12.41	12.41	1.068
Acetaminophen	24.02	24.02	1.032
Alpha-tocopherol	3.82	3.73	1.077
Aspirine	6.08	6.08	1.057
Astaxanthin	52.98	52.49	1.036
Atorvastatin	8.86	10.26	1.026
Beta-carotene	26.69	29.75	1.027
Budesonide	11.86	11.82	1.047
Caffeic acid	56.75	57.26	1.041
Caffeine	5.16	4.43	1.070
Cholesterol	23.23	23.23	1.064
Cholesterolbenzoate	7.25	7.80	1.062
Clofibric acid	5.06	4.97	1.064
Clozapine	21.08	19.13	1.040
Cyproterone acetate	24.74	24.79	1.081
Diflunisal	21.08	21.01	1.039
Exemestane	33.46	33.46	1.023
Fenofibrate	8.90	7.99	1.064
Flurbiprofen	8.67	8.70	1.033
Fluvastatin	14.73	14.73	1.031
Gemfibrozil	7.83	7.49	1.051
Hexadecanoic acid	2.61	2.07	1.160
Irgacure 2959	3.49	3.37	1.035
Ketoprofen	11.72	11.72	1.047
Lamotrigine	5.74	5.75	1.076
Letrozole	38.46	39.09	1.025
Licopene	5.71	5.60	1.040
Lidocaine	34.45	34.46	1.044
Lovastatin	5.89	6.09	1.069
Medroxyprogesterone acetate	18.91	18.23	1.055
Methimazole	12.69	12.39	1.054
Nabumetone	11.55	11.55	1.045
Naproxen	9.77	9.80	1.059
Nimesulide	19.13	18.08	1.057
Nitrendipine	16.10	15.58	1.055
Octadecanoic acid	8.31	8.31	1.140
o-Hydroxybenzoic acid	8.15	8.15	1.043
Penicillin G	25.43	25.65	1.035
Penicillin V	18.17	18.17	1.076
Phenazopyridine	15.46	15.59	1.051
Procaine	14.25	14.25	1.068
Progesterone	17.27	17.26	1.054
Propanolol	38.42	36.75	1.021
Propyl *p*-hydroxybenzoate	30.81	30.92	1.022
p-toluenesulfonamide	7.50	7.87	1.032
Rosuvastatin	6.96	6.84	1.047
Simvastatin	13.05	12.77	1.042
Taxol	4.34	4.28	1.057
Testosterone	23.48	23.51	1.038
Tetradecanoic acid	13.82	13.82	1.150
Theobromine	6.62	6.70	1.067
Theophylline	5.50	5.39	1.079
Vitamin D2	10.53	11.82	1.062
Vitamin D3	34.11	34.33	1.049
Average AARD ± standard deviation	15.45 ± 11.27	15.42 ± 11.31	

of ketoprofen in $scCO_2$ are depicted, in linear–linear, linear–log and log–log scales. Another point of interest is that the value of the parameter q is almost close to unity for all systems. If the parameter q tends to one, the q-exponential reduces to the original exponential, and as consequence the q-Chrastil reduces to the original Chrastil's equation. As q tends to unity for all binary systems investigated, the similar AARD obtained for both models are expected. Chrastil's equation can be seen as a particular case of the q-Chrastil's with q equal to one. A correlation between q and temperature applicable to all systems (thus independent from the API) was investigated. Finding a $q = q(T)$ equation valid for a wide range

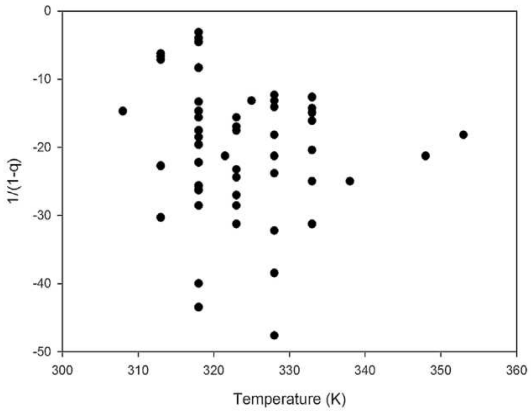

Fig. 2. Temperature effect on parameter q for all the binary systems.

of solutes would allow the reduction of the number of parameters of q-Chrastil's model from three to two.

The temperature effect on the parameter q was studied by plotting the average temperature of the experimental data for each system against $1/1 - q$ (Fig. 2). In this Fig. 2 it can be seen that there is not a clear behaviour the parameter q as a function of the temperature. As a consequence, it is not possible to obtain a simple expression to correlate q as a function of the temperature.

It was also observed that for highly linear molecules (fatty acids) such as hexadecanoic, octadecanoic and tetradecanoic acids the parameter q is around 1.15, differing of the common values found for molecules constituted by aromatic and/or polycyclic aliphatic rings (between 1.030 and 1.075). The results indicate a dependency of the value of parameter q on the molecular structure of the solid with the possibility of developing a group contribution method to estimate this parameter. The development of such group contribution method would reduce the total number of parameters in the q-Chrastil's equation.

5.2. Calculation of solubility of solid APIs in sc-CO_2 and cosolvents

In this section, the first six models shown in Table 1 were used for fitting experimental solubility data of different APIs in $scCO_2$ and cosolvents (see Table 3). Table 5 shows the AARD calculated and the standard deviations for each of the six semiempirical equations; the values of the corresponding parameters are given in Appendices A and B.

As explained before, Chrastil3 equation cannot be used for systems with different concentrations of cosolvent at the same temperature. However, the equation was used when there were experimental data for the same concentration of cosolvent at different temperatures. As an example, system 1 comprises three different concentrations of cosolvent, but only one temperature (333 K). In this case, Chrastil3 was not employed. On the other hand, system 2 (comprising also three different concentrations of cosolvent) was studied for two different temperatures (323 and 333 K) for 3.5% molar of concentration of cosolvent. In this case, Chrastil3 was used for this constant concentration of cosolvent (Indicated in Table 5).

Fig. 3 illustrates the average AARD for each equation with their standard deviations. From this Fig. 3 and Table 3 it is possible to extract several conclusions. All models yield similar results in terms of AARD and standard deviations. RedMa7 provides an AARD around 6–7%, which is the lowest. However, seven parameters should be estimated and this a disadvantage because the number of experimental data points necessary increases with the number of

Please cite this article in press as: A. Tabernero, et al., Modelling solubility of solid active principle ingredients in sc-CO_2 with and without cosolvents: A comparative assessment of semiempirical models based on Chrastil's equation and its modifications, J. Supercrit. Fluids (2013), http://dx.doi.org/10.1016/j.supflu.2013.11.017

Table 5
AARD calculated for the ternary systems with six models.

Number	Chrastil3	González	Tang	MST	RedMa5	RedMa7
1	**	11.08	5.31	18.77	13.67	12.27
2 (3.5%)	3.63	11.61	5.66	16.34	12.73	12.51
3 (3.0%)	7.22	8.22	4.94	9.49	6.08	2.37
4 (3.0%)	3.3	7.25	3.81	4.28	2.00	1.65
5 (3.5%)	2.15	2.15	**	3.15	1.95	1.97
6 (3.5%)	9.98	13.69	8.64	14.34	13.92	10.90
7 (3.5%)	2.48	2.48	4.56	4.59	3.16	2.77
8 (3.5%)	16.67	16.67	25.35	17.60	18.35	15.20
9 (3.5%)	22.77	22.77	26.07	25.33	10.81	9.27
10 (5.0%)	5.48	4.79	**	4.90	3.83	3.76
11 (3.0%)	6.55	6.55	27.36	9.12	8.11	5.66
12 (0.73%)	2.34	10.09	6.27	0.51	11.49	0.41
13 (3.5%)	7.12	10.21	8.36	16.25	11.92	11.07
14 (0.73%)	5.70	14.78	11.20	2.85	13.80	2.99
15 (3.5%)	32.17	22.59	15.44	26.11	7.17	6.71
16 (0.73%)	12.02	13.04	3.85	11.93	13.09	5.11
17 (3.5%)	14.92	14.78	9.61	14.42	9.51	9.52
18	**	16.59	7.93	17.60	17.36	17.63
19 (3.0%)	7.28	7.27	6.94	9.57	10.12	4.39
20 (3.0%)	4.91	4.92	4.35	5.99	5.47	4.19
21 (3.0%)	3.19	3.19	6.69	3.60	2.70	2.99
22 (3.5%)	2.67	2.67	**	4.70	3.13	3.21
23 (3.5%)	4.93	11.46	25.27	19.66	14.80	12.59
24 (3.5%)	3.11	2.13	5.05	3.52	2.24	2.37
25 (0.73%)	2.61	1.88	1.52	0.55	0.41	0.45
26 (0.73%)	2.24	1.82	3.23	0.58	0.45	0.47
27 (0.73%)	13.40	11.73	2.78	10.52	9.38	9.39
Average AARD ± Standard deviation	7.95 ± 6.62	9.50 ± 6.02	9.59 ± 8.07	10.23 ± 7.55	8.43 ± 5.38	6.36 ± 4.91

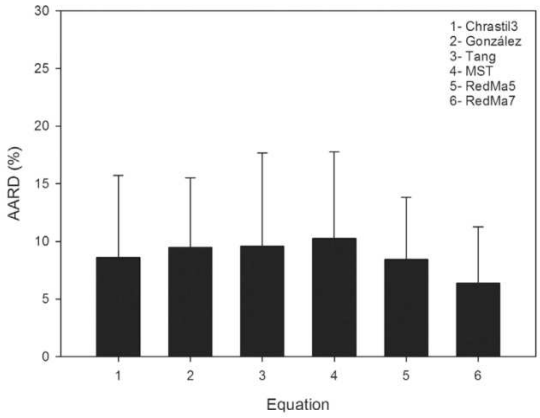

Fig. 3. Average AARD for each equation.

parameters of the model in order to allow the optimization numerical method to perform adequately the estimation procedure.

Tang (Eq. (10)) and González (Eq. (9)) models fit the experimental solubility data with an AARD lower than 10%, and with only four adjustable parameters. However, Tang's equation requires the knowledge of the solubility data of the compound in the pure SCF, which sometimes is unknown (as happens with system 22). In this case, Tang's model cannot be used. This shortcoming can be avoided by the RedMa5 model, which provides an AARD less than 9% but with one additional parameter.

When possible, it is better to use Chrastil3 as it has the lower number of parameters. However, Chrastil3 cannot be used if several concentration of cosolvents at the same temperature are included in the modelling process. This drawback can be avoided by using González's equation that generates an average AARD slightly higher (average AARD lower than 10%) and a similar standard deviation. However, its use requires one additional parameter. Finally, MST provides the highest average AARD: between 10% and 11%.

It can be concluded from these results that Chrastil3 can be used to perform an accurate fit of the solubility data as long as there is only one composition of cosolvent. On the other hand, for different concentrations of cosolvent at the same temperature, Tang and González models, with four parameters each, or RedMa5 with five parameters are good alternatives. However, Tang's equation provides the highest standard deviation. Moreover, if the solubility of the solid in the pure SCF is unknown, RedMa5 or González equations can be employed, increasing the accuracy of the fitting around 1%, but adding one or two parameters, respectively. Although RedMa7 provides the best fit, estimation of seven parameters can be difficult and for this reason this model is not recommendable.

5.3. Effect of the vicinity to the solvent-cosolvent mixture critical point on the solubility

The mixture critical point of the system solvent-cosolvent is defined as the pressure above which (for a fixed temperature) vapour and liquid phase merge into one single supercritical phase. Due to the transition from a biphasic to a monophasic region, a drastic increase in the solubility can occur when the systems are close to this point.

Experimental runs with cosolvents are usually carried out at a pressure higher than the MCP in order to avoid the biphasic region and achieve higher solubility. However, to take into account the influence of proximity to the MCP, the modelling results for systems which experimental pressures were less than 10 bar above the MCP are examined (Table 6). Data about the relevant MCPs were taken from different experimental studies (references reported in the fifth column of Table 3).

Table 6 shows the AARD values for each ternary system and the average AARD and standard deviations for each equation. It can be noted that the average AARD for Chrastil3, González, Tang and MST models increases about 30–40% in comparison with their average AARD given in Table 5. In general, the statistical parameter also increases, although decreases for RedMa5 and RedMa7 equations.

Please cite this article in press as: A. Tabernero, et al., Modelling solubility of solid active principle ingredients in sc-CO_2 with and without cosolvents: A comparative assessment of semiempirical models based on Chrastil's equation and its modifications, J. Supercrit. Fluids (2013), http://dx.doi.org/10.1016/j.supflu.2013.11.017

Table 6
AARD calculated for systems with experimental conditions less than 10 bars above the MCP.

Number	Chrastil3	González	Tang	MST	RedMa5	RedMa7
6	9.98	13.69	8.64	14.34	13.92	10.90
7	2.48	2.48	4.56	4.59	3.16	2.77
9	22.77	22.77	26.07	25.33	10.81	9.27
13	7.12	10.21	8.36	16.25	11.92	11.07
15	32.17	22.59	15.44	26.11	7.17	6.71
17	14.92	14.78	9.61	14.42	9.51	9.52
22	2.67	2.67	**	4.70	3.13	3.21
23	4.93	11.46	25.27	19.66	14.80	12.59
27	13.40	11.73	2.78	10.52	9.38	9.39
Average AARD ± Standard deviation	12.27 ± 9.92	12.49 ± 7.22	12.59 ± 8.89	15.10 ± 7.81	9.31 ± 4.19	8.38 ± 3.45

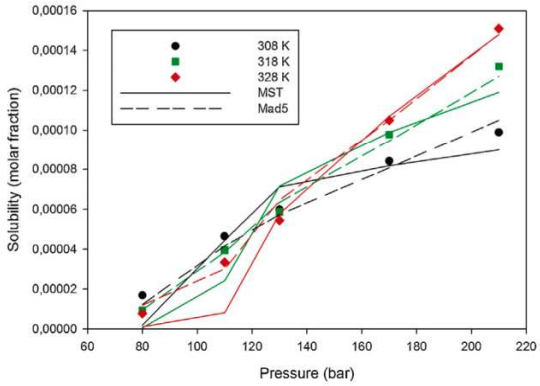

Fig. 4. Solubility of pTSA in sc-CO_2 with ethanol as a cosolvent. Experimental data from [73].

The only equations that fit these data with an average AARD value lower than 10% are RedMa5 and RedMa7. In fact, the average AARD values of these equations do not significantly increase close to the MCP. Particularly, the average AARD for RedMa5 increases only from 8.43% to 9.31%, for RedMa7 it increases from 6.36% to 8.38%. In summary, the RedMa5 equation can reproduce the transition from a biphasic to a monophasic region with five parameters, losing only 1% of accuracy compared to RedMa7 model, thus RedMa5 equation appears to be the most suitable to model solubility data of APIs in SCF + co-solvent systems in the proximity of the corresponding MCP.

Fig. 4 depicts the solubility of pTSA with ethanol as a cosolvent (experimental conditions close to the MCP) and the fit with MST and RedMa5. It can be observed how MST model does not predict accurately experimental data at high temperatures (closer to the MCP). However, at conditions farther from the MCP (lower temperature), the model is more accurate. On the other hand, RedMad5 fits better the experimental data for all the investigated conditions, although the fit is less accurate for low temperatures and pressures.

5.4. Effect of higher experimental pressure on modelling solubility data

Results have shown that there is an increase in the average AARD value for all equations tested when the highest experimental pressure is below 200 bar (Table 7).

The average AARD of all the semiempirical models increases significantly when the higher experimental pressure is lower than 200 bar. It is important to highlight that the average AARD for RedMa5 and RedMa7 almost the doubles to 14.0% and 12.8%, respectively, although the standard deviation decreases significantly for all the equations except for Tang's model (decreasing only around one unit). Chrastil's equation provides the lower average deviation. However, there are only four systems that can be modelled with Chrastil's equation at these conditions, and perhaps more systems are required to get clearer results.

However, the higher experimental pressure in solubility studies of APIs in SCFs are usually higher than 200 bar due to the occurrence lower and upper crossover pressures, Specifically, it is recommended to operate at conditions above the upper crossover pressure, in order to avoid a region in which the solubility of the solute decreases with an isobaric increase of temperature. The knowledge of this region is needed to properly design the extraction and separation steps of supercritical fluid extraction processes [87].

Overall González's equation seems to be the more convenient as the corresponding average AARD is not affected by lack of solubility data above 200 bar and does not require the knowledge of solubility data of the solid in pure CO_2 (as in Tang's model), and can take into account different concentrations of cosolvent and requires only four adjustable parameters.

Fig. 5 illustrates the solubility of naproxen with 2-propanol as a cosolvent. It can be observed how RedMad5 and MST models predict less accurately regions of low pressure and low temperature. However, the fit improves at higher pressures.

5.5. Effect of the concentration of cosolvent and the interactions solute-cosolvent on the solubility

The knowledge of experimental solubility data in SCF with cosolvents is crucial to process design. Usually, the cosolvent is added to

Table 7
AARD calculated for systems with higher experimental pressure lower than 200 bars.

Number	Chrastil3	González	Tang	MST	RedMa5	RedMa7
1	**	11.08	5.31	18.77	13.67	12.27
2	3.63	11.61	5.66	16.34	12.73	12.51
6	9.98	13.69	8.64	14.34	13.92	10.90
13	7.12	10.21	8.36	16.25	11.92	11.07
18	**	16.59	7.93	17.60	17.36	17.63
23	4.93	11.46	25.27	19.66	14.80	12.59
Average AARD ± Standard deviation	6.41 ± 2.78	12.44 ± 2.33	10.19 ± 7.52	17.16 ± 1.92	14.07 ± 1.85	12.83 ± 2.46

Please cite this article in press as: A. Tabernero, et al., Modelling solubility of solid active principle ingredients in sc-CO_2 with and without cosolvents: A comparative assessment of semiempirical models based on Chrastil's equation and its modifications, J. Supercrit. Fluids (2013), http://dx.doi.org/10.1016/j.supflu.2013.11.017

G Model
SUPFLU-2862; No. of Pages 12
ARTICLE IN PRESS
A. Tabernero et al. / J. of Supercritical Fluids xxx (2013) xxx–xxx

Table 8
AARD calculated for systems with the concentration of the cosolvent higher than 3%.

Number	Chrastil3	González	Tang	MST	Madras5	Madras7
1	**	11.08	5.31	18.77	13.67	12.27
2	3.63	11.61	5.66	16.34	12.73	12.51
5	2.15	2.15	**	3.15	1.95	1.97
6	9.98	13.69	8.64	14.34	13.92	10.90
7	2.48	2.48	4.56	4.59	3.16	2.77
8	16.67	16.67	25.35	17.60	18.35	15.20
9	22.77	22.77	26.07	25.33	10.81	9.27
10	5.48	4.79	**	4.90	3.83	3.76
11	6.55	6.55	27.36	9.12	8.11	5.66
12	2.34	10.09	6.27	0.51	11.49	0.41
13	7.12	10.21	8.36	16.25	11.92	11.07
14	5.70	14.78	11.20	2.85	13.8	2.99
15	32.17	22.59	15.44	26.11	7.17	6.71
16	12.02	13.04	3.85	11.93	13.09	5.11
17	14.92	14.78	9.61	14.42	9.51	9.52
18	**	16.59	7.93	17.60	17.36	17.63
22	2.67	2.67	**	4.70	3.13	3.21
23	4.93	11.46	25.27	19.66	14.80	12.59
24	3.11	2.13	5.05	3.52	2.24	2.37
Average AARD ± Standard deviation	9.09 ± 8.35	11.06 ± 6.39	12.24 ± 8.69	12.19 ± 7.90	10.05 ± 5.18	7.68 ± 4.59

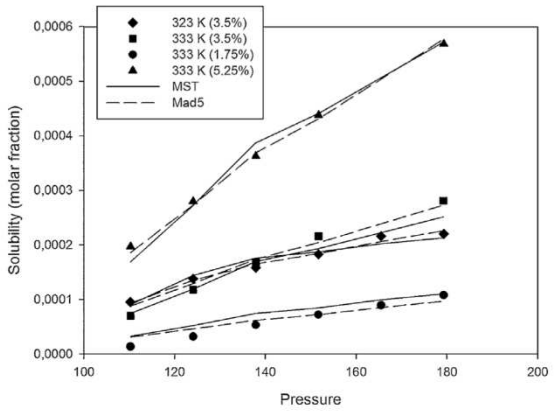

Fig. 5. Solubility of naproxen in sc-CO_2 with ethanol as a cosolvent. Experimental data from [66].

enhance the solubility of the solid in the SCF. However, the cosolvent should be added in moderate amounts-typical 5–6% molar- in order to avoid shortcomings such as residual solvent in the products and mass transfer resistances due to the existence of biphasic fluid regions. Therefore, in order to study the effect of the cosolvent concentration, experimental data were divided based on the molar percentage of cosolvent in scCO_2 used: under and above 3% molar.

Table 8 shows the corresponding AARD values for the systems with these characteristics.

Overall, semiempirical equations can predict the increase in solubility due to the addition of a higher concentration of cosolvent (at least until around 6%) with only a slight increase in the average AARD. However RedMa7 provides the best fit, RedMa5 and González models can be used obtaining an average AARD value close to 10%, with a lower number of adjustable parameters.

Interactions between solute and cosolvent were considered by studying the relation (R) between the corresponding Hildebrand solubility parameters (Eq. (16)). Solvent power can be quantified by using this parameter: a strong solvent effect is produced when the Hildebrand parameters for the cosolvent and the solute are similar. In this case, the investigation was performed for systems with an R between 0.85–1.15. The results are shown in Table 9.

It is clear that all the models provide an accurate fit for systems with R close to unity, in fact all but MST generate average AARD values lower than 10% with similar standard deviations. The average AARD obtained for systems with R close to 1 are similar to the overall average AARDs reported in Table 5.

5.6. Application of q-exponential function for ternary systems

The proposed q-Chrastil (Eq. (6)) and q-González (Eq. (15)) models were also used to fit solubility data of the solid APIs in scCO_2 with cosolvents. The obtained AARD values were compared with the results with original Chrastil3 and González's models, results are reported in Table 10.

Table 9
AARD calculated for systems with R values between 0.85 and 1.15.

Number	Chrastil3	González	Tang	MST	RedMad5	RedMad7
1	**	11.08	5.31	18.77	13.67	12.27
2	3.63	11.61	5.66	16.34	12.73	12.51
3	7.22	8.22	4.94	9.49	6.08	2.37
4	3.30	7.25	3.81	4.28	2.00	1.65
11	6.55	6.55	27.36	9.12	8.11	5.66
13	7.12	10.21	8,36	16.25	11.92	11.07
14	5.70	14.78	11.20	2.85	13.80	2.99
15	32.17	22.59	15.44	26.11	7.17	6.71
22	2.67	2.67	**	4.70	3.13	3.21
24	3.11	2.13	5.05	3.52	2.24	2.37
26	2.24	1.82	3.23	0.58	0.45	0.47
27	13.40	11.73	2.78	10.52	9.38	9.39
Average AARD ± Standard deviation	7.67 ± 8.29	9.22 ± 5.70	8.46 ± 8.50	10.21 ± 7.86	7.55 ± 5.05	5.89 ± 4.60

Please cite this article in press as: A. Tabernero, et al., Modelling solubility of solid active principle ingredients in sc-CO_2 with and without cosolvents: A comparative assessment of semiempirical models based on Chrastil's equation and its modifications, J. Supercrit. Fluids (2013), http://dx.doi.org/10.1016/j.supflu.2013.11.017

Table 10
AARD calculated for the ternary systems with different equations and q value for both q-models.

Number	Chrastil3	q-Chrastil	q(Chrastil)	González	q-González	q(González)
1	**	**	**	11.08	11.08	0.9999
2	3.63	3.62	1.44	11.61	11.73	0.9999
3	7.22	7.22	1.26	8.22	7.22	0.9999
4	3.30	3.30	1.19	7.25	3.30	0.9999
5	2.15	2.15	1.71	2.15	2.15	0.9999
6	9.98	9.89	1.42	13.69	20.98	1
7	2.48	3.33	1.42	2.48	2.48	0.9937
8	16.67	18.65	0.83	16.67	16.67	0.9999
9	22.77	22.77	1.20	22.77	22.77	0.9999
10	5.48	7.27	19.23	4.79	5.45	1
11	6.55	6.55	1.49	6.55	6.55	0.9999
12	2.34	2.38	19.84	10.09	10.09	1.0091
13	7.12	7.13	0.67	10.21	10.91	1
14	5.70	5.70	1.22	14.78	14.78	1.0739
15	32.17	32.15	1.64	22.59	22.60	0.9999
16	12.02	12.06	1.16	13.04	13.42	0.9999
17	14.92	14.74	0.82	14.78	16.68	1
18	**	**	**	16.59	16.59	0.9999
19	7.28	7.27	1.44	7.27	7.28	0.9999
20	4.91	4.92	1.25	4.92	4.92	0.9999
21	3.19	3.19	1.18	3.19	3.19	0.9999
22	2.67	3.62	1.025	2.67	2.67	0.9999
23	4.93	4.99	1.32	11.46	14.01	1
24	3.11	3.11	1.50	2.13	2.13	0.9999
25	2.61	2.32	1.24	1.88	1.88	0.9986
26	2.24	2.25	1.22	1.82	1.99	0.9999
27	13.40	13.40	1.16	11.73	13.49	1
Average AARD ± Standard deviation	7.95 ± 6.62	8.16 ± 6.35		9.50 ± 6.02	9.89 ± 6.71	

q(Chrastil): value of q in Chrastil equation; q(González): value of q in González equation.

Chrastil3 and q-Chrastil's models provide almost the same deviation and the same standard deviation, as the González and q-González's do. Chrastil's model provides a better fit than González's model, but González's equation can be used for different concentrations of cosolvent.

Since almost identical AARD values were obtained with the use of q-models either for binary or ternary systems, the q-exponential function could be employed to develop new models in the field of the solubility of solids in SCF with or without cosolvents. The modelling process for the q-models and the former models would be identical with the same number of parameters. Furthermore, as a generalization model, it can be expected that q-Chrastil and q-González equations can outperform the original models in predicting the solubility of solid APIs in SCFs at high temperature conditions.

The results with the q-models were not included in the comparison with the other six models because the deviation is almost identical in comparison with the original Chrastil and González models, and the same influence of the experimental conditions in the AARD would be produced.

We also observe that the value parameter q for q-González's equation tends strongly to 1. In this case q-González's equation is reduced to the original González's one. On the other hand, with q-Chrastil's equation, q value differs from 1. However, the value ranges from 1 to 19 independently from molecular structure, type of cosolvent or the temperature.

Results from modelling the 27 ternary systems, show within three-parameters equations Chrastil3 provides the lower average AARD (8.6%), whereas the original González equation provides the best fit (average AARD 9.5%) between the four-parameters equations. Finally, it is possible to see that Chrastil3 for binary systems provides higher AARD than in ternary systems. The AARD for binary systems is around 15%, whereas for ternary systems is between 8% and 9%. Similarly, MST applied to ternary systems generated lower average AARD than for binary systems [24]: for binary systems, MST provides an average AARD of around 15–20%, whereas for ternary systems it is reduced to 10%.

The reason can be the effect of temperature. It was shown that equations for binary systems provide a less accurate fit when experimental data are distributed over a wide temperature range (about 50 K). However, systems with cosolvents are usually investigated over a smaller range of experimental temperatures (about 10–20 K), in order to avoid problems with organic solvent evaporation and biphasic phases. This narrow temperature range will not affect the obtained deviation in a modelling process with semiempirical models, and since there are not many available studies with a high temperature range with cosolvents, the effect of the temperature was not investigated.

6. Conclusions

Solubility modelling of solid active principle ingredients in supercritical carbon dioxide with and without cosolvents was performed using Chrastil's equations and its modifications for different binary and ternary systems. Two new models were proposed and a comparative assessment of eight models was done considering as criteria the deviations, the number of parameters, the concentration of cosolvent and the proximity to the mixture critical point. The new models were developed based on a generalization of Chrastil's and González's equations by using a q-exponential function. The q-models generated similar AARD than the original models: Chrastil and q-Chrastil models for binary systems and González's and q-González's for ternary systems.

For ternary systems, six models fit experimental data with a deviation lower than 10%. RedMa7 equation provides the most accurate fit (average AARD 6.4%), although it requires the use of seven parameters. Chrastil3 (average AARD 8.6%) and Tang (average AARD 9.6%) models need less parameters (three and four, respectively), but they cannot be used for data with different concentrations of cosolvent, or if the solubility of the compound in absence of cosolvent is unknown, respectively. Therefore the use of González (average AARD 9.5%, four parameters) and RedMa5 (average AARD 8.6%, five parameters) models are considered the most useful.

Please cite this article in press as: A. Tabernero, et al., Modelling solubility of solid active principle ingredients in sc-CO_2 with and without cosolvents: A comparative assessment of semiempirical models based on Chrastil's equation and its modifications, J. Supercrit. Fluids (2013), http://dx.doi.org/10.1016/j.supflu.2013.11.017

In general, all equations provide an average AARD around 10%. González and RedMa5 equations were shown to be the most suitable, because they do not have drawbacks concerning the number of parameters and either can be used for different concentrations of cosolvent. For all the equations investigated, it is possible to observe the ability to properly reproduce the solubility behaviour dependence on the concentration of cosolvent. However, the deviation increases when the conditions are close to the mixture critical point.

The original Chrastil's equation can be seen as a particular case of the *q*-Chrastil model. Similarly, the *q*-González's equation reduces to the original González's equation when the value of parameter *q* tends to unity. The main advantage of using the new *q*-models is that they have not the physical inconsistency of the original models. Whilst the original models are based on Boltzmann's weight argument, the *q*-models express the energy exponential term based on the Tsallis's weight argument. Although the new *q*-Chrastil and *q*-González's models proposed have shown deviations similar to the other models investigated in this study, they appears with a great potential for highly complex systems and should be further explored mainly at higher temperatures. Moreover, due to the relationship molecular structure-parameter *q*, it might be possible to develop a group contribution method to estimate *q* and thus reduce the number of parameters of *q*-Chrastil's model.

Acknowledgements

S.A.B.V.M. wishes to thank Prof. E.P. Borges for his enrichful discussions about *q*-exponential models and gratefully acknowledge the support of CNPq–Brazilian National Science and Technology Foundation (grant 201127/2011-3) during his sabbatical period at the University of New South Wales.

Antonio Tabernero acknowledges the grant provided by the Spanish Ministerio de Ciencia y Innovacion (project CTQ 2009-08222).

Appendix A. Supplementary data

Supplementary data associated with this article can be found, in the online version, at http://dx.doi.org/10.1016/j.supflu.2013.11.017.

References

[1] R.L. Mendes, B.P. Nobre, M.T. Cardoso, A.P. Pereira, A.F. Palavra, Supercritical carbon dioxide extraction of compounds with pharmaceutical importance from microalgae, Inorganica Chimica Acta 356 (2003) 328–334.
[2] E. Reverchon, I. De Marco, Supercritical fluid extraction and fractionation of natural matter, J. Supercritical Fluids 38 (2006) 146–166.
[3] N. Bahramifar, Y. Yamini, M. Shamsipur, Investigation on the supercritical carbon dioxide extraction of some polar drugs from spiked matrices and tablets, J. Supercritical Fluids 35 (2005) 205–211.
[4] E.J. Beckman, Supercritical and near-critical CO_2 in green chemical synthesis and processing, J. Supercritical Fluids 28 (2004) 121–191.
[5] H. Sovova, L. Opletal, M. Bartlova, M. Sajfrtova, M. Krenkova, Supercritical fluid extraction of lignans and cinnamic acid from *Schichandra chinensis*, J. Supercritical Fluids 42 (2007) 88–95.
[6] H. Sovova, A.A. Galushko, R.P. Stateva, K. Rochova, M. Sajfrtova, M. Bartlova, Supercritical food extraction of minor compounds of vegetable oils: β-sitosterol, J. Food Engineering 101 (2010) 201–209.
[7] H. Sovova, Mathematical model for supercritical fluid extraction of natural extraction of natural products and extraction curve evaluation, J. Supercritical Fluids 33 (2005) 35–52.
[8] C.-S. Su, M. Tang, Y.-P. Chen, Micronization of nabumetone using the rapid expansion of supercritical solution (RESS) process, J. Supercritical Fluids 50 (2009) 69–76.
[9] M. Turk, G. Upper, P. Hils, Formation of composite drug-polymer particles by coprecipitation during the rapid expansion of supercritical fluids, J. Supercritical Fluids 39 (2006) 253–263.
[10] M. Charoenchaitrakool, F. Dehghani, N.R. Foster, Utilization of supercritical carbon dioxide for complex formation of ibuprofen and methyl-β-cyclodextrin, International J. Pharmaceutics 239 (2002) 103–112.
[11] B. Kongsombut, A. Tsutsumi, N. Suankaew, T. Charinpanitkul, Encapsulation of SiO_2 and TiO_2 fine powders with poly(DL-lactic-co-glycolic acid) by rapid expansion of supercritical CO_2 incorporated with ethanol cosolvent, Industrial and Engineering Chemistry Research 48 (2009) 11230–11235.
[12] L.T. Danh, P. Truong, R. Mammucari, N. Foster, Extraction of vetiver essential oil by ethanol-modified supercritical carbon dioxide, Chemical Engineering J. 165 (2010) 26–34.
[13] A. Chafer, T. Fornari, A. Berna, R.P. Stateva, Solubility of quercetin in supercritical CO_2 + ethanol as a modifier: measurements and thermodynamic modelling, J. Supercritical Fluids 32 (2004) 89–96.
[14] A. Caballero, L.N. Hernandez, L.A. Estevez, Calculation of interaction parameters for binary solid-SCF equilibria using several EOS and mixing rules, J. Supercritical Fluids 5 (1992) 293–295.
[15] I. Kikic, M. Lora, A. Bertucco, A thermodynamic analysis of three-phase equilibria in binary and ternary systems for applications in rapid expansion of a supercritical solution (RESS), particles from gas-saturated solutions (PGSS), and supercritical antisolvent (SAS), Industrial and Engineering Chemistry Research 36 (1997) 5507–5515.
[16] I. Kikic, N. De Zordi, M. Moneghini, D. Solinas, Solubility estimation of drugs in ternary systems of interest for the antisolvent precipitation processes, J. Supercritical Fluids 55 (2010) 616–622.
[17] A. Tabernero, E.M. Martin del Valle, M.A. Galan, Estimation of sublimation enthalpies of solids constituted by aromatic and/or polycyclic aliphatic rings by using a group contribution method, AIChE J. 58 (2012) 2875–2884.
[18] L. Constantinou, R. Gani, New group contribution method for estimating properties of pure compounds, AIChE J. 40 (1994) 1697–1710.
[19] J. Chrastil, Solubility of solids and liquids in supercritical gases, J. Phys. Chem. 86 (1982) 3016–3021.
[20] R. Ch, G. Madras, An association model for the solubilities of pharmaceuticals in supercritical carbon dioxide, Thermochimica Acta 507-508 (2010) 99–105.
[21] X. Bian, Z. Du, Y. Tang, An improved density-based model for the solubility of same compounds in supercritical carbon dioxide, Thermochimica Acta 519 (2011) 16–21.
[22] D.L. Sparks, R. Hernandez, L.A. Estevez, Evaluation of density-based models for the solubility of solids in supercritical carbon dioxide and formulation a new model, Chemical Engineering Science 63 (2008) 4292–4301.
[23] A. Jouyban, H.K. Chan, N.R. Foster, Mathematical representation of solute solubility in supercritical carbon dioxide using empirical expressions, J. Supercritical Fluids 24 (2002) 19–35.
[24] A. Tabernero, E.M. Martin del Valle, M.A. Galan, A comparison between semiempirical equations to predict the solubility of pharmaceutical compounds in supercritical carbon dioxide, J. Supercritical Fluids 52 (2010) 161–174.
[25] C. Tsallis, Possible generalization of Boltzmann–Gibbs statistics, J. Statistical Physics 52 (1988) 479–487.
[26] E.P. Borges, On a q-generalization of circular and hyperbolic functions, J. Physics A: General Physics 31 (1998) 5281–5288.
[27] E.K. Lenzi, R.S. Mendes, A.K. Rajagopal, Quantum statistical mechanics for nonextensive systems, Physical Review E: Statistical, Nonlinear, and Soft Matter Physics 59 (1999) 1398–1407.
[28] Y. Adachi, B.C.Y. Lu, Supercritical fluid extraction with carbon dioxide and ethylene, Fluid Phase Equilibria 14 (1983) 147–156.
[29] J.M. Del Valle, J.M. Aguilera, An improved equation for predicting the solubility of vegetable oils in supercritical CO_2, Industrial and Engineering Chemistry Research 27 (1988) 1551–1553.
[30] C. Tsallis, Introduction to Nonextensive Statistical Mechanics: Approaching a Complex World, Springer, New York, NY, 2009.
[31] I. Sartori, E.M. Assis, A.L. Silva, R.L.F.V. Melo, E.P. Borges, S.A.B. Vieira de Melo, Reliability modeling of a natural gas recovery plant using q-Weibull distribution, Computer Aided Chemical Engineering 27 (2009) 1797–1802.
[32] V. Aquilanti, K.C. Mundim, M. Elango, S. Kleijn, T. Kasai, Temperature dependence of chemical and biophysical rate processes: phenomenological approach to deviations from Arrhenius law, Chemical Physics Letters 498 (2010) 209–213.
[33] M. Gell-Mann, C. Tsallis (Eds.), Nonextensive Entropy—Interdisciplinary Applications, Oxford University Press, Oxford, 2003.
[34] M. Sauceau, J.-J. Letourneau, D. Richon, J. Fages, Enhanced density-based models for solid compound solubilities in supercritical carbon dioxide with cosolvents, Fluid Phase Equilibria 208 (2003) 99–113.
[35] J.C. González, M.R. Vieytes, A.M. Botana, J.M. Vieites, L.M. Botana, Modifies mass action law-based model to correlate the solubility of solids and liquids in entrained supercritical carbon dioxide, J. Chromatography A 910 (2001) 119–125.
[36] H. Sovova, Solubility of ferulic acid in supercritical carbon dioxide with ethanol as cosolvent, J. Chemical and Engineering Data 46 (2001) 1255–1257.
[37] Z. Tang, J.-su Jin, Z.-ting Zhang, X.-yun Yu, J.-niang Xu, Solubility of 3,5-dinitrobenzoic acid in supercritical carbon dioxide with cosolvent at temperatures from (308 to 328) K and pressures from (10.0 to 21.0) MPa, J. Chemical and Engineering Data 55 (2010) 3834–3841.
[38] J. Mendez-Santiago, A.S. Teja, The solubility of solids in supercritical fluids, Fluid Phase Equilibria 158 (1999) 501–510.
[39] S.N. Reddy, G. Madras, Modeling of ternary solubilities of solids in supercritical carbon dioxide in the presence of cosolvents or cosolutes, J. Supercritical Fluids 63 (2012) 105–114.
[40] S.N. Reddy, G. Madras, A new semi-empirical model for correlating the solubilities of solids in supercritical carbon dioxide with cosolvents, Fluid Phase Equilibria 310 (2011) 207–212.

Please cite this article in press as: A. Tabernero, et al., Modelling solubility of solid active principle ingredients in sc-CO_2 with and without cosolvents: A comparative assessment of semiempirical models based on Chrastil's equation and its modifications, J. Supercrit. Fluids (2013), http://dx.doi.org/10.1016/j.supflu.2013.11.017

[41] E. W. Lemmon, M. O. McLinden, D. G. Friend, Thermophysical properties of fluid systems, NIST chemistry webbook, NIST Standard Reference Data Base, Eds. P.J. Linstrom and W.G. Mallard, National Institute of Standards and Technology, Gaithersburg MD, 20899, http://webbook.nist.gov,.(retrieved August 16, 2012).
[42] K.-L. Tsai, F.N. Tsai, Solubilities of methylbenzoic acid isomers in supercritical carbon dioxide, J. Chemical and Engineering Data 40 (1995) 264–266.
[43] Y.-M. Chen, Y.-P. Chen, Measurements for the solid solubilities of antipyrine, 4-aminoantipyrine and 4-dimethylaminoantipyrine in supercritical carbon dioxide, Fluid Phase Equilibria 282 (2009) 82–87.
[44] S. Bristow, B.Y. Shekunov, P. York, Solubility analysis of drug compounds in supercritical carbon dioxide using static and dynamic extraction systems, Industrial and Engineering Chemistry Research 40 (2001) 1732–1739.
[45] M. Johannsen, G. Brunner, Solubilities of the fat-soluble vitamins A, D, E and K in supercritical carbon dioxide, J. Chemical and Engineering Data 42 (1997) 106–111.
[46] Z. Huang, Y.C. Chiew, W.-D. Lu, S. Kawi, Solubility of aspirin in supercritical carbon dioxide/alcohol mixtures, Fluid Phase Equilibria 237 (2005) 9–15.
[47] J.C. De La Fuente, B. Oyarzun, N. Quezada, J.M. Del Valle, Solubility of carotenoid pigments (lycopene and astaxanthin) in supercritical carbon dioxide, Fluid Phase Equilibria 247 (2007) 90–95.
[48] M. Hojjati, Y. Yamini, M. Khajeh, A. Vatanara, Solubility of some statin drugs in supercritical carbon dioxide and representing the solute solubility data with several density-based correlations, J. Supercritical Fluids 41 (2007) 187–194.
[49] A. Vatanara, A.R. Najafabadi, M. Khajeh, Y. Yamini, Solubility of some inhaled glucocorticoids in supercritical carbon dioxide, J. Supercritical Fluids 33 (2005) 21–25.
[50] R. Murga, M.T. Sanz, S. Beltran, J.L. Cabezas, Solubility of three hydroxycinnamic acids in supercritical carbon dioxide, J. Supercritical Fluids 27 (2003) 239–245.
[51] M. Johannsen, G. Brunner, Solubilities of the xanthenes caffeine, theophylline and theobromine in supercritical carbon dioxide, Fluid Phase Equilibria 95 (1994) 215–226.
[52] Z. Huang, S. Kawi, Y.C. Chiew, Solubility of cholesterol and its esters in supercritical carbon dioxide with and without cosolvents, J. Supercritical Fluids 30 (2004) 25–39.
[53] Y.-M. Chen, P.-C. Lin, M. Tang, Y.-P. Chen, Solid solubility of antilipemic agents and micronization of gemfibrozil in supercritical carbon dioxide, J. Supercritical Fluids 52 (2010) 175–182.
[54] M.H. Hosseini, N. Alizadeh, A.R. Khanchi, Solubility analysis of clozapine and lamotrigine in supercritical carbon dioxide using static system, J. Supercritical Fluids 52 (2010) 30–35.
[55] M. Asghari-Khiavi, Y. Yamini, M.A. Farajzadeh, Solubilities of two steroid drugs and their mixtures in supercritical carbon dioxide, J. Supercritical Fluids 30 (2004) 111–117.
[56] P. Coimbra, D. Fernandes, M.H. Gil, H.C. de Sousa, Solubility of diflunisal in supercritical carbon dioxide, J. Chemical and Engineering Data 53 (2008) 1990–1995.
[57] M. Hojjati, A. Vatanara, Y. Yamini, M. Moradi, A.R. Najafabadi, Supercritical CO_2 and highly selective aromatase inhibitors: experimental solubility and empirical data correlation, J. Supercritical Fluids 50 (2009) 203–209.
[58] A.R. Duarte, P. Coimbra, H.C. de Sousa, C.M.M. Duarte, Solubility of flurbiprofen in supercritical carbon dioxide, J. Chemical and Engineering Data 49 (2004) 449–452.
[59] C. Garlapati, G. Madras, Solubilities of hexadecanoic and octadecanoic acids in supercritical CO_2 with and without cosolvents, J. Chemical and Engineering Data 53 (2008) 2913–2917.
[60] P. Coimbra, D. Fernandes, P. Ferrerir, M.H. Gil, H.C. de Sousa, Solubility of irgacure® 2959 photoinitiator in supercritical carbon dioxide: experimental determination and correlation, J. Supercritical Fluids 45 (2008) 272–281.
[61] S.J. Macnaughton, I. Kikic, N.R. Foster, P. Alessi, A. Cortessi, I. Colombo, Solubility of anti-inflammatory drugs in supercritical carbon dioxide, J. Chemical and Engineering Data 41 (1996) 1083–1086.
[62] J. Shi, M. Khatri, S.J. Xue, G.S. Mittal, Y. Ma, D. Li, Solubility of lycopene in supercritical CO_2 fluid as affected by temperature and pressure, Separation and Purification Technology 66 (2009) 322–328.
[63] R.D. Weinstein, K.R. Muske, J. Moriarty, E.K. Schmidt, The solubility of benzocaine, lidocaine, and procaine in liquid and supercritical carbon dioxide, J. Chemical and Engineering Data 49 (2004) 547–552.
[64] Y. Yamini, J. Arab, M. Asghari-Khiavi, Solubilities of phenazopyridine, propanolol, and methimazole in supercritical carbon dioxide, J. Pharm. Biomed. Anal. 32 (2003) 181–187.
[65] C.-S. Su, Y.-P. Chen, Measurement and correlation for the solid solubility of non-steroidal anti-inflammatory drugs (NSAIDs) in supercritical carbon dioxide, J. Supercritical Fluids 43 (2008) 438–446.
[66] S.S. Ting, S. Macnaughton, D.L. Tomasko, N.R. Foster, Solubility of naproxen in supercritical carbon dioxide with and without cosolvents, Industrial and Engineering Chemistry Research 32 (1993) 1471–1481.
[67] Z. Knez, M. Skerget, P. Sencar-Bozic, A. Ridner, Solubility of nifedipine and nitrendipine in supercritical CO_2, J. Chemical and Engineering Data 40 (1995) 216–220.
[68] G.S. Gurdial, N.R. Foster, Solubility of *o*-hydroxybenzoic acid in supercritical carbon dioxide, Industrial and Engineering Chemistry Research 30 (1991) 575–580.
[69] M.D. Gordillo, M.A. Blanco, A. Molero, E. Martinez de la Ossa, Solubility of the antibiotic penicillin G in supercritical carbon dioxide, J. Supercritical Fluids 15 (1999) 183–190.
[70] M. Ko, V. Shah, P.R. Bienkowski, H.D. Cochran, Solubility of the antibiotic penicillin V in supercritical CO_2, J. Supercritical Fluids 4 (1991) 32–39.
[71] E. Kosal, C.H. Lee, G.D. Holder, Solubility of progesterone, testosterone, and cholesterol in supercritical fluids, J. Supercritical Fluids 5 (1992) 169–179.
[72] J. Jin, Z. Zhang, Q. Li, E. Yu, Solubility of propyl *p*-hydroxybenzoate in supercritical carbon dioxide with and without cosolvents, J. Chemical and Engineering Data 50 (2005) 801–803.
[73] J. Li, J. Jin, Z. Zhang, X. Pei, Solubility of *p*-toluenesulfonamide in pure and modified supercritical carbon dioxide, J. Chemical and Engineering Data 54 (2009) 1142–1146.
[74] C.A. Nalesnik, B.N. Hansen, J.T. Hsu, Solubility of pure taxol in supercritical carbon dioxide, Fluid Phase Equilibria 146 (1998) 315–323.
[75] C. Garlapati, G. Madras, Solubilities of dodecanoic and tetradecanoic acids in supercritical CO_2 with and without entrainers, J. Chemical and Engineering Data 53 (2008) 2637–2641.
[76] R.F. Fedors, A method for estimating both the solubility parameters and molar volumes of liquids, Polymer Engineering and Science 14 (1974) 147–154.
[77] G.S. Gurdial, S.J. Macnaughton, D.L. Tomasko, N.R. Foster, Influence of chemical modifiers on the solubility of *o*- and *m*-hydroxybenzoic acid in supercritical CO_2, Industrial and Engineering Chemistry Research 32 (1993) 1488–1497.
[78] A.R. Duarte, S. Santiago, H.C. de Sousa, C.M.M. Duarte, Solubility of acetazolimide in supercritical carbon dioxide in the presence of ethanol as a cosolvent, J. Chemical and Engineering Data 50 (2005) 216–220.
[79] V. Vandana, A. Teja, Vapor-liquid equilibria in the carbon dioxide + 1-propanol system, J. Chemical and Engineering Data 40 (1995) 459–461.
[80] C. Secuianu, V. Feroiu, D. Geana, High-pressure vapour-liquid equilibria in the system carbon dioxide and 2-propanol at temperatures from 293.15 K to 323.15 K, J. Chemical and Engineering Data 48 (2003) 1384–1386.
[81] C.J. Chang, C.-Y. Day, C.-M. Ko, K.-L. Chiu, Densities and *P-x-y* diagrams for carbon dioxide dissolution in methanol, ethanol and acetone mixtures, Fluid Phase Equilibria 131 (1997) 243–258.
[82] J. M. Anderson, M. W. Barrick, R. L. Robinson Jr., Solubilities of carbon dioxide in cyclohexane and trans-decalin at pressures to 10.7 MPa and temperatures from 323 to 423 K, *J. Chem. Eng. Data* **31**, 1986, 72-175.
[83] Z. Knez, M. Skerget, L. Ilic, C. Lutge, Vapor-liquid equilibria of binary CO_2-organic solvent systems (ethanol, tetrahydrofuran, *ortho*-xylene, *meta*-xylene, *para*-xylene), J. Supercritical Fluids 43 (2008) 383–389.
[84] Y.-L. Tian, H.-G. Zhu, Y. Xue, L. Yin, Vapor-liquid equilibria of the carbon dioxide + ethyl propanoate and carbon dioxide + ethyl acetate systems at pressure from 2.96 MPa to 11.79 MPa and temperature from 313 K to 393 K, J. Chemical and Engineering Data 49 (2004) 1554–1559.
[85] J.H. Hong, R. Kobayashi, Vapor-liquid equilibrium studies for the carbon dioxide-methanol system, Fluid Phase Equilibria 41 (1988) 269–276.
[86] M. Vazquez Da Silva, D. Barbosa, High pressure vapor-liquid equilibrium data for the systems carbon dioxide/2-methyl-1-propanol and carbon dioxide/3-methyl-1-butanol at 288.2, 303.2 and 313.2 K, Fluid Phase Equilibria 198 (2002) 229–237.
[87] S.A.B. Vieira d Melo, G.M.N. Costa, A.C.C. Viana, F.L.P. Pessoa, Solid pure component property effects on modeling upper crossover pressure for supercritical fluid process synthesis: a case study for the separation of Annato pigments using sc-CO_2, J. Supercritical Fluids 49 (2009) 1–8.

Please cite this article in press as: A. Tabernero, et al., Modelling solubility of solid active principle ingredients in sc-CO_2 with and without cosolvents: A comparative assessment of semiempirical models based on Chrastil's equation and its modifications, J. Supercrit. Fluids (2013), http://dx.doi.org/10.1016/j.supflu.2013.11.017

Table A1. Parameters of the Chrastil´s equation for the binary systems CO_2-solid.

Solid	***k***	***A (K)***	***B***
2-Methylbenzoic acid	5.24	-6642	-12.41
3-Methylbenzoic acid	5.49	-6263	-15.27
3,5-Dinitrobenzoic acid	3.91	-8538	-4.16
4-Aminoantipyrine	4.77	-4188	-18.73
4-Methylbenzoic acid	4.89	-5609	-15.23
Acetaminophen	4.86	-7192	-15.40
Alfa-tocopherol	7.09	-3358	-34.48
Aspirine	4.42	-4586	-15.57
Astaxanthin	4.98	-9531	-9.41
Atorvastatin	11.21	-10832	-41.29
Beta-carotene	9.59	-10209	-33.97
Budesonide	8.25	-6433	-31.75
Caffeic acid	7.21	-7119	-36.47
Caffeine	6.07	-4429	-26.67
Cholesterol	6.08	-4615	-26.01
Cholesterolbenzoate	7.18	-7180	-9.08
Clofibric acid	4.89	-4278	-18.51
Clozapine	7.21	-7197	-26.67
Cyproterone acetate	10.29	-3949	-57.05
Diflunisal	6.63	-7030	-26.54
Examestane	7.93	-10058	-21.86
Fenofibrate	6.14	-3938	-25.86
Flurbiprofen	7.25	-7634	-25.15
Fluvastatin	9.47	-9160	-35.58
Gemfibrozil	7.44	-5605	-29.87
Hexadecanoic acid	5.92	-10606	-4.87
Irgacure2959	4.50	-6440	-16.70
Ketoprofen	6.98	-6098	-28.28
Lamotrigine	4.35	-3951	-19.10
Letrozole	7.68	-9791	-24.09
Lycopene	1.18	-3314	-2.52
Lidocaine	11.38	-6538	-56.83
Lovastatin	3.44	-3767	-12.41
Medroxyprogesterone acetate	8.52	-5716	-39.61
Methimazole	6.80	-5619	-30.31
Nabumetone	5.31	-5492	-16.21
Naproxen	4.84	-4750	-19.62
Nimesulide	7.79	-5338	-36.17
Nitrendipine	4.98	-5489	-11.63

Octadecanoic acid	6.88	-11871	-8.44
Orto-hydroxybenzoic acid	4.21	-5248	-11.63
PenicillinG	3.07	-3283	-9.42
Penicillin V	3.07	-3283	-9.42
Phenazopyridine	6.27	-5735	-25.76
Procaine	2.28	-3045	-6.34
Progesterone	8.63	-5612	-39.07
Propanolol	13.27	-13143	-48.82
Propyl *p*-hydroxybenzoate	4.37	-8405	-10.86
p-toluenesulfonamide	1.59	-3198	-8.67
Rosuvastatin	6.96	-6201	-28.04
Simvastatin	9.31	-7241	-40.18
Taxol	12.74	-5446	-75.18
Testosterone	9.29	-7484	-40.18
Tetradecanoic acid	6.35	-7405	-15.98
Theobromine	3.56	-4256	-15.90
Theophylline	3.23	-3604	-13.63
Vitamine D2	5.66	-4731	-22.10
Vitamine D3	6.70	-5907	-25.36

Table A2. Parameters of the q-Chrastil´s equation for binary systems CO_2-solid.

Solid	k	A_q **(K)**	q
2-Methylbenzoic acid	5.24	588	1.032
3-Methylbenzoic acid	5.49	868	1.037
3,5-Dinitrobenzoic acid	26.72	$3 \cdot 10^{20}$	1.025
4-Aminoantipyrine	4.76	2491	1.068
4-Methylbenzoic acid	4.89	1027	1.043
Acetaminophen	4.86	769	1.032
Alfa-tocopherol	7.10	25193	1.077
Aspirine	4.48	1485	1.057
Astaxanthin	4.99	-167	1.036
Atorvastatin	11.22	2022	1.026
Beta-carotene	9.57	1614	1.027
Budesonide	8.25	3871	1.047
Caffeic acid	7.20	3337	1.041
Caffeine	6.11	5338	1.070
Cholesterol	6.09	4047	1.064
Cholesterolbenzoate	22.53	$8 \cdot 10^{9}$	1.062
Clofibric acid	4.89	2222	1.064
Clozapine	7.21	1910	1.040
Cyproterone acetate	10.33	94671	1.081
Diflunisal	6.64	1730	1.039
Examestane	7.90	785	1.023
Fenofibrate	6.15	5180	1.064
Flurbiprofen	7.24	1293	1.033
Fluvastatin	9.48	2078	1.031
Gemfibrozil	7.45	3364	1.051
Hexadecanoic acid	33.89	$1 \cdot 10^{17}$	1.16
Irgacure2959	5.54	902	1.035
Ketoprofen	6.98	2648	1.047
Lamotrigine	4.35	3224	1.076
Letrozole	7.68	958	1.025
Lycopene	1.18	214	1.040
Lidocaine	11.39	11279	1.044
Lovastatin	3.44	1486	1.069
Medroxyprogesterone acetate	8.56	7278	1.055
Methimazole	6.81	3971	1.054
Nabumetone	5.31	1169	1.045
Naproxen	4.85	2129	1.059
Nimesulide	7.79	6318	1.057
Nitrendipine	3.86	2120	1.055
Octadecanoic acid	37.94	$4 \cdot 10^{16}$	1.140

Orto-hydroxybenzoic acid	4.21	747	1.043
PenicillinG	6.87	1379	1.035
Penicillin V	3.07	1134	1.076
Phenazopyridine	6.28	2695	1.051
Procaine	2.27	611	1.068
Progesterone	8.63	6483	1.054
Propanolol	13.35	1978	1.021
Propyl *p*-hydroxybenzoate	26.31	$6 \cdot 10^{18}$	1.022
p-toluenesulfonamide	11.47	$2 \cdot 10^{12}$	1.032
Rosuvastatin	6.97	2736	1.047
Simvastatin	9.35	4288	1.042
Taxol	12.74	61949	1.057
Testosterone	9.29	3486	1.038
Tetradecanoic acid	23.66	$1 \cdot 10^{12}$	1.150
Theobromine	3.57	1959	1.067
Theophylline	3.25	1998	1.079
Vitamine D2	5.74	3007	1.062
Vitamine D3	6.76	2569	1.049

Table A3. Parameters for Chrastil3 equation for ternary systems.

System	***k***	***A (K)***	***B***
1-propanol-Naproxen	**	**	**
2-propanol-Naproxen	2.25	-4861	-8.33
Acetone-Cholesterol	3.84	-5238	-3.67
Acetone-Cholesterolbenzoate	5.32	-5680	-7.83
Acetone-mHBA	1.40	-2569	-6.67
Acetone-naproxen	2.37	-3909	-12.96
Acetone-oHBA	1.19	-2810	-5.30
Acetone-Propyl *p*-hydroxybenzoate	6.27	209655	-729.81
Cyclohexane-Propyl *p*-hydroxybenzoate	4.95	$6 \cdot 10^6$	-20329.8
Ethanol-acetazolimide	2.87	-3714	-19.26
Ethanol-aspirine	2.02	-2806	-11.29
Ethanol-hexadecanoic acid	3.97	-10437	-0.13
Ethanol-naproxen	2.79	-5759	-8.95
Ethanol-octadecanoic acid	4.42	-10022	-5.50
Ethanol-*p*-toluenesulfonamide	0.66	1506	-18.66
Ethanol-tetradecanoic acid	4.79	-9844	-5.72
Ethyl acetate-3,5-Dinitrobenzoicacid	7.27	-12755	-18.81
Ethyl acetate-naproxen	**	**	**
Methanol-aspirine	2.24	-2047	-15.10
Methanol-cholesterol	3.97	-3540	-9.39
Methanol-cholesterolbenzoate	5.47	-4456	-12.12
Methanol-mHBA	1.03	-2269	-5.30
Methanol-naproxen	3.15	-4239	-16.16
Methanol-oHBA	1.97	-3164	-8.69
3-Methyl-1-butanol-hexadecanoic acid	4.15	-10517	-7.39
3-Methyl-1-butanol-octadecanoic acid	4.43	-10838	-3.29
3Methyl-1-butanol-tetradecanoic acid	5.97	-7600	-14.09

Table A4. Parameters for Gonzalez's equation for ternary systems.

System	***k***	***γ***	***A (K)***	***B***
1-propanol-Naproxen	1.59	1.81	60132	-193
2-propanol-Naproxen	1.92	1.73	-4765	-0.61
Acetone-Cholesterol	3.84	-29.68	-5238	-107
Acetone-Cholesterolbenzoate	5.32	-52.50	-5688	-191
Acetone-mHBA	1.41	-80357.00	-2509	-269396
Acetone-naproxen	2.25	1.18	-4429	-6.63
Acetone-oHBA	1.19	54.11	-2810	176
Acetone-Propyl *p*-hydroxybenzoate	6.27	30.72	-51425	220
Cyclohexane-Propyl *p*-hydroxybenzoate	4.96	621.43	$-2\cdot10^{6}$	8965
Ethanol-acetazolimide	2.79	0.86	-3996	-15.24
Ethanol-aspirine	2.03	36.88	-2806	118
Ethanol-hexadecanoic acid	4.05	0.78	-8278	-3.85
Ethanol-naproxen	2.28	1.64	-5416	-1.47
Ethanol-octadecanoic acid	4.58	1.09	-6213	-13.59
Ethanol-*p*-toluenesulfonamide	4.36	15.34	-5289	29.85
Ethanol-tetradecanoic acid	4.94	0.64	-9201	-5.58
Ethyl acetate-3,5-Dinitrobenzoicacid	7.50	1.15	-12864	-16.11
Ethyl acetate-naproxen	1.96	1.17	-53037	141
Methanol-aspirine	2.24	203.99	-2047	700
Methanol-cholesterol	3.97	-18.78	-3540	-75.06
Methanol-cholesterolbenzoate	5.47	49.76	-4456	162
Methanol-mHBA	1.03	25.99	-2269	81.85
Methanol-naproxen	2.87	1.41	-3866	-10.76
Methanol-oHBA	1.97	-8.43	-3164	-36.96
3-Methyl-1-butanol-hexadecanoic acid	4.22	0.49	-10558	0.74
3-Methyl-1-butanol-octadecanoic acid	4.50	0.61	-10882	-0.58
3Methyl-1-butanol-tetradecanoic acid	4.75	0.38	-7500	-11.23

Table A5. Parameters for Tang's equation for ternary systems.

System	***k***	***m***	***n***	***A(K)***
1-propanol-Naproxen	2.13	1.92	0.43	661
2-propanol-Naproxen	774	1.88	0.50	-1101
Acetone-Cholesterol	0.0056	-1.10	0.27	-1897
Acetone-Cholesterolbenzoate	0.28	1.17	0.34	-677
Acetone-mHBA	**	**	**	**
Acetone-naproxen	12.23	1.58	0.51	428
Acetone-oHBA	0.99	0.81	0.24	-550
Acetone-Propyl *p*-hydroxybenzoate	240	7.58	0.83	532
Cyclohexane-Propyl *p*-hydroxybenzoate	0.042	1.06	0.18	-378
Ethanol-acetazolimide	**	**	**	**
Ethanol-aspirine	0.59	1.36	-0.27	-1253
Ethanol-hexadecanoic acid	10.49	1.16	0.74	369
Ethanol-naproxen	41.27	1.82	0.56	-46.86
Ethanol-octadecanoic acid	0.0011	1.42	0.65	3372
Ethanol-*p*-toluenesulfonamide	4.06	-2.42	2.90	3259
Ethanol-tetradecanoic acid	$7 \cdot 10^4$	0.99	0.80	-9764
Ethyl acetate-3,5-Dinitrobenzoicacid	0.55	1.20	2.70	9398
Ethyl acetate-naproxen	0.86	1.63	0.41	97.08
Methanol-aspirine	0.22	1.26	0.49	1096
Methanol-cholesterol	0.37	1.19	0.43	-197
Methanol-cholesterolbenzoate	0.000079	2.98	0.30	3806
Methanol-mHBA	**	**	**	**
Methanol-naproxen	0.020	1.42	0.026	45.14
Methanol-oHBA	1.58	1.02	0.47	359
3-Methyl-1-butanol-hexadecanoic acid	565664	1.02	0.70	-3469
3-Methyl-1-butanol-octadecanoic acid	641498	1.08	0.52	-3903
3Methyl-1-butanol-tetradecanoic acid	$1 \cdot 10^8$	1.22	0.50	-5309

Table A6. Parameters for MST equation for ternary systems.

System	***A* (K)**	***B* ($K \cdot m^3 \cdot mol^{-1}$)**	***C***	***D* (K)**
1-propanol-Naproxen	$-7 \cdot 10^7$	1.53	236388	15974
2-propanol-Naproxen	-7475	1.72	14.14	15671
Acetone-Cholesterol	$1 \cdot 10^7$	124	19.98	$-4 \cdot 10^8$
Acetone-Cholesterolbenzoate	$-6 \cdot 10^6$	155	20.21	$2 \cdot 10^8$
Acetone-mHBA	$1 \cdot 10^7$	1.40	13.97	$-3 \cdot 10^8$
Acetone-naproxen	-7738	1.91	14.07	11037
Acetone-oHBA	$1 \cdot 10^7$	1.26	13.95	$-4 \cdot 10^8$
Acetone-Propyl *p*-hydroxybenzoate	$1 \cdot 10^8$	3.99	-25268	$-8 \cdot 10^7$
Cyclohexane-Propyl *p*-hydroxybenzoate	$4 \cdot 10^8$	3.61	$-1 \cdot 10^6$	$-3 \cdot 10^8$
Ethanol-acetazolimide	-8788	2.52	14.25	3701
Ethanol-aspirine	$7 \cdot 10^7$	1.85	14.42	-2.33
Ethanol-hexadecanoic acid	-15663	2.92	40.13	10741
Ethanol-naproxen	-8431	1.93	16.59	14696
Ethanol-octadecanoic acid	-15402	3.15	37.96	14083
Ethanol-*p*-toluenesulfonamide	$-4 \cdot 10^6$	3.44	23.23	$1 \cdot 10^8$
Ethanol-tetradecanoic acid	-16328	3.37	43.40	9005
Ethyl acetate-3,5-Dinitrobenzoicacid	-19848	4.38	45.14	9915
Ethyl acetate-naproxen	$4 \cdot 10^7$	1.75	-135397	11044
Methanol-aspirine	$2 \cdot 10^8$	1.97	12.16	$-8 \cdot 10^9$
Methanol-cholesterol	$3 \cdot 10^6$	126	14.57	$-1 \cdot 10^8$
Methanol-cholesterolbenzoate	$2 \cdot 10^6$	157.72	16.43	$-9 \cdot 10^7$
Methanol-mHBA	$-4 \cdot 10^7$	1.17	12.94	$1 \cdot 10^9$
Methanol-naproxen	-7409	2.31	12.93	12704
Methanol-oHBA	$1 \cdot 10^7$	1.73	16.23	$-5 \cdot 10^8$
3-Methyl-1-butanol-hexadecanoic acid	-15722	3.01	40.16	12529
3-Methyl-1-butanol-octadecanoic acid	-16171	3.12	40.15	15628
3-Methyl-1-butanol-tetradecanoic acid	-12934	3.31	32.45	9747

Table A7. Parameters for RedMa5 equation for ternary systems.

System	***k***	***A* (K)**	***B* (K)**	***C* ($m^3 \cdot mol^{-1}$)**	***D***
1-propanol-Naproxen	1.21	3679	7043	0.0026	-19.50
2-propanol-Naproxen	1.19	-4586	6534	0.0031	5.07
Acetone-Cholesterol	1.15	18700	-793625	0.21	5.82
Acetone-Cholesterolbenzoate	0.82	87808	$-3 \cdot 10^6$	0.34	7.59
Acetone-mHBA	0.37	831	-136270	0.16	10.80
Acetone-naproxen	1.00	-4763	1889	0.17	5.56
Acetone-oHBA	0.43	1771	-166715	0.14	10.40
Acetone-Propyl *p*-hydroxybenzoate	-2.69	44328	-390496	1.21	-107
Cyclohexane-Propyl *p*-hydroxybenzoate	1.89	-47360	$-1 \cdot 10^6$	0.088	345
Ethanol-acetazolimide	2.27	-361	-560	0.080	-12.52
Ethanol-aspirine	0.97	-7621	149438	0.15	4.28
Ethanol-hexadecanoic acid	0.094	-9092	-2034	0.39	24.42
Ethanol-naproxen	0.38	-6768	5668	0.0051	14.42
Ethanol-octadecanoic acid	0.036	-8522	1705	0.43	21.04
Ethanol-*p*-toluenesulfonamide	1.86	$-3 \cdot 10^6$	$9 \cdot 10^7$	0.13	-2.00
Ethanol-tetradecanoic acid	-2.80	-17335	-4264	1.00	56.44
Ethyl acetate-3,5-Dinitrobenzoicacid	0.50	-14384	1304	0.52	31.24
Ethyl acetate-naproxen	1.24	106455	1784	0.0032	-329
Methanol-aspirine	0.95	2371	-159470	0.16	1.87
Methanol-cholesterol	0.65	8991	-448437	0.29	5.02
Methanol-cholesterolbenzoate	0.63	-39378	$1 \cdot 10^6$	0.37	5.23
Methanol-mHBA	0.51	42463	$-1 \cdot 10^6$	0.12	8.60
Methanol-naproxen	1.03	-4258	3770	0.0048	3.86
Methanol-oHBA	0.49	-66038	$1 \cdot 10^6$	0.19	10.76
3-Methyl-1-butanol-hexadecanoic acid	0.0075	-12809	-12855	0.40	36.34
3-Methyl-1-butanol-octadecanoic acid	0.085	-13134	-9755	0.42	35.92
3Methyl-1-butanol-tetradecanoic acid	-1.37	-13509	-15643	0.73	42.04

Table A8. Parameters for RedMa7 equation for ternary systems.

System	K	γ	A (K)	B ($K \cdot m^3 \cdot mol^{-1}$)	C (K)	D ($m^3 \cdot mol^{-1}$)	E
1-propanol-Naproxen	-0.059	1.27	$-1 \cdot 10^8$	$-1 \cdot 10^7$	4662	43373	549880
2-propanol-Naproxen	0.17	1.06	-3652	-56.06	6011	0.30	2.89
Acetone-Cholesterol	119424	-119422	$-1 \cdot 10^8$	-712	$6 \cdot 10^9$	2.36	-418800
Acetone-Cholesterolbenzoate	-77073	77074	$6 \cdot 10^7$	-255	$-2 \cdot 10^9$	1.08	270254
Acetone-mHBA	-11.67	12.03	34214	2.54	$-1 \cdot 10^6$	0.15	47.92
Acetone-naproxen	1.42	0.020	3674	-468	10874	1.56	-26.01
Acetone-oHBA	23.94	-23.50	38348	-91.89	$-1 \cdot 10^6$	0.42	-76.13
Acetone-Propyl *p*-hydroxybenzoate	-2.16	-2.90	4.99	7.99	-0.10	-1.05	2.92
Cyclohexane-Propyl *p*-hydroxybenzoate	-2.16	-3.90	3.99	8.03	-0.50	-1.14	3.92
Ethanol-acetazolimide	2.61	-0.50	1231	-102	5788	0.25	-20.01
Ethanol-aspirine	129	-128	-155691	-473	$5 \cdot 10^6$	1.58	477
Ethanol-hexadecanoic acid	0.10	$2 \cdot 10^{-6}$	-12007	-43.00	10741	0.52	28.73
Ethanol-naproxen	-0.62	1.17	-2808	-233	4163	0.92	1.54
Ethanol-octadecanoic acid	0.076	-0.0001	-6906	-292	14085	1.34	11.09
Ethanol-*p*-toluenesulfonamide	-49.05	51.04	$8 \cdot 10^6$	-280	$-2 \cdot 10^8$	0.99	148
Ethanol-tetradecanoic acid	-3.37	0.37	-48811	1511	3886	-3.72	152
Ethyl acetate-3,5-Dinitrobenzoicacid	-0.66	1.04	-16256	91.42	1012	0.26	36.09
Ethyl acetate-naproxen	0.81	0.42	$1 \cdot 10^8$	$9 \cdot 10^7$	7088	-272051	-371072
Methanol-aspirine	-181	182	-389935	-823	$1 \cdot 10^7$	2.67	592
Methanol-cholesterol	-254812	154813	$4 \cdot 10^8$	-211	$-1 \cdot 10^{10}$	0.93	893053
Methanol-cholesterolbenzoate	-150932	150933	$3 \cdot 10^7$	536	$-1 \cdot 10^9$	-1.17	529286
Methanol-mHBA	-56.48	57.01	6658	-24.91	-273621	0.19	195
Methanol-naproxen	-0.13	1.50	2874	-407	-538	1.41	-16.76
Methanol-oHBA	120	-120	75334	122	$-2 \cdot 10^6$	-0.18	-388
3-Methyl-1-butanol-hexadecanoic acid	35.47	-35.37	-18663	-43.31	910390	0.53	-145
3-Methyl-1-butanol-octadecanoic acid	-21.99	22.09	-8216	-49.57	-545273	0.60	136
3Methyl-1-butanol-tetradecanoic acid	-234	236	63997	-1134	$6 \cdot 10^6$	4.33	1087

Table A9. Parameters for q-Chrastil´s equation for ternary systems.

System	***k***	***A (K)***	***q***
1-propanol-Naproxen	**	**	**
2-propanol-Naproxen	14.82	$9 \cdot 10^{20}$	1.44
Acetone-Cholesterol	16.21	$6 \cdot 10^{12}$	1.26
Acetone-Cholesterolbenzoate	17.60	$2 \cdot 10^{10}$	1.19
Acetone-mHBA	7.95	$5 \cdot 10^{18}$	1.71
Acetone-naproxen	12.00	$2 \cdot 10^{17}$	1.42
Acetone-oHBA	-0.86	492	1.42
Acetone-Propyl *p*-hydroxybenzoate	-0.47	-436	0.83
Cyclohexane-Propyl *p*-hydroxybenzoate	11.94	$4 \cdot 10^{9}$	1.20
Ethanol-acetazolimide	-2.06	-616	19.23
Ethanol-aspirine	8.69	$1 \cdot 10^{15}$	1.49
Ethanol-hexadecanoic acid	-1.20	-266	19.84
Ethanol-naproxen	-1.30	-212	0.67
Ethanol-octadecanoic acid	32.02	$5 \cdot 10^{21}$	1.22
Ethanol-*p*-toluenesulfonamide	8.74	$-1 \cdot 10^{20}$	1.64
Ethanol-tetradecanoic acid	31.46	$5 \cdot 10^{19}$	1.16
Ethyl acetate-3,5-Dinitrobenzoicacid	-2.93	165	0.82
Ethyl acetate-naproxen	**	**	**
Methanol-aspirine	6.34	$1 \cdot 10^{11}$	1.44
Methanol-cholesterol	10.96	$1 \cdot 10^{9}$	1.25
Methanol-cholesterolbenzoate	13.79	$2 \cdot 10^{8}$	1.18
Methanol-mHBA	-0.84	13.29	1.025
Methanol-naproxen	12.93	$2 \cdot 10^{14}$	1.32
Methanol-oHBA	9.80	$3 \cdot 10^{16}$	1.50
3-Methyl-1-butanol-hexadecanoic acid	33.61	$6 \cdot 10^{23}$	1.24
3-Methyl-1-butanol-octadecanoic acid	34.63	$1 \cdot 10^{23}$	1.22
3Methyl-1-butanol-tetradecanoic acid	24.28	$4 \cdot 10^{15}$	1.16

Table A10. Parameters for q-Gonzalez equation for ternary systems.

System	k	γ	A (K)	q
1-propanol-Naproxen	1.59	1.81	-0.17	0.9999
2-propanol-Naproxen	1.91	1.71	-0.0026	0.9999
Acetone-Cholesterol	3.84	1.05	-0.15	0.9999
Acetone-Cholesterolbenzoate	5.32	2.23	-0.24	0.9999
Acetone-mHBA	1.40	1.99	-0.035	0.9999
Acetone-naproxen	1.98	1.11	-0.0014	1
Acetone-oHBA	1.19	1.65	-16.55	0.9937
Acetone-Propyl *p*-hydroxybenzoate	6.27	0.14	-0.39	0.9999
Cyclohexane-Propyl *p*-hydroxybenzoate	4.95	0.15	-0.35	0.9999
Ethanol-acetazolimide	0.62	1.05	-0.0016	1
Ethanol-aspirine	2.02	3.22	-0.13	0.9999
Ethanol-hexadecanoic acid	4.05	0.78	100	1.0091
Ethanol-naproxen	2.26	1.62	-0.0023	1
Ethanol-octadecanoic acid	4.57	1.09	-6213	1.0739
Ethanol-*p*-toluenesulfonamide	0.061	0.11	-15.07	0.9999
Ethanol-tetradecanoic acid	4.81	0.63	-0.0072	0.9999
Ethyl acetate-3,5-Dinitrobenzoicacid	5.70	1.49	-0.0017	1
Ethyl acetate-naproxen	1.96	1.17	-0.36	0.9999
Methanol-aspirine	2.24	4.31	-0.15	0.9999
Methanol-cholesterol	3.97	2.68	-0.14	0.9999
Methanol-cholesterolbenzoate	5.47	3.46	-0.17	0.9999
Methanol-mHBA	1.03	1.58	-0.028	0.9999
Methanol-naproxen	2.58	1.31	-0.0019	1
Methanol-oHBA	1.97	2.59	-0.0036	0.9999
3-Methyl-1-butanol-hexadecanoic acid	4.22	0.49	-13.57	0.9986
3-Methyl-1-butanol-octadecanoic acid	4.47	0.61	-0.025	0.9999
3Methyl-1-butanol-tetradecanoic acid	3.90	0.34	-0.0019	1

6.3. Conclusiones

En el artículo anterior se ha procedido al ajuste de datos experimentales de solubilidad de sólidos en CO_2sc con y sin cosolventes con distintas ecuaciones semiempíricas. Además, se han desarrollado dos nuevos modelos basados en la generalización de las ecuaciones de Chrastil y de González mediante el empleo de la función exponencial *q*.

Todos estos modelos fueron comparados en términos de error de ajuste, dependiendo de criterios tales como el número de parámetros, la concentración de cosolvente y la proximidad al punto crítico de mezcla CO_2-cosolvente.

Para sistemas ternarios, seis modelos ajustaron los datos experimentales con una desviación inferior al 10%. La ecuación RedMa7 proporcionó el menor error (6,4%), aunque requiere el cálculo de siete parámetros ajustables.

La ecuación Chrastil3 (8,6%) necesita tres parámetros, pero únicamente puede ser utilizada para una concentración de cosolvente, mientras que la ecuación de Tang (9,6%) con cuatro parámetros ajustables requiere conocer datos experimentales de la solubilidad del sólido en CO_2sc puro.

Las ecuaciones de González (9,5% con cuatro parámetros) y RedMa5 (8,6% con cinco parámetros) son las más convenientes para ajustar la solubilidad de sólidos en CO_2sc con cosolventes, ya que no necesitan un gran número de parámetros y pueden ser empleadas para una amplio intervalo de concentraciones de cosolvente.

Por otra parte, los modelos *q* desarrollados (*q*-Chrastil y *q*-González) proporcionaban el mismo error que los modelos originales. Sin embargo, no

presentan inconsistencias teóricas con la temperatura, por lo que deben ser estudiados en sistemas a alta temperatura y con sólidos complejos.

Además, los resultados indican que el parámetro q está estrechamente relacionado con la estructura del compuesto, por lo que podría ser utilizado en trabajos futuros para el desarrollo de un test de consistencia para la solubilidad de sólidos en CO_2sc.

● Referencias también citadas

[1] R. L. Mendes; B. P. Nobre; M. T. Cardoso; A. P. Pereira; A. F. Palabra, Supercritical carbon dioxide extraction of compounds with pharmaceutical importance for microalgae, Inorg. Chim. Acta 356 (2003) 328-334.

[2] L. T. Danh; P. Truong; R. Mammucari; N. Foster, Extraction of vetiver essential oil by ethanol-modified supercritical carbon dioxide, Chem. Eng. J. 165 (2010) 26-34.

[3] M. Sauceau; J.-J. Letourneau; D. Richon, J. Fages, Enhanced density-based models for solid compound solubilities in supercritical carbon dioxide with cosolvents, Fluid Phase Equilib. 208 (2003) 99-113.

[4] J. C. González; M. R. Vieites; A. M. Botana; J. M. Vieites; L. M. Botana, Modified mass action law-based model to correlate the solubility of solids and liquids in entrained supercritical carbon dioxide, J. Chromatogr. A 910 (2001) 119-125.

[5] H. Sovova, Solubility of ferulic acid in supercritical carbon dioxide with ethanol as cosolvent, J. Chem. Eng. Data 46 (2001) 1255-1257.

[6] Z. Tang; J.-su Jin; Z.-ting Zhan; X-yun Yu; J.-niang Xu; Solubility of 3,5-dinitrobenzoic acid in supercritical carbon dioxide with cosolvents at temperatures from (308 to 328) K and pressures from (10.0 to 21.0) MPa, J. Chem. Eng. Data 55 (2010) 3834-3841.

[7] S. N. Reddy; G. Madras, Modeling of ternary solubilities of solids in supercritical carbon dioxide in the presence of cosolvents or cosolutes, J. Supercrit. Fluids 63 (2012) 105-114.

[8] S. N. Reddy; G. Madras, A new semi-empirical model for correlating the solubilities of solids in supercritical carbon dioxide with cosolvents, Fluid Phase Equilib. 310 (2011) 207-212.

[9] C. Tsallis, Possible generalization of Boltamann-Gibbs statistics, J. Stat. Phys. 52 (1988) 479-487.

[10] E. P. Borges, On a q-generalization of circular and hyperbolic functions, J. Phys. A: Math. Gen. 31 (1998) 5281-5288.

[11] C. Tsallis, Introduction to nonextensive statistical mechanics, approaching a complex world, 1º Ed.- NewYork: Ed. Springer, 2009.

CAPÍTULO 7.

Estimación de propiedades de sublimación de sólidos

En el capítulo 4 se ajustaron datos experimentales de solubilidad de fármacos en CO_2sc con ecuación cúbica de Peng-Robinson. A partir de este estudio se observó los problemas al utilizar ecuaciones de estado cúbicas para el ajuste, el error obtenido para moléculas complejas era elevado (más del 20%) y las propiedades del sólido eran difíciles de obtener.

A fin de reducir el error en el ajuste de estos equilibrios se usaron y estudiaron diferentes ecuaciones semiempíricas (capítulos 5 y 6). Sin embargo, quedaba sin resolver el problema referido a la estimación de diferentes propiedades del sólido.

Entre estas propiedades, es especialmente compleja la estimación de la presión y entalpía de sublimación debido a la dificultad de su obtención tanto de forma teórica así como experimental.

7.1. Importancia de la presión de sublimación.

Para proceder al ajuste de un equilibrio sólido-fluido supercrítico mediante la aproximación de isofugacidad con una ecuación de estado cúbica se requiere conocer diferentes propiedades del sólido Específicamente, se necesita conocer las propiedades críticas, el factor acéntrico y la presión de sublimación del sólido.

Debido a la dificultad de encontrar en bibliografía valores de estas propiedades obtenidos de forma experimental, se desarrollaron metodologías para su estimación a través de modelos de contribución de grupos como los desarrollados en [1] y [2].

En el caso de las propiedades críticas o del factor acéntrico existen diversos modelos de este tipo que proporcionan valores con un error entre el 5% y el 10% en su predicción [1-2]. Sin embargo, la estimación de la presión de sublimación de una molécula compleja es más complicada debido a sus bajos valores, con lo que su determinación experimental es muchas veces errónea o sólo válida para unas ciertas condiciones-

7.1.1. Presión de sublimación en el equilibrio sólido-vapor.

La solubilidad de un sólido en un fluido supercrítico está directamente relacionada con la presión de sublimación del soluto [3], como es observa en la definición de la solubilidad del sólido en la fase supercrítica (ecuación 7.1).

En esta ecuación y_2 representa la solubilidad en fracción molar, P la presión, P^{sub} la presión de sublimación del sólido, R la constante de los gases ideales, T la temperatura y V el volumen del sólido. Finalmente, Φ^{Sat} es el coeficiente de fugacidad del sólido (que se supone la unidad) y Φ^{SCF} es el coeficiente de fugacidad del sólido en el fluido supercrítico.

$$y_2 = \frac{P_2^{sub}\phi_2^{sat}}{P\phi_2^{SCF}} \exp\left(\frac{\left(P - P_2^{sub}\right)V_2^S}{RT}\right) \qquad \text{(Ec. 7.1)}$$

Por tanto no es posible emplear la ecuación anterior si no se conoce dicha presión de sublimación del sólido. Como se ha indicado y se hace incidencia, su determinación experimental es complicada debido a que las presiones de sublimación de sólidos complejos suelen tener un valor muy bajo, y por ello una diferencia en el procedimiento experimental puede conducir a la obtención de errores muy elevados.

Esta dificultad en su obtención experimental obliga en muchas ocasiones al uso de aproximaciones para su estimación.

Sin embargo, aunque existen ecuaciones o modelos de contribución de grupos para su cálculo, estos modelos necesitan de la estimación de otras propiedades como puede ser la entropía de fusión [4], lo que se traduce en una desventaja importante, ya que el aumento del número de modelos de contribución de grupos incrementa el error final de predicción.

Como muestra de lo anterior, en la tabla 7.1 se observa la gran diferencia entre valores experimentales y calculados de la presión de sublimación de un fármaco con varios modelos de contribución de grupos [5].

Table 7.1. Relación entre la presión de sublimación del Irgacure 2959 a 298 K calculada con distintos modelos de contribución de grupos y su presión de sublimación experimental [5].

$(P^{sub})_{calc}$ (Pa)		$(P^{sub})_{calc}/(P^{sub})_{exp}$
Método de estimación	**Valor**	
Ambrose-Walton (set 1)	$1{,}46\cdot10^{-2}$	$2{,}1\cdot10^{2}$
Ambrose Walton (set 2)	$1{,}86\cdot10^{-4}$	2,7
Ambrose-Walton (set 3)	$1{,}42\cdot10^{-2}$	$2{,}0\cdot10^{2}$
Ambrose-Walton (set 4)	1,42	$2{,}0\cdot10^{4}$
Ambrose-Walton (set 5)	$8{,}51\cdot10^{-15}$	$1{,}2\cdot10^{-10}$
Coutsikos (set 6)	$1{,}86\cdot10^{-6}$	$2{,}7\cdot10^{-2}$

Además del uso de modelos de contribución de grupos existen otras formas de determinación de la presión de sublimación de sólidos como son:

- Mediante el ajuste del equilibrio sólido-fluido supercrítico con una ecuación de estado cúbica.

En este procedimiento, la presión de sublimación debe ser considerada como un parámetro ajustable junto a los correspondientes parámetros de interacción de la regla de mezcla. Sin embargo, mediante este procedimiento el parámetro de interacción y la presión de sublimación pierden su significado físico y su estimación podría resultar errónea [6].

• Mediante el uso de la aproximación de Clausius-Clapeyron en el punto triple del sólido (ec. 7.2).

Este método evita el cálculo previo de propiedades como la entropía de fusión o las propiedades críticas del sólido [3].Sin embargo, es necesario conocer la entalpía de sublimación del sólido. Esta entalpía en el punto triple se puede desdoblar en la suma de las correspondientes entalpías de fusión y de vaporización (ec. 7.3).

$$Ln\left(\frac{P^{sub}}{P_{pt}}\right) = -\frac{\Delta H^{sub}}{R}\left(\frac{1}{T} - \frac{1}{T_{tt}}\right) \qquad \text{(Ec. 7.2)}$$

$$\Delta H^{sub} = \Delta H^{vap} + \Delta H^{fus} \qquad \text{(Ec. 7.3)}$$

Las dos ecuaciones anteriores (ecuaciones 7.2 y 7.3) serán la base para el desarrollo de una nueva metodología para calcular la presión de sublimación.

7.1.2. Ecuaciones semiempíricas para estimar la presión de sublimación.

Como puede deducirse de las ecuaciones 7.2 y 7.3, para el cálculo de la presión de sublimación de un sólido mediante la ecuación de Clausius-Clapeyron se necesita un conocimiento de su entalpía de sublimación.

Sin embargo, la estimación de la entalpía de sublimación para sólidos farmacéuticos es compleja ya que no existe un método adecuado basado en la

contribución de grupos. Además, no existe una base de datos con muchos valores experimentales de esta propiedad para sólidos orgánicos complejos como son los farmacéuticos.

En este contexto, como se indicó en el capítulo 5, varios parámetros ajustables de diferentes ecuaciones semiempíricas están relacionados con diferentes entalpías de transición entre fases del sólido. En concreto, se observó una similitud entre el valor estimado a partir de la ecuación de Bartle et al. [7] y la entalpía de vaporización del sólido para pasar de estado líquido a gas, como se observa en la tabla 7.2 [8].

Tabla 7.2. Entalpías de vaporización estimadas a partir de la ecuación de Bartle et al. y su comparación con las propiedades experimentales [8].

Compuesto	$(\Delta H^{vap})_{est}$ (kJ·mol^{-1})	$(\Delta H^{vap})_{exp.}$ (kJ·mol^{-1})
Naftaleno	58,65	55,40
Acetaminofén	74,11	89,40
2-Ácido hidroxibenzoico	60,20	66,70

De acuerdo con la ecuación 7.3, para calcular la entalpía de sublimación del sólido se debería añadir el valor de la entalpía de fusión a la entalpía de vaporización.

La entalpía de fusión puede ser estimada de forma precisa (con un error menor del 5%) para fármacos a través de contribución de grupos, tal como se indica en [9].

Teniendo en cuenta lo anteriormente descrito, más adelante, apartado 7.3.1, se describirá la metodología usada para el cálculo de la presión de sublimación, que está basada en ecuaciones semiempíricas y datos experimentales de solubilidad de sólidos en CO_2sc.

Los valores obtenidos de presión de sublimación se compararán con los correspondientes valores experimentales, y posteriormente podrán ser usados en diferentes áreas de la termodinámica en las que se necesite el valor de esta propiedad, como por ejemplo en los ciclos de solvatación, etc…

7.2. Estimación de la entalpía de sublimación.

Como se ha indicado, para la determinación de la presión de sublimación se ha de calcular la entalpía de fusión y de vaporización del sólido y la presión en el punto triple.

La determinación de la entalpía de fusión se ha realizado por un método de contribución de grupos [9], mientras que la presión en el punto triple se puede calcular mediante una ecuación de estado cúbica para un componente puro sin necesidad de parámetros de interacción.

Sin embargo no existe un método para la estimación de la entalpía de sublimación de moléculas complejas como las farmacéuticas. Esta entalpía de sublimación es además una propiedad requerida para el estudio de ciclos termodinámicos de solvatación, muy importantes en este tipo de industria.

Por otra parte, el conocimiento de este ciclo es fundamental para conocer los distintos mecanismos moleculares de solvatación de moléculas de fármacos, como se ha indicado en [10-11].

Con el fin de evitar un procedimiento experimental para el cálculo de la entalpía de sublimación, se procedió al desarrollo de un método de contribución de grupos para estimar esta entalpía de compuestos farmacéuticos.

Por tanto, en el apartado 7.3.2 se describirá el procedimiento utilizado para el desarrollo de un modelo para dicho cálculo de la entalpía de sublimación de sólidos constituidos por anillos aromáticos y/o alifáticos, básicos para la industria farmacéutica.

Asimismo se mostrará la compilación de los valores de entalpía de sublimación recogidos de bibliografía para el desarrollo de este modelo.

7.3. Resultados y discusión

7.3.1. Cálculo de la presión de sublimación

Durante estos últimos años, los modelos semiempíricos se han establecido como una buena opción para ajustar el equilibrio de datos de solubilidad de sólidos en fluidos supercríticos.

En el primero de los artículos que se encuentran a continuación, se ha estudiado el empleo de estas ecuaciones para la determinación de las propiedades de sublimación de sólidos. En concreto, se emplea la ecuación de Bartle para el cálculo de la entalpía de vaporización de diferentes sólidos objeto de estudio.

Mediante este procedimiento, se obtuvieron desviaciones alrededor del 10% en la determinación de presiones y entalpías de sublimación.

Los valores calculados de la presión de sublimación fueron utilizados para el estudio de equilibrios multifásicos, como sólido-fluido supercrítico y sólido-líquido-fluido supercrítico con la ecuación de estado de Peng-Robinson (sin considerar la presión de sublimación como parámetro ajustable).

Por otro lado, las presiones de sublimación se usaron para calcular más propiedades de sublimación (entropía de sublimación y energía libre de Gibbs de sublimación) y propiedades de solvatación del acetaminofén en varios solventes.

También se procedió al modelado con distintas ecuaciones semiempíricas (Chrastil, Kumar-Johnston y Bartle) de 62 sistemas constituidos por fármacos y CO_2 supercrítico para calcular la entalpía de solvatación de esos sólidos en CO_2sc junto con sus entalpías de vaporización.

7.3.2. Desarrollo de un modelo de contribución de grupos para estimar la entalpía de sublimación de fármacos

Asimismo, se ha procedido en el segundo trabajo que se expone en este capítulo al desarrollo de un modelo de contribución de grupos para estimar la entalpía de sublimación de sólidos constituidos por anillos aromáticos y/o anillos policíclicos alifáticos.

Este modelo predice esta propiedad de estos sólidos con un error relativo de 8,98% y un error absoluto de 9,22 $kJ \cdot mol^{-1}$.

A fin de evaluar la consistencia de este modelo, se realizó un análisis ANOVA y dos pruebas de validación. Este modelo de contribución de grupos puede ser empleado para facilitar el cálculo de la entalpía de sublimación de un sólido de estas características, como pueden ser los fármacos. Sin embargo, el inconveniente de este modelo es que no puede ser usado con sólidos sin anillos en su estructura o con compuestos inorgánicos.

ARTÍCULO

On the use of semiempirical models (solid+supercritical fluid systems) to determine solid sublimation properties

The Journal of Chemical Thermodynamics 43(2011) 711-718

J. Chem. Thermodynamics 43 (2011) 711–718

Contents lists available at ScienceDirect

J. Chem. Thermodynamics

journal homepage: www.elsevier.com/locate/jct

On the use of semiempirical models of (solid + supercritical fluid) systems to determine solid sublimation properties

Antonio Tabernero, Eva M. Martín del Valle *, Miguel A. Galán

Department of Chemical Engineering, University of Salamanca, P/Los Caídos S/N, 37008, Spain

ARTICLE INFO

Article history:
Received 19 May 2010
Received in revised form 13 December 2010
Accepted 22 December 2010
Available online 5 January 2011

Keywords:
Supercritical fluids
Sublimation properties
Solvation properties
Semiempirical models

ABSTRACT

Experimental solubility data of solid–supercritical fluids have significantly increased in the last few years, and semiempirical models are emerging as one of the best choices to fit this type of data. This work establishes a methodology to calculate sublimation pressures using this type of equations. It requires the use of Bartle's equation to model equilibria data solid–supercritical fluids with the aim of determining the vaporization enthalpy of the compound. Using this method, low deviations were obtained by calculating sublimation pressures and sublimation enthalpies. The values of the sublimation pressures were subsequently used to successfully model different multiphasic equilibria, as solid–supercritical fluids and solid–solvent–supercritical fluids with the Peng–Robinson equation of state (without considering the sublimation pressure as an adjustable parameter). On the other hand, the sublimation pressures were also used to calculate solid sublimation properties and acetaminophen solvation properties in some solvents. Also, solubility data solid–supercritical fluids from 62 pharmaceuticals were fitted with different semiempirical equations (Chrastil, Kumar-Johnston and Bartle models) in order to present the values of solvation enthalpies in sc-CO_2 and vaporization enthalpies for these compounds. All of these results highlight that semiempirical models can be used for any other purpose as well as modeling (solid + supercritical fluids) equilibria.

© 2010 Elsevier Ltd. All rights reserved.

1. Introduction

During these last few years, supercritical fluids (SCFs) have been used in pharmaceutical applications for extracting ultra-purity actives from natural sources [1–3] or for drug processing with processes like RESS, SAS or SEDS among others. Advantages of these techniques are widely presented in literature [4–6]. The compound most used as an SCF is the supercritical carbon dioxide (sc-CO_2) because of its light properties and their environmental benefits [7].

In these processes, it is crucial to know the solubility of the solids in the SCF. Different models have been employed to predict the solubility of solids in sc-CO_2. Cubic equations of state (EOS) or semiempirical models are currently the most employed.

Semiempirical equations are emerging as a good choice to model the (solid + SCF) equilibrium for several reasons, like their accuracy. In a previous work, our research group studied the nine most used semiempirical equations with 27 pharmaceutical solids, determining which of these equations should be used depending on the operating conditions, and proving that these models provide, in terms of error, a better fit compared with cubic EOS [8]. Furthermore, these equations are relatively easy to handle, solid properties are not required, and due to their semiempirical character, the parameters of some of these equations are related to the total reaction heat (ΔH^{tot}) or to solid properties like vaporization enthalpy (ΔH^{vap}). Another advantage is that some of these models can be applied to determine the consistency of the experimental data [9]. Nevertheless, although the correlation is accurate and long computational methods are not required, experimental data are needed. In this context, it is important to point out that in the last decade, the studies aiming at determining the experimental solubility of compounds in sc-CO_2 data have increased significantly [10–13] due to the great number of applications of the SCFs in the pharmaceutical industry.

On the other hand, deviations could be obtained fitting experimental data at high pressures with cubic EOS if the solid is a heavy polar compound (like many drugs), although the tendency is still always present [8,14]. Furthermore, it is necessary to estimate the critical properties by group contribution, which can lead to a larger error in the adjustment. Besides, the computational method is longer and more difficult with respect to semiempirical models.

Regarding multicomponent equilibria, although semiempirical models have been employed in systems with cosolvents [15,16], it is not a very common fact because they were thought to fit only the solubility of pure solids in SCFs. Moreover, experimental data from multicomponent systems are more difficult to find in

* Corresponding author. Tel.: +34 923 294479; fax: +34 923 294579.
E-mail address: emvalle@usal.es (E.M. Martín del Valle).

0021-9614/$ - see front matter © 2010 Elsevier Ltd. All rights reserved.
doi:10.1016/j.jct.2010.12.011

literature, and since a component is added, the number of combinations solid–solvent–SCF is practically infinite. In this context, cubic EOS are perhaps the best choice to estimate a multicomponent equilibrium, because despite the deviation, the tendency is always predicted.

Nevertheless, cubic EOS need the knowledge of certain properties. Among these properties, the sublimation pressure (P^{sub}) plays an important role to predict the solubility of solids in SCFs. In some studies, it is established that large deviations produced with cubic EOS are mainly due to no accurate estimations of the P^{sub} [17–20]. However, its calculation is very complicated for solids like pharmaceuticals, since these obtained values with different methods or by different estimation group contributions can vary more than an order of magnitude [18–20].

There are some approaches to determine the P^{sub} from experimental data. Usually, its value is calculated considering it as an adjustable parameter together with the interaction parameter k_{ij} when the equilibrium (solid + SCF) is correlated with an EOS. But upon these conditions, the fitted parameters are highly correlated and the computational method is even more difficult. Besides, the k_{ij} cannot be related with the structure of the compound [19].

Another approach is to calculate the sublimation pressures using fusion properties and the Clausius–Clapeyron approach. Neau et al. [18] proposed a method in which Antoine's equation might be used to calculate the component vapor pressures (P^{sat}) at different temperatures, with the aim of determining subsequently the ΔH^{vap} using the Clausius–Clapeyron equation. This step is very complicated for pharmaceuticals, because Antoine's parameters for these components are usually unavailable. Then, knowing the ΔH^{vap}, due to the singularity of the triple point, the sublimation enthalpy (ΔH^{sub}) can be calculated as the sum of fusion enthalpy ΔH^{fus} (this parameter can be relatively easy measured) and ΔH^{vap}. Finally, the P^{sub} can be defined with the ΔH^{sub} using again the Clausius–Clapeyron approach. Therefore, ΔH^{sub} is the key parameter to calculate the P^{sub} [18]. Its value is related to a parameter from Bartle's model [21] in such a matter that by using this equation, the enthalpy can be determined directly and without intermediate calculations. However, when this value is tested with experimental data, the enthalpy from Bartlés model is always lower (usually around 60-70 % of the experimental values with an inert gas flow method) [12-13]. A possible explanation might be that, at high pressures and in presence of a SCF, the semiempirical models predict a lower value of the sublimation enthalpy (near the vaporization enthalpy of the compound), given that at these conditions the solid might even melt at a lower temperature due to the melting point depression. Therefore, although solids sublime directly from solid to vapour at temperatures below their triple point, and the melting point depression can not be enough to melt the solid, a more accurate result would be achieved when it is performed a comparison with experimental data if the value of the fusion enthalpy is added (a 20-30 % of the sublimation enthalpy). This assumption will be used in this work in order to reduce the deviation, considering the value of the ΔH^{sub} obtained from semiempirical models as the value of the ΔH^{vap} of the compound.

This work tries to prove if semiempirical models (with only three parameters) can be used in a proposed methodology to determine accurately sublimation pressures. The sublimation pressures might be used to predict easier multicomponent equilibria with cubic EOS, or to determine solid sublimation properties. Afterwards, if the solution properties are known, the sublimation properties might be used to calculate solid solvation properties in different solvents.

To do that a methodology to calculate sublimation pressures using experimental solubility data solid–supercritical fluids will be proposed. It requires the use of Bartle's model to fit this type of experimental data. The results will be compared with data from literature and the P^{sub} will be used to model binary and ternary systems with a cubic EOS (Peng–Robinson with classic Van der Waals mixing rules). Another aim will be to prove if the sublimation pressures can be used to determine sublimation properties. Finally, 62 experimental data sc-CO_2-pharmaceuticals will be modeled with semiempirical models (Chrastil [22], Kumar–Johnston (KJ) [23] and Bartle et al. [21]) in order to present new values of properties for these solids using semiempirical equations.

2. Semiempirical models that can be used to determine different enthalpies

Chrastil [22] described one of the first density-based models, based on the solvato complex formed between the solute and solvent molecules at equilibrium (equation (1)):

$$S = \rho_1^k \exp\left(\frac{A}{T} + B\right). \tag{1}$$

Equation (1) establishes a relationship between the solubility of the solute (S in $kg \cdot m^{-3}$) and the pure density of the SCF (ρ_1 in $kg \cdot m^{-3}$). The parameter k is the association number which describes the number of SCF molecules in the solvated complex. The ΔH^{tot} can be calculated from the parameter $A = -\Delta H^{tot}/R$ (R is the gas constant). ΔH^{tot} is given by the sum of the vaporization enthalpy (ΔH^{vap}) and solvation enthalpy (ΔH^{solv}) of the solute in the SCF. Finally, T is the temperature (K).

Kumar and Johnston [23] proposed a new density-based model with a linear relationship between $\ln(y_2)$ and ρ_1 equation (2).

$$ln(y_2) = A + B \cdot \rho_1 + \frac{C}{T}. \tag{2}$$

In the previous equation, y_2 is the solubility of the solute in the SCF, ρ_1 ($kg \cdot m^{-3}$) is the density of the SCF and T is the temperature (K). In this equation, the parameter C is, again, related to the ΔH^{tot} by means of $C = -\Delta H^{tot}/R$.

Finally, Bartle et al. [21] established a relation between the enhancement factor (ratio of the actual solubility to the ideal solubility, but changing P^{sub} for P^{ref} and adding a ρ_{ref}) of the solute and the density of the solvent (equation (3)).

$$ln\left(y_2 \cdot \frac{P}{P_{ref}}\right) = A + \frac{B}{T} + C \cdot (\rho - \rho_{ref}). \tag{3}$$

The value of P_{ref} is taken as 1 bar, whereas the reference density ρ_{ref} is taken as 700 $kg \cdot m^{-3}$. The ΔH^{vap} is directly related to the parameter B, where $B = -\Delta H^{vap}/R$.

As it was defined previously, the ΔH^{solv} can be obtained as the difference between ΔH^{tot} and ΔH^{vap}. The ΔH^{tot} can be calculated from the parameters given by Chrastil or KJ models. Therefore, when experimental solubility data is modeled with some semiempirical equations, the obtained parameters might be used to determine ΔH^{vap}, ΔH^{tot} and ΔH^{solv}.

3. Methodology to calculate sublimation pressures

The next steps were followed to calculate the sublimation pressure from solubility data solid–SCFs:

(1) The ΔH^{fus} and the T_f should be known or can be determined by different group contribution methods [24,25]. The P_{tp} should be known or can be calculated with an EOS [19].
(2) The ΔH^{vap} is determined modeling solubility data solid–SCFs with Bartle's model. The parameter B of Bartle's equation is related to the value of the ΔH^{vap}.
(3) In the triple point, the value of the ΔH^{sub} can be assumed as the sum of ΔH^{fus} and ΔH^{vap}.

(4) The sublimation pressure P^{sub} at a given temperature T is calculated using the well-known Clausius–Clapeyron equation at the triple point (equation (4)):

$$Ln\left(\frac{P^{sub}}{P_{tp}}\right) = -\left(\frac{\Delta H^{sub}}{R}\right)\cdot\left(\frac{1}{T}-\frac{1}{T_{tp}}\right). \quad (4)$$

Although this methodology is not valid to estimate P^{sub}, several improvements (compared with other methods to calculate the P^{sub} from solubility data) are presented:

- It is not necessary to use the Antoine's equation to calculate the vapor pressure to determine ΔH^{vap}. Sometimes, the parameters given by this equation are not available (it is very difficult to find them for pharmaceuticals) or are only suitable for certain conditions.
- Although it is possible to use a cubic EOS to calculate the sublimation pressure from solubility data solid–SCFs (taking the P^{sub} as an adjustable parameter together with the binary interaction parameter), this method presents several drawbacks, like building a long algorithm or obtaining a highly correlated parameters [18].

Therefore, calculating P^{sub} with our procedure is more accurate and faster (in our case the computational method is shorter because it is not necessary to build an algorithm).

Furthermore, an advantage of this method is that the use of semiempirical models is increasing because these models are the best option (in terms of average deviation) to correlate solubility data (SCFs + solid) systems. Therefore, this type of experimental data might be a new source to calculate P^{sub} or other type of enthalpies.

4. Results and discussion

4.1. Validation of the P^{sub}

In order to validate the sublimation pressure results, naphthalene was chosen as the reference. Experimental solubility data CO_2–naphthalene between (308 and 338) K were taken from McHugh and Paulaitis [26] and were modeled in this work with Bartle, Chrastil and KJ models (parameters are showed in table 1). Bartle's model was used to calculate the ΔH^{vap} and subsequently the sublimation pressure was calculated with the methodology described previously.

The parameters from Chrastil and KJ models were also introduced in table 1 with the aim of calculating the ΔH^{tot} and ΔH^{solv} of the solid in sc-CO_2 with the relationships explained before (section 2). This methodology to determine these enthalpies will be followed in section 4.5. It is important to point out that the ΔH^{tot} was taken as the average between the values given by Chrastil and KJ. The ΔH^{solv} was defined as the difference between ΔH^{tot} and ΔH^{vap}. Table 1 shows the enthalpies for the naphthalene as well as the parameters from the three equations.

TABLE 1
Parameters given by semiempirical models for naphthalene.

Equation	Parameters			Enthalpies (kJ · mol^{-1})
Chrastil	k = 4.90	A = −6991.68	B = −6.62	ΔH^{tot} = 58.10
KJ	A = 10.92	B = 0.05	C = −5833.47	ΔH^{tot} = 48.47
Bartle	A = 23.26	B = −7057.48	C = 0.09	ΔH^{vap} = 58.65
				$\Sigma\Delta H^{tot}/2$ = 53.28
				ΔH^{solv} = −5.37

TABLE 2
Fusion properties of the studied solids.

Solid	Tf (K)	ΔH^{fus} (kJ · mol^{-1})
Naphthalene	353 [19]	19.06 [19]
Acetaminophen	443 [29]	27.10 [29]
2-Hydroxybenzoic	431 [28]	28.80 [28]
3-Hydroxybenzoic	473 [28]	34.90 [28]

TABLE 3
Values of the calculated sublimation enthalpies using semiempirical models and the values given by [27–29] (Error = 100 · (ΔH^{sub} this work. − ΔH^{sub} lit.)/ΔH^{sub} lit.). For naphthalene $AARD$ = (100/N) · Σ(ΔH^{sub} this work. − ΔH^{sub} lit.)/ΔH^{sub} lit.).

Solid	ΔH^{sub} (this work)/ (kJ · mol^{-1})	ΔH^{sub} (lit.)/ (kJ · mol^{-1})	Error or $AARD$ (%)
Naphthalene	77.71	22 values	9.14
Acetaminophen	101.22	116.50	13.11
2-Hydroxybenzoic acid	89.00	95.50	6.81
3-Hydroxybenzoic acid	98.65	104.30	5.42

TABLE 4
Deviations (error in %) for the method proposed for naphthalene. (Error = 100 · (P^{sub} this work. − P^{sub} lit.)/P^{sub} lit.).

P^{sub} (bar) [19]	Error (%) (333 K)	Error (%) (353 K)	Error (%) (373 K)
$10^{(8.58-3734/T)}$ (equation (5))	12.53	0.90	9.20

TABLE 5
Sublimation pressures of the different solids in function of the temperature. P^{sub} (bar) and T (K).

Solid	Sublimation pressure (bar)
Naphthalene	$P^{sub}(T) = \exp(21.88 - 9351/T)$
Acetaminophen	$P^{sub}(T) = \exp(24.57 - 12{,}167/T)$
2-Hydroxybenzoic acid	$P^{sub}(T) = \exp(21.24 - 10{,}710/T)$
3-Hydroxybenzoic acid	$P^{sub}(T) = \exp(23.24 - 11{,}871/T)$

Knowing the fusion properties of the naphthalene (table 2) and the triple point pressure (P_{tp} = 0.01 bar [19]), by means of equation (4) it is possible to determine the P^{sub} for every T. The value of the ΔH^{sub} (77.71 kJ · mol^{-1}) was compared with 22 values for the sublimation enthalpy of naphthalene (21 from NIST webbook (http://webbook.nist.gov/chemistry/) and one from [27]), obtaining an $AARD$ around 9% (table 3). This $AARD$ is low, considering that the values of naphthalene sublimation enthalpies vary approximately from 66 to 75 kJ · mol^{-1}.

The calculated P^{sub} was compared with equation (5), which is given in literature [19] (equation (5) is: P^{sub} (bar) = $10^{(8.58-3734/T)}$). The results are showed in table 4.

The deviation values (table 4) are 0.90% at 353 K (triple point), whereas at 373 K and 333 K is near 10%. The deviation increases slightly (from an average value of 5% to our average value around 7%) in comparison with another method found in literature [18]. This difference can be due to the slight error in the calculation of the sublimation enthalpy of the naphthalene (table 3). As in other studies, the deviation increases far away from the triple point because of the temperature extrapolation of the experimental data [18,20].

This procedure was later applied to other solids (acetaminophen and isomers of hydroxybenzoic acid), which can be used in the pharmaceutical industry, determining an equation which relates the sublimation pressure with the temperature. Table 2 shows the properties of the studied solids whereas table 3 shows the values of the sublimation enthalpies given by [27–29] and the values obtained with the proposed methodology. In table 3, it is possible to observe how the deviation in the ΔH^{sub} is low when the values are compared with literature data (an average value between 8% and 9%). This difference can be attributed to the fact that the sublimation enthalpy is not totally independent of the temperature (the obtaining value was compared with the value at 298 K).

Therefore, due to the low error in the sublimation enthalpies, it can be concluded that the proposed methodology, in which it is required the use of a semiempirical model, can be applied to calculate the sublimation pressures for several solids with a low deviation. The equations of the sublimation pressure of naphthalene, acetaminophen and two isomers of hydroxybenzoic acid are given in table 5. The triple point pressure of naphthalene was taken from [19], whereas the triple point pressures of the other compounds were taken from [30].

4.2. Modeling binary mixtures

A bad calculation of the sublimation pressure can be responsible for a large deviation when a cubic EOS is used to fit experimental data (solid + SCFs) systems [17–20]. This section is introduced with the aim of verifying whether the calculated

sublimation pressures can be applied to model the equilibrium (solid + SCF). As a reference, the system (CO_2 + naphthalene) was modeled with the well-established and well-known Peng–Robinson EOS (PR-EOS) [31].

$$P = \frac{R \cdot T}{v - b} - \frac{a(T)}{v^2 + 2b \cdot v - b^2}. \quad (5)$$

In equation (5), v is the molar volume, a is the attractive parameter which depends on the temperature, and b is the covolume. Both terms equations (6) and (7) for pure compounds) are function of the critical properties Pc and Tc of the solid. The dependence of the parameter a with the temperature is considered with the corrector term α (equation (8)), in which the acentric factor w takes into account the no esfericity of the molecule. In order to considerer the interactions between the compounds, classical Van der Waals mixing rules with one single parameter were used (equations (9) and (10)). Only one parameter was chosen in the mixing rule because the P^{sub} is calculated previously, and according to Ashour et al. [32] the addition of several parameters in the mixing rule does not improve significantly the fit.

$$a = 0.45724 \cdot \frac{R^2 \cdot Tc^2}{Pc} \cdot \alpha(T_R), \quad (6)$$

$$b = 0.07780 \cdot \frac{R \cdot Tc}{Pc}, \quad (7)$$

$$\alpha(T_R) = [1 + (0.374 + 1.542w - 0.269w^2)(1 - T_R)^{0.5}]^2, \quad (8)$$

$$a_m = \sum_i \sum_j y_i \cdot y_j \sqrt{a_i \cdot a_j}(1 - k_{ij}), \quad (9)$$

$$b_m = \sum_i \sum_j y_i \cdot y_j \left(\frac{b_i + b_j}{2}\right). \quad (10)$$

The equilibrium (solid + SCF) was modeled with iso-fugacity criteria, assuming the solid phase in the system as a pure solute. The molar fraction in the SCF is described by equation (11). In this equation V_2 is the solid molar volume and $\hat{\Phi}_2^{SCF}$ is the fugacity coefficient of the solid in the supercritical phase. The fugacity coefficient is calculated with the PR-EOS with the mixing rules described in equations (9) and (10).

$$y_2 = \frac{P_2^{sub}}{P \cdot \hat{\Phi}_2^{SCF}} \exp\left(\frac{V_2 \cdot (P - P_2^{sub})}{R \cdot T}\right). \quad (11)$$

Naphthalene and acetaminophen were modeled with the previous assumptions (experimental data CO_2-naphthalene from [26] and CO_2-acetaminophen from [33]). The critical properties of these solids are shown in table 6. The binary interaction parameters k_{ij} from both solids (table 7) were obtained by minimizing the following objective function equation (12).

$$Objective\ function = \sum_{i=1}^{N} 1/N \cdot (y_{exp\,i} - y_{calc\,i})^2, \quad (12)$$

$$AARD = (100/N) \cdot \sum_{i=1}^{N} \frac{|y_{calc} - y_{exp}|}{y_{exp}}. \quad (13)$$

The *AARD* equation (13) between experimental data and predicted values is 14.43% for the naphthalene (figure 1) and 20.92% for the acetaminophen (figure 2). Comparing with literature, Caballero et al. [34] obtained an *AARD* around 15% modeling several experimental data (SCF + naphthalene) with the same number of parameters in the mixing rule (the sublimation pressure was not calculated as an adjustable parameter). With acetaminophen (figure 2), the *AARD* is higher because the acetaminophen is a heavy molecule with polar character, which makes the fit worse with cubic EOS at high pressures [14]. However, it is possible to observe that the tendency of the experimental data is always present. Higher deviations were found in literature when PR-EOS is used to fit solubility data of different solids in sc-CO_2 like indole (33.20%), penicillin V (37.90%) or dodecanoic acid (37.80%) [35].

TABLE 6
Properties of the investigated substances [30].

Property	Toluene	Ethanol	Naphthalene	Acetaminophen	CO_2
MW	92.14	46.07	128.17	151.16	44.01
Tc (K)	591.80	513.92	748.15	736.10	304.21
Pc (bar)	41.08	61.37	40.50	42.60	73.83
W	0.26	0.64	0.30	0.80	0.22
V ($l \cdot mol^{-1}$)			0.11	0.12	

TABLE 7
Binary interaction parameters k_{ij}.

	Toluene	Ethanol	Naphthalene	Acetaminophen
CO_2	0.087 Refitted from [39]	0.080 Refitted from [38]	0.107 Refitted from [26]	0.221 Refitted from [33]

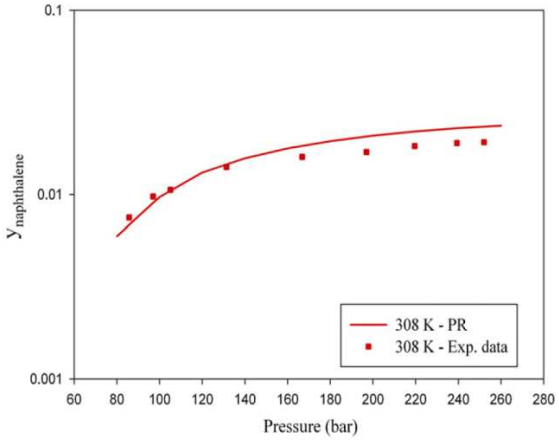

FIGURE 1. Naphthalene solubility in CO_2 as function of pressure at 308 K. Experimental data from [26].

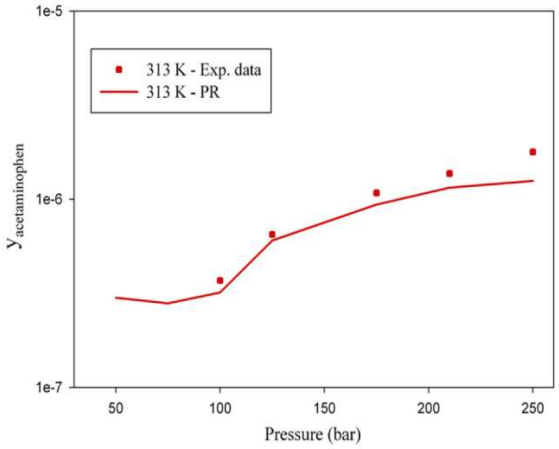

FIGURE 2. Acetaminophen solubility in CO_2 as function of pressure at 313 K. Experimental data from [33].

4.3. Modeling ternary mixtures

In this section it is proved whether the sublimation pressure calculated previously can be used to predict equilibria of multicomponent systems at high pressures. For processes in which an antisolvent is used (like SAS or SEDS) it is very important to know the ternary diagram. In these processes, the main driving force of the precipitation is the supersaturation [36]. This diagram might provide some valuable information in terms of the evolution of the fraction molar of the solid in the liquid phase at equilibrium (knowing the conditions at which the molar fraction at equilibrium would be the minimum) and might give information about the cosolvent effect of the solvent. For modeling this kind of systems, semiempirical equations can not be used because these models are not able to extrapolate equilibria without experimental data. The systems (CO_2 + toluene + naphthalene) and (CO_2 + ethanol + acetaminophen) were modeled with iso-fugacity criteria with the equations described by De la Fuente et al. [37] using PR-EOS. Subscript 1 is given for the CO_2, 2 for the solvent and 3 for the solid. The (liquid + vapor) equilibria CO_2–ethanol (experimental data from [38]) and CO_2–toluene (experimental data from [39]) were also refitted with PR-EOS to obtain the corresponding binary interaction parameters k_{ij} (the parameters are given in table 7) using a different objective function equation (14). The interaction parameters of the system (CO_2 + naphthalene) and (CO_2 + acetaminophen) were obtained in the previous section using equation (12).

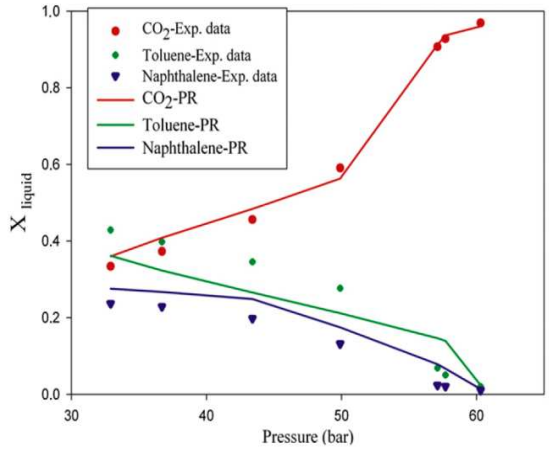

FIGURE 3. Naphthalene solubility as function of pressure in the ternary system (CO_2 + toluene + naphthalene) at 298 K. Experimental data from [40].

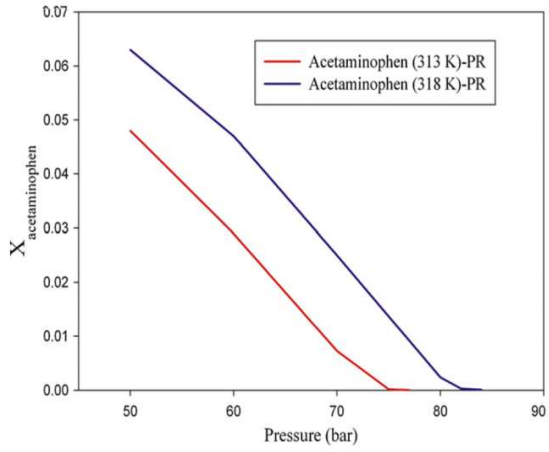

FIGURE 4. Acetaminophen solubility as function of pressure in the ternary system (CO_2 + ethanol + acetaminophen) at (313 and 318) K.

$$Objective\ function = (1/N)\cdot\sum_{i=1}^{N}(x_{exp\,i}-x_{calci})^2+(y_{exp\,i}-y_{calci})^2. \quad (14)$$

The system (CO_2 + toluene + naphthalene) was chosen to check the accuracy, because experimental data at 298 K are available in literature [40]. To model these data at 298 K, the binary interaction parameters k_{12} and k_{13} were considered independent of the temperature. The value of the parameter k_{23} (toluene + naphthalene) was considered negligible because at high pressures the main interactions come from antisolvent–solid and antisolvent–solvent [40]. Figure 3 describes the evolution of the molar fraction of each component in the liquid phase. Moreover, in this figure it can be observed the reasonable good fit provided with PR-EOS using the naphthalene sublimation pressure calculated in this work. The *AARD* from the toluene and naphthalene in the liquid phase are relatively high (*AARD* of CO_2 is 4.35%, *AARD* of toluene is 34.92% and *AARD* of naphthalene is 39.84%). Nevertheless, the tendency of the curve and the maximums and minimums are properly captured. Therefore, the pressure (at a certain temperature) at which the molar fraction of the solid at equilibrium is the minimum can be observed in the diagram. Also the cosolvent effect of the solvent is shown. The solubility of pure naphthalene in CO_2 is about 10^{-2}, whereas if toluene is added the molar fraction increases until values of 0.2.

Finally, the evolution of the molar fraction at equilibrium of the acetaminophen in the liquid phase for the ternary system (CO_2 + ethanol + acetaminophen) was estimated at two different temperatures (figure 4). The binary interaction parameters k_{12} and k_{13} were considered constant (their variation with the temperature is minimum), and again, the parameter k_{23} was considered negligible due to the reasons explained before.

The tendency of the curve which describes the evolution of the fraction molar at equilibrium of the solid in the liquid phase is similar for both systems. An increase in pressure is accompanied by a reduction in the solid molar fraction. This fact can be explained taking into account that the CO_2 is used as an antisolvent. At higher pressures the CO_2 dissolves better in the cosolvent. Therefore, the solvent loses its "solvent power" with the solid and a supersaturation is reached. In figure 4 it can be observed the big cosolvent effect of the ethanol. In the system with acetaminophen, the molar fraction of the acetaminophen increases from 10^{-6} in the binary equilibrium (figure 2) to 10^{-2} in the ternary equilibrium (CO_2 + ethanol + acetaminophen) due to the ethanol cosolvente effect. In this system it is also possible to observe how the curve moves toward higher pressures if the temperature increases. This is due to the density of the CO_2 decreases with the temperature, and consequently the antisolvent effect also decreases.

It should be noticed that in the system with naphthalene, liquid CO_2 is used as an antisolvent because the experimental data were determined at 298 K (under the critical temperature of CO_2, 304 K). On the other hand, in the system with acetaminophen the temperature and the pressure are higher than the critical pressure and critical temperature of CO_2, so that sc-CO_2 is used as an antisolvent.

With this section, it is proved that the calculated sublimation pressure might be applied to estimate molar fraction at equilibrium of multicomponent systems at high pressures with a cubic EOS in order to get a better understanding (for instance) of the processes which employs supercritical fluids as antisolvent.

4.4. Calculating more solid sublimation properties and acetaminophen solvation properties in different solvents

In the previous subsections, the P^{sub} was calculated for different solids from experimental solubility data solid–SCFs (modeling previously this type of equilibria with Bartle's model in order to determine the ΔH^{vap}) (4.1). Then, those values of P^{sub} were used to model different binary (4.2) and ternary systems (4.3) with PR-EOS.

But, sublimation pressures are required in other fields as well as thermodynamic equilibria. For instance, in the thermodynamics of solution the sublimation pressures are needed to calculate the solid sublimation properties of a pure compound. These last properties are required to calculate the solvation properties of a solid in different solvents. In these cases, the sublimation properties are usually determined experimentally by different methods. Although this work is not focused on this topic, this section is dedicated to check if the sublimation pressures determined previously in this work can be used to calculate sublimation properties, and if the calculated sublimation properties can be used to determine solvation properties. In case of good results, experimental solubility data solid–SCFs might be another source to calculate sublimation properties with the aim of using these values in the field of thermodynamic of solutions.

Firstly, the thermodynamics parameters of sublimation of a pure compound are related to its structure. Therefore, knowing the values of these properties for a family of derivatives, it could be possible to determine the role of the different substituents for the crystal lattice energy (for instance with the naphthalene derivatives [27]). A decrease in the crystal lattice energy (Gibbs free energy of sublimation of a pure compound) increases the solubility ability of the compound.

The next equations (15)–(18) were used with the aim of calculating the sublimation properties of the pure compounds at different temperatures (P^o = 1 bar) and the relative contributions by enthalpy (ξ_H) and entropy (ξ_{TS}). The equations to treat the relative contributions have been used previously [27–29], and are used to identify the dominant effect on molecular organization changes in the structure. On the other hand, ΔG^T_{sub}, ΔS^T_{sub}, ΔH^T_{sub} are Gibbs free energy, entropy and enthalpy of sublimation at a given temperature T. Table 8 shows the values of the entropy (ΔS°_{sub}) and Gibbs free energy of sublimation (ΔG°_{sub}) at 298 K for the solids studied previously and the respective deviations from the results found in literature [27–29]. It can be observed that the average error in the Gibbs free energy is near 16% whereas with entropy this error is near 6%. The biggest deviation is found with

TABLE 8
Entropy and Gibbs free energy of sublimation at 298 K and the deviation when these values are compared with literature [27–29]. (Error = 100 · (property this work. – property lit.)/property lit.).

Solid	ΔG°_{sub}/(kJ · mol^{-1})	Error ΔG°_{sub} (%)	ΔS°_{sub}/(kJ · mol^{-1} · K^{-1})	Error ΔS°_{sub} (%)	ξ_H (%)	ξ_{TS} (%)
Naphthalene	23.52	5.00	0.18	5.88	59.16	40.84
Acetaminophen	40.26	32.90	0.20	7.40	61.97	38.03
2-Hydroxibenzoic acid	36.41	5.43	0.18	5.26	62.39	37.61
3-Hydroxibenzoic acid	41.09	18.79	0.19	5.55	63.53	36.47

TABLE 9
Entropy and Gibbs free energy of solvation of acetaminophen in different solvents at 298 K and the error when these values are compared with literature. Enthalpies and Gibbs free energy of solution in the different solvents were taken from [29] (error = 100 · (property this work. – property lit.)/property lit.).

Solvent	ΔG°_{sol}/ (kJ · mol^{-1})	ΔH°_{sol}/ (kJ · mol^{-1})	$-\Delta G^{\circ}_{solv}$/ (kJ · mol^{-1})	Error $-\Delta G^{\circ}_{solv}$ (%)	$-T\Delta S^{\circ}_{solv}$/ (kJ · mol^{-1})	Error $-T\Delta S^{\circ}_{solv}$ (%)	$-\Delta H^{\circ}_{solv}$/ (kJ · mol^{-1})	*Error* $-\Delta H^{\circ}_{solv}$ (%)	ξ_{Hsolv} (%)	ξ_{TSolv} (%)
n-Hexane	30.70	41.90	9.56	32.62	49.75	6.31	59.31	22.10	54.30	45.70
2-Propanol	7.30	13.70	32.96	37.53	54.55	5.72	87.51	16.11	61.62	38.38
Ethanol	7.20	12.20	33.06	37.38	55.93	5.56	88.99	15.89	61.42	38.58

TABLE 10
Enthalpies of different pharmaceuticals estimated from different semiempirical models. ΔH^{tot} is the medium value between the ΔH^{tot} obtained by Chrastil and KJ equations.

Solid	ΔH^{tot}/(kJ · mol^{-1})	ΔH^{vap}/(kJ · mol^{-1})	$-\Delta H^{solv}$/(kJ · mol^{-1})	Reference
Acetaminophen	61.37	74.11	12.74	[33]
Alfa-tocopherol	28.86	45.71	16.85	[41]
Anastrozole	72.90	94.19	21.29	[42]
Astaxanthin	80.26	96.94	16.68	[43]
Atorvastatin	91.61	107.25	15.64	[44]
Beclomethasone dipropionate	40.33	57.15	16.82	[45]
Beta-carotene	86.17	101.18	15.01	[41]
Budesonide	42.28	59.12	16.84	[45]
Butyl hydroxyl anisole	35.53	54.01	18.48	[46]
Caffeine	64.85	80.60	15.75	[47]
Cholesterol	58.54	74.00	15.46	[48]
Coumarin	39.37	55.28	15.91	[49]
Cyproterone acetate	32.82	50.53	17.71	[50]
Eflucimibe	84.16	97.26	13.10	[51]
Erythromycin	44.72	62.15	17.43	[52]
Examestane	84.55	99.28	14.73	[42]
Flurboprifen	63.37	83.26	19.89	[53]
Fluvastatin	77.41	92.79	15.38	[44]
Irgacure 2959®	55.96	79.41	23.45	[17]
Ketoprofen	61.56	74.01	12.45	[54]
Letrozole	81.33	94.68	13.35	[42]
Licopene	28.01	43.47	15.46	[43]
Lidocaine	53.82	71.93	18.11	[14]
Lovastatin	32.12	47.17	15.05	[44]
Medroxyprogesterone acetate	48.28	64.94	16.66	[50]
Methimazole	47.43	63.54	16.11	[55]
Methyl gallate	52.28	68.01	15.73	[56]
Nabumetone	46.92	63.24	16.32	[12]
Narasin	54.22	61.14	6.92	[57]
Nifedipine	57.36	71.60	14.24	[58]
Nimesulide	45.13	58.35	13.22	[54]
Nitrendipine	47.25	61.44	14.19	[58]
o-Hydroxybenzoic acid	44.65	60.21	15.56	[59]
p-Hydroxybenzoic acid	48.10	63.75	15.65	[59]
Paclitaxel	35.51	57.38	21.87	[60]
Penicillin G	63.64	80.30	16.66	[61]
Penicillin V	28.25	43.79	15.54	[62]
Phenazopyridine	51.35	69.77	18.42	[55]
Piroxicam	28.63	42.32	13.69	[54]
Procaine	25.89	51.39	25.50	[14]
Propanolol	109.86	124.79	14.93	[55]
Propyl gallate	51.61	69.16	17.55	[46]
Progesterone	47.48	67.04	19.56	[48]
Protocatochaldehyde	89.07	103.47	14.40	[56]
Protocatechuic acid	79.00	93.37	14.37	[56]
Retinol	27.96	44.67	16.71	[41]
Rosuvastatin	52.71	68.31	15.60	[44]
Salicylamide	45.04	60.76	15.72	[12]
Salinomycin	117.94	132.28	14.34	[57]
Sigma-tocopherol	41.09	57.68	16.59	[41]
Simvastatin	61.57	77.28	15.71	[44]
Taxol	45.58	61.71	16.13	[63]
Testosterone	63.04	82.55	19.51	[48]
Theobromine	56.80	70.89	14.09	[47]
Theophylline	71.65	86.29	14.64	[47]
Vitamine D2	41.52	55.58	14.06	[41]
Vitamine D3	46.09	55.54	9.45	[64]
2-Methylbenzoic acid	56.30	73.99	17.69	[65]
3-Methylbenzoic acid	53.08	70.92	17.84	[65]
4-Methylbenzoic acid	47.56	65.27	17.71	[65]
4-Aminoantipyrine	35.89	51.80	15.91	[66]
4- Dimethylaminoantipyrine	45.60	61.25	15.65	[66]

the acetaminophen (near 33%) as a consequence of several factors, like the deviation in the sublimation enthalpy (table 3) or due to a different choice of the source of the triple point pressure.

$$\Delta G^{T}_{sub} = -R \cdot T \cdot Ln\left((T)P^{sub}(T)\Big/P^{0}\right), \quad (15)$$

$$\Delta S^{T}_{sub} = \frac{\Delta H^{T}_{sub} - \Delta G^{T}_{sub}}{T}, \quad (16)$$

$$\xi_{H} = \frac{\Delta H^{T}_{sub}}{\Delta H^{T}_{sub} + T \cdot \Delta S^{T}_{sub}} \cdot 100, \quad (17)$$

$$\xi_{TS} = \frac{T\Delta S^{T}_{sub}}{\Delta H^{T}_{sub} + T \cdot \Delta S^{T}_{sub}} \cdot 100. \quad (18)$$

In a second case, when a solute diffuses through biological membranes, it is established an interaction between drug–membrane. It is necessary to calculate the solid sublimation properties to determine the solid solvation properties in different solvents, which are important to understand the energetic parameters of the drug-membrane interactions, the nature of these interactions and the corresponding energetic barriers.

If the Gibbs free energy of solution (ΔG°_{sol}) and the enthalpy of solution (ΔH°_{sol}) at 298 K for different solvents are available, the different solid solvation properties, Gibbs free energy (ΔG°_{solv}), enthalpy (ΔH°_{solv}), entropy (ΔS°_{solv}) and the respective enthalpy (ξ_{HSolv}) and entropy (ξ_{TSolv}) contributions at 298 K could be calculated by means of equations (19)–(23).

$$\Delta G^{0}_{solv} = \Delta G^{0}_{sol} - \Delta G^{0}_{sub}, \quad (19)$$

$$\Delta H^{0}_{solv} = \Delta H^{0}_{sol} - \Delta H^{0}_{sub}, \quad (20)$$

$$T \cdot \Delta S^{0}_{solv} = \Delta H^{0}_{solv} - \Delta G^{0}_{solv}, \quad (21)$$

$$\xi_{HSolv} = \frac{\Delta H^{0}_{solv}}{\Delta H^{0}_{solv} + T \cdot \Delta S^{0}_{solv}} \cdot 100, \quad (22)$$

$$\xi_{TSolv} = \frac{T \cdot \Delta S^{0}_{solv}}{\Delta H^{0}_{solv} + T \cdot \Delta S^{0}_{solv}} \cdot 100. \quad (23)$$

Table 9 shows the solvation properties of acetaminophen in some solvents and the deviations when the values are compared with literature data. Only three solvents were chosen from bibliography because the target of our study is to prove if the same conclusions can be obtained using the sublimation properties (calculated with our methodology) to determine solvation properties. To make a complete study, more solvents should be introduced. It can be concluded from our values of solvation properties in different solvents that the acetaminophen solvates stronger in the ethanol than in the n-hexane and in the 2-propanol due to the value of the Gibbs free energy. This fact involves that the solubility of the drug in ethanol would be nearer from the ideal solubility (the value of the coefficient activity near to the unit). According to the values of the enthalpic and entropic contributions, for all solvents the driving force for the solvation process is the enthalpy. In spite of the produced deviation in some properties, the same conclusions were obtained in literature [29].

It is important to realize that if the hydroxybenzoic acids are studied, the deviation would be lesser because the error in the sublimation properties is lower. Therefore, with these results, it can be concluded that the methodology described in section 3 can be applied to obtain sublimation pressures for calculating sublimation properties in order to use them in future studies related to solvation processes.

4.5. Properties given by semiempirical equations of several pharmaceuticals

Section 4.1 was focused on calculating sublimation pressures (with the methodology given in section 3) and the validation of its values. In this case, to calculate the sublimation pressures, it is a required step to model experimental solubility data solid–SCFs with Bartle's model in order to determine the vaporization enthalpy of the solids. Later, in sections 4.2 and 4.3 the obtaining values of sublimation pressures were used to estimate different equilibria diagrams of binary and ternary systems (thermodynamic equilibria) wheras in section 4.4 the sublimation pressures were used to calculate solid sublimation properties, and these sublimation properties were to determine solid solvation properties in some solvents (thermodynamics of solutions).

But, as it was proved in section 2, it is possible to calculate the total reaction heat or the solvation enthalpy of the solid in the SCFs from the parameters given by Chrastil and KJ models, as it was done in section 4.1 with the naphthalene. The aim of this section is to give the values of the vaporization enthalpy, the total enthalpy and the solvation enthalpy in sc-CO_2 for 62 pharmaceuticals using the parameters given from different semiempirical models. The vaporization enthalpy will be got from Bartle's model, the total enthalpy will be taken as the average value given by Chrastil and KJ models, and the solvation enthalpy will be determined as the difference between the total enthalpy and the vaporization enthalpy. These values for different 62 pharmaceuticals are showed in table 10. To build this table, different experimental solubility data of solids in sc-CO_2 were taken from literature (column of references) and were fitted with Bartle, Chrastil and KJ models. As a result of the fits, different parameters were obtained. The different enthalpies were calculated from those parameters.

The precision of our results can be estimated from the comparison of the values of the same enthalpies for the same molecule, calculated each one from different experimental data sources. As an example, it can be seen in table 10 the different values of enthalpies for the compounds paclitaxel and taxol (taxol is the trade name for paclitaxel). The vaporization enthalpy value of the paclitaxel and the taxol are practically the same (a difference around 7%), whereas the solvation enthalpies for these compounds in CO_2 are only relatively similar (a difference around a 25%). Those deviations can be attributed to differences between the solubility data of the different works. For instance, in [60], at near 311 K and 210 bars, the solubility of the paclitaxel in CO_2 is $2 \cdot 10^{-6}$. On the other hand, in [63], at 205 bars and 308 K, the value of solubility in CO_2 is $0.7 \cdot 10^{-7}$ (at similar conditions there is a difference around 96% between both studies). Since the experimental data are very different, when the solubility is modeled with a semiempirical equation, the value of the parameters varies. This would surely induce a difference in the calculated enthalpies. Considering the differences in the solubility data between [60] and [63], the deviations in the enthalpies are even low. The reason why the variation in the vaporization enthalpy is not high is due to the value of the parameter *B* from Bartle's model. Parameter *B* remains relatively constant against the variations in the solubility data (−6904 K for paclitaxel and −7426 K for taxol), whereas more differences are observed for the parameter *A* of ChrastilÍs model (−4065 K for paclitaxel and −5546 K for taxol) and for the parameter *C* of KĴs model (−4481 K for paclitaxel and −5523 K for taxol) [8]. However, it should be specified that if the experimental conditions reach an upper critical end point, a big deviation can be produced fitting the solubility data with semiempirical models [8]. This deviation might provide an error in the value of the different enthalpies.

In relation to table 10, all published data were considered correct. This table might be used for several studies, such as to determine sublimation pressures for pharmaceuticals with the methodology established in section 3 (if the fusion properties for the corresponding solid are known).

This table might be also used for a previous thermodynamic study to micronize a drug using SCFs as a solvent (RESS) or as an antisolvent (SAS or SEDS). If experimental solubility data solid–SCF is available, a semiempirical model could be used to predict the equilibria accurately. If the solubility of the solid is low in the sc-CO_2 (this happens frequently due to the polar character of several pharmaceutical compounds) the RESS process would be rejected. Therefore, the SCF must be used as an antisolvent and the multicomponent equilibrium (taking into account the solvent) should be described.

With Bartle's equation it might be possible to determine the sublimation pressure of the solid (if the fusion enthalpy is known). Using the sublimation pressure to model the multicomponent equilibria with a cubic EOS (only parameters in the mixing rule would be required given that the sublimation pressure is known), the multiphasic diagram would be depicted. Therefore, the cosolvent effect of the solvent and the conditions (pressure and temperature) at which the molar fraction at equilibrium is the minimum would be established.

And finally, from the sublimation pressure it would be possible to determine the sublimation properties of the pharmaceutical. If the solution properties of the pharmaceutical in different solvents are known, the thermodynamics solvation properties might be calculated.

5. Conclusions

In this work, it was checked that experimental solubility data (solid + SCFs) can be used to determine different sublimation properties. A methodology was proposed, in which Bartle's model must be used. If the fusion properties are known, the sublimation enthalpy can be determined as the sum of the fusion and vaporization enthalpy. Finally, with Clausius–Clapeyron approach, the sublimation pressure can be obtained. With this methodology, low deviations were produced with sublimation pressures (around 10% at 20 K far from the triple point) and sublimation enthalpies (around an average value of 9%). Furthermore, those pressures were used to model binary systems (solid + SCF), and to estimate equilibria diagrams (SCF + solvent + solid) with PR-EOS, obtaining similar deviations in comparison with literature.

More sublimation properties were calculated using the sublimation pressures (Gibbs free energy and entropy), which then they were employed to obtain acetaminophen solvation properties in different solvents. Although in this last case a relative high deviation might be produced (specifically in Gibbs free energy), it was checked that the solubility of the acetaminophen in ethanol is nearer from the ideal solubility (in comparison with other solvents), as it was obtained in literature experimental studies.

Finally, another main interest of this work is that if the experimental solubility data of a solid in the SCF are available and are

modeled with Chrastil's model, KJ's model and Bartle's model, it would be possible to use the parameters given by these equations to determine different enthalpies.

Therefore, solubility data solid–SCF can be a new source to determine solid sublimation properties.

Acknowledgements

This research was supported by funds from the Ministerio de Ciencia e Innovación (Spain), project CTQ2009-08222 (PPQ subprogram). Antonio Tabernero is supported by a F.P.I. grant from the Ministerio de Ciencia y Innovación (Spain). This grant is also appreciated by the author.

References

[1] N. Vedaraman, C. Srinavasakannan, G. Brunner, B.V. Ramabrakmam, P.G. Brao, J. Supercrit. Fluids 34 (2005) 27–34.
[2] E. Reverchon, I. De Marco, J. Supercrit. Fluids 38 (2006) 146–166.
[3] G.L. Filho, V.V. De Rosso, M.A.A. Meireles, P.T.V. Rosa, A.L. Oliveira, A.Z. Mercadante, F.A. Cabral, J. Supercrit. Fluids 46 (2008) 33–39.
[4] J. Jung, M. Perrut, J. Supercrit. Fluids 20 (2001) 179–219.
[5] M.J. Cocero, A. Martin, F. Mattea, S. Varona, J. Supercrit. Fluids 47 (2009) 545–555.
[6] E.M. Martín del Valle, M.A. Galán, R.G. Carbonell, Ind. Eng. Chem. Res. 48 (2009) 2475–2486.
[7] M. Kemmere, T. Meyer, Supercritical Carbon Dioxide, first ed., Wiley-VCH, Germany, 2005.
[8] A. Tabernero, Eva M. Martín del Valle, M.A. Galán, J. Supercrit. Fluids 52 (2010) 161–174.
[9] J. Mendez-Santiago, A.S. Teja, Fluid Phase Equilib. 158 (1999) 501–510.
[10] A. Jouyban, H.K. Chan, N.R. Foster, J. Supercrit. Fluids 24 (2002) 19–35.
[11] Chie-Shaan Su, Yan-Ping Chen, Fluid Phase Equilib. 254 (2007) 167–173.
[12] D.J. Miller, S.B. Hawthorne, A.A. Clifford, S. Zhu, J. Chem. Eng. Data 41 (1996) 779–786.
[13] Ch. Garlapati, G. Madras, Thermochim. Acta 496 (2009) 54–58.
[14] R.D. Weinstein, K.R. Muske, J. Moriarty, E.K. Schmidt, J. Chem. Eng. Data 49 (2004) 547–552.
[15] Ch. Garlapati, G. Madras, Fluid Phase Equilib. 283 (2009) 97–101.
[16] M. Sauceau, J. Letourneau, D. Richon, J. Fages, Fluid Phase Equilib. 208 (2003) 99–113.
[17] P. Coimbra, D. Fernandes, P. Ferreira, Maria H. Gil, Herminio C. de Sousa, J. Supercrit. Fluids 45 (2008) 272–281.
[18] E. Neau, S. Garnier, L. Avaullée, Fluid Phase Equilib. 164 (1999) 173–186.
[19] S. Garnier, E. Neau, P. Alessi, A. Cortesi, I. Kikic, Fluid Phase Equilib. (1999) 491–500.
[20] P. Coutsikos, E. Voutsas, K. Magoulas, D. Tassios, Fluid Phase Equilib. 207 (2003) 263–281.
[21] K.D. Bartle, A.A. Clifford, S.A. Jafar, G.F. Shilstone, J. Phys. Chem. Ref. Data 20 (1991) 201–219.
[22] J. Chrastil, J. Phys. Chem. 86 (1982) 3016–3021.
[23] S. Kumar, K.P. Johnston, J. Supercrit. Fluids 1 (1988) 15–22.
[24] A. Jain, G. Yang, S.H. Yalkowsky, Ind. Eng. Chem. Res. 43 (2004) 7618–7621.
[25] B.E. Poling, J.M. Prausnitz, J.P. ÓConnell, The Properties of Gases and Liquids, fifth ed., McGraw-Hill, 2004.
[26] M. McHugh, M.E. Paulaitis, J. Chem. Eng. Data 25 (1980) 326–338.
[27] G.L. Perlovich, S.V. Kurkov, A.N. Kinchin, A. Bauer-Brandl, Eur. J. Pharm. Biopharm. 57 (2004) 411–420.
[28] G.L. Perlovich, T.V. Volkova, A. Bauer-Brandl, J. Pharm. Sci. 7 (2006) 1448–1458.
[29] G.L. Perlovich, T.V. Volkova, A. Bauer-Brandl, J. Pharm. Sci. 10 (2006) 2158–2169.
[30] ASPEN HYSYS v. 7.0. ASPEN Technologies, ing.
[31] D.Y. Peng, D.B. Robinson, Ind. Eng. Chem. Fund. 15 (1976) 59–64.
[32] I. Ashour, R. Almehaideb, S.-E. Fateen, G. Aly, Fluid Phase Equilib. 167 (2000) 41–61.
[33] S. Bristow, B.Y. Shekunov, P. York, Ind. Eng. Chem. Res. 40 (2001) 1732–1739.
[34] A.C. Caballero, L.N. Hernández, L.A. Estévez, J. Supercrit. Fluids 5 (1992) 283–295.
[35] P. Coutsikos, K. Magoulas, G.M. Kontogeorgis, J. Supercrit. Fluids 25 (2003) 197–212.
[36] A. Martin, M.J. Cocero, Adv. Drug Delivery Rev. 60 (2008) 339–350.
[37] J.C. De la Fuente Badilla, A. Shariati, C.J. Peters, J. Supercrit. Fluids 32 (2004) 55–61.
[38] Z. Knez, M. Skerget, L. Ilic, C. Lütge, J. Supercrit. Fluids 43 (2008) 383–389.
[39] H.J. Ng, D.B. Robinson, J. Chem. Eng. Data 4 (1978) 325–327.
[40] D. Dixon, K.P. Johnston, AICHE J. 37 (1991) 1441–1449.
[41] M. Johannsen, G. Brunner, J. Chem. Eng. Data 42 (1997) 106–111.
[42] M. Hojjati, A. Vatanara, Y. Yamini, M. Moradi, A. Rouholamini Najafabadi, J. Supercrit. Fluids 50 (2009) 203–209.
[43] J.C. de la Fuente, B. Oyarzun, N. Quezada, J.M. del Valle, Fluid Phase Equilib. 247 (2006) 90–95.
[44] M. Hojjati, Y. Yamini, M. Khajeh, A. Vatanara, J. Supercrit. Fluids 41 (2007) 187–194.
[45] A. Vatanara, A. Rouholamini Najafabadi, M. Khajeh, Y. Yamini, J. Supercrit. Fluids 33 (2005) 21–25.
[46] A. Cortesi, I. Kikic, P. Alessi, G. Turtoi, S. Garnier, J. Supercrit. Fluids 14 (1999) 139–144.
[47] M. Johannsen, G. Brunner, Fluid Phase Equilib. 95 (1994) 215–226.
[48] E. Kosal, C.H. Lee, G.D. Holder, J. Supercrit. Fluids 5 (1992) 169–179.
[49] R.F. Rodrigues, A.K. Tashima, R.M.S. Pereira, R.S. Mohameda, F.A. Cabral, J. Supercrit. Fluids 43 (2008) 375–382.
[50] M. Asghari-Khiavi, Y. Yamini, M.A. Farajzadeh, J. Supercrit. Fluids 30 (2004) 111–117.
[51] M. Sauceau, J.-J. Letourneau, B. Freiss, D. Richon, J. Fages, J. Supercrit. Fluids 31 (2004) 133–140.
[52] G.I. Burgos-Solórzano, J.F. Brennecke, M.A. Stadtherr, Fluid Phase Equilib. 220 (2004) 57–69.
[53] A.R.C. Duarte, P. Coimbra, H.C. de Sousa, C.M.M. Duarte, J. Chem. Eng. Data 49 (2004) 449–452.
[54] S.J. Macnaughton, I. Kikic, N.R. Foster, P. Alessi, A. Cortesi, I. Colombo, J. Chem. Eng. Data 41 (1996) 1083–1086.
[55] Y. Yamini, J. Arab, M. Asghari-khiavi, J. Pharm. Biomed. Anal. 32 (2003) 181–187.
[56] R. Murga, M.T. Sanz, S. Beltrán, J.L. Cabezas, J. Supercrit. Fluids 23 (2002) 113–121.
[57] R.J. Maxwell, J.W. Hampson, M.L. Cygnarowicz-Provost, J. Supercrit. Fluids 5 (1992) 31–37.
[58] Z. Knez, M. Skerget, P. Sencar-Bozic, A. Rizner, J. Chem. Eng. Data 40 (1995) 216–220.
[59] F.P. Lucien, N.R. Foster, Ind. Eng. Chem. Res. 35 (1996) 4686–4699.
[60] V. Vandana, A.S. Teja, Fluid Phase Equilib. 135 (1997) 83–87.
[61] M.D. Gordillo, M.A. Blanco, A. Molero, E. Martinez de la Ossa, J. Supercrit. Fluids 15 (1999) 183–190.
[62] M. Ko, V. Shah, P.R. Bienkowski, H.D. Cochran, J. Supercrit. Fluids 4 (1991) 32–39.
[63] C.A. Nalesnik, B.N. Hansen, J.T. Hsu, Fluid Phase Equilib. 146 (1998) 315–323.
[64] Z. Knez, M. Skerget, J. Supercrit. Fluids 20 (2001) 131–144.
[65] Kuen-Long Tsai, Fuan-Nan Tsai, J. Chem. Eng. Data 40 (1995) 264–266.
[66] Yen-Ming Chen, Yan-Ping Chen, Fluid Phase Equilib. 282 (2009) 82–87.

JCT 10-172

ARTÍCULO

Estimation of sublimation enthalpies of solids constituted by aromatic and/or polycyclic aliphatic rings by using a group contribution method

AIChE Journal, 58 (2012) 2885-2874

AIChE

THERMODYNAMICS AND MOLECULAR-SCALE PHENOMENA

Estimation of Sublimation Enthalpies of Solids Constituted by Aromatic and/or Polycyclic Aliphatic Rings by Using a Group Contribution Method

Antonio Tabernero, Eva M. Martín del Valle, and Miguel A. Galán
Dept. of Chemical Engineering, University of Salamanca, P/Los Caídos S/N 37008, Spain

DOI 10.1002/aic.12779
Published online October 25, 2011 in Wiley Online Library (wileyonlinelibrary.com).

A group contribution (GC) method is developed to predict the sublimation enthalpy of only any compound constituted with polycyclic aromatic hydrocarbons and/or polycyclic aliphatic rings with an average absolute relative deviation of 8.98% and an average absolute error of 9.22 kJ·mol^{-1}. A statistical analysis (ANOVA table) and two validation tests are performed to show the consistency of the method. This GC method can speed up several processes in which it is required the value of the sublimation enthalpy of a solid with these characteristics (pharmaceuticals for instance). However, this method must not be used with inorganic compounds or organic solids with noncyclic structure. © 2011 American Institute of Chemical Engineers *AIChE J,* 58: 2875–2884, 2012

Keywords: sublimation enthalpies, group contribution, pharmaceuticals, polycyclic aromatic hydrocarbons

Introduction

Solid sublimation enthalpy is an important and required property for several thermodynamics applications. Its value is needed in different thermodynamic cycles to study the molecular mechanism of solvation of drug molecules.[1–4] Furthermore, if it is desired to depict a solid–vapor equilibrium diagram, the sublimation pressure must be known. This pressure can be determined by a Clausius–Clapeyron equation, but to use this equation the sublimation enthalpy must be determined.[5,6]

Although several articles in relation to these topics have been published in these last years,[1–8] and there are several database of sublimation enthalpies,[9–11] there is not a group contribution (GC) model to estimate this type of enthalpies for solids like pharmaceuticals. In addition, there are additional problems due to the transitions in the solid phase, avoiding the existence of generalized correlations.[12] Therefore, the value of the required enthalpy must be determined experimentally, although it can be determined with the fusion and vaporization enthalpies of the solid.

Theoretically, the sublimation enthalpy can be considered as the sum of the fusion and the vaporization enthalpies.[9,13] With a low variation, these values can be considered temperature independent, so that this approach is usually used to calculate the sublimation enthalpy. As there are methods to estimate fusion enthalpy,[14,15] it would be only necessary to determine the vaporization enthalpy.

However, there are not estimations for vaporization enthalpies of pharmaceuticals, although there are databases[9,16] and estimations to determine the value of this property for hydrocarbons and more organic compounds.[17] In this context, a work was recently published[18] in which this enthalpy was directly determined (with a deviation around a 10%) fitting experimental solubility data of solids in supercritical fluids (SCFs) using Bartle's semiempirical model.[19] In this equation, a term is related to the sublimation enthalpy of the solid given that the sublimation pressure appears on the development of the model. However, when it is performed a comparison between experimental sublimation enthalpies and calculated sublimation enthalpies from Bartle's model (calculated at high pressure and in the presence of a SCF), the calculated values were always around a 60–70% of the experimental value,[20,21] nearer to the value of the vaporization enthalpy of the solid.

A possible explanation might be that, at high pressures and in the presence of a SCF, this equation predicts a lower value of the sublimation enthalpy (near the vaporization enthalpy of the compound), given that at these conditions the solid might even melt at a lower temperature due to the melting point depression.[22]

The aim of this work is to develop a consistent GC method to estimate the sublimation enthalpy of pharmaceuticals, based only on the structural form of the molecule. This method might be used to speed up processes in which the sublimation enthalpy should be determined to study the solvation process of pharmaceuticals or to determine the sublimation pressure of the solid by means of a Clausius–Clapeyron equation.

It can be found in literature several GC methods to estimate properties of pure compounds.[23,24] However, there is not a GC method for estimating sublimation enthalpies of pharmaceuticals.

Although it is difficult to establish a boundary between drugs and other organic solids, drugs are usually constituted

Correspondence concerning this article should be addressed to E. M. Martín del Valle at emvalle@usal.es.

© 2011 American Institute of Chemical Engineers

by aromatic hydrocarbons and/or cyclic molecules. Therefore, the GC was developed by building a set of 253 compounds of polycyclic aromatic hydrocarbons (PAHs) and different compounds constituted by PHAs and/or polycyclic aliphatic rings to define the values of the sublimation enthalpies for the most common groups in this type of compounds.

Methodology

The creation of this type of models should be first oriented on the molecular crystals with definite structures with a known value of their sublimation enthalpies with the aim of creating a first set of data.

Therefore, a set of values of sublimation enthalpies for 253 compounds was built. All of them present PAHs and/or polycyclic aliphatic rings in their molecular structures, considering that these are the groups that can be commonly found in pharmaceuticals. There are neither noncyclic molecules nor inorganic compounds in this set.

The methodology to obtain these sublimation enthalpies is the following:

1. Values of sublimation enthalpies were directly collected from literature (mainly from databases[9,10]), neglecting the unreasonable low reported values or
2. Sublimation enthalpies were considered as the sum of the fusion enthalpy and the vaporization enthalpy. If the sublimation enthalpy is calculated, then,
   2.1. Fusion enthalpies were collected from literature or were determined using a GC method and
   2.2. Vaporization enthalpies were estimated modeling experimental solubility data solid-SCFs with Bartle's semiempirical equation (SE). This model (Eq. 1) establishes a relation between the enhancement factor (ratio of the actual solubility to the ideal solubility, but changing P^{sub} for P^{ref} and adding a ρ_{ref}) of the solute and the density of the solvent. The equilibrium molar fraction of the solid in supercritical CO_2 is denoted with y_2. The value of P_{ref} is taken as 1 bar, whereas the reference density ρ_{ref} is taken as 700 kg m^{-3} (around the density value of the CO_2 at supercritical conditions) because the solvent is always supercritical CO_2. The parameters A, B, and C must be determined with a regression between experimental data and theoretical data to obtain the best fit. Initially, the value of the sublimation enthalpy is related to the parameter B, ($B = -\Delta H^{sub}/R$).[19–21]

$$\mathrm{Ln}\left(y_2 \cdot \frac{P}{P_{ref}}\right) = A + \frac{B}{T} + C \cdot (\rho - \rho_{ref}) \qquad (1)$$

However, when it is performed a comparison between the enthalpies given by this model and the experimental enthalpies, the estimated values are always lower than the experimental values. Actually, the experimental values are always nearer than the vaporization enthalpy of the solid.[20,21] A possible explanation might be the melting point depression. In the presence of a SCF (high pressure), the solid melting temperature can decrease significantly.[22] Therefore, it might be considered that the solid can melt, and the value of the enthalpy would be the vaporization enthalpy instead of the sublimation enthalpy,[18] being thus the vaporization enthalpy ($\Delta H^{vap} = B{\cdot}R$). An example of this calculation can be found in the Appendix. It is important to take into account several limitations in this methodology to calculate sublimation enthalpies:

1. The vaporization enthalpies were obtained fitting experimental solubility data of solids in sc-CO_2 with a semiempirical model. The use of a semiempirical model can provide an important deviation if the experimental conditions reach an upper critical end point. This phenomenon might induce an error in the value of the vaporization enthalpy.[25]
2. If the fusion enthalpy is determined with a GC model, a deviation can be produced in the outcome due to the error of the method.[14,15]

To avoid the previous error sources, the values of the calculated enthalpies were evaluated, discarding the solids with a value of the fusion enthalpy more than 1/3 of the sublimation enthalpy. Although Poling et al.[12] established the previous value less or equal than 1/4, this value was increased to 1/3 because 1/4 might not be valid for all compounds.[9] Finally, the enthalpies were considered temperature independent.

With these assumptions, values of sublimation enthalpies for 253 solids were collected and were divided into functional groups, defining 41 different groups. These groups are the most common in this type of solids and were chosen because all of these molecules can be structurally defined with these functional groups. The chosen solids have a high average value of carbon atoms (around 10), and the frequency of repetition in most of the mainly groups is high.

It is important to realize that the goal is to develop a method only for solids constituted by PAHs and/or polycyclic aliphatic rings. Therefore, it is also important to highlight that this method will not be able to predict sublimation enthalpies of inorganic molecules or solids with noncyclic structures.

Table 1 depicts the chosen compounds. If the value of the sublimation enthalpy is collected from literature, the reference and the conditions (if they are available in the corresponding article) are specified.

On the other hand, if the sublimation enthalpy is calculated with the methodology previously described, the vaporization enthalpy is calculated with Bartle's SE, and the respective reference for the solubility data of this solid in supercritical CO_2 is given. Finally, the method to determine the value of the fusion enthalpy (if it is used a GC or from literature) is indicated.

In that table, it is possible to observe that the sublimation enthalpies of 225 compounds were directly taken from experimental works or from different databases. The remaining sublimation enthalpies (28 compounds) were calculated using fusion and vaporization enthalpies.

When more than two values for the same compound are presented in the correspondent databases, it was chosen the suggested value (if it is indicated[9,10]) or the value when the conditions are near to 298 K. On the other hand, when the solid vaporization enthalpy is calculated from solubility data, the solubility data are always at high pressure (more than 70 bar) and at temperatures higher than 300 K.

Finally, the multiple linear regression with a least squares method was performed with the aim of determining the values of each of the groups.

Results and Discussion

The values for the 41 groups are given in Table 2. Subscripts apr and ar denote aliphatic ring and aromatic ring,

Table 1. Set of Compounds

Compounds	Temp. Range (K)	Fusion Enthalpy (kJ mol^{-1})	Vaporization Enthalpy (kJ mol^{-1})	Sublimation Enthalpy (kJ mol^{-1})	References
[4-(Benzyloxy)phenyl] acetic acid	–	–	–	106.4	26
1-(3-Nitrophenyl)-1*H*-pyrrole-2,5-dione	(350–370)	–	–	115.7	10
1,1,1,2-Tetraphenylethane	298	–	–	132.6	10
1,1,1-Triphenylethane	298	–	–	108.6	10
1,1′-Diphenyl-1,1′-bicyclopentyl	–	–	–	141.4	10
1,2,3,4,4a,7,8,9,10,11,12,12a-Dodecahydrochrysene	(293–313)	–	–	115.4	10
1,2,3,6,7,8-Hexahydropyrene	398	–	–	92.3	10
1,2:4,5-Dibenzopyrene	298	–	–	155.2	9
1,2:5,6-Dibenzanthracene	298	–	–	149.0	9
1,2-Benzodiphenylene sulfide	349	–	–	111.9	10
1,2-Dimethylbenzene	248	–	–	60.1	10
1,2-Dimethylnaphthalene	–	–	–	84.0	7
1,3,5-Triazine	298	–	–	54.2	10
1,3,5-Triethiane	298	–	–	93.2	10
1,3,5-Triphenylbenzene	298	–	–	149.8	9
1,3,5-Tri-*tert*-butylbenzene	298	–	–	81.2	10
1,3-Diamino-2,4,6-trinitrobenzene	298	–	–	143.5	10
1,3-Dimethyl-5-ethyluracil	(312–321)	–	–	98.7	10
1,3-Dithiolan-2-one	–	–	–	80.3	10
1,4-Benzenedicarboxamide	(373–498)	–	–	57.3	10
1,4-Bromoiodobenzene	(279–355)	–	–	78.5	10
1,4-Chloroiodobenzene	(259–320)	–	–	71.9	10
1,4-Diaminobenzene	298	–	–	92.2	10
1,4-Di-*tert*-butylbenzene	298	–	–	82.8	10
1,5-Diphenyltetrazole	343	–	–	119.7	10
1,*N*-Dimethylcytosine	(401–426)	–	–	132.8	10
1-Amino-4-hydroxy-2-phenoxy-9,10-anthraquinone	(359–366)	–	–	152.2	10
1-Amino-cyclopentanecarboxylic acid	298	–	–	77.6	10
1-Hydroxypyrene	382	–	–	129.0	10
1-Naphthalenamine	–	–	–	90.0	10
1-Naphthol	–	–	–	91.2	7
1-Naphtholic acid	–	–	–	110.4	7
1-Nitroanthraquinone	396	–	–	115.5	10
1-Phenyldodecane	298	–	–	135.1	10
2,2,4,4-Tetramethyl-1,3-cyclobutanedione	–	–	–	70.3	10
2,2′-Bipyridine	298	–	–	81.8	10
2,2′-Biquinoline	298	–	–	134.7	10
2,3-Benzofluorene	298	–	–	122.0	9
2,3-Benzothiophene	(273–403)	–	–	65.7	10
2,3-Dichloropyridine	298	–	–	73.5	10
2,3-Dimethyl-2,3-diphenylbutane	320	–	–	96.7	10
2,3-Diphenylbutane	326	–	–	96.7	10
2,4,5,7-Tetramethylphenanthrene	–	–	–	114.2	10
2,4,6-Triisopropylbenzophenone	298	–	–	116.0	10
2,4,6-Tri-*tert*-butylaniline	298	–	–	92.5	10
2,4,6-Tri-*tert*-butylnitrosobenzene	298	–	–	96.4	10
2,5-Dihydroxybenzoic acid	–	–	–	109.0	10
2,5-Dinitrophenol	306	–	–	93.4	10
2,6-Dibromopyridine	298	–	–	85.6	10
2,6-Di-*tert*-butylphenol	298	–	–	92.9	10
2,6-Methoxybenzoic acid	298	–	–	129.8	10
2-Acetylnaphthalene	305	–	–	84.0	7
2-Amino-3-methylbenzoic acid	298	–	–	107.3	10
2-Aminoanthraquinone	–	–	–	136.8	10
2-Aminophenol	298	–	–	98.8	10
2-Aminotropone	(273–333)	–	–	71.1	10
2-Bromonaphthalene	298	–	–	81.2	10
2-Chlorobenzoic acid	298	–	–	100.9	10
2-Ethylimidazole	298	–	–	89.6	10
2-Fluorobenzoic acid	298	–	–	94.4	10
2-Hydroxybenzoic acid	–	–	–	95.5	2
2-Imidazolidinone	298	–	–	103.2	10
2-Iodobenzoic acid	298	–	–	92.6	10
2-Methylphenol	288	–	–	76.0	10
2-Methylthio-4-ethylamino-6-isopropylamino-1,3,5-triazine	338	–	–	100.9	10
2-Nitroaniline	(310–319)	–	–	90.0	10
2-Phenylquinoline	298	–	–	105.4	10

(*Continued*)

Table 1. (Continued)

Compounds	Temp. Range (K)	Fusion Enthalpy (kJ mol^{-1})	Vaporization Enthalpy (kJ mol^{-1})	Sublimation Enthalpy (kJ mol^{-1})	References
2-Pyridinecarboxamide	298	–	–	93.0	10
2-Pyridinecarboxylic acid	298	–	–	91.0	10
2-Thiouracil	–	–	–	129.3	10
3,4:9,10-Dibenzopyrene-5,8-quinone	–	–	–	112.5	10
3,5-Dichlorophenol	298	–	–	82.8	10
3,5-Dimethylpyrazole	298	–	–	83.4	10
3,5-Di-*tert*-butylbenzoic acid	348	–	–	108.4	10
3-Bromobenzoic acid	298	–	–	99.2	10
3-Cyanopyridine	–	–	–	72.1	10
3-Methylcholanthrene	413	–	–	127.2	10
3-Nitrobenzoic acid	298	–	–	110.0	10
4-Aminopyridine	–	–	–	87.1	10
4-Benzylphenol	(313–335)	–	–	97.4	10
4-Bromophenol	(260–302)	–	–	87.3	10
4-Chlorobenzoic acid	298	–	–	107.9	10
4-Diacetylbenzene diethyl ketal	316.5	–	–	112.5	10
4-Dimethylaminoantipyrine	–	GC[14,15]	SE[27]	80.2	–
4-Ethylphenol	(278–317)	–	–	84.0	10
4-Isopropylaminodiphenylamine	335	–	–	120.7	10
4-Methylthiopyridine	365	–	–	75.3	10
4-Phenylpyridine	298	–	–	81.4	10
4-*tert*-Butyl phenol	298	–	–	85.9	10
5,12-Dihydrotetracene	298	–	–	118.9	9
5,12-Tetracenequinone	–	–	–	108.8	10
5,6-Dimethylchrysene	394	–	–	135.0	10
5,7-Dichloro-8-hydroxyquinoline	298	–	–	109.3	10
5-Aminotetrazole	(383–443)	–	–	112.6	10
5-Bromouracil	–	–	–	128.4	10
5-Iodo-7-chloro-8-hydroxyquinoline	(383–414)	–	–	131.0	10
6,13-Pentacenequinone	298	–	–	116.3	10
6-Azauracil	–	–	–	141.0	10
8-Azaadenine	(418–463)	–	–	128.4	10
9,10-Anthraquinone	298	–	–	107.9	10
9,10-Diphenylanthracene	298	–	–	170.0	9
9,9-Bifluorenyl	298	–	–	134.0	9
9,9′-Biphenanthryl	–	–	–	151.5	10
9-Amidoanthracene	461	–	–	134.8	10
9-Aminoacridone	–	–	–	115.0	10
9-Ethylhypoxanthine	–	–	–	108.8	10
9-Methyl carbazole	298	–	–	95.5	10
9-Methyl fluorene	298	–	–	82.8	10
9-Methylanthracene	–	–	–	98.9	10
9-Phenylanthracene	298	–	–	120.5	9
Acenaphthacene	298	–	–	84.8	9
Acenaphthylene	298	–	–	72.5	9
Acetaminophen	–	–	–	117.9	8
Acetanilide	(317–336)	–	–	99.8	10
Acridine	298	–	–	92.0	10
Acridone	–	–	–	136.2	10
Alfa-terpineol	(283–328)	–	–	80.3	10
Alfatocopherol	–	GC[14,15]	SE[28]	102.2	–
Aminobenzoic acid	298	–	–	111.6	10
Anastrozole	–	GC[14,15]	SE[29]	129.4	–
Anthanthrone	465	–	–	152.2	10
Anthracene	298	–	–	101.9	9
Anthranthrene	479	–	–	135.0	10
Anthrone	298	–	–	106.1	10
Aspirin	–	–	–	109.7	30
Astaxanthina	–	GC[14,15]	SE[31]	138.2	–
Atorvastatin	–	GC[14,15]	SE[32]	167.4	–
Barbituric acid	(294–438)	–	–	111.3	10
Benzanilide	360	–	–	99.2	10
Benzanthrone	298	–	–	126.6	10
Benzene	298	–	–	44.7	9
Benzenemethanol	298	–	–	105.7	10
Benzil	329	–	–	98.4	10
Benzimidazole	(340–359)	–	–	102.2	10
Benzofurazan	298	–	–	64.4	10
Benzoic acid	298	–	–	88.3	10
Benzo[*e*]pyrene	298	–	–	122.5	9

(*Continued*)

Table 1. (Continued)

Compounds	Temp. Range (K)	Fusion Enthalpy (kJ mol^{-1})	Vaporization Enthalpy (kJ mol^{-1})	Sublimation Enthalpy (kJ mol^{-1})	References
Benzo[*ghi*]perylene	298	–	–	132.9	9
Benzophenone	298	–	–	93.1	10
Benzoxazole	–	–	–	69.5	10
Beta-carotene	–	–[33]	SE[28]	128.7	–
Binaphthalene	383	–	–	138.3	10
Biphenyl	298	–	–	82.1	9
Biphenylene	298	–	–	83.8	9
Butylparaben	–	–	–	108.4	3
Caffeine	(413–463)	–	–	105.1	10
ε-Caprolactam	298	–	–	87.3	10
Cholesterol	–	–[34]	SE[34]	114.6	–
Chromone	298	–	–	81.3	10
Coronene	298	–	–	143.0	9
Coumarin	(293–353)	–	–	83.1	10
Cyanuric acid	298	–	–	131.0	10
Cyclotetradecane	298	–	–	134.8	10
Cytosine	298	–	–	147.2	10
Desoxybenzoin	–	–	–	99.3	10
Dibenzofuran	298	–	–	84.4	10
Dibenzosuberone	298	–	–	109.3	10
Dibenzoylmethane	298	–	–	115.7	10
Dibenzyl	298	–	–	84.0	26
Dibenzyl sulfide	–	–	–	93.3	10
Dibenzyl sulfone	–	–	–	125.5	10
Dibenzylideneazine	298	–	–	93.3	10
Diflunisal	–	–	–	120.1	21
Dimethylparaben	–	–	–	100.9	3
Diphenyl oxalate	–	–	–	102.5	10
Diphenylfulvene	–	–	–	104.6	10
Diphenylmethane	298	–	–	87.2	26
Eflucimibe	–	GC[14,15]	SE[35]	157.9	–
Examestane	–	GC[14,15]	SE[29]	122.8	–
Fluorene	298	–	–	86.5	9
Flurboprifen	–	–	–	104.9	21
Fluvastatin	–	GC[14,15]	SE[32]	136.1	–
Formanilide	(298–318)	–	–	77.8	10
Fuflenamic acid	–	–	–	119.4	4
Glutarimide	298	–	–	94.1	10
Hexacyclopropylethane	–	–	–	109.0	10
Hexaethylbenzene	340	–	–	95.0	10
Hexamethoxycarbonylbenzene	298	–	–	154.3	10
Ibuprofen	–	–	–	115.8	36
Imidazole	(292–309)	–	–	83.4	10
Indane	298	–	–	55.4	9
Indene	298	–	–	61.8	9
Iodobenzene	(243–255)	–	–	43.1	10
Irgacure	–	GC[14,15]	SE[37]	110.2	–
Ketoprofen	–	–	–	112.0	21
Letrozole	–	GC[14,15]	SE[29]	129.9	–
Lidocaine	–	GC[14,15]	SE[38]	104.8	–
Lovastatin	–	GC[14,15]	SE[32]	90.6	–
Medroxyprogesterone acetate	–	–[40]	SE[39]	92.1	–
Methimazole	–	–[40]	SE[41]	87.2	–
Methyl benzyl sulfone	–	–	–	99.2	10
Methyl-2-aminobenzoate	292.5	–	–	78.4	10
Methylbiphenyl	298	–	–	80.2	10
Methyparaben	–	–	–	98.8	3
N-Phenyl benzephenone imine	298	–	–	115.5	10
N,*N*′-Bis-(2-methoxyphenyl)terphthalamide	–	–	–	197.5	10
N,*N*-Diphenylacetamide	358	–	–	122.7	10
Naphthacene	298	–	–	135.9	9
Naphthalene	298	–	–	72.6	9
Naproxen	–	–	–	128.3	7
Niflumic acid	–	–	–	130.2	4
Nimesulide	–	–[40]	SE[42]	82.2	–
Nitrendipine	–	–[40]	SE[43]	94.8	–
N-Methylsuccinimide	298	–	–	80.1	10
N-Phenylbenzylamine	303	–	–	103.6	10
Penicillin G	–	–[40]	SE[44]	122.2	–
Pentafluorobenzoic acid	(335–359)	–	–	91.6	10

(*Continued*)

Table 1. (Continued)

Compounds	Temp. Range (K)	Fusion Enthalpy (kJ mol^{-1})	Vaporization Enthalpy (kJ mol^{-1})	Sublimation Enthalpy (kJ mol^{-1})	References
Pentafluorophenol	(273–299)	–	–	67.4	10
Phenanthridine	298	–	–	98.6	10
Phenazine	298	–	–	91.8	10
Phenazopyridine	–	–[40]	SE[41]	93.0	–
Phenyl benzoate	298	–	–	99.0	10
Phenyl salicylate	294	–	–	109.1	10
Phenyl vinyl sulfone	–	–	–	82.0	10
Phthalimide	(378–418)	–	–	85.8	10
Phthalazine	298	–	–	81.1	10
Phthalic acid	298	–	–	129.8	10
Picene	298	–	–	149.4	9
Piperazine	(413–450)	–	–	103.8	10
Progesterone	–	–[34]	SE[34]	93.9	–
Propylparaben	–	–	–	123.7	3
Protocate acid	–	–[40]	SE[45]	120.1	–
Protocatechu	–	–[40]	SE[45]	127.6	–
p-Phenacetin	(312–387)	–	–	121.8	10
p-Terphenyl	(353–383)	–	–	125.6	10
p-Toluidine	298	–	–	78.8	10
Pyracene	298	–	–	89.6	9
Pyracyclene	298	–	–	83.2	9
Pyrene	298	–	–	100.3	9
Quinone	–	–	–	68.0	10
Resorcinol dibenzoate	338	–	–	165.8	10
Rosuvastatin	–	GC[14,15]	SE[32]	122.2	–
Salicylamide	–	–[46]	SE[47]	89.76	–
Simvastatin	–	–[40]	SE[32]	109.4	–
Succinic acid	(292–320)	–	–	73.6	10
Succinimide	(317–340)	–	–	83.1	10
Sulfanilic acid	–	–	–	66.9	10
Sulfonamide I	–	–	–	114.0	48
Sulfonamide II	–	–	–	124.9	48
Testosterone	–	–[34]	SE[34]	110.5	–
Tetrabenzonaphthalene	298	–	–	151.0	9
Tetrahydro-4*H*-thiopyran-4-one	298	–	–	72.6	10
Tetramethyl pyrazine	298	–	–	94.6	10
Tetrathiofulvalene	351	–	–	92.0	10
Tetrazole	(333–363)	–	–	97.5	10
Theophylline	–	–[40]	SE[49]	126.0	–
Thiophene	(192–213)	–	–	49.0	10
Thymol	(283–323)	–	–	89.1	10
Toluene	298	–	–	48.0	9
Tricyclohexylmethane	298	–	–	117.4	10
Triphenylmethane	298	–	–	108.4	9
Triphenylmethanol	298	–	–	121.8	10
Uracil	(394–494)	–	–	127.0	10

respectively. To obtain the sublimation enthalpy ΔH_{sub} of the solid, the compound should be divided in groups, applying subsequently the Eq. 2. In Eq. 2, n_i is the number of times a group i appears in the solid, and X_i is the contribution of group i to the values of the sublimation enthalpy. It is important to point out that when a carbon atom belongs at the same time to an aromatic and cyclic ring, the value of that carbon atom should be taken as the value of the carbon atom of the aromatic ring. An example can be found in the Appendix.

$$\Delta H^{sub}(\text{kJ mol}^{-1}) = \sum n_i \cdot X_i \tag{2}$$

The average absolute relative deviation (AARD) in percent and the average absolute error (AAE) in kJ mol^{-1} were calculated with Eqs. 3 and 4, respectively. Subscript exp denotes experimental value or the calculated value from experimental solubility data solid-SCFs. On the other hand, subscript pre denotes the predicted values with our method. Finally, N is the number of compounds

$$\text{AARD} = \left(100/N\right) \cdot \sum_{i=1}^{N} \frac{\left|\Delta H_{pre} - \Delta H_{exp}\right|}{\Delta H_{exp}} \tag{3}$$

$$\text{AAE} = \frac{\sum \left|\Delta H_{exp} - \Delta H_{pre}\right|}{N} \tag{4}$$

Our method predicts experimental values with an AARD of 8.98% and an AAE of 9.22 kJ mol^{-1}. These values are low, taking into account that the usual value of the sublimation enthalpy of this type of compounds is around 80–110 kJ mol^{-1}.

Figure 1 depicts a plot that shows the predicted sublimation enthalpies vs. the experimental sublimation enthalpies of the 253 solids. On the other hand, Figure 2 depicts the Bland–Altman plot. In this case, the dashed lines depict the

Table 2. Group Contribution Values (kJ mol^{-1})

Molecular Fragment	X (kJ mol^{-1})	Molecular Fragment	X (kJ mol^{-1})
Nonring C Increments			
—CH_3	11.57	=CH_2	40.54
—CH_2—	3.38	=CH—	3.43
>CH—	−11.26	=C<	−9.40
>C<	−16.46		
Aliphatic Ring Increments			
—CH_2— (apr)	10.38	—O— (apr)*	−9.28
>CH— (apr)	−4.75	—N< (apr)	15.37
>C< (apr)	−7.25	—NH— (apr)	34.34
=CH— (apr)	11.78	—N= (apr)	19.08
=C< (apr)	−13.04	—S— (apr)	17.19
Halogen Increments			
—F	3.92	—Cl	18.43
—Br	21.85	—I	17.49
Oxygen and Carboxyl Increments			
—OH (phenol)	26.17	>C=O (no ring)	6.47
—OH	16.79	>C=O (ring)	13.01
—CHO	30.36	—O— (no ring)	5.89
—COOH	40.37	—C(=O)O—	12.09
Aromatic Ring Increments			
CHar	8.10	Nar	11.15
Car	2.60		
Nitrogen and Sulfur Increments			
—CN*	1.16	=N—*	−10.12
—NO_2	23.17	C=S	29.66
—NH_2	25.21	SO_2	−4.39
—NH—	17.08	—S—*	−5.82
>N—*	−17.59		

limits of agreement (average difference (1.30 kJ mol^{-1}) ± 1.96·standard deviation) and the solid line depicts the value of the average of the differences between the experimental and predicted value (our result is 1.30 kJ mol^{-1}). It can be observed in these figures the accuracy of our estimations.

These errors can be considered low, given that bigger differences can sometimes be found for the same solid depending on the experimental work,[10] and the values of sublimation enthalpies usually range from 90 to 120 kJ mol^{-1}. For instance (see NIST webbook http://webbook.nist.gov/chemistry/), the value of the sublimation enthalpy for the anthracene ranges from 84 to 104 kJ mol^{-1} (a difference around 20%), and something similar occurs for the naphthalene, finding a difference between the different experimental works around 15%.

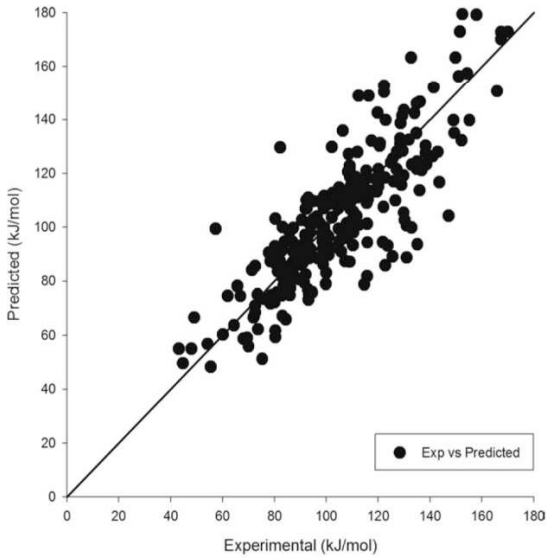

Figure 1. Predicted vs. experimental values of the sublimation enthalpy for the compounds.

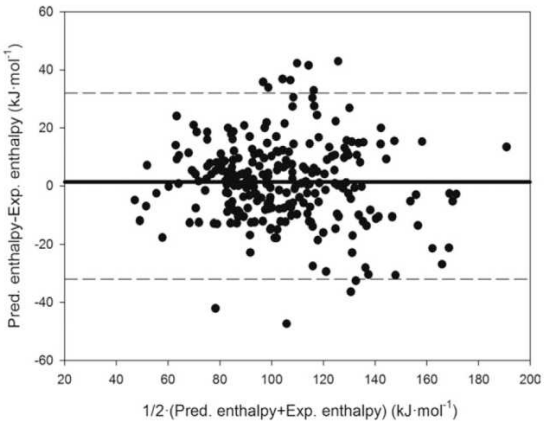

Figure 2. Bland–Altman plot.

A statistical analysis was performed. The multiple regression gave an R^2 value of 0.988, a standard deviation of 14.77, and a coefficient variation of 0.155. Table 3 shows the ANOVA table, whereas in Table 2 the * shows the functional groups with statistical insignificance (confidence level $\alpha < 0.05$).

The prediction ability of the method was validated by randomizing the database with 253 compounds. Forty compounds were chosen at random in order to use them as a test set, using the remaining data (213 solids) as a data set to generate the values of the functional groups. This validation was performed two times. The AAE and the AARD were calculated for each data and test set.

Table 4 shows these results. Although the AARD and the AAE of the test sets are higher than the deviations of their correspondent sets of compounds, these differences are not significant. Indeed, these values are near to the AARD and AAE of the set of 253 compounds, and in addition both test sets give similar deviations.

These facts indicate that this method is suitable for any solid constituted by aromatic and/or polycyclic aliphatic rings. However, this GC method presents two limitations: (1) it is impossible to distinguish between isomers and (2) the number of groups.

Only 41 groups were defined, and although there are not drawbacks with solids with a molecular structure similar to pharmaceuticals because these groups are the most common, it is possible to find solids constituted with groups that were not considered in the calculations. This fact might hinder to extend the values of the groups to other type of solids like inorganic compounds.

Table 3. ANOVA Table

Model	Squares Sum (SS)	Mean Squares (MS)	Freedom Deg. (fd)
Regression	2863870.80	69850.80	41
Residuals	56129.20	264.76	212
Total	$2.92 \cdot 10^6$		253

Table 4. AARD and AAE for the Respective Validation Tests

Set Type	AARD (%)	AAE (kJ mol^{-1})
Set of compounds 1	8.75	9.18
Set of compounds 2	8.32	9.15
Test set 1	9.63	10.93
Test set 2	9.37	10.70

About the drawbacks related to isomers, although the sublimation enthalpy of a solid varies depending on the geometric properties as occurs with other properties (e.g., fusion enthalpy), it should be specified that this variation is not usually high taking into account the big values of the sublimation enthalpies. For instance, for the three isomers of the methylbenzoic acid (MBA), the difference between their sublimation enthalpies is only 2.90 kJ mol^{-1} (95.90 kJ mol^{-1} for 2-MBA, 97.00 kJ mol^{-1} for 3-MBA, and 98.80 kJ mol^{-1} for 4-MBA). Therefore, the relative error of the estimation would not suffer a great increase. The values for these compounds can be found in the NIST webbook.

Conclusions

This work presents a consistent GC method to estimate the sublimation enthalpy of only any solid constituted by aromatic and/or polycyclic aliphatic rings (for instance pharmaceuticals). An AARD of 8.98% and an AAE of 9.22 kJ mol^{-1} were obtained predicting values of sublimation enthalpies for 253 solids. The main limitation is that only 41 groups were defined, hindering the prediction for other types of solids.

Acknowledgments

This research was supported by funds from the Ministerio de Ciencia e Innovación (Spain), project CTQ2009-08222 (PPQ Subprogram). The authors thank Prof. D. J. Rodríguez Díaz (Statistics Department of University of Salamanca) for his helpful advice.

Literature Cited

1. Tomé LIN, Rosado MTS, Nunes SCC, Maria TMR, Canotilho J, Eusébio MES. Enthalpy of sublimation/vaporization of *trans*-cyclohexyl-1,4-diamine and *cis*-cyclohexyl-1,2-diamine. *J Chem Thermodyn*. 2007;39:1354–1356.
2. Perlovich GL, Volkova TV, Bauer-Brandl A. Towards and understanding of the molecular mechanism of solvation of drug molecules: a thermodynamic approach by crystal lattice energy, sublimation, and solubility exemplified by hydroxybenzoic acids. *J Pharm Sci*. 2006;95:1448–1458.
3. Perlovich GL, Rodionov SV, Bauer-Brandl A. Thermodynamics of solubility, sublimation and solvation processes of parabens. *Eur J Pharm Sci*. 2005;24:25–33.
4. Perlovich GL, Surov AO, Bauer-Brandl A. Thermodynamic properties of flufenamic and niflumic acids—specific and non-specific interactions in solutions and in crystal lattices, mechanism of solvation, partitioning and distribution. *J Pharm Biomed Anal*. 2007;45:679–687.
5. Garnier S, Neau E, Alessi P, Cortesi A, Kikic I. Modelling solubility of solids in supercritical fluids using fusion properties. *Fluid Phase Equilib*. 1999;158–160:491–500.
6. Neau E, Garnier S, Avaullée L. A consistent estimation of sublimation pressures using a cubic equation of state and fusion properties. *Fluid Phase Equilib*. 1999;164:173–186.
7. Perlovich GL, Kurkov SV, Kinchin AN, Bauer-Brandl A. Thermodynamics of solution III: comparison of the solvation of (+)-naproxen with other NSAIDs. *Eur J Pharm Biopharm*. 2004;57:411–420.
8. Perlovich GL, Volkova TV, Bauer-Brandl A. Towards and understanding of the molecular mechanism of solvation of drug molecules: a thermodynamic approach by crystal lattice energy, sublimation, and solubility exemplified by paracetamol, acetanilide, and phenacetin. *J Pharm Sci*. 2006;95:2158–2169.
9. Roux MV, Temprado M, Chickos JS, Nagano Y. Critically evaluated thermochemical properties of polycyclic aromatic hydrocarbons. *J Phys Chem Ref Data*. 2008;4:1855–1996.
10. Chickos JS, Acree W Jr. Enthalpies of sublimation of organic and organometallic compounds. 1910–2001. *J Phys Chem Ref Data*. 2002;2:537–698.
11. Chickos JS, Acree W Jr. Phase transition enthalpy measurements of organic and organometallic compounds. Sublimation, vaporization and fusion enthalpies from 1880 to 2010. *J Phys Chem Ref Data*. 2010;4:43101–43942.
12. Poling BE, Prausnitz JM, O'Connell. *The Properties of Gases and Liquids*, 5th ed. New York: McGraw-Hill, 2004.
13. Chickos JS, Annunziata R, Ladon LH, Hyman AS, Liebman JF. Estimating heats of sublimation of hydrocarbons. A semiempirical approach. *J Org Chem*. 1986;51:4311–4314.
14. Jain A, Yang G, Yalkowsky SH. Estimation of melting points of organic compounds. *Ind Eng Chem Res*. 2004;43:7618–7621.
15. Jain A, Yalkowsky SH. Estimation of melting points of organic compounds-II. *J Pharm Sci*. 2006;95:2562–2618.
16. Chickos JS, Acree WE Jr. Enthalpies of vaporization of organic and organometallic compounds, 1880–2002. *J Phys Chem Ref Data*. 2003;32:1–361.
17. Chickos JS, Hesse DG. Estimating vaporization enthalpies of organic compounds with single and multiple substitution. *J Org Chem*. 1989;22:5250–5256.
18. Tabernero A, Martín del Valle EM, Galán MA. On the use of semiempirical models of solid-supercritical fluid systems to determine solid sublimation properties. *J Chem Thermodyn*. 2010;43:711–718.
19. Bartle KD, Clifford AA, Jafar SA, Shilstone GF. Solubilities of solids and liquids of low volatile in supercritical carbon dioxide. *J Phys Chem Ref Data*. 1991;20:713–756.
20. Miller DJ, Hawthorne SB, Clifford AA, Zhu S. Solubility of polycyclic aromatic hydrocarbons in supercritical carbon dioxide from 313 K to 523 K and pressures from 100 bar to 450 bar. *J Chem Eng Data*. 1996;41:779–786.
21. Garlapati C, Madras G. Temperature independent mixing rules to correlate the solubilities of antibiotics and anti-inflammatory drug in $scCO_2$. *Thermochim Acta*. 2009;496:54–58.
22. Lucien FP, Foster NR. Solubilities of solid mixtures in spuercritical carbon dioxide: a review. *J Supercrit Fluids*. 2000;17:111–134.
23. Marrero J, Gani R. Group-contribution based estimation of pure component properties. *Fluid Phase Equilib*. 2001;183/184:183–208.
24. Constantinou L, Gani R. New group contribution method for estimating properties of pure compounds. *AIChE J*. 1994;40:1697–1710.
25. Tabernero A, Martín del Valle EM, Galán MA. A comparison between semiempirical equations to predict the solubility of pharmaceutical compounds in supercritical carbon dioxide. *J Supercrit Fluids*. 2010;52:161–174.
26. Kurkov SV, Perlovich GL, Zielenkiewicz W. Thermodynamic investigations of sublimation, solubility and solvation of [4-(benzyloxy)-phenyl] acetic acid. *J Therm Anal Calorim*. 2006;3:549–556.
27. Chen Y-M, Chen Y-P. Measurements for the solid solubility of antipyrine, 4-aminoantipyrine and 4-dimethylaminoantipyrine in supercritical carbon dioxide. *Fluid Phase Equilib*. 2009;282:82–87.
28. Johannsen M, Brunner G. Solubility of the fat-soluble vitamins A, D, E and K in supercritical carbon dioxide. *J Chem Eng Data*. 1997;42:106–111.
29. Hojjati M, Vatanara A, Yamini Y, Moradi M, Rouholamini Najafabadi A. Supercritical CO_2 and highly selective aromatase inhibitors: experimental solubility and empirical data correlation. *J Supercrit Fluids*. 2009;50:203–209.
30. Perlovich GL, Kurkov SV, Kinchin AN, Bauer-Brandl A. Solvation and hydration characteristics of ibuprofen and acetylsalycilic acid. *AAPS PharmSci*. 2006;6:1–9.
31. De la Fuente JC, Oyarzun B, Quezada N, Del Valle JM. Solubility of carotenoid pigments (lycopene and astaxanthin) in supercritical carbon dioxide. *Fluid Phase Equilib*. 2006;247:90–95.
32. Vatanara A, Rouholamini Najafabadi A, Khajeh M, Yamini Y. Solubility of some statin drugs in supercritical carbon dioxide and representing the solubility data with several density-based correlations. *J Supercrit Fluids*. 2007;33:21–25.

33. Miguel F, Martín A, Mattea F, Cocero MJ. Precipitation of lutein and co-precipitation of lutein and poly-lactic acid with the supercritical anti-solvent process. *Chem Eng Process*. 2008;47:1594–1602.
34. Kosal E, Lee CH, Holder GD. Solubility of progesterone, testosterone and cholesterol in supercritical fluids. *J Supercrit Fluids*. 1992;5:169–179.
35. Sauceau M, Letourneau J-J, Freiss B, Richon D, Fages J. Solubility of eflucimibe in supercritical carbon dioxide with or without a co-solvent. *J Supercrit Fluids*. 2004;31:133–140.
36. Perlovich GL, Kurkov SV, Hansen LK, Bauer-Brandl A. Thermodynamics of sublimation, crystal lattice energies, and crystal structures of racemates and enantiomers: (+)- and (+/−)- ibuprofen. *J Pharm Sci*. 2004;93:654–666.
37. Coimbra P, Fernandes D, Ferreira P, Gil María H, De Sousa Herminio C. Solubility of Irgacure®2959 photoinitiator in supercritical carbon dioxide. Experimental determination and correlation. *J Supercrit Fluids*. 2008;45:272–281.
38. Weinstein RD, Muske KR, Moriarty J, Schmidt EK. The solubility of benzocaine, lidocaine and procaine in supercritical carbon dioxide. *J Chem Eng Data*. 2004;49:547–552.
39. Su C-S, Chen Y-P. Correlation for the solubilities of pharmaceutical compounds in supercritical carbon dioxide. *Fluid Phase Equilib*. 2007;257:167–173.
40. Asghari-Khiavi M, Yamini Y, Farajzadeh MA. Solubility of two steroid drugs and their mixtures in supercritical carbon dioxide. *J Supercrit Fluids*. 2004;30:111–117.
41. Yamini Y, Arab J, Asghari-Khiavi M. Solubilities of phenazopyridine, propanolol and methimazole in supercritical carbon dioxide. *J Pharm Biomed Anal*. 2003;32:181–187.
42. Macnaughton SJ, Kikic I, Foster NR, Alessi P, Cortesi A, Colombo I. Solubilities of anti-inflammatory drugs in supercritical carbon dioxide. *J Chem Eng Data*. 1996;41:1083–1086.
43. Knez Z, Skerget M, Sencar-Bozic P, Rizner A. Solubility of nifedipine and nitrendipine in supercritical carbon dioxide. *J Chem Eng Data*. 1995;40:216–220.
44. Gordillo MD, Blanco MA, Molero A, Martinez de la Ossa E. Solubility of the antibiotic Penicillin G in supercritical carbon dioxide. *J Supercrit Fluids*. 1999;15:183–190.
45. Murga R, Sanz MT, Beltrán S, Cabezas JL. Solubility of some phenolic compounds contained in grape seeds, in supercritical carbon dioxide. *J Supercrit Fluids*. 2002;23:113–121.
46. Nordström FL, Rasmusen AC. Prediction of solubility curves and melting properties of organic and pharmaceutical compounds. *Eur J Pharm Sci*. 2009;36:330–344.
47. Su C-S, Chen Y-P. Measurement and correlation for the solid solubility of non-steroidal anti-inflammatory drugs (NSAIDs) in supercritical carbon dioxide. *J Supercrit Fluids*. 2008;43:438–446.
48. Perlovich GL, Strakhova NN, Kazachenko VP, Volkova TV, Tkachev VV, Schaper K-J, Raevsky OA. Studying thermodynamic aspects of sublimation, solubility and solvation processes and crystal structure analysis of some sulphonamides. *Int J Pharm*. 2007;334:115–124.
49. Johannsen M, Brunner G. Solubilities of the xanthines caffeine, theophylline and theobromine in supercritical carbon dioxide. *Fluid Phase Equilib*. 1994;95:215–226.
50. McHugh M, Paulaitis ME. Solid solubilities of naphthalene and biphenyl in supercritical carbon dioxide. *J Chem Eng Data*. 1980;25:326–328.
51. Aspen HYSYS® [computer program]. Version 7.0. Burlington, MA: Aspen Technology, Inc. Accessed March 2011.

Appendix: Examples

Using Bartle's model to determine vaporization enthalpies of several solids

Experimental solubility data (around 45 points at different conditions of pressure and temperature) of naphthalene in supercritical CO_2 between 308 and 338 K were determined by McHugh and Paulaitis[50] and were modeled with Bartle's model. The parameters A, B, and C from Eq. 1 are given in Table A1. If the parameter $-B$ is multiplied by the gas constant (R), the estimated enthalpy is 58.65 kJ mol^{-1}. This result is obviously nearer to the vaporization enthalpy (55.4 kJ mol^{-1})[9] than the sublimation enthalpy (72.60 kJ mol^{-1}).[9] The same can be observed for other solids such as acetaminophen or 2-hydroxybenzoic acid (2-HBA). Table A1 shows the results and the comparison with experimental data. In these last two cases, the experimental vaporization enthalpies were obtained as the difference between the experimental values of the sublimation enthalpies (acetaminophen[8] and 2-HBA[2]) and the respective fusion enthalpies.[51] It should also be indicated that the relative deviation in the sublimation enthalpies will be lower, taking into account the bigger value of this enthalpy compared to the vaporization enthalpies.

Sublimation enthalpy of 1,2,3,4,4a,7,8,9,10,11,12,12a-dodecahydrochrysene ($C_{18}H_{24}$)

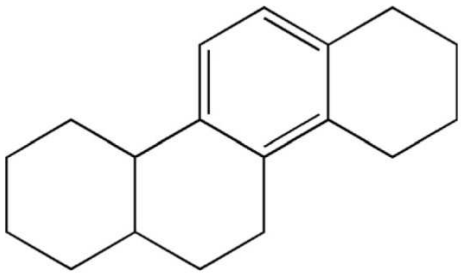

This solid is constituted with a benzene ring and several aliphatic rings. In this case, four carbon atoms belong to an aromatic and to different cyclic rings. When a similar case occurs, the values of those four carbon atoms should be taken as the values of the carbon atoms of the benzene ring. Then:

$$\Delta H^{\mathrm{sub}}(\mathrm{predict.}) = \sum n_i \cdot X_i = 2 \cdot (X_{\mathrm{CHar}}) + 4 \cdot (X_{\mathrm{Car}}) + 10 \cdot (X_{-\mathrm{CH2}-(\mathrm{apr})}) + 2 \cdot (X_{>\mathrm{CH}-(\mathrm{apr})}) = 2 \cdot (8.10) + 4 \cdot (2.60) + 10 \cdot (10.38) - 2 \cdot (4.75) = 120.90\ \mathrm{kJmol}^{-1}.$$

The experimental value of the sublimation enthalpy of this compound[10] is 115.40 kJ mol^{-1}. The difference between the predicted and the experimental value is 5.50 kJ mol^{-1}.

Table A1. Estimated Vaporization Enthalpies Using Bartle's Model and the Comparison with the Experimental Values

Compound	Parameter A	Parameter B	Parameter C	ΔH_{vap} Estim. (kJ mol^{-1})	ΔH_{vap} Exp. (kJ mol^{-1})
Naphthalene	23.26	−7057.48	0.09	58.65	55.40[9]
Acetaminophen	19.11	−8917.97	0.008	74.11	89.40
2-HBA	19.49	−7244.96	0.007	60.20	66.70

Sublimation enthalpy of 3-bromobenzoic acid ($C_7H_5BrO_2$)

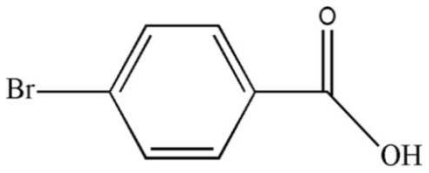

$$\Delta H^{\mathrm{sub}}(\mathrm{predict.}) = \sum n_i \cdot X_i = 4 \cdot (X_{\mathrm{CHar}}) + 2 \cdot (X_{\mathrm{Car}}) + 1 \cdot (X_{-\mathrm{Br}}) + 1 \cdot (X_{-\mathrm{COOH}}) = 4 \cdot (8.10) + 2 \cdot (2.60) + 1 \cdot (21.85) + 1 \cdot (40.37) = 99.82\,\mathrm{kJ\,mol^{-1}}.$$

The experimental value of the sublimation enthalpy of this compound[10] is 99.20 kJ mol^{-1}. The difference between the predicted and the experimental value is less than 1.00 kJ mol^{-1}.

Manuscript received Jun. 21, 2011, revision received Aug. 30, 2011, and final revision received Sept. 14, 2011.

7.4. Conclusiones

En los artículos anteriores se ha procedido al desarrollo de dos procedimientos para determinar la presión y entalpía de sublimación de compuestos farmacéuticos.

Mediante el uso de datos experimentales de solubilidad de varios sólidos en CO_2sc y la ecuación de Clausius-Clapeyron se ha definido un método para el cálculo de la presión de sublimación de dichos sólidos con errores aproximados del 10%. Los valores obtenidos de presión de sublimación fueron empleados posteriormente de manera exitosa para el cálculo de diferentes equilibrios multifásicos y de diferentes propiedades (energía libre de Gibbs y entalpía) de sublimación y de solvatación de acetaminofén en varios disolventes. Ello pone de manifiesto la utilidad de este procedimiento para diferentes cálculos termodinámicos relacionados con la industria farmacéutica.

Asimismo, se desarrolló un modelo robusto de contribución de grupos para la estimación de la entalpía de sublimación de sólidos compuestos por anillos aromáticos y/o policíclicos sustituidos. Este modelo predice la entalpía de sublimación de este tipo de sólidos con un error inferior al 10%. Su única desventaja es que no puede ser empleado con otro tipo de sólidos, como pueden ser los inorgánicos.

• Referencias también citadas

[1] L. Constantinou; R. Gani, New group contribution method for estimating properties of pure compounds, AIChE J. 10 (1994) 1697-1710.

[2] J. Marrero; R. Gani, Group-contribution based estimation of pure component properties, Fluid Phase Equilib. 183-184 (2001) 183-208.

[3] S. Garnier; E. Neau; P. Alessi; A. Cortesi; I. Kikic, Modelling solubility of solids in supercritical fluids using fusion properties, Fluid Phase Equilib. 158-160 (1999) 491-500.

[4] P. Coutsikos; E. Voutsas; K. Magoulas; D. P. Tassios, Prediction of vapor pressures of solid organic compounds with a group-contribution method, Fluid Phase Equilib. 207 (2003) 263-281.

[5] P. Coimbra; D. Fernandes; P. Ferreira; M. H. Gil; H. C. de Sousa, Solubility of irgacure® 2959 photoinitiator in supercritical carbon dioxide: Experimental determination and correlation, J. Supercrit. Fluids 45 (2008) 272-281.

[6] M. D. Gordillo; M. A. Blanco; A. Molero; E. Martínez de la Ossa, Solubility of the antibiotic penicillin G in supercritical carbon dioxide, J. Supercrit. Fluids 15 (1999) 183-190.

[7] K. D. Bartle; A. A. Clifford; S. A. Jafar; G. F. Shilstone, Solubilities of solids and liquids of low volatility in supercritical carbon dioxide, J. Phys. Chem. Ref. Data 20 (1991) 201-219.

[8] A. Tabernero; Eva M. Martín del Valle; Miguel A. Galán, Estimation of sublimation enthalpies of solids constituted by aromatic and/or polycyclic

aliphatic rings by using a group contribution method, AIChE J. 52 (2012) 2875-2884.

[9] A. Jain; G. Yang; S. H. Yalkowsy, Estimation of melting points of organic compounds, Ind. Eng. Chem. Res. 43 (2004) 7618-7621.

[10] G. L. Perlovich; T. V. Volkova; A. Bauer-Brandl, Towards an understanding of the molecular mechanism of solvation of drug molecules: A thermodynamic approach by crystal lattice energy, sublimation, and solubility exemplified by paracetamol, acetanilide, and phenacetin, J. Pharm. Sci. 95 (2006) 2158-2169.

[11] G. L. Perlovich; S. V. Rodionov; A. Bauer-Brandl, Thermodynamics of solubility, sublimation and solvation processes of parabens, European J. Pharm. Sci. 24 (2005) 25-33.

CAPÍTULO 6.

Evaluación de la solubilidad de fármacos en CO_2sc

8.1. Estudio de solubilidad de sólidos en CO_2sc.

Como se ha comentado repetidamente en capítulos anteriores (1, 5, 6 y 7), la determinación de la solubilidad de sólidos en fluidos supercríticos es fundamental para conocer la viabilidad de su aplicación en técnicas de extracción o de generación de partículas.

Sin embargo, la determinación de forma precisa de la solubilidad de fármacos, compuestos generalmente polares, en CO_2sc puede resultar una tarea compleja, debido a que normalmente son poco solubles (con fracciones molares en torno 10^{-5}-10^{-8}). Por ello, un simple error de pesada o en la pureza del sólido puede dar lugar a un error de varios órdenes de magnitud.

Este hecho puede observarse en la figura 8.1, donde se representan los valores de solubilidad del beta-caroteno en CO_2sc a 313 K recogidos en bibliografía [1]. Como se puede observar en esta figura, existe una gran dispersión entre los valores experimentales obtenidos por diferentes grupos de investigación, todos ellos pueden ser observados en [1].

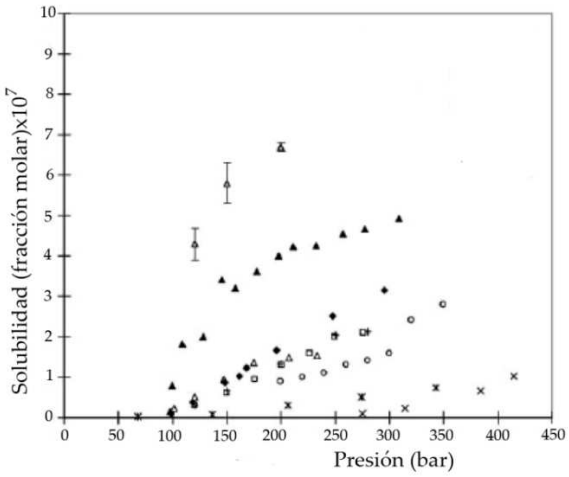

Figura 8.1. Diferentes resultados experimentales de la solubilidad de beta-caroteno en CO_2sc [1].

La solubilidad de sólidos en fluidos supercríticos puede determinarse de forma experimental mediante diferentes técnicas en discontinuo o en continuo. Sin embargo, al igual que podían aparecer errores debido a la pureza del sólido. También, dependiendo del procedimiento experimental seguido se pueden obtener desviaciones superiores a un orden de magnitud [2].

De lo anterior, se puede colegir la dificultad existente en la determinación de forma precisa de la solubilidad de sólidos con carácter polar en CO_2sc.

Este hecho implica la importancia de la existencia de tests de consistencia para conocer la precisión de esos datos experimentales.

A pesar de todo ello, no existe ningún test completamente fiable para evaluar la precisión de los datos experimentales de solubilidad de sólidos en CO_2sc.

8.1.1. Tests de consistencia. Test de Méndez-Santiago y Teja [3].

Los tests de consistencia son herramientas teóricas para determinar la bondad (exactitud) de los datos experimentales. Sin embargo, como se comentó anteriormente, no existe un test de consistencia para analizar la solubilidad de sólidos en CO_2sc.

Hasta ahora, el único procedimiento existente es el desarrollado por Méndez-Santiago y Teja [3]. Estos autores observaron, a partir de la teoría de las disoluciones diluidas, que la relación lineal entre la expresión $T \cdot Ln(E)$ y la densidad del fluido supercrítico, debe ser la misma para los diferentes estudios de la solubilidad del mismo sólido en CO_2sc (figura 8.2). En la expresión anterior, T es la temperatura en K y E es el factor de mejora (*"enhancement factor"*).

Por tanto, esta relación lineal se puede utilizar para discernir la exactitud de los datos experimentales.

Este hecho puede ser observado en la figura 8.2, que representa diferentes estudios de la solubilidad del pireno en CO_2sc [3].

Según la figura, los datos de solubilidad con forma de triángulo tomados de uno de los trabajos que Méndez-Santiago y Teja consideran [3], se alejan de los datos publicados por otros autores (según el test de consistencia de Méndez-Santiago y Teja) por lo que pueden resultar inexactos.

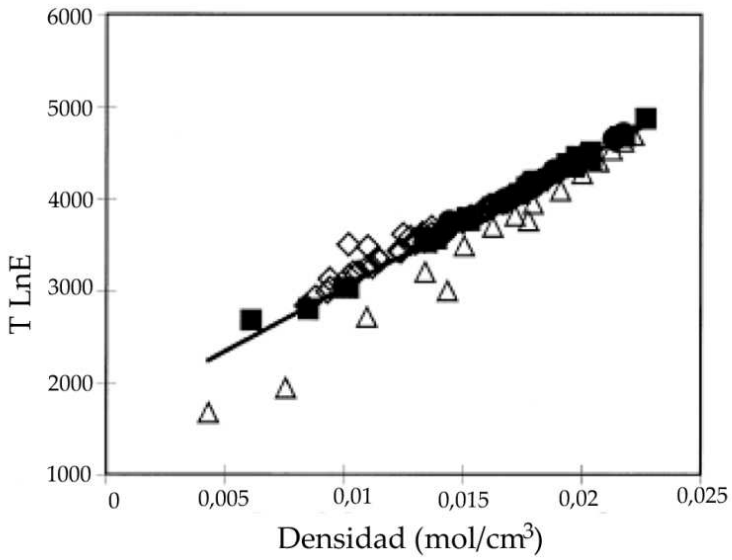

Figura 8.2. Test de consistencia para la solubilidad del pireno en sc-CO_2 [3].

Sin embargo, este test presenta varias limitaciones:

● Su carácter comparativo. Se necesitan al menos dos estudios para poder distinguir si los datos experimentales objeto de estudio caen en el intervalo adecuado de solubilidad, por lo que no puede ser aplicado a datos experimentales de sólidos que hayan sido investigados previamente.

● Requerimiento de la presión de sublimación del sólido para calcular el factor de mejora. Con el fin de resolver este inconveniente, Méndez-Santiago y Teja introdujeron la ecuación de Clausius-Clapeyron, y definieron la expresión

($T \cdot Ln(y \cdot P) - T \cdot C$) que estaba también relacionada linealmente con la densidad del fluido supercrítico. En la expresión anterior, T es la temperatura en K, y es la solubilidad en fracción molar, P es la presión en atm. y C es uno de los parámetros ajustables de la ecuación de Méndez-Santiago y Teja obtenido después del modelado de los datos experimentales de solubilidad. El principal inconveniente de esta metodología es de nuevo su carácter únicamente comparativo.

A pesar de las desventajas explicadas previamente, a partir de la teoría del test de Méndez-Santiago y Teja se pueden obtener varias conclusiones para un desarrollo futuro de un test de consistencia, a saber:

- La posibilidad de predecir el factor de mejora (E) de la solubilidad del sólido en el fluido supercrítico permitiría la estimación del término $T \cdot Ln(E)$. Por tanto, conociendo las condiciones experimentales, se podría realizar una estimación previa de la relación lineal entre el término $T \cdot Ln(E)$ y a la densidad. De esa forma, la recta estimada podría ser comparada con la recta experimental. Si la diferencia entre las dos rectas es elevada, la precisión de los datos experimentales sería dudosa.

- Debido a la relación entre el factor de mejora (E) y las propiedades de sublimación del sólido, se pone de manifiesto la posibilidad de que la solubilidad de un sólido esté relacionada con las propiedades de sublimación de dicho sólido. Esta teoría fue explorada previamente por Vetere [4] y también por Chrastil [5], aunque éste último de manera indirecta.

Vetere intentó predecir la solubilidad de fármacos en CO_2sc en función de la entalpía de sublimación del sólido, aunque su método podía llegar a producir un error de estimación superior al 60% [4].

Además, la ecuación de Chrastil está basada en la formación de un complejo de solvatación entre el sólido y el fluido supercrítico. El primer paso en un ciclo de solvatación es la sublimación del sólido, por lo que confirmaría la relación entre las propiedades de sublimación de un sólido y su solubilidad en un fluido supercrítico.

Teniendo en cuenta lo anteriormente descrito, a continuación se describirá el desarrollo de un test de consistencia basado en las teorías anteriores.

Este test de consistencia será definido con el uso de más de 2000 datos experimentales y dependerá exclusivamente de la entalpía de sublimación del sólido y de una modificación realizada al factor de mejora. Dicho estudio se recoge en el trabajo siguiente (artículo 7).

8.2. Resultados y discusión.

En el artículo del presente capítulo se procedió al desarrollo de un test de consistencia para la solubilidad de fármacos en CO_2sc, basado en un modelo de contribución de grupos para determinar la entalpía de sublimación y en un factor de mejora modificado.

De acuerdo a los resultados obtenidos, sólidos polares con similares valores de entalpías de sublimación, y a las mismas condiciones experimentales, muestran una parecida solubilidad en términos del factor de mejora modificado.

Varias ecuaciones a diferentes temperaturas fueron deducidas para la predicción del logaritmo del factor de mejora modificado con un error menor del 5%.

Estas ecuaciones junto con el modelo de contribución de grupos pueden ser usadas como una técnica para identificar datos experimentales erróneos de solubilidad de compuestos polares en CO_2sc. Sin embargo, esta metodología no puede ser usada con otro tipo de sólidos, como compuestos inorgánicos.

ARTÍCULO

An empirical analysis of the solubility of pharmaceuticals in supercritical carbon dioxide using sublimation enthalpies

Industrial and Engineering Chemistry Research

52 (2013) 18447-18457

I&EC research
Industrial & Engineering Chemistry Research

Article

pubs.acs.org/IECR

An Empirical Analysis of the Solubility of Pharmaceuticals in Supercritical Carbon Dioxide Using Sublimation Enthalpies

Antonio Tabernero, Eva M. Martín del Valle,* and Miguel A. Galán

Department of Chemical Engineering, University of Salamanca, P/Los Caídos S/N, Salamanca, 37008, Spain

Supporting Information

ABSTRACT: An empirical study of the solubility of pharmaceuticals in supercritical carbon dioxide has been performed by using a modified enhancement factor and a group contribution method. According to the results, polar solids with similar sublimation enthalpies, and at similar experimental conditions, show similar solubility in terms of the proposed modified enhancement factor. Several equations to estimate that modified enhancement factor (depending on the experimental conditions and the sublimation enthalpies) with a deviation less than 5% have been determined. These equations can be used as a tool to identify if experimental data follow the common solubility tendency. However, they cannot be used with other type of solids, such as inorganic compounds.

1. INTRODUCTION

Over these last years, supercritical fluids (SCFs) have been used in several pharmaceutical applications, such as the extraction of compounds from natural sources[1,2] and the micronization of different solids.[3,4] In this context, sc-CO_2 is the fluid most used in supercritical conditions because is a nonflammable, nontoxic, and inert compound and is naturally abundant with a high threshold limit value (TLV) (less toxic than other compounds).[5] Concerning the previous topics, different reviews have been published covering the different techniques with their advantages and disadvantages.[6−10] Nevertheless, prior to the use of these techniques, several studies should be performed.

One of the main studies is to acquire knowledge of the solubility of the solid in the sc-CO_2. This information can be used to identify the most appropriate technique for processing the chosen solid.[11]

However, the determination of the solubility of pharmaceuticals in sc-CO_2 is not an easy task. Since there is (usually) a great difference of polarity between those solids and the sc-CO_2, the solubility is usually very low (around 10^{-5} to 10^{-8} in molar fraction). That means that a small difference in the purity, in the source of the compound or in the protocol can provide high deviations (even more than 1 order of magnitude) in the experimental data. The used technique for determining the solubility is also very important. For example, Rodríguez-Meizoso et al.[12] investigated the solubility of alkyl ketene dimmer in sc-CO_2 with different methodologies, and the implications of the use of different techniques. They showed that depending on the methodology, significant differences can be obtained (sometimes around 1 order of magnitude) in the experimental data. Moreover, the solubility measuring apparatus should be chosen depending on the subsequent application.[12] Therefore, it seems there is not a standard way to determine these solubility data. As an example, discrepancies were observed for the solubility of beta-carotene[13] or paclitaxel[14,15] in sc-CO_2 at the same experimental conditions.

The previous facts highlight the importance of the development of consistency tests or methodologies to assess the experimental data of highly polar compounds in sc-CO_2. The accuracy of the solubility data can be evaluated by first using a theoretical methodology for predicting the solubility data and then subsequently perform a comparison between the predicted and the experimental values. Theoretical tools, such as equations of state and semiempirical models need adjustable parameters that must be obtained with experimental data.[11,16] As a consequence, they can not be used for that purpose.

Furthermore, equations of state need solid properties such as the sublimation pressure or the critical properties. Those properties (mainly the sublimation pressure) are not usually available for drugs. In this context, it is important to specify that sublimation pressures and sublimation enthalpies of pharmaceuticals can be regressed by using mixing rules combined with cubic equations of state, or can be calculated from different parameters from semiempirical models. As an example, Garlapati and Madras[17] calculated the sublimation enthalpies of different antibiotics by using temperature independent mixing rules with a cubic equation of state and by using semiempirical models. In that case, the authors obtained more accurate results with mixing rules combined with cubic equations of state.[17]

On the other hand, methodologies such as EoS/G^E have several drawbacks. An adjustable parameter can be needed in the covolume, and solid properties have to be previously determined.[18,19] Sometimes, the methodology, such as the COSMO base activity coefficient model, is more convenient for predicting solubility only at certain conditions.[20] Finally, prior to the previous references for predicting solubility of solids in sc-CO_2, Vetere published in 1998 a short-cut method with only two input parameters (molecular weight and melting temper-

Received: September 13, 2013
Revised: November 21, 2013
Accepted: November 26, 2013
Published: November 26, 2013

ACS Publications © 2013 American Chemical Society

ature of the solids), but deviations of about 40−60% (mainly at low pressures) were obtained for several solids.[21]

Consistency tests can be also used for evaluating experimental solubility data (e.g., Méndez-Santiago and Teja (MST)[22]). Although the MST test has been used in different articles,[23] it is a comparative methodology, so it needs two or three different studies to distinguish the accuracy of the experimental data.

In this context, the main aim of this work is to perform an empirical analysis of the solubility of pharmaceuticals in sc-CO_2 at different conditions based on the sublimation enthalpies of the solids, avoiding the use of the sublimation pressure. More than 2300 solubility data (more than 100 solids) points of solids constituted by substituted aromatic and/or polycyclic aliphatic rings are studied by defining several correlations for predicting a modified enhancement factor at different experimental conditions. As will be shown in a later section, an accurate estimation of this factor can be used as a tool to identify less accurate experimental data.

2. THEORETICAL BACKGROUND

The enhancement factor E establishes a relation between the observed solubility and the ideal solubility. As a matter of fact, the enhancement factor E takes into account the different interaction forces between the solute and the solvent molecules in the solubilization process of any solid in a SCF. Because of that, E is also related to the second and third virial coefficients, and to the SCF density.[21,24] Equation 1 shows the previous considerations:

$$E = \frac{y_1 P}{P^{sub}} = \exp(a + b\rho_{SCF}) \quad (1)$$

where y_1 is the molar fraction of the solid in the SCF, P^{sub} is the sublimation pressure of the solid, ρ_{SCF} is the SCF density, and a and b are parameters.

On the other hand, Vetere[21] developed an equation to establish a relation between the molar fraction of the solid in the SCF at equilibrium y_1, the sublimation enthalpy of the solid ΔH_{sub} and the density of the SCF ρ_{SCF} (eq 2).

$$y_1 = 1/P \exp(-\frac{\Delta H_{sub}}{RT} + a_1 + b\rho_{SCF}) \quad (2)$$

Although eq 2 does not directly derive from eq 1, the constant b is the same for both equations, whereas the constant a_1 includes information concerning the sublimation pressure. Equation 2 provides a significant advantage, since the knowledge of the sublimation pressure is not required.

In this article, a modified enhancement factor (E_{mod}) was defined (eq 3) with the constants from the eq 2. The main difference between the modified and the original enhancement factors is the addition of information of the sublimation pressure in the modified factor. This fact can be seen as an advantage, since the sublimation pressure for pharmaceuticals is not usually available, and its estimation is one of the most important drawbacks to study the solubility of solids in SCFs.[25]

$$E_{mod} = \exp(a_1 + b\rho_{SCF}) \quad (3)$$

On the other hand, Méndez-Santiago and Teja[22] showed that the term $T\ln(E)$ collapses to a single straight line when plotted against SCF density (at any temperature).

Following that theory, it was noticed that the term $T\ln(E_{mod})$ presents the same tendency when plotted against SCF density, although not at any temperature. A change in the temperature produces a small variation on the value of the constants a_1 and b. Therefore, those constants should be calculated for each temperature. That slight temperature change can be attributed to the addition of the constant from the Clausius−Clapeyron approach.

Furthermore, the term $a_1+b\rho_{SCF}$ (or $\ln(E_{mod})$) is strongly related to the sublimation enthalpy of the solid and to the experimental conditions (pressure and temperature).

Due to the previous observations (as will be shown later), it was concluded that the term $a_1+b\rho_{SCF}$ (or $\ln(E_{mod})$) for any polar solid might be predicted depending on the experimental conditions and its molecular structure. To do that, different equations must be defined. Therefore, if the experimental lines $T\ln(E_{mod})_{exp}$ are close to the predicted lines $T\ln(E_{mod})_{pre}$, experimental data would lie within the limits of the accuracy.

3. METHODOLOGY

This section is divided in different subsections. The first one is related to the methodology to develop the equations for predicting the modified enhancement factor. On the other hand, the second subsection is dedicated to the methodology to analyze solubility data of solids in sc-CO_2 with the previously obtained equations.

3.1. Development of Equations for Predicting the Term $a_1+b\rho_{SCF}$. The steps to determine the equations to predict the modified enhancement factor are indicated in Figure 1.

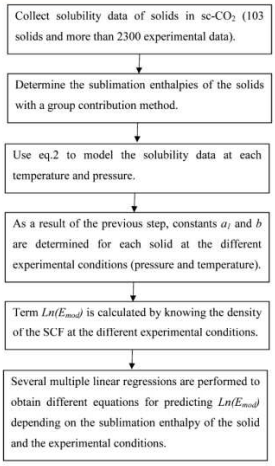

Figure 1. Steps to determine the equations to predict $\ln(E_{mod})$.

To determine those equations, solubility data of 103 solids in sc-CO_2 (around 2300 experimental data) were modeled with eq 2. Those solids and the experimental temperatures are shown in Table 1. As can be observed, all solids are constituted by substituted aromatic and/or polycyclic aliphatic rings, that is the usually structure of pharmaceuticals. References for the solubility of the solids in sc-CO_2 were mainly taken from different works.[26−29]

To use eq 2, the sublimation enthalpy of the solid must be previously calculated. Since this property is not usually available for complex solids such as pharmaceuticals, a group

Table 1. Solids with Their Sublimation Enthalpies, Number of Experimental Data *N* and Temperatures *T*

solid	ΔH_{sub} (kJ·mol^{-1})	*N*	*T* (K)	ref
1,5-naphthalenediamine	109.92	27	313−333	32
2,3,5-trimethylphenol	87.48	7	308	33
2,3-dimethylnaphthalene	80.14	15	308−328	34
2,3-dimethylphenol	81.41	7	308	33
2,4,6-trichlorophenol	108.6	24	308−318	35
2,4,6-trimethylphenol	93.10	6	308	33
2,4-dichloro-1-naphthol	116.53	24	308−328	36
2,4-dichlorophenol	95.13	16	308−313	35
2,5-dimethylphenol	81.41	7	308	33
2,6-dimethylnaphthalene	80.14	15	308−328	34
2-methylbenzoic acid	89.54	18	313−333	37
2-methyl-*N*-phenylacetamide	84.29	21	308−328	38
3-methylbenzoic acid	89.54	18	313−333	37
4-aminoantipyrine	135.20	14	318−328	39
4-chlorophenol	82.20	16	308−313	35
4-dimethylaminoantipyrine	80.20	14	318−328	39
4-methyl benzoic acid	89.54	18	313−333	37
4-methoxyphenylacetic acid	98.81	22	308−328	40
4-methyl-*N*-phenylacetamide	84.29	21	308−328	38
4-phenylphenol	105.37	7	308	33
4-*tert*-butyl-phenol	82.02	7	308	33
4,4′-diaminodiphenylmethane	135.60	27	313−333	32
acetaminophen	117.90[82]	4	313	41
acid protocatechuic	124.81	21	313−333	42
alpha-tocopherol	102.20	16	313−333	43
anastrozole	129.40	45	308−348	44
antipyrine	109.90	14	318−328	39
AQ1[a](1-hydroxy-9,10-anthraquinone)	121.89	45	308−348	45
AQ2[a](1-hydroxy-9,10-anthraquinone)	127.96	45	308−348	45
AQ3[a](1-hydroxy-9,10-anthraquinone)	137.23	45	308−348	45
AQ4[a](1-hydroxy-9,10-anthraquinone)	140.61	45	308−348	45
AQ5[a](1-hydroxy-9,10-anthraquinone)	143.99	45	308−348	45
AQ6[a](1-hydroxy-9,10-anthraquinone)	143.99	45	308−348	45
AQ7[a](1-hydroxy-9,10-anthraquinone)	147.37	45	308−348	45
aspirin	109.70[83]	24	308−328	46
atorvastatin	167.40	45	308−348	47
benzoic acid	83.47	15	318−338	34
beta-carotene	128.70	16	313−333	43
boldine	188.29	37	308−333	48
caffeic acid	117.17	24	313−333	49
caffeine	105.10[84]	16	313−333	50
cinnamic acid	90.33	19	308−328	40
climbazole	124.38	24	313−333	51
clofibric acid	108.97	21	308−328	52
clozapine	212.34	27	318−348	53
coumarin	83.10[84]	7	318−328	54
chalcone	98.95	26	308−338	55
cholesterol	114.60	22	313−333	56
dibenzofuran	82.00	21	308−338	57
ethyl vanillin	101.50	19	313−333	58
examestane	122.80	45	308−348	44
fenofibrate	131.91	21	308−328	52
ferulic acid	122.96	27	313−333	49
flutamide	86.00	36	318−348	59
fluvastatin	136.10	45	308−348	47
gemfibrozil	140.28	21	308−328	52
ibuprofen	93.54	29	308−318	60
Irgacure 2959	110.20	21	308−328	61
ketoprofen	112.00	10	313−333	62
lamotrigine	160.63	36	318−348	53
letrozole	129.90	45	308−348	44

dx.doi.org/10.1021/ie403031k | *Ind. Eng. Chem. Res.* 2013, 52, 18447−18457

Table 1. continued

solid	ΔH_{sub} (kJ·mol^{-1})	N	T (K)	ref
lovastatin	90.60	45	308−348	47
maleic acid	105.40	21	318−348	63
methimazole	87.20	40	308−348	64
nabumetone	101.26	14	318−328	65
naproxen	128.30[85]	18	313−333	66
nimesulide	82.20	8	313−333	62
nitrendipine	94.80	15	333	67
N-phenylacetamide	78.22	24	308−328	38
o-HBA	104.14	12	318−328	68
o-phthalic acid	118.34	15	308−328	69
p-aminobenzoic acid	103.18	15	308−328	69
p-bromobenzaldehyde	89.81	12	313−333	70
penicillin G	122.20	18	313−333	71
p-HBA	104.14	11	318−328	68
phenacetin	93.56	16	308−328	72
phenazopyridine	93.00	45	308−348	64
phenoxyacetic acid	89.36	22	308−328	40
phenylacetic acid	86.85	24	308−318	73
phytosterol	93.65	15	323−333	74
piroxicam	122.45	9	313−333	62
progesterone	93.90	27	313−328	56
propanolol	123.40	45	308−348	64
propyl gallate	135.53	8	313−333	75
protocatechualdehyde	127.60	22	313−333	42
retinol	66.04	12	313−333	43
rosuvastatin	122.20	45	308−348	47
salicylamide	89.76	14	318−328	65
salicylic acid	104.14	20	313−333	76
simvastatin	109.40	45	308−348	47
testosterone	110.50	29	313−328	56
tetramethylpyrazine	94.60	15	318−338	77
theobromine	126.00	15	313−333	50
theophylline	126.00	16	313−333	50
triclocarban	160.12	24	313−333	51
triphenylmethyl chloride	131.27	18	308−338	78
uracil	127.00[84]	11	313−333	79
vanillic acid	116.10	13	313−328	80
vanillin	88.70	20	313−333	58
vitamin D2	122.50	13	313−333	43
vitamin D3	122.40	9	313−333	43
vitamin K1	87.93	16	313−333	43
xanthone	89.31	16	308−328	81

[a]AQ1, AQ2, AQ3, AQ4, AQ5, AQ6, and AQ7 are different 1-hydroxy-9,10-anthraquinone derivatives.

contribution method was used.[30] The sublimation enthalpies of the 103 solids are given in Table 1. The reference is given in the table if the sublimation enthalpy is taken from an experimental work. It should be specified that the effect of the temperature on that property has been neglected. For the previous calculations, the density of the sc-CO_2 was taken from the NIST webbook.[31]

Once the sublimation enthalpies were determined, solubility data of the 103 solids were modeled with eq 2 at different experimental temperatures, obtaining as a result the terms a_1 and b. Since the density of the sc-CO_2 is known, $a_1+b\rho_{SCF}$ for each temperature and pressure can be calculated.

Subsequently, by performing several multiple linear regressions, equations based only in the sublimation enthalpy and in the experimental pressure were defined to predict the term $a_1+b\rho_{SCF}$ for each temperature.

Therefore, after developing these equations, only the sublimation enthalpy of the solid and the experimental conditions are required to predict the modified enhancement factor. Since there is a group contribution method for estimating that enthalpy, only the knowledge of the molecular structure of the solid is needed to calculate the $a_1+b\rho_{SCF}$.

Finally, concerning the modeling process with eq 2, it is important to highlight that a very small percentage of experimental data of solids (less than 5%) were rejected (and consequently were not considered in the multiple linear regression) when the value of the constants a_1 and b were far different from the common values for the other 103 solids.

3.2. Methodology to Analyze Experimental Data of Solubility of Solids in sc-CO_2. With the aim of analyzing the accuracy of new experimental solubility data, the sublimation enthalpy of the solid must be known.

Subsequently, the term $\ln(E_{mod})_{pre}$ must be predicted (at the experimental conditions) by using the previously obtained correlations. Afterward, the term $\ln(E_{mod})_{exp}$ should be determined by modeling the experimental data with eq 2. As a result, the constants a_1 and b for each temperature and pressure are obtained.

Finally, the corresponding terms $T\ln(E_{mod})_{pre}$ and $T\ln(E_{mod})_{exp}$ at the experimental temperature can be calculated. By means of a comparison between those values, it will be possible to analyze the solubility data in terms of accuracy. Figure 2 shows a diagram of the previous steps.

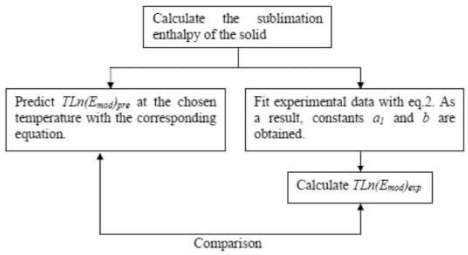

Figure 2. Steps to analyze the solubility of pharmaceuticals in sc-CO_2.

4. RESULTS AND DISCUSSION

4.1. Predicting the Term $a_1+b\rho_{SCF}$ and Its Applications for Polar Compounds. After determining the sublimation enthalpies of the 103 solids, parameters a_1 and b for each solid were determined by modeling the solubility of the solid in sc-CO_2 at each experimental temperature. Knowing the density of the sc-CO_2, the term $a_1+b\rho_{SCF}$ (or $\ln(E_{mod})_{exp}$) is calculated for the different experimental conditions. Tables 1 through 8 in the Supporting Information show the results of the solubility modeling for 308 K, 313 K, 318 K, 323 K, 328 K, 333 K, 338 K, and 348 K.

In those tables, although the term $\ln(E_{mod})_{exp}$ was calculated for all of the experimental conditions, only the values for the lowest and the highest pressure at each experimental temperature are shown. Several conclusions can be obtained from the previous tables.

First, at the same temperature, $\ln(E_{mod})_{exp}$ increases with an increase in the sublimation enthalpy. In addition, the value of the modified enhancement factor (at the same experimental conditions) is always similar for solids with similar sublimation enthalpies.

For the same solid, the $\ln(E_{mod})_{exp}$ slightly decreases with increasing temperature, although increases obviously with the pressure. Moreover, for a similar pressure range, the increase of the $\ln(E_{mod})_{exp}$ is greater for higher temperatures. For instance, for the clofibric acid, the increase in the $\ln(E_{mod})_{exp}$ at 308 K is around 1.50, whereas at 328 K the increase is around 4.00. This increase is similar (at the same temperature) for solids with similar sublimation enthalpies. That is the reason why, in order to improve the accuracy, the term $\ln(E_{mod})_{exp}$ was calculated for each temperature.

The explanation for these last facts is based on the solubility of any solid in sc-CO_2. At higher temperatures, the solubility increase for the same pressure range is greater in comparison with the increase at lower temperatures. In fact, the upper critical end point (temperature at which two phases merge in one single phase) can even be reached, and as a consequence, at these conditions there is a strong increase in solubility. Furthermore, the increase on the saturation pressure of the solid at high temperature becomes predominant over the density reduction of the SCF. This phenomenon is well-known and has been reported in several articles.[17,86]

Owing to the observed dependence between sublimation enthalpy, pressure, and temperature with the modified enhancement factor, it is possible to develop different equations to predict that factor based on the previous properties. To do that, several multiple linear regressions were performed to determine an equation to estimate the $\ln(E_{mod})$ at each temperature, depending on the pressure and the sublimation enthalpy of the solid.

Table 2 shows the obtained equations and the average absolute relative deviation (AARD, eq 4) as well as the average absolute error (AAE, eq 5). In those equations, the sublimation enthalpies are in kJ·mol^{-1} and the pressure is in bar.

Table 2. Obtained Equations for Predicting $\ln(E)$ at Different Temperatures with Their AARD and AAE

temp (K)	equation	AARD (%)	AAE
308	$\ln(E_{mod})_{pre} = 0.3452\Delta H_{sub} + 0.0088P$	5.58	2.05
313	$\ln(E_{mod})_{pre} = 0.3231\Delta H_{sub} + 0.0112P$	5.15	1.96
318	$\ln(E_{mod})_{pre} = 0.3224\Delta H_{sub} + 0.0127P$	5.30	1.88
323	$\ln(E_{mod})_{pre} = 0.3139\Delta H_{sub} + 0.0096P$	6.12	2.27
328	$\ln(E_{mod})_{pre} = 0.2989\Delta H_{sub} + 0.0178P$	5.26	1.80
333	$\ln(E_{mod})_{pre} = 0.2837\Delta H_{sub} + 0.0189P$	6.68	2.48
338	$\ln(E_{mod})_{pre} = 0.2920\Delta H_{sub} + 0.0175P$	5.82	2.02
348	$\ln(E_{mod})_{pre} = 0.278\cdot\Delta H_{sub} + 0.0181P$	5.68	1.96

$$\text{AARD}\ (\%) = \frac{100}{n}\sum_{i=1}^{n}\left(\frac{\ln(E_{mod})_{pre} - \ln(E_{mod})_{exp}}{\ln(E_{mod})_{exp}}\right) \quad (4)$$

$$\text{AAE} = \frac{1}{n}\sum_{i=1}^{n}\left|\ln(E_{mod})_{pre} - \ln(E_{mod})_{exp}\right| \quad (5)$$

As can be seen in Table 2, the defined equations from 308 to 323 K are very similar. That means that the $\ln(E_{mod})$ at any intermediate temperature might be determined by using the equation at the closest temperature. However, equations for temperatures ranging from 328 to 348 K (although similar between them) are different from the equations from 308 to 323 K.

Concerning the deviations, Figure 3 illustrates the comparison between experimental and predicted values by using the equations given in Table 4.

Figure 4a and Figure 4b illustrate the terms $T\ln(E_{mod})_{pre}$ and $T\ln(E_{mod})_{exp}$ for the cholesterol at 313 K and for the naproxen at 323 K, respectively. As can be observed, the term $T\ln(E_{mod})$ is predicted accurately for both solids with our equations (with an AARD of around 5%). Those solids were chosen because their solubility in sc-CO_2 has been reported in different articles.

Figure 4a shows the experimental and the predicted terms with the modified enhancement factors for different studies dealing with the solubility of cholesterol at 313 K. In that case, data from refs 56 and 88 are shown in this figure. Data from Huang et al.[87] were similar to that in ref 88 and for that reason were not included. Data from ref 89 were determined at different temperatures.

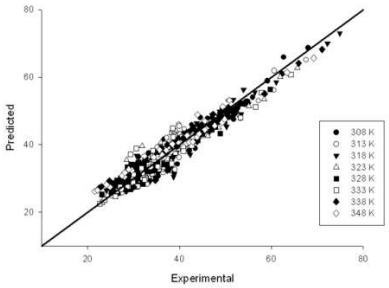

Figure 3. Comparison between experimental and predicted Ln-(Emod).

Discrepancies between experimental data from references 88 and 56 were found, although always with a difference of less than 1 order of magnitude. According to Yun et al.,[88] these differences were produced mainly due to the different experimental procedure. To check it, we performed an analysis of the solubility of cholesterol in sc-CO_2 with our test. If the difference between the experimental and the predicted terms is relevant for one of these studies, that study would not be accurate according to our methodology. However, as can be seen in Figure 4a, the AARD for both studies is always less than 5%, so the differences between the experimental works can be attributed to experimental reasons.

On the other hand, Figure 4b shows that the solubility of the naproxen in sc-CO_2 at 323 K for both works[23,66] is almost identical. Moreover, we did not find a significant deviation between the experimental and the predicted terms with the modified enhancement factor and as a consequence these data can be considered accurate according to our methodology. It is important to realize that in Figure 4b, the line for the predicted modified enhancement factor crosses the experimental modified enhancement factor. This fact can occur when a wide CO_2 density range is studied (in this case from 350 kg·m^{-3} to 950 kg·m^{-3}). Nevertheless, the AARD between the predicted and the experimental terms with the modified enhancement factor is always less than 5% at all the investigated densities.

The methodology proposed was used with more solids that were not included in our initial set (Table 1). Solubility data of norfloxacin at 313 K,[90] vitamin K3 at 313 K,[43] and ofloxacin at 318 K[90] were analyzed. The methodology described in Figure 2 was followed, and the steps (with the calculations) for norfloxacin (example A.1) and vitamin K3 (example A.2) are given in the Appendix.

Figure 5 panels a and b and Figure 6 illustrate the $T\ln(E_{mod})_{exp}$ and the $T\ln(E_{mod})_{pre}$ for the previous solids. It can be observed that the AARD between the predicted and the experimental terms with the modified enhancement factors is always around 5%. In these cases the curve of the predicted term is almost completely straight because the initial density of these studies was always at least around 500 kg·m^{-3}.

Figure 6 shows the results with inaccurate data. Those data were supposed with a difference of about 16% between the $T\ln(E_{mod})_{exp}$ and $T\ln(E_{mod})_{inaccurate}$ (a difference of 10 units between the experimental and the inaccurate enhancement factor). The experimental modified enhancement factor was 58, the inaccurate value was considered 48, and the predicted value was close to 60. As can be seen in Figure 8, there is a huge difference between the inaccurate and the predicted data, and as a result the proposed methodology can be used to perform a previous analysis of the accuracy of the experimental data.

It is important to specify that solids with a sublimation enthalpy greater than 212 kJ·mol^{-1} were not studied. That value might be a limitation for the test, because according to eq 2, the sublimation enthalpy multiplies an exponential term. As a consequence, the deviation might increase drastically.

In summary, by means of a comparison between the $T\ln(E_{mod})_{exp}$ and $T\ln(E_{mod})_{pre}$, the accuracy of the experimental data can be studied. If the values of the both terms are relatively close, the solubility of the solid would lie in the standard values.

4.2. Application for Other Types of Compounds. To extend the previous methodology to other compounds, the equations of Table 2 were used for fatty acids.

However, the used group contribution method in this work cannot determine sublimation enthalpies of highly linear solids without rings.[30] With the aim of overcoming this drawback, a correlation was defined for calculating the sublimation enthalpy of these compounds.

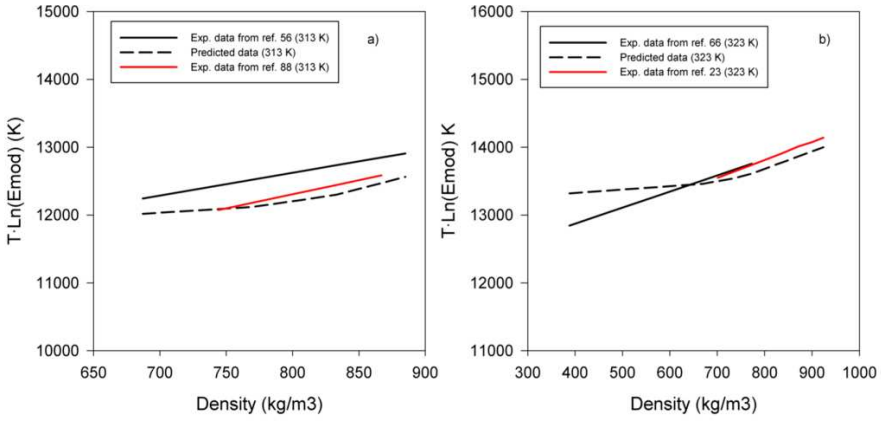

Figure 4. $T\ln(E_{mod})_{pre}$ and $T\ln(E_{mod})_{exp}$ for the solubility of different pharmaceuticals in sc-CO2: (a) cholesterol at 313 K[56,88] and (b) naproxen at 323 K.[23,66]

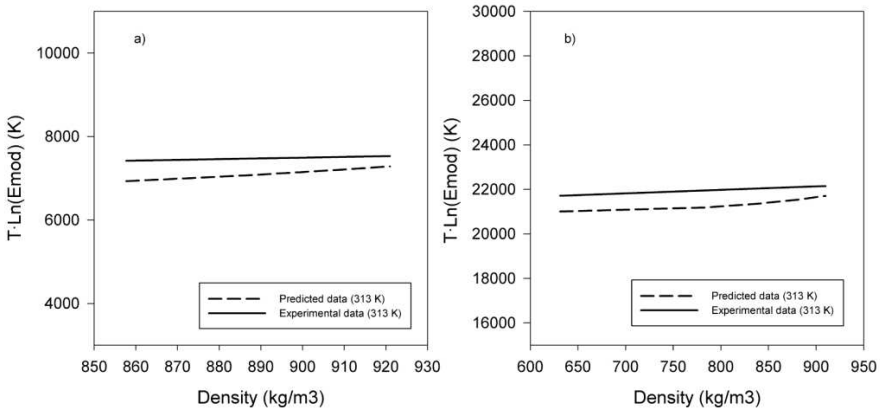

Figure 5. $T\ln(E_{mod})_{pre}$ and $T\ln(E_{mod})_{exp}$ for the solubility of different pharmaceuticals in sc-CO2 at 313 K: (a) vitamin K3[43] and (b) norfloxacin.[90]

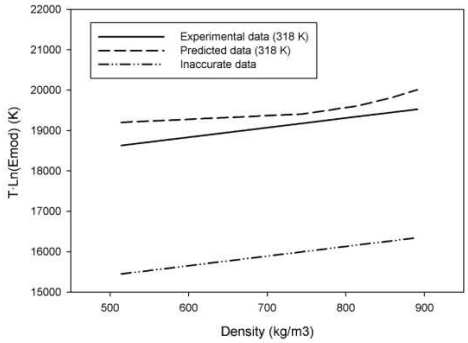

Figure 6. $T\ln(E_{mod})_{pre}$ and $T\ln(E_{mod})_{exp}$ for the solubility of ofloxacin in sc-CO2 at 318 K.[90]

Sublimation enthalpies of fatty acids were collected from different works. Nevertheless, only nine values were found (from octanoic acid (eight carbon atoms) to eicosanoic acid (20 carbon atoms). These values are shown in Table 3 with their references. In this context, it is important to highlight that for the octanoic acid, the sublimation enthalpy was calculated as the sum of its fusion and vaporization enthalpies. This assumption can be considered (at least with polycyclic aromatic hydrocarbons) when the sublimation enthalpy[91] is less than 160 kJ·mol^{-1}.

Table 3. Sublimation Enthalpies of Fatty Acids and References

compound	ΔH_{sub} (kJ·mol^{-1})	ref
octanoic acid	101.38	31
decanoic acid	117.10	84
undecanoic acid	121.30	84
dodecanoic acid	127.90	84
tetradecanoic acid	139.70	84
hexadecanoic acid	154.40	84
octadecanoic acid	166.50	84
nonadecanoic acid	192.00	31
eicosanoic acid	199.60	84

Subsequently, the molecules must be divided into molecular fragments, and a multiple linear regression should be performed to determine the value of each functional group. The values of the functional groups are given in Table 4.

Therefore, with Table 4 and eq 6, the sublimation enthalpy of any fatty acid can be calculated with and AARD and AAE of 4.90% and 6.97 kJ·mol^{-1}, respectively. In eq 6, n_i is the number of times a group i appears in the solid, and X_i is the contribution of group i to the value of the sublimation enthalpy.

Table 4. Molecular Fragments and Their Contribution X (kJ·mol^{-1}) to the Sublimation Enthalpy

molecular fragment	X (kJ·mol^{-1})
CH_3	57.47
$-CH_2-$	7.82
$-COOH$	−5.79

$$\Delta H_{sub}\ (\text{kJ·mol}^{-1}) = \sum n_i \cdot X_i \qquad (6)$$

Since we were not able to find more sublimation enthalpies of fatty acids in the literature, it was not possible to split the values of Table 3 into a training test and in a test set. As a consequence, the predicting ability of the method cannot be checked, and its use for fatty acids with more than 20 carbon atoms is not appropriate (although the method can be used to estimate sublimation enthalpies of any fatty acid with a number of carbon atoms between 8 and 20). The comparison between the predicted and the experimental values for these fatty acids is illustrated in Figure 7.

In order to test the proposed methodology with fatty acids, the term $a_1+b\rho_{SCF}$ (or $\ln(E_{mod})$) at different temperatures and pressures for nonanoic, tetranoic, hexadecanoic, and octadecanoic acids were predicted by using eq 6 (sublimation enthalpies) and equations from Table 2. Table 5 shows the calculated sublimation enthalpies, references for the solubility data and the experimental term $a_1+b\rho_{SCF}$ (calculated by modeling the solubility data).

According to the results (table 5), our methodology predicts the tendency of the $\ln(E_{mod})$, although always with a deviation of about 10%. This fact highlights that the proposed equations cannot be used to analyze the solubility of fatty acids in sc-CO_2. The different molecular structure of the fatty acids changes

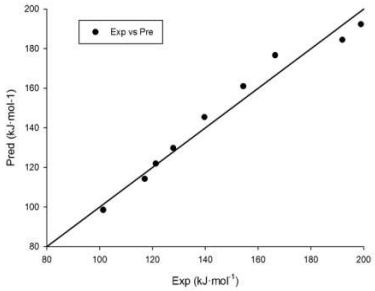

Figure 7. Comparison between predicted and experimental values of sublimation enthalpies of fatty acids.

drastically their solubility in sc-CO_2 in comparison with other solids with substituted aromatic and/or polycyclic rings.

However, as can be seen in Table 5, the modified enhancement factor depends strongly on the sublimation enthalpy of the fatty acid and on the experimental conditions. This fact highlights that fatty acids with similar sublimation enthalpies give as a result a similar modified enhancement factor. Then, the previous theory can be used with another type of compounds as well as with polar solids, although different equations must be proposed depending on the main structure of the compound.

However, it was not possible to find enough solubility data of fatty acids in sc-CO_2 to determine consistent equations to predict the $\ln(E_{mod})$.

5. CONCLUSIONS

An analysis of more than 2300 experimental solubility data points of pharmaceuticals in supercritical carbon dioxide has been performed by proposing a modified enhancement factor, which has been defined from an equation that determines the solubility of the solid depending on the sublimation enthalpy of the solid. According to the results, solids with similar sublimation enthalpies, and at the same experimental conditions, provide a similar modified enhancement factor. On the basis of this conclusion, a set of equations to estimate that factor have been proposed. Those equations provide a deviation in the estimation of about 5%, and they can be used (as long as a group contribution method to determine the sublimation enthalpy is available) as a tool to distinguish the accuracy of the experimental values.

To check the obtained equations with fatty acids, a group contribution method to predict the sublimation enthalpy of this type of solids has been developed (with a deviation less than 5%). The results indicated that fatty acids with similar sublimation enthalpies have the same modified enhancement factor at similar experimental conditions.

However, the proposed equations to estimate the modified enhancement factor for polar solids provided a large deviation in the estimation of that factor for fatty acids, highlighting that the proposed equations can be only used for polar solids with aromatic and/or polycyclic aliphatic rings.

APPENDIX

Example A.1. Norfloxacin

Figure 8 illustrates the molecular structure of the norfloxacin.

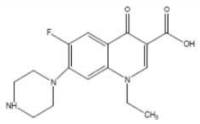

Figure 8. Molecular structure of norfloxacin.

The sublimation enthalpy of the norfloxacin should be estimated with a GC.[30] To do that, the molecule must be divided into different functional groups as follows: 2[CHar] + 4[Car] + 4[(−CH_2−)apr] + 1[−CH_2−] + 1[−CH_3] + 1[COOH] + 2[(−N<)apr] + 1[(−NH−)apr] + 1[F−] + 1[(>C═O)ring] + 1[(=C<)apr] + 1[(=CH−)apr].

After that, the sublimation enthalpy can be predicted: ΔH_{sub} = (2·8.10) + (4·2.60) + (4·10.38) + 3.38 + 11.57 + 40.37 + (2·15.37) + 34.34 + 3.92 + 13.01 −13.04 + 11.78 = 204.19 kJ·mol^{-1}.

By using Table 4, and the equation at 313 K, the $\ln(E_{mod})$ at 300 bar is predicted: $\ln(E_{mod})_{pred}$ (313 K) = 0.3231·ΔH_{sub}+0.0112·P = 0.3231·215.19 kJ·mol^{-1} + 0.0112·300 = 72.92; $T\ln(E_{mod})_{pre}$ (313 K) = 313·72.92 = 22823.96 K.

By modelling the solubility data of this compound[90] in sc-CO_2 with eq 2, the $\ln(E_{mod})_{exp}$ at 313 K and 300 bar was calculated. The value was 75.00. Then $T\ln(E_{mod})_{pre}$ (313 K) = 313·75.00 = 23475.00 K.

This procedure must be followed to calculate more experimental data. As can be seen from the results, both terms are similar, with a deviation of less than 5%.

Example A.2. Vitamin K3

The molecular structure of the vitamin K3 is given in Figure 9.

Firstly, the molecule must be divided into its functional groups to calculate its sublimation enthalpy with the GC.[30] That molecule is constituted by the following groups: 4[−CHar] + 2[Car] + 2[(>C═O)ring] + 1[−CH_3] + 1[(=CH−)apr] + 1[(>C=)apr].

Table 5. Terms $(a_1+b\rho_{SCF})_{exp}$ and $(a_1+b\rho_{SCF})_{pre}$ for Several Fatty Acids at Different Experimental Conditions

compound	ΔH_{sub} (kJ·mol^{-1})	temp (K)	pressure (bars)	$(a_1+b\rho_{SCF})_{exp}$	$(a_1+b\rho_{SCF})_{pred}$	ref
nonanoic acid	106.34	313	100−300	40.45−41.64	35.49−37.74	92
nonanoic acid	106.34	323	100−300	37.99−40.41	34.35−36.28	92
nonanoic acid	106.34	328	100−300	36.36−39.29	33.57−37.13	92
tetradecanoic acid	145.39	308	99−226	54.95−56.85	51.06−52.18	93
tetradecanoic acid	145.39	318	128−226	53.93−55.55	48.51−49.76	93
hexadecanoic acid	161.01	308	128−226	59.50−60.60	56.71−57.58	94
hexadecanoic acid	161.01	318	128−226	57.87−59.46	53.55−54.80	94
octadecanoic acid	176.63	308	128−226	64.37−65.55	62.10−62.97	94
octadecanoic acid	176.63	318	128−226	62.41−64.25	58.59−59.84	94

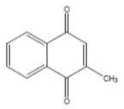

Figure 9. Molecular structure of vitamin K3.

Therefore, the sublimation enthalpy is calculated as ΔH_{sub} = (4·8.10) + (2·2.60) + (2·6.47) + 11.57 + 11.78 − 13.04 = 60.85 kJ·mol^{-1}.

Knowing the sublimation enthalpy, it is possible to estimate the $\ln(E_{mod})$ at 313 K at any pressure. To make a comparison with the experimental data,[43] the previous term at 320 bar is predicted with the equation in Table 4: $\ln(E_{mod})_{pre}$ (313 K) = $0.3231 \cdot \Delta H_{sub} + 0.0112 \cdot P = 0.3231 \cdot 60.85$ kJ·mol^{-1} + 0.0112·320 = 23.27; $T\ln(E_{mod})_{pre}$ (313 K) = 313·23.27 = 7283.51 K.

After modelling the solubility data in sc-CO_2 with eq 2, the $\ln(E_{mod})_{exp}$ at 313 K and 320 bar was obtained. The value was 24.08. Then $T\ln(E_{mod})_{pre}$ (313 K) = 313·24.08 = 7537.04 K.

This procedure must be followed to calculate more experimental data. As can be seen from the results, both terms are similar, with a deviation of less than 5%.

■ ASSOCIATED CONTENT

Supporting Information

The obtained data for the modified enhancement factor at the different temperatures are given in Supplementary Tables 1−8. This material is available free of charge via the Internet at http://pubs.acs.org.

■ AUTHOR INFORMATION

Corresponding Author

*E-mail: emvalle@usal.es. Tel.: (+34) 923-294479. Fax: (+34) 923-294579.

Notes

The authors declare no competing financial interest.

■ ACKNOWLEDGMENTS

This research was supported by funds from the Ministerio de Ciencia e Innovación (Spain), project CTQ2012-32929 (PPQ subprogram).

■ REFERENCES

(1) Içen, H.; Gürü, M. Extraction of caffeine from tea stalk and fiber waste using supercritical carbon dioxide. *J. Supercrit. Fluids* **2009**, *50*, 225.

(2) Mendes, R. L.; Nobre, B. P; Cardoso, M. T.; Pereira, A. P; Palavra, A. F. Supercritical carbon dioxide extraction of compounds with pharmaceutical importance from microalgae. *Inorg. Chim. Acta* **2003**, *356*, 328.

(3) Tabernero, A.; Martín del Valle, E. M.; Galán, M. A. Precipitation of tretinoin and acetaminophen with solution enhanced dispersion by supercritical fluids (SEDS). Role of phase equilibria to optimize particle diameter. *Powder Technol.* **2012**, *217*, 177.

(4) Thiering, R.; Dehghani, F.; Dillow, A.; Foster, N. R. The influence of operating conditions on the dense gas precipitation of model proteins. *J. Chem. Technol. Biot.* **2000**, *75*, 29−41.

(5) Beckman, E. J. Supercritical and near-critical CO_2 in green chemical synthesis and processing. *J. Supercrit. Fluids* **2004**, *28*, 121.

(6) Tandya, A.; Mammucari, R.; Dehghani, F.; Foster, N. R. Dense gas processing of polymeric controlled release formulations. *Int. J. Pharm.* **2007**, *328*, 1.

(7) Tabernero, A.; Martín del Valle, E. M.; Galán, M. A. Supercritical fluids for pharmaceutical particle engineering: Methods, basic fundamentals and modelling. *Chem. Eng. Process.* **2012**, *60*, 9.

(8) Martín, A.; Cocero, M. J. Micronization processes with supercritical fluids: Fundamentals and mechanisms. *Adv. Drug. Delivery Rev.* **2008**, *60*, 339.

(9) Reverchon, E.; Adami, R. Nanomaterials and supercritical fluids. *J. Supercrit. Fluids* **2006**, *37*, 1.

(10) Herrero, M.; Cifuentes, A.; Ibañez, E. Sub- and supercritical fluid extraction of functional ingredients from different natural sources: Plants, food-by-products, algae and microalgae: A review. *Food Chem.* **2006**, *98*, 136.

(11) Higashi, H.; Iwai, Y.; Arai, Y. Solubilities and diffusion coefficients of high boiling compounds in supercritical carbon dioxide. *Chem. Eng. Sci.* **2001**, *51*, 3027.

(12) Rodríguez-Meizoso, I.; Werner, O.; Quan, C.; Knez, Z.; Turner, C. Phase behaviour of alkyl ketene dimmer (AKD) in supercritical carbon dioxide. The implications of using different solubility measurement methods. *J. Supercrit. Fluids* **2012**, *61*, 25.

(13) Saldaña, M. D. A.; Sun, L.; Guigard, S. E.; Temelli, F. Comparison of the solubility of β-carotene in supercritical CO_2 based on a binary and a multicomponent complex system. *J. Supercrit. Fluids* **2006**, *37*, 342.

(14) Vandana, V.; Teja, A. S. The solubility of paclitaxel in supercritical CO_2 and N_2O. *Fluid Phase Equilib.* **1997**, *135*, 83.

(15) Nalesnik, C. A.; Hansen, B. N.; Hsu, J. T. Solubility of pure taxol in supercritical carbon dioxide. *Fluid Phase Equilib.* **1998**, *146*, 315.

(16) Tabernero, A.; Martín del Valle, E. M.; Galán, M. A. A comparison between semiempirical equations to predict the solubility of pharmaceutical compounds in supercritical carbon dioxide. *J. Supercrit. Fluids* **2010**, *52*, 161.

(17) Garlapati, C.; Madras, G. Temperature independent mixing rules to correlate the solubilities of antibiotics and anti-inflammatory drugs in scCO_2. *Thermochim. Acta* **2009**, *496*, 54.

(18) Kontogeorgis, G. M.; Coutsikos, P. Thirty years with EoS/G^E models—What have we learned? *Ind. Eng. Chem. Res.* **2012**, *51*, 4119.

(19) Vieira de Melo, S. A. B.; Vieira de Melo, R. L. F.; Costa, G. M. N.; Alves, T. L. M. Solubility of L-DOPA in supercritical carbon dioxide: Prediction using a cubic equation of state. *J. Supercrit. Fluids* **2005**, *34*, 231.

(20) Shimoyama, Y.; Iwai, Y. Development of activity coefficient model based on COSMO method for prediction of solubilities OS solid solutes in supercritical carbon dioxide. *J. Supercrit. Fluids* **2009**, *50*, 210.

(21) Vetere, A. A short-cut method to predict the solubilities of solids in supercritical carbon dioxide. *Fluid Phase Equilib.* **1998**, *148*, 83.

(22) Méndez-Santiago, J.; Teja, A. S. The solubility of solids in supercritical fluids. *Fluid Phase Equilib.* **1999**, *158−160*, 501.

(23) Turk, M.; Kraska, T. Experimental and theoretical investigation of the phase behaviour of naproxen in supercritical CO_2. *J. Chem. Eng. Data* **2009**, *54*, 1592.

(24) Vetere, A. An empirical method to evaluate the enhancement factors of solids in supercritical gases. *J. Supercrit. Fluids* **1998**, *12*, 129.

(25) Johnston, K. P.; Peck, D. G.; Kim, S. Modeling supercritical mixtures: How predictive is it? *Ind. Eng. Chem. Res.* **1989**, *28*, 1115.

(26) Dohrn, R.; Peper, S.; Fonseca, J. M. S. High pressure fluid-phase equilibria: Experimental methods and systems investigated (2000−2004). *Fluid Phase Equilib.* **2010**, *288*, 1.

(27) Fonseca, J. M. S.; Dohrn, R.; Peper, S. High pressure fluid-phase equilibria: Experimental methods and systems investigated (2005−2008). *Fluid Phase Equilib.* **2011**, *300*, 1.

(28) Fornari, R. E.; Alessi, P.; Kikic, I. High pressure fluid-phase equilibria: Experimental methods and systems investigated (1978−1987). *Fluid Phase Equilib.* **1990**, *57*, 1.

(29) Skerget, M.; Knez, Z.; Knez-Hrncic, M. Solubility of solids in sub- and supercritical fluids: A review. *J. Chem. Eng. Data* **2011**, *56*, 694.

(30) Tabernero, A.; Martín del Valle, E. M.; Galán, M. A. Estimation of sublimation enthalpies of solids constituted by aromatic and/or

polycyclic aliphatic rings by using a group contribution method. *AIChE J.* **2012**, *58*, 2875.
(31) Lemmon, E. W.; McLinden, M. O.; Friend, D. G. Thermophysical properties of fluid systems, NIST chemistry webbook. *NIST Standard Reference Data Base*; Linstrom, P.J., Mallard, W.G., Eds; National Institute of Standards and Technology: Gaithersburg MD; http://webbook.nist.gov, (retrieved Febrary 25, 2013).
(32) Khimeche, K.; Alessi, A.; Kikic, I.; Dahmani, A. Solubility of diamines in supercritical carbon dioxide: Experimental determination and correlation. *J. Supercrit. Fluids* **2007**, *41*, 10.
(33) Ravipaty, S.; Sclafani, A. G.; Fonslow, B. R.; Chesney, D. J. Solubilities of substuted phenols in supercritical carbon dioxide. *J. Chem. Eng. Data* **2006**, *51*, 1301.
(34) Kurnik, R.; Holla, S. J.; Reid, R. C. Solubility of solids in supercritcal carbon dioxide. *J. Chem. Eng. Data* **1981**, *26*, 47.
(35) Garlapati, Ch.; Madras, G. Solubilities of some chlorophenols in supercritical CO_2 in the presence and absence of cosolvents. *J. Chem. Eng. Data* **2010**, *55*, 273.
(36) Yoon, J. H.; Lee, H. S.; Lee, H. Solubilities of 2,4-dichloro-1-naphthol in supercritical carbon dioxide. *J. Chem. Thermodyn.* **1993**, *25*, 193.
(37) Tsai, K. L.; Tsai, F. N. Solubilities of methylbenzoic acid isomers in supercritical carbon dioxide. *J. Chem. Eng. Data* **1995**, *40*, 264.
(38) Huang, S. Y.; Tang, M.; Ho, S. L.; Chen, Y. P. Solubilities of *N*-phenylacetamide, 2-methyl-*N*-phenylacetamide and 4-methyl-*N*-phenylacetamide in supercritical carbon dioxide. *J. Supercrit. Fluids* **2007**, *42*, 165.
(39) Chen, Y. M.; Chen, Y. P. Measurements of solid solubilities of antipyrine, 4-aminoantipyrine and 4-dimethylaminoantipyrine in supercritical carbon dioxide. *Fluid Phase Equilib.* **2009**, *282*, 82.
(40) Chen, Y. P.; Chen, Y. M.; Tang, M. Solubilities of cinnamic acid, phenoxyacetic acid and 4-methoxyphenylacetic acid in supercritical carbon dioxide. *Fluid Phase Equilib.* **2009**, *275*, 33.
(41) Bristow, S.; Shekunov, B. Y.; York, P. Solubility analysis of drug compounds in supercritical carbon dioxide using static and dynamic extraction systems. *Ind. Eng. Chem. Res.* **2001**, *40*, 1732.
(42) Murga, R.; Sanz, M. T.; Beltrán, S.; Cabezas, J. L. Solubility of some phenolic compounds contained in grape seeds, in supercritical carbon dioxide. *J. Supercrit. Fluids* **2002**, *23*, 113.
(43) Johannsen, M.; Brunner, G. Solubilities of the fat-soluble vitamins A, D, E and K in supercritical carbon dioxide. *J. Chem. Eng. Data* **1997**, *42*, 106.
(44) Hojjati, M.; Vatanara, A.; Yamini, Y.; Moradi, M.; Najafabadi, A. R. Supercritical CO_2 and highly selective aromatase inhibitors: Experimental solubility and empirical data correlation. *J. Supercrit. Fluids* **2009**, *50*, 203.
(45) Shamsipur, M.; Karami, A. R.; Yamini, Y.; Sharghi, H. Solubilities of some 1-hydroxy-9,10-anthraquinone derivatives in supercritical carbon dioxide. *J. Supercrit. Fluids* **2004**, *32*, 47.
(46) Huang, Z.; Lu, W. D.; Kawi, S.; Chiew, Y. C. Solubility of aspirin in supercritical carbon dioxide with and without acetone. *J. Chem. Eng. Data* **2004**, *49*, 1323.
(47) Hojjati, M.; Yamini, Y.; Khajeh, M.; Vatanara, A. Solubility of some statin drugs in supercritical carbon dioxide and representing the solute solubility data with several density-based correlations. *J. Supercrit. Fluids* **2007**, *41*, 187.
(48) de la Fuente, J. C.; Quezada, N.; del Valle, J. M. Solubility of boldo leaf antioxidant components (Boldine) in high-pressure carbon dioxide. *Fluid Phase Equilib.* **2005**, *235*, 196.
(49) Murga, R.; Sanz, M. T.; Beltrán, S.; Cabezas, J. L. Solubility of three hydroxycinnamic acids in supercritical carbon dioxide. *J. Supercrit. Fluids* **2003**, *27*, 239.
(50) Johannsen, M.; Bruneer, G. Solubilities of the xanthines caffeine, theophylline and theobromine in supercritical carbon dioxide. *Fluid Phase Equilib.* **1994**, *95*, 215.
(51) Park, C. I.; Shin, M. S.; Kim, H. Solubility of climbazole and triclocarban in supercritical carbon dioxide: Measurement and correlation. *J. Chem. Thermodyn.* **2009**, *41*, 30.
(52) Chen, Y. M.; Lin, P. C.; Tang, M.; Chen, Y. P. Solid solubility of antilipemic agents and micronization of gemfibrozil in supercritical carbon dioxide. *J. Supercrit. Fluids* **2010**, *52*, 175.
(53) Hosseini, M. H.; Alizadeh, N.; Khanchi, A. R. Solubility analysis of clozapine and lamotrigine in supercritical carbon dioxide using static system. *J. Supercrit. Fluids* **2010**, *52*, 30.
(54) Rodrigues, R. F.; Tashima, A. K.; Pereira, R. S. M.; Mohamed, R. S.; Cabral, F. A. Coumarin solubility and extraction from emburana (*Torresea cearensis*) seeds with supercritical carbon dioxide. *J. Supercrit. Fluids* **2008**, *43*, 375.
(55) Nunes, A. V. M; Sampaio de Sousa, A. R.; Nunes da Ponte, M.; Duarte, C. M. M. Phase behaviour study of chalcone in dense CO_2. *J. Supercrit. Fluids* **2009**, *49*, 9.
(56) Kosal, E.; Lee, C. H.; Holder, G. D. Solubility of progesterone, testosterone, and cholesterol in supercritical fluids. *J. Supercrit. Fluids* **1992**, *5*, 169.
(57) Pérez, E.; Cabañas, A.; Sánchez-Vicente, Y.; Renuncio, J. A. R.; Pando, C. High-pressure phase equilibria for the binary system carbon dioxide + dibenzofuran. *J. Supercrit. Fluids* **2008**, *46*, 238.
(58) Skerget, M.; Cretnik, L.; Knez, Z.; Skrinjar, M. Influence of the aromatic ring substituents on phase equilibria of vanillins in binary systems with CO_2. *Fluid Phase Equilib.* **2005**, *231*, 11.
(59) Yamini, Y.; Kalantarian, P.; Hojjati, M.; Esrafily, A.; Moradi, M.; Vatanara, A.; Harrian, I. Solubilities of flutamide, dutasteride, and finasteride as antiandrogenic agents, in supercritical carbon dioxide: Measurement and correlation. *J. Chem. Eng. Data* **2010**, *55*, 1056.
(60) Charoenchaitrakool, M.; Dehghani, F.; Foster, N. R.; Chan, H. K. Micronization by rapid expansion of supercritical solutions to enhance the dissolution rates of poorly water-soluble pharmaceuticals. *Ind. Eng. Chem. Res.* **2000**, *39*, 4794.
(61) Coimbra, P.; Fernandes, D.; Ferreira, P.; Gil, M. H.; de Sousa, H. C. Solubility of Irgacure 2959 photoinitiator in supercritical carbon dioxide: Experimental determination and correlation. *J. Supercrit. Fluids* **2008**, *45*, 272.
(62) Macnaughton, S. J.; Kikic, I.; Foster, N. R.; Alessi, P.; Cortesi, A.; Colombo, I. Solubility of anti-inflammatory drugs in supercritical carbon dioxide. *J. Chem. Eng. Data* **1996**, *41*, 1083.
(63) Sahihi, M.; Ghaziaskar, H. S.; Hajebrahimi, M. Solubility of maleic acid in supercritical carbon dioxide. *J. Chem. Eng. Data* **2010**, *55*, 2596.
(64) Yamini, Y.; Arab, J.; Asghari-Khiavi, M. Solubilities of phenazopyridine, propranolol, and methimazole in supercritical carbon dioxide. *J. Pharm. Biomed. Anal.* **2003**, *32*, 181.
(65) Su, C. S.; Chen, Y. P. Measurement and correlation for the solid solubility of non-steroidal anti-inflammatory drugs (NSAIDs) in supercritical carbon dioxide. *J. Supercrit. Fluids* **2008**, *43*, 438.
(66) Ting, S. S. T.; Macnaughton, S. J.; Tomasko, D. L.; Foster, N. R. Solubility of naproxen in supercritical carbon dioxide with and without cosolvents. *Ind. Eng. Chem. Res.* **1993**, *32*, 1471.
(67) Knez, Z.; Skerget, M.; Sencar-Bozic, P.; Rizner, A. Solubility of nifedipine and nitrendipine in supercritical CO_2. *J. Chem. Eng. Data* **1995**, *40*, 216.
(68) Lucien, F. P.; Foster, N. R. Influence of matrix composition on the solubility of hydroxybenzoic acid isomers in supercritical carbon dioxide. *Ind. Eng. Chem. Res.* **1996**, *35*, 4686.
(69) Tian, G.; Jin, J.; Zhang, Z.; Guo, J. Solubility of mixed solids in supercritical carbon dioxide. *Fluid Phase Equilib.* **2007**, *251*, 47.
(70) Favareto, R.; Fregadolli, P. H.; Cabral, V. F.; Antunes, O. A. C.; Cardozo-Filho, L. Phase equilibria of acrylonitrile and *p*-bromobenzaldehyde in carbon dioxide. *J. Chem. Eng. Data* **2008**, *53*, 1080.
(71) Gordillo, M. D.; Blanco, M. A.; Molero, A.; Martínez de la Ossa, E. Solubility of the antibiotic Penicillin G in supercritical carbon dioxide. *J. Supercrit. Fluids* **1999**, *15*, 183.
(72) Ch, R.; Garlapati, C.; Madras, G. Solubility of *n*-(4-Ethoxyphenyl)ethanamide in supercritical carbon dioxide. *J. Chem. Eng. Data* **2010**, *55*, 1437.
(73) Wells, P. A.; Chaplin, R. P.; Foster, N. R. Solubility of phenylacetic acid and vanillan in supercritical carbon dioxide. *J. Supercrit. Fluids* **1990**, *3*, 8.

(74) Türk, M.; Upper, G.; Hils, P. Formation of composite drug–polymer particles by co-precipitation during the rapid expansion of supercritical fluids. *J. Supercrit. Fluids* **2006**, *39*, 253.
(75) Cortesi, A.; Kikic, I.; Alessi, P.; Turtoi, G.; Garnier, S. Effect of chemical structure on the solubility of antioxidants in supercritical carbon dioxide: experimental data and correlation. *J. Supercrit. Fluids* **1999**, *14*, 139.
(76) Reverchon, E.; Donsi, G. Salicylic acid solubilization in supercritical CO_2 and its micronization by RESS. *J. Supercrit. Fluids* **1993**, *6*, 241.
(77) Sun, Y.; Li, S.; Quan, C. Solubility of ferulic acid and tetramethylpyrazine in supercritical carbon dioxide. *J. Chem. Eng. Data* **2005**, *50*, 1125.
(78) Liu, T.; Li, S.; Zhou, R.; Jia, D.; Tian, S. Solubility of triphenylmethyl chloride and triphenyltin chloride in supercritical carbon dioxide. *J. Chem. Eng. Data* **2009**, *54*, 1913.
(79) Burgos-Solórzano, G. I.; Brennecke, J. F.; Stadtherr, M. A. Solubility measurements and modeling of molecules of biological and pharmaceutical interest with supercritical CO_2. *Fluid Phase Equilib.* **2004**, *220*, 55.
(80) Stassi, A.; Bettini, R.; Gazzaniga, A.; Giordano, F.; Schiraldi, A. Assessment of solubility of ketoprofen and vanillic acid in supercritical carbon CO_2 under dynamic conditions. *J. Chem. Eng. Data* **2000**, *45*, 161.
(81) Huang, Z.; Yang, X. W.; Sun, G. B.; Song, S. W.; Kawi, S. The solubilities of xanthone and xanthene in supercritical carbon dioxide: Structure effect. *J. Supercrit. Fluids* **2005**, *36*, 91.
(82) Perlovich, G. L.; Volkova, T. V.; Bauer-Brandl, A. Towards and understanding of the molecular mechanism of solvation of drug molecules: A thermodynamic approach by crystal lattice energy, sublimation, and solubility exemplified by paracetamol, acetanilide, and phenacetin. *J. Pharm. Sci.* **2006**, *95*, 2158.
(83) Perlovich, G. L.; Kurkov, S. V.; Kinchin, A. N.; Bauer-Brandl, A. Solvation and hydration characteristics of ibruprofen and acetylsalycilic acid. *AAPS Pharm. Sci.* **2006**, *6*, 1.
(84) Chickos, J. S.; Acree, W., Jr. Enthalpies of sublimation of organic and organometallic compounds. 1910–2001. *J. Phys. Chem. Ref. Data* **2002**, *2*, 537.
(85) Perlovich, G. L.; Kurkov, S. V.; Kinchin, A. N.; Bauer-Brandl, A. Thermodynamics of solution III: Comparison of the solvation of (+)-naproxen with other NSAIDs. *Eur. J. Pharm. Biopharm.* **2004**, *57*, 411.
(86) McHugh, M.; Paulaitis, M. E. Solid solubilities of naphthalene and biphenyl in supercritical carbon dioxide. *J. Chem. Eng. Data* **1980**, *25*, 326.
(87) Huang, Z.; Kawi, S.; Chiew, Y. C. Solubility of cholesterol and its esters in supercritical carbon dioxide with and without cosolvents. *J. Supercrit. Fluids* **2004**, *30*, 25.
(88) Yun, S. L. J.; Liong, K. K.; Gurdial, G. S.; Foster, N. R. Solubility of cholesterol in supercritical carbon dioxide. *Ind. Eng. Chem. Res.* **1991**, *30*, 2476.
(89) Wong, J. M.; Johnston, K. P. Solubilization of biomolecules in carbon dioxide based supercritical fluids. *Biotechnol. Prog.* **1986**, *2*, 29.
(90) Chim, R.; Marceneiro, S.; Braga, M. E. M.; Dias, A. M. A.; de Sousa, H. C. Solubility of norfloxacin and ofloxacin in supercritical carbon dioxide. *Fluid Phase Equilib.* **2012**, *331*, 6.
(91) Roux, M. V.; Temprado, M.; Chickos, J. S.; Nagano, Y. Critically evaluated thermochemical properties of polycyclic aromatic hydrocarbons. *J. Phys. Chem. Ref. Data* **2008**, *37*, 1855.
(92) Sparks, D. L.; Estévez, L. A.; Hernández, R.; McEwen, J.; French, T. Solubility of small-chain carboxylic acids in supercritical carbon dioxide. *J. Chem. Eng. Data* **2010**, *55*, 4922.
(93) Garlapati, C.; Madras, G. Solubilities of dodecanoic and tetradecanoic acids in supercritical CO_2 with and without entrainers. *J. Chem. Eng. Data* **2008**, *53*, 2637.
(94) Garlapati, C.; Madras, G. Solubilities of hexadecanoic and octadecanoic acids in supercritical CO_2 with and without cosolvents. *J. Chem. Eng. Data* **2008**, *53*, 2913.

Supporting information for the article:

An empirical analysis of the solubility of pharmaceuticals in supercritical carbon dioxide using sublimation enthalpies.

Antonio Tabernero, Eva M. Martín del Valle, Miguel A. Galán

Department of Chemical Engineering, University of Salamanca, P/Los Caídos S/N, 37008 Salamanca, Spain

Table 1. Results of $a_1+b\cdot\rho$ at 308 K for different pressures.

Solid	ΔH_{sub}(kJ·mol^{-1})	Pressure (atm)	$a_1+b\cdot\rho$
2,3,5-Trimethylphenol	87.48	100-280	32.72-34.48
2,3-Dimethylnaphthalene	80.14	97-280	29.77-31.88
2,3-Dimethylphenol	81.41	100-280	31.19-33.27
2,4,6-Trichlorophenol	108.60	90-160	42.12-43.45
2,4,6-Trimethylphenol	93.10	100-280	36.70-38.18
2,4-Dichloro-1-naphthol	116.53	100-350	41.91-44.22
2,4-Dichlorophenol	95.13	90-160	38.21-39.50
2,5-Dimethylphenol	81.41	100-280	31.32-32.95
2,6-Dimethylnaphthalene	80.14	97-280	29.50-31.50
2-Methyl-N-phenylacetamide	84.29	121-225	27.51-29.69
4-Chlorophenol	82.20	90-160	32.14-33.34
4-Methoxyphenylacetic acid	98.81	116-236	33.58-35.88
4-Methyl-N-phenylacetamide	84.29	121-225	27.98-29.60
4-Phenylphenol	105.37	100-280	35.69-37.87
4-Tert-butyl-phenol	82.02	100-280	30.84-32.77
Anastrozole	129.40	122-355	43.91-46.10
AQ1[a] (1-hydroxy-9,10-anthraquinone)	121.89	121-355	43.07-44.56
AQ2 [a] (1-hydroxy-9,10-anthraquinone)	127.96	121-355	45.32-47.55
AQ3 [a] (1-hydroxy-9,10-anthraquinone)	137.23	121-355	49.14-51.07
AQ4 [a] (1-hydroxy-9,10-anthraquinone)	140.61	121-355	50.63-52.80
AQ5 [a] (1-hydroxy-9,10-anthraquinone)	143.99	121-355	52.17-54.47
AQ6 [a] (1-hydroxy-9,10-anthraquinone)	143.99	121-355	52.67-54.87
AQ7 [a] (1-hydroxy-9,10-anthraquinone)	147.37	121-355	54.15-54.93
Aspirin	109.70	120-250	38.29-39.69
Atorvastatin	167.40	121-355	59.17-62.31
Boldine	188.29	100-410	62.69-67.98
Cinnamic acid	90.33	149-231	31.40-32.47
Clofibric acid	108.97	100-220	38.93-40.53
Chalcone	98.95	120-190	36.36-37.46
Dibenzofuran[b]	82.00	105-275	30.98-32.79
Examestane	122.80	122-355	41.36-44.47
Fenofibrate	131.91	100-220	49.92-51.74
Fluvastatin	136.10	121-355	47.08-49.53
Gemfibrozil	140.28	100-220	48.80-50.61
Ibuprofen	93.54	80-220	31.20-36.53
Irgu2959	110.20	101-255	37.51-39.62
Letrozole	129.90	121-355	42.62-44.54
Lovastatin	90.60	121-355	29.53-31.05

Methimazole	87.20	122-355	27.98-30.23
N-phenylacetamide	78.22	104-225	25.41-27.46
o-phthalic acid	118.34	80-210	36.71-39.03
p-aminobenzoic acid	103.18	80-210	31.07-33.25
Phenacetin	93.56	90-190	29.70-31.36
Phenazopyridine	93.00	122-355	29.96-32.41
Phenoxyacetic acid	89.36	123-225	30.74-32.38
Phenylacetic acid	86.85	83-184	35.36-38.85
Propanolol	123.40	122-355	42.79-45.29
Rosuvastatin	122.20	122-355	41.79-43.88
Simvastatin	109.40	122-355	37.11-39.74
Triphenylmethyl chloride	131.27	150-400	48.54-50.24
Xanthone	89.31	120-300	30.48-32.60

[a] AQ1, AQ2, AQ3, AQ4, AQ5, AQ6 and AQ7 are different 1-hydroxy-9,10-anthraquinone derivatives.
[b] The experimental temperature is 309 K.

Table 2. Results of $a_1+b\cdot\rho$ at 313 K for different pressures.

Solid	ΔH_{sub}(kJ·mol^{-1})	Pressure (atm)	$a_1+b\cdot\rho$
1,5-Naphthalenediamine	109.92	110-200	34.65-36.31
2,4,6-Trichlorophenol	108.60	90-160	40.29-42.85
2,4-Dichlorophenol	95.13	90-160	36.49-39.00
2-Methylbenzoic acid	89.54	110-246	32.03-33.93
3-Methyl benzoic acid	89.54	110-246	32.06-33.96
4-Chlorophenol	82.20	90-160	30.61-32.94
4-Methyl benzoic acid	89.54	110-246	30.18-31.00
4,4'-Diaminodiphenylmethane	135.60	110-200	43.96-45.79
Acetaminophen	117.90	100-250	35.15-37.33
Acid protocatechuic	124.81	150-500	37.17-39.80
Alpha-tocopherol	102.20	199-349	38.07-39.34
Beta-carotene	128.70	200-350	38.39-39.97
Boldine	188.29	95-380	60.63-67.54
Caffeic acid	117.17	150-500	37.59-41.15
Caffeine	105.10	199-349	37.68-38.73
Climbazole	119.38	150-400	43.28-46.56
Chalcone[a]	98.95	90-220	33.26-37.63
Cholesterol	114.60	99-272	38.39-41.24
Ethyl vanillin	101.50	100-301	38.07-39.94
Ferulic acid	122.96	100-500	34.63-38.77
Ibuprofen	93.54	95-220	32.96-36.38
Ketoprofen[b]	112.00	100-220	36.29-39.09
Naproxen	128.30	90-193	40.54-43.93
Nimesulide	82.20	130-220	25.28-27.51
p-bromobenzaldehyde	89.81	90-109	32.44-32.93
Penicillin G	122.20	100-300	38.69-42.07
Piroxicam[b]	122.45	100-220	38.67-42.45
Progesterone	93.90	104-240	30.93-34.28
Propyl gallate	135.53	150-250	44.91-46.04
Protocatechualdehyde	127.60	100-500	39.00-43.84
Retinol	66.04	200-350	24.36-25.71
Salicylic acid	104.14	100-350	35.90-38.40
Testosterone	110.50	103-238	34.62-38.11
Theobromine	126.00	213-345	39.95-41.07
Theophylline	126.00	199-349	42.21-43.01
Triclocarban	160.12	110-390	57.17-60.51
Uracil	127.00	125-300	40.71-44.26

Vanillic acid	116.10	86-250	35.89-38.80
Vanillin	88.70	87-235	29.49-34.07
Vitamin D2	122.50	200-320	44.45-45.28
Vitamin D3	122.40	151-297	43.85-45.16
Vitamin K1	87.93	200-350	32.37-34.04

[a]The experimental temperature is 315 K.
[b]The experimental temperature is 312 K.

Table 3. Results of $a_1+b\cdot\rho$ at 318 K for different pressures.

Solid	ΔH_{sub}(kJ·mol^{-1})	Pressure (atm)	$a_1+b\cdot\rho$
2,3-Dimethylnaphthalene	80.14	98-280	28.29-31.03
2,4,6-Trichlorophenol	108.60	90-160	38.61-42.28
2,4-Dichloro-1-naphthol	116.53	100-350	39.70-43.05
2,6-Dimethylnaphthalene	80.14	90-280	27.78-30.95
2-Methyl-N-phenylacetamide	84.29	121-225	26.43-29.14
4-Aminoantipyrine	135.20	100-220	45.85-48.37
4-Dimethylaminoantipyrine	80.20	100-220	26.85-29.30
4-Methoxyphenylacetic acid	98.81	126-230	32.28-35.08
4-Methyl-N-phenylacetamide	84.29	121-225	26.97-29.02
Anastrozole	129.40	122-355	41.96-45.05
Antipyrine	109.90	100-220	36.89-39.55
AQ1[a] (1-hydroxy-9,10-anthraquinone)	121.89	121-355	40.73-43.33
AQ2[a] (1-hydroxy-9,10-anthraquinone)	127.96	121-355	43.28-46.19
AQ3[a] (1-hydroxy-9,10-anthraquinone)	137.23	121-355	47.08-49.57
AQ4[a] (1-hydroxy-9,10-anthraquinone)	140.61	121-355	48.75-51.43
AQ5[a] (1-hydroxy-9,10-anthraquinone)	143.99	121-355	50.23-53.16
AQ6[a] (1-hydroxy-9,10-anthraquinone)	143.99	121-355	50.23-53.39
AQ7[a] (1-hydroxy-9,10-anthraquinone)	147.37	121-355	51.65-54.93
Aspirin	109.70	120-250	36.49-38.73
Atorvastatin	167.40	121-355	56.39-61.03
Benzoic acid	83.47	120-280	29.60-31.82
Cinnamic acid	90.33	123-230	29.00-31.67
Clofibric acid	108.97	100-220	36.37-39.40
Clozapine	212.34	121-354	72.20-74.88
Coumarin	83.10	110-240	30.53-33.33
Dibenzofuran[b]	82.00	105-225	29.32-31.83
Diflunisal	120.10	94-246	33.17-38.81
Eflucimibe	157.90	93-301	46.65-51.93
Examestane	122.80	122-355	40.82-44.19
Fenofibrate	131.91	100-220	46.53-50.20
Flutamide	86.00	121-355	26.44-29.62
Fluvastatin	136.10	121-355	44.82-48.51
Gemfibrozil	140.28	100-220	45.61-49.17
Ibuprofen	93.54	85-170	29.52-35.39
Irgu2959	110.20	101-256	35.11-38.65
Lamotrigine	160.63	121-355	51.66-53.92
Letrozole	129.90	121-355	41.04-43.71
Lovastatin	90.60	121-355	28.51-30.27

Maleic acid	105.40	70-300	32.73-34.74
Methimazole	87.20	122-355	26.34-29.45
Nabumetone	101.26	101-220	34.70-37.51
N-phenylacetamide	78.22	104-225	24.07-27.04
o-HBA	104.14	101-202	34.75-36.93
o-phthalic acid	118.34	80-210	35.26-37.83
p-aminobenzoic acid	103.18	80-210	29.78-32.15
p-HBA	104.14	101-202	29.61-31.88
Phenacetin	93.56	110-190	28.66-30.45
Phenazopyridine	93.00	122-355	28.32-31.70
Phenoxyacetic acid	89.36	125-220	29.49-31.63
Phenylacetic acid	86.85	93-191	33.61-38.67
Progesterone	93.90	105-240	29.86-33.73
Propanolol	123.40	122-355	40.83-44.39
Rosuvastatin	122.20	122-355	39.57-42.91
Salicylamide	89.76	101-221	28.17-30.52
Simvastatin	109.40	122-355	35.10-38.74
Testosterone	110.50	86-240	30.65-37.61
Tetramethylpyrazine	94.60	100-300	35.42-37.57

[a] AQ1, AQ2, AQ3, AQ4, AQ5, AQ6 and AQ7 are different 1-hydroxy-9,10-anthraquinone derivatives.
[b] The experimental temperature is 309 K.

Table 4. Results of $a_1+b\cdot\rho$ at 323 K for different pressures.

Solid	**ΔH_{sub}(kJ·mol^{-1})**	**Pressure (atm)**	**$a_1+b\cdot\rho$**
1,5-Naphthalenediamine	109.92	110-200	33.05-35.11
2-Methylbenzoic acid	89.54	110-246	30.22-33.27
3-Methyl benzoic acid	89.54	110-246	30.05-33.28
4-Methyl benzoic acid	89.54	110-246	28.35-31.26
4,4'-Diaminodiphenylmethane	135.60	110-200	41.92-44.40
Acid protocatechuic	124.81	150-500	35.93-39.20
Boldine	188.29	105-380	61.90-65.66
Caffeic acid	117.17	150-500	36.58-40.13
Climbazole	124.38	130-365	42.10-45.07
Chalcone	98.95	100-210	32.37-36.58
Ferulic acid	122.96	100-500	31.83-38.21
Naproxen	128.30	100-193	39.77-42.58
p-bromobenzaldehyde	89.81	102-111	31.50-31.88
Penicillin G	122.20	150-350	38.70-41.39
Phytosterol	93.65	143-312	29.62-31.75
Protocatechualdehyde	127.60	150-500	39.44-42.79
Triclocarban	160.12	120-335	55.04-58.43
Triphenylmethyl chloride	131.27	150-400	46.15-48.47

Table 5. Results of $a_1+b\cdot\rho$ at 328 K for different pressures.

Solid	ΔH_{sub}(kJ·mol^{-1})	Pressure (atm)	$a_1+b\cdot\rho$
2,3-Dimethylnaphthalene	80.14	98-280	26.52-30.33
2,4-Dichloro-1-naphthol	116.53	100-350	38.26-41.98
2,6-Dimethylnaphthalene	80.14	96-280	26.20-30.31
2-Methyl-N-phenylacetamide	84.29	123-225	25.14-28.68
4-Aminoantipyrine	135.20	100-220	43.28-47.00
4-Dimethylaminoantipyrine	80.20	100-220	25.08-28.76
4-Methoxyphenylacetic acid	98.81	142-234	31.37-34.35
4-Methyl-N-phenylacetamide	84.29	123-225	25.39-28.67
Anastrozole	129.40	122-355	38.83-44.37
Antipyrine	109.90	100-220	34.95-38.44
AQ1[a] (1-hydroxy-9,10-anthraquinone)	121.89	121-355	38.96-42.17
AQ2 [a] (1-hydroxy-9,10-anthraquinone)	127.96	121-355	40.89-45.08
AQ3 [a] (1-hydroxy-9,10-anthraquinone)	137.23	121-355	44.94-48.24
AQ4 [a] (1-hydroxy-9,10-anthraquinone)	140.61	121-355	46.25-50.08
AQ5 [a] (1-hydroxy-9,10-anthraquinone)	143.99	121-355	47.66-51.76
AQ6 [a] (1-hydroxy-9,10-anthraquinone)	143.99	121-355	47.57-52.07
AQ7 [a] (1-hydroxy-9,10-anthraquinone)	147.37	121-355	49.37-54.45
Aspirin	109.70	120-230	35.19-37.64
Atorvastatin	167.40	121-355	53.25-59.76
Benzoic acid	83.47	120-280	27.47-31.30
Cinnamic acid	90.33	125-231	27.66-30.83
Clofibric acid	108.97	100-220	34.48-38.33
Coumarin	83.10	110-200	29.02-32.07
Cholesterol	114.60	101-272	34.61-39.38
Dibenzofuran	82.00	130-185	29.32-30.81
Examestane	122.80	122-355	38.75-43.54
Fenofibrate	131.91	100-220	43.94-48,80
Flutamide	86.00	121-355	24.61-28.98
Fluvastatin	136.10	121-355	42.07-47.49
Gemfibrozil	140.28	100-200	41.93-47.80
Irgu2959	110.20	102-253	33.16-37.79
Lamotrigine	160.63	121-355	49.35-52.31
Letrozole	129.90	121-355	39.35-42.92
Lovastatin	90.60	121-355	26.98-29.51
Methimazole	87.20	122-355	24.47-28.78
Nabumetone	101.26	101-220	32.73-36.61
N-phenylacetamide	78.22	104-225	23.06-26.44
o-HBA	104.14	101-202	33.05-36.02

o-phthalic acid	118.34	80-210	33.92-36.56
p-aminobenzoic acid	103.18	80-210	28.63-31.07
p-HBA	104.14	121-202	28.74-31.00
Phenacetin	93.56	110-190	27.12-29.49
Phenazopyridine	93.00	122-355	26.37-30.85
Phenoxyacetic acid	89.36	117-222	27.54-31.02
Progesterone	93.90	107-240	26.01-32.77
Propanolol	123.40	122-355	37.79-43.72
Rosuvastatin	122.20	122-355	37.50-41.79
Salicylamide	89.76	100-220	26.60-29.79
Simvastatin	109.40	122-355	32.59-37.87
Testosterone	110.50	86-239	28.49-36.48
Tetramethylpyrazine	94.60	100-300	34.82-37.39
Vanillic acid	116.10	90-250	32.54-37.45
Xanthone	89.31	120-300	27.82-30.84

[a] AQ1, AQ2, AQ3, AQ4, AQ5, AQ6 and AQ7 are different 1-hydroxy-9,10-anthraquinone derivatives.

Table 6. Results of $a_1+b\cdot\rho$ at 333 K for different pressures.

Solid	ΔH_{sub}(kJ·mol^{-1})	Pressure (atm)	$a_1+b\cdot\rho$
1,5-Naphthalenediamine	109.92	110-200	31.67-34.02
2-Methylbenzoic acid	89.54	110-246	28.85-32.67
3-Methyl benzoic acid	89.54	110-246	28.64-32.62
4-Methyl benzoic acid	89.54	110-246	27.04-30.57
4,4'-Diaminodiphenylmethane	135.60	110-200	40.44-43.07
Acid protocatechuic	124.81	150-500	34.22-38.45
Alpha-tocopherol	102.20	199-349	35.38-37.14
Beta-carotene	128.70	200-350	36.77-38.81
Boldine	188.29	105-390	57.78-64.21
Caffeic acid	137.17	150-500	35.31-38.95
Caffeine	105.10	199-349	35.21-36.60
Climbazole	119.38	145-360	40.83-43.73
Cholesterol	114.60	99-269	33.73-39.06
Ethyl vanillin	101.50	81-296	31.93-38.27
Ferulic acid	122.96	100-500	29.98-37.09
Ketoprofen[a]	112.00	115,6-220	33.26-37.27
Maleic acid	105.40	70-300	32.05-34.39
Naproxen	128.30	124-193	39.12-41.24
Nimesulide	82.20	130-220	23.14-26.01
Nitrendipine	94.80	117-300	26.24-29.92
p-bromobenzaldehyde	89.81	109-118	30.56-30.92
Penicillin G	122.20	100-350	34.07-40.33
Phytosterol	93.65	176-271	29.28-30.61
Piroxicam[a]	122.45	130-220	36.32-39.67
Propyl gallate	135.53	150-250	42.10-43.58
Protocatechualdehyde	127.60	150-500	37.65-42.31
Retinol	66.04	200-260	22.63-23.60
Salicylic acid	104.14	115-325	33.68-36.14
Theobromine	126.00	193-344	37.51-38.60
Theophylline	126.00	199-349	39.74-40.50
Triclocarban	160.12	140-305	53.28-56.52
Uracil	127.00	125-300	35.36-42.64
Vanillin	88.70	84-233	27.36-32.37
Vitamin D2	122.50	200-300	41.47-42.73
Vitamin D3	122.40	99,5-209	40.76-42.51
Vitamin K1	87.93	200-350	29.88-31.95

[a]The experimental temperature is 331 K.

Table 7. Results of $a_1+b\cdot\rho$ at 338 K for different pressures.

Solid	ΔH_{sub}(kJ·mol^{-1})	Pressure (atm)	$a_1+b\cdot\rho$
Anastrozole	129.40	122-355	38.22-43.55
AQ1 [a] (1-hydroxy-9,10-anthraquinone)	121.89	121-355	37.28-41.29
AQ2 [a] (1-hydroxy-9,10-anthraquinone)	127.96	121-355	39.41-43.93
AQ3 [a] (1-hydroxy-9,10-anthraquinone)	137.23	121-355	42.65-47.02
AQ4 [a] (1-hydroxy-9,10-anthraquinone)	140.61	121-355	43.70-48.77
AQ5 [a] (1-hydroxy-9,10-anthraquinone)	143.99	121-355	45.59-50.53
AQ6 [a] (1-hydroxy-9,10-anthraquinone)	143.99	121-355	45.38-50.81
AQ7 [a] (1-hydroxy-9,10-anthraquinone)	147.37	121-355	46.66-52.04
Atorvastatin	167.40	121-355	50.65-58.48
Benzoic acid	83.47	120-280	25.44-30.72
Clozapine	212.34	121-354	65.92-71.05
Chalcone	98.95	120-205	31.20-34.52
Dibenzofuran	82.00	135-200	28.36-30.08
Examestane	122.80	122-355	36.93-42.85
Flutamide	86.00	121-355	22.55-28.51
Fluvastatin	136.10	121-355	39.72-46.49
Lamotrigine	160.63	121-355	47.26-50.77
Letrozole	129.90	121-355	37.29-42.25
Lovastatin	90.60	121-355	25.67-28.76
Methimazole	87.20	122-355	23.04-28.09
Phenazopyridine	93.00	122-355	24.72-30.28
Propanolol	123.40	122-355	35.52-43.00
Rosuvastatin	122.20	122-355	35.46-40.78
Simvastatin	109.40	122-355	30.45-37.02
Tetramethylpyrazine	94.60	100-300	34.70-37.33
Triphenylmethyl chloride	131.27	150-400	43.76-46.79

[a]AQ1, AQ2, AQ3, AQ4, AQ5, AQ6 and AQ7 are different 1-hydroxy-9,10-anthraquinone derivatives.

Table 8. Results of $a_1+b\cdot\rho$ at 348 K for different pressures.

Solid	ΔH_{sub}(kJ·mol^{-1})	Pressure (atm)	$a_1+b\cdot\rho$
Anastrozole	129.40	122-355	37.10-42.73
AQ1 [a] (1-hydroxy-9,10-anthraquinone)	121.89	121-355	36.46-40.31
AQ2 [a] (1-hydroxy-9,10-anthraquinone)	127.96	121-355	38.13-42.91
AQ3 [a] (1-hydroxy-9,10-anthraquinone)	137.23	121-355	41.47-45.84
AQ4 [a] (1-hydroxy-9,10-anthraquinone)	140.61	121-355	41.99-47.64
AQ5 [a] (1-hydroxy-9,10-anthraquinone)	143.99	121-355	43.79-49.27
AQ6 [a] (1-hydroxy-9,10-anthraquinone)	143.99	121-355	44.26-49.77
AQ7 [a] (1-hydroxy-9,10-anthraquinone)	147.37	121-355	43.90-50.88
Atorvastatin	167.40	121-355	49.18-57.22
Clozapine	212.34	121-354	63.36-69.22
Examestane	122.80	122-355	36.08-42.06
Flutamide	86.00	121-355	21.52-27.99
Fluvastatin	136.10	121-355	38.40-45.51
Lamotrigine	160.63	121-355	45.45-49.38
Letrozole	129.90	121-355	35.58-41.63
Lovastatin	90.60	121-355	24.79-28.07
Maleic acid	105.40	70-300	32.58-34.73
Methimazole	87.20	122-355	22.09-27.44
Phenazopyridine	93.00	122-355	24.07-29.55
Propanolol	123.40	122-355	32.27-42.85
Rosuvastatin	122.20	122-355	34.32-39.81
Simvastatin	109.40	122-355	28.88-36.16

[a]AQ1, AQ2, AQ3, AQ4, AQ5, AQ6 and AQ7 are different 1-hydroxy-9,10-anthraquinone derivatives.

8.3. Conclusiones

En el artículo anterior se ha procedido al desarrollo de un test de consistencia para evaluar la solubilidad de nuevos datos experimentales de fármacos en CO_2sc.

Este test se basa en la definición de un factor de mejora modificado, cuyo valor se mantiene constante para sólidos polares con similares entalpías de sublimación a las mismas condiciones experimentales.

Después de estudiar más de 2300 datos experimentales de solubilidad de sólidos en CO_2sc, se obtuvieron varias ecuaciones para predecir el anterior factor de mejora modificado en función de varias variables (entalpía de sublimación, presión y temperatura) con un error inferior al 5%. Estas ecuaciones pueden ser utilizadas como una herramienta para identificar la exactitud de nuevos datos experimentales.

Sin embargo, este test de consistencia no puede ser empleado con sólidos inorgánicos o con sólidos con larga cadena lineal, como los ácidos grasos.

● Referencias también citadas

[1] M. A. Saldaña; L. Sun; S. E. Guigard; F. Temelli, Conparison of the solubility of β-carotene in supercritical CO_2 based on a binary and a multicomponent complex system, J. Supercrit. Fluids 37 (2006) 342-349.

[2] I. Rodríguez-Maizoso; O. Werner; C. Quan; Z. Knez; C. Turner, Phase-behaviour of alkyl ketene dimmer (AKD) in supercritical carbon dioxide. The implications of using different solubility measurements methods. J. Supercrit. Fluids 61 (2012) 25-33.

[3] J. Méndez-Santiago; A. S. Teja, The solubility of solids in supercritical fluids, Fluid Phase Equilib. 158-160 (1999) 501-510.

[4] A. Vetere, A short-cut method to predict the solubilities of solids in supercritical carbon dioxide, Fluid Phase Equilib. 148 (1998) 83-93.

[5] J. Chrastil, Solubility of solids and liquids in supercritical gases, J. Phys. Chem. 86 (1982) 3016-3021.

CAPÍTULO 9.

Análisis teórico-experimental de la precipitación de sólidos mediante SEDS

Anteriormente, capítulo 4, se ha estudiado la influencia de la presión y la temperatura en la distribución de tamaño de partícula y la aparición de agregados en el proceso de precipitación de partículas con SEDS.

Sin embargo, otros parámetros importantes que pueden condicionar el proceso son los caudales de disolución y de antisolvente. Es por ello por lo que el presente apartado se estudiará la influencia de los mismos.

Este estudio es importante, ya que la variación de los caudales puede producir un cambio en el régimen de atomización de la disolución a alta presión y alterar de forma significativa el tamaño y morfología de las partículas obtenidas.

Lo que se pretende en este capítulo es correlacionar la distribución y tamaño de partícula y la formación de agregados con los diferentes regímenes de desintegración producidos debido al cambio de flujos.

Por otro lado, como se ha comentado con anterioridad existe un proceso de transferencia de materia entre la gota de disolución (formada debido al proceso de atomización) y el medio supercrítico.

Esta transferencia de materia puede caracterizarse en función de los respectivos coeficientes de película de transferencia tanto en la película del líquido como en la del fluido supercrítico.

Mediante el estudio de estos coeficientes se podrá definir el efecto de dicho transporte de materia sobre la distribución de tamaño de partícula y la morfología obtenida.

A continuación se comentarán las características especiales de los procesos de atomización y transferencia de materia que tienen lugar en un proceso SEDS.

9.1. Proceso de atomización.

La atomización se define como un proceso en el cuál un chorro líquido se convierte en gotas pequeñas.

Básicamente, esa ruptura es producida por la acción de unas fuerzas externas e internas, que sobrepasan las fuerzas de cohesión.

Después de esa ruptura, la tensión superficial transforma el líquido en gotas con forma de esfera, ya que esta geometría presenta la energía superficial mínima. Por otra parte, constituida la gota, la viscosidad del líquido se opone a un cambio en la geometría de la misma ejerciendo un efecto estabilizador [1].

Este efecto puede observarse en la figura 9.1

Figura 9.1. Desintegración de un chorro debido a fuerzas externas [1].

En el proceso de desintegración del chorro en gotas es importante conocer propiedades como la longitud de ruptura del chorro, el tamaño de gota, y también la manera en la que el chorro se desintegra (regímenes de desintegración). Dichos regímenes de desintegración son descritos en el siguiente apartado.

9.1.1. Regímenes de desintegración a condiciones atmosféricas

El mecanismo de desintegración de un chorro líquido en gotas lleva investigándose durante más de 100 años, debido a su influencia en el tamaño final de la gota [1].

Este fenómeno de desintegración depende de propiedades como la densidad del líquido y del gas, tensión superficial y viscosidad. Además, en la ruptura del chorro es muy importante la relación de velocidades entre la disolución y el gas que produce la desintegración.

Todas estas variables son introducidas en los números adimensionales de Reynolds, Weber y Ohnesorge (ecuaciones 9.1 a 9.3), donde ρ_D es la densidad de la disolución, v_D es la velocidad de la disolución, d_B es el diámetro de la boquilla, σ es la tensión superficial y μ es la viscosidad cinemática de la disolución.

$$\mathrm{Re} = \rho_D \cdot v_D \cdot d_B \Big/ \mu \qquad \text{(Ec. 9.1)}$$

$$We = \rho_D \cdot v_D^2 \cdot d_B \Big/ \sigma \qquad \text{(Ec. 9.2)}$$

$$Oh = \mu \Big/ (\rho_D \cdot \sigma \cdot d_B) \qquad \text{(Ec. 9.3)}$$

A partir de estos números adimensionales se describen los distintos mecanismos de desintegración del chorro.

Estos mecanismos de desintegración fueron clasificados por Ohnesorge, basándose en las distintas fuerzas que intervienen en un proceso de atomización en medio gaseoso. Dichas fuerzas se pueden identificar en capilares, inerciales, viscosas y aerodinámicas.

A partir de ellas, se establecieron tres mecanismos que rigen todo proceso de desintegración de un chorro líquido en un ambiente atmosférico [1].

Estos mecanismos se clasifican dependiendo del número de Reynolds y del número de Ohnesorge, como se muestra en la siguiente figura (fig. 9.2):

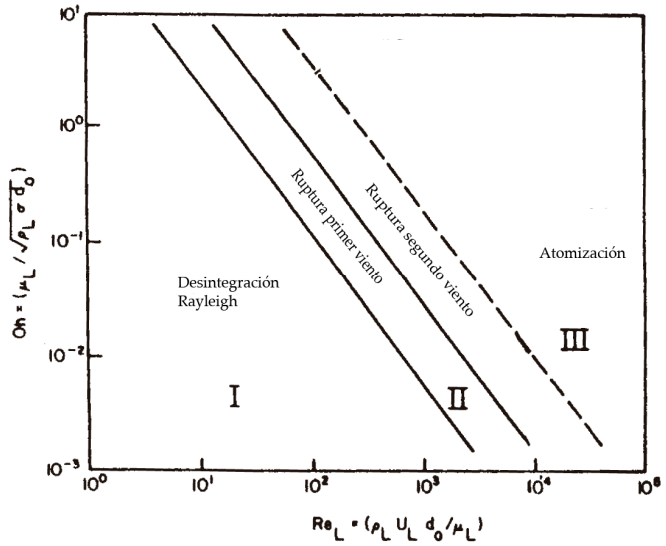

Figura 9.2. Diferentes mecanismos de desintegración de un chorro en función del Reynolds y del Ohnesorge [1].

A valores bajos de Reynolds, el chorro presenta unas perturbaciones axisimétricas, que producen una ruptura en gotas relativamente grandes. Este tipo de ruptura (zona I) está controlada por la tensión superficial, y fue enunciado por Rayleigh, por lo que se conoce mecanismo de desintegración de Rayleigh.

En la zona II (valores intermedios de Reynolds) se produce la desintegración del chorro debido a las oscilaciones producidas alrededor de su eje. La magnitud de estas oscilaciones aumenta con el incremento de la diferencia entre

la resistencia del chorro y del fluido que le rodea. El tamaño de las gotas producidas en este caso varía en un amplio intervalo.

Para valores altos del número de Reynolds (zona III), se produce la atomización a poca distancia del orificio de descarga. En estas condiciones se obtienen las gotas de menor tamaño.

Finalmente, cuando el valor de flujo de la disolución sobrepasa un cierto valor límite, las fuerzas aerodinámicas controlan la ruptura del chorro y después de la zona de desintegración se forma una especie de cono de disolución atomizada. En este caso se produce además una atomización secundaria (ruptura de las primeras gotas producidas).

Otra de las propiedades más importantes de un proceso de atomización es la longitud previa a la desintegración.

Partiendo de la representación de este parámetro frente a la velocidad, se pueden representar los distintos mecanismos de desintegración: Primeramente aumenta la longitud de ruptura con la velocidad, posteriormente este comportamiento se invierte, disminuyendo la longitud del chorro con un incremento de velocidad hasta alcanzar un cierto valor de velocidad. A partir de esta velocidad la longitud del chorro se mantiene constante, existiendo además atomización secundaria.

Este fenómeno puede observarse en las figuras 9.3, que representa la ruptura de un chorro en un medio gaseoso de CO_2 a condiciones subcríticas [2].

A partir de esta figura se pueden identificar los distintos regímenes de desintegración. De la fotografía a) a la d) el chorro adquiere una forma axisimétrica, que coincide con un aumento de la longitud de ruptura del chorro (zona I en la figura 9.2).

Por otra parte, de la imagen e) a la h) el chorro presenta una forma asimétrica, y la longitud de ruptura disminuye. Esa disminución de la longitud de ruptura corresponde a la zona II en la figura 9.2

Finalmente, en la fotografía h) se observa un chorro totalmente atomizado. La longitud de ruptura del chorro es prácticamente constante Por tanto, la imagen h) correspondería a la zona III de la figura 9.2.

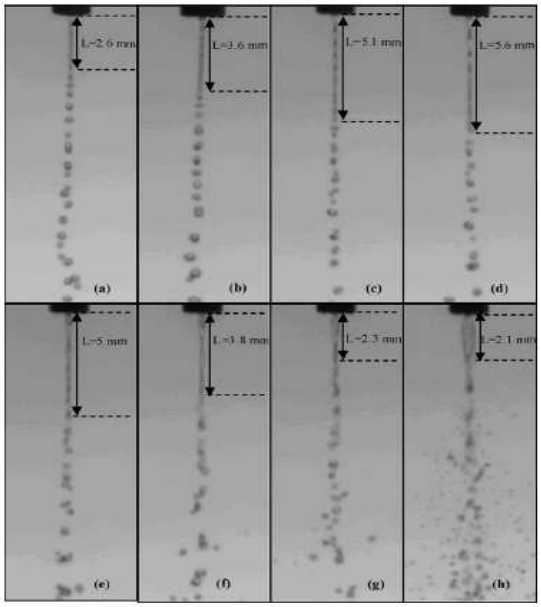

Figura 9.3. Distintos regímenes de desintegración de un chorro [2].

9.1.2. Influencia de la presión. Tensión superficial

La tensión superficial del líquido es un parámetro que contribuye activamente en los procesos de atomización.

En un proceso SEDS se produce una atomización en un medio a alta presión y como consecuencia, el proceso de desintegración del chorro experimenta variaciones con respecto al comportamiento en un ambiente a presión atmosférica.

En un ambiente a alta presión, la tensión superficial alcanza de una forma paulatina el valor nulo.

Para justificar esta desaparición debe tenerse en cuenta que en este proceso de atomización, el fluido supercrítico difunde hacia el interior de cada gota de disolución. Este hecho genera que la tensión superficial vaya disminuyendo hasta alcanzar un valor prácticamente nulo, cuando se alcanza el punto crítico de mezcla del fluido supercrítico-disolvente.

Este fenómeno puede observarse en la figura 9.4, que muestra la evolución de la tensión superficial de una gota de diferentes disolventes con la presión [2].

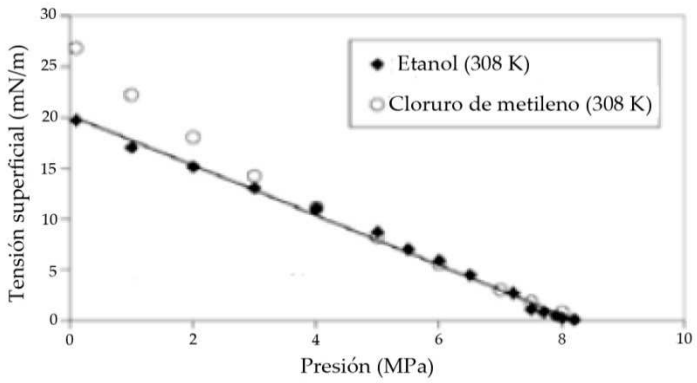

Figura 9.4. Reducción de la tensión superficial de varios disolventes con un aumento de la presión [2]

Como consecuencia de esta disminución de la tension superficial al aumentar la presión, la gota pierde su esfericidad a la vez que disminuye su tamaño. Así, en condiciones subcríticas, cercanas al punto crítico, la forma de la gota es totalmente axisimétrica, existiendo interfase.

A medida que las condiciones de presión y temperatura se acercan a las condiciones críticas de la mezcla disolvente-fluido supercrítico, la forma de la gota se modifica hasta que desaparece la interfase líquido-fluido supercrítico. Por tanto, un aumento de presión modifica la inestabilidad de la gota,

perdiendo su forma esférica a la vez que disminuye su tamaño [3]. Este efecto puede observarse en la figura 9.5.

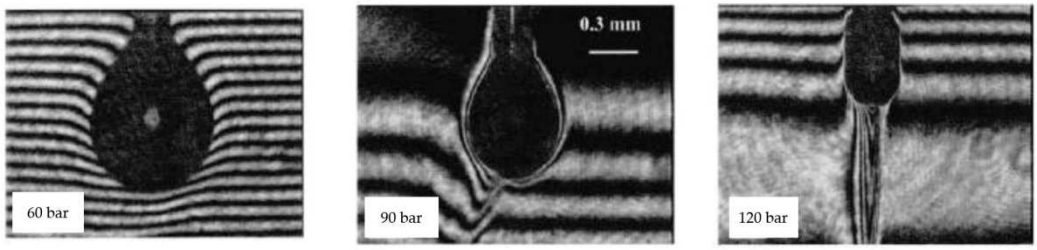

Figura 9.5. Evolución de una gota de etanol al aumentar la presión [3]

Sin embargo, a pesar de lo anteriormente descrito, varios autores [4] han puesto de manifiesto que la tensión superficial no desaparece totalmente en las condiciones establecidas por el punto crítico de mezcla. Estos mismos autores diferencian entre dos tipos de tensión superficial, tensión superficial en equilibrio que se hace cero en el punto crítico de mezcla y tensión superficial dinámica (o tensión superficial a tiempo cero).

Como se ha indicado, la tensión superficial en equilibrio desaparece en condiciones supercríticas de la mezcla. Sin embargo, debido a la existencia de un gradiente de densidad y de temperatura, la tensión superficial no alcanza un valor nulo automáticamente, existiendo entonces una tensión superficial muy pequeña, la llamada tensión superficial dinámica. Esta tensión superficial es la encargada de estabilizar el chorro frente a las perturbaciones aerodinámicas. Sin embargo, después de un tiempo, esta tensión superficial alcanza también el valor nulo [4].

La desaparición de la tensión superficial es tan importante, que algunos autores [5] han logrado correlacionar el tamaño de las partículas con el tiempo para la ruptura del chorro y el tiempo para la desaparición completa de la tensión superficial [5].

9.1.3. Influencia de la presión en los regímenes de desintegración.

Como se ha descrito previamente la atomización a alta presión se diferencia de la atomización convencional por el efecto que la presión ejerce en la tensión superficial.

Sin embargo, además de este efecto, la presión también va a modificar las condiciones hidrodinámicas del chorro y por tanto su régimen de atomización. Así, la influencia de la presión hace que se produzca la atomización del chorro a velocidades menores.

Esta influencia de la presion hace necesario el establecer unos límites de Ohnesorge y Reynolds, distintos a los definidos a presión atmosférica, para diferenciar los distintos tipos de desintegración de un chorro líquido a alta presión [6].

Por todo lo anterior, en estos procesos a alta presión es necesario definir un número de Ohnesorge modificado (Oh*) con el que se tenga en cuenta la viscosidad y la densidad del gas a alta presión (ecuación 9.4).

Asimismo, es necesario en el número de Reynolds (ecuación 9.5) y en el número de Weber (ecuación 9.6) introducir la velocidad relativa entre el antisolvente y el disolvente, debido a que es la principal causa de la rotura del chorro [6].

De acuerdo con lo anterior los números adimensionales modificados quedarán:

$$Oh^* = \mu_L \cdot \frac{v_A}{\sigma} \sqrt{\frac{\rho_G}{\rho_L}} \cdot \sqrt{\frac{\mu_L}{\mu_G}} \qquad \text{(Ec. 9.4)}$$

$$\mathrm{Re}_L = \frac{\rho_L \cdot (v_A - v_D) \cdot D_b}{\sigma} \qquad \text{(Ec. 9.5)}$$

$$We_G = \frac{\rho_G \cdot D_b \cdot (v_A - v_D)^2}{\sigma} \qquad \text{(Ec 9.6)}$$

Con estos números adimensionales modificados fueron desarrolladas [6] las ecuaciones 9.7 y 9.8 que establecen los límites de las distintas zonas.

Así, la ecuación 9.7 limita las condiciones para la desintegración de Rayleigh (zona I) y la zona II, mientras que la ecuación 9.8 establece los límites entre la zona II y la región de atomización (zona III) [6].

$$Oh^* = 10^{3,9} \cdot \mathrm{Re}_L^{-1,66} \qquad \text{(Ec. 9.7)}$$

$$Oh^* = 10^{5} \cdot \mathrm{Re}_L^{-1,73} \qquad \text{(Ec. 9.8)}$$

9.2. Transferencia de materia.

En un proceso SEDS, después de la atomización de la disolución se produce un mezclado íntimo entre las gotas de la disolución y el medio supercrítico.

En este proceso de mezclado existe un proceso de transporte de materia que debido a las condiciones de operación (presiones elevadas, etc…) conducen a un grado de sobresaturación muy alto. Esa sobresaturación tan elevada lleva a la precipitación del fármaco.

A continuación, se estudiará el proceso de transporte de materia.

9.2.1. Etapas de transferencia de materia en un proceso SEDS

La trayectoria una gota aislada en un proceso de atomización en un medio supercrítico puede observarse en la figura 9.6 [7].

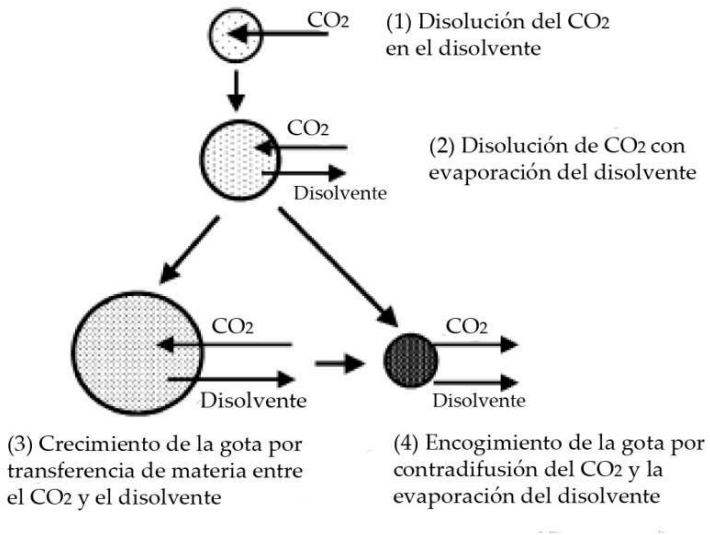

Figura 9.6. Etapas de transferencia de materia fluido supercrítico-disolvente de una gota individual en el proceso SEDS [7].

Como se deduce de la figura, la gota generada en el proceso de atomización (estado 1) no contiene fluido supercrítico, aunque está rodeada por una atmósfera en estado supercrítico. En estas condiciones la fuerza impulsora de la transferencia de materia es máxima y, el fluido supercrítico comienza a disolverse en la gota, aumentando su fracción molar. A medida que aumenta la fracción molar de fluido supercrítico en la gota, la velocidad de transferencia de materia entre el fluido supercrítico y la gota disminuye.

En el estado 2, teóricamente aumentaría la temperatura de la gota debido al carácter exotérmico del proceso de disolución. Sin embargo, debido a que el medio fluido supercrítico es infinito en relación a la gota, no se aprecia un drástico cambio de temperatura en el sistema.

En este proceso existe transferencia de calor desde el interior de la gota hacia su superficie (que está a la temperatura del medio supercrítico), lo que indica que se produce una evaporación del disolvente y la transferencia de materia de moléculas en fase vapor del disolvente al medio supercrítico.

Esa transferencia de materia es pequeña debido a que la fracción molar en equilibrio del disolvente en el fluido supercrítico es prácticamente nula. Por tanto el número de moléculas entrante del fluido supercrítico a la gota serían mayores que las salientes de la gota al fluido supercrítico. Como consecuencia la gota aumentaría su tamaño (estado 2 y 3)

Posteriormente, en el estado 4 existe un fenómeno de contradifusión y la gota disminuye de tamaño.

Ello es debido al aumento de la fracción molar del fluido supercrítico en el interior de la gota, y como por otra parte el proceso es exotérmico, con transporte de energía hacia el exterior, el equilibrio se modifica en el sentido de qué habrá uno nuevo que obligará a salir a una serie de moléculas de la gota de la disolución al medio supercrítico, de acuerdo a las nuevas condiciones de equilibrio.

A continuación se realizará un estudio teórico-experimental de la influencia de los diferentes regímenes de atomización y de los diferentes coeficientes de película de transferencia de materia en la precipitación de dos fármacos (acetaminofén y tretinoína) con un proceso SEDS.

Estos resultados son completados con los resultados obtenidos en el capítulo 4, intentando estudiar la interacción entre equilibrio de fases, atomización y transferencia de materia para un proceso de estas características.

9.3. Resultados y discusión.

El objetivo de este trabajo es el estudio de las condiciones óptimas para la generación de partículas con la técnica SEDS. Para ello se determinarán los equilibrios de fases que intervienen en los sistemas, los distintos regímenes de atomización y los coeficientes de película de transferencia de materia.

Estos resultados teóricos se correlacionarán con los resultados experimentales obtenidos en la generación de partículas de acetaminofén y tretinoína mediante la técnica SEDS.

La mejor distribución de tamaño de partícula y morfología (pocos agregados) para ambos sólidos fueron obtenidas a unas condiciones experimentales ligeramente por encima del punto crítico de mezcla antisolvente-disolvente y con una alta relación de flujos antisolvente-disolvente.

Los resultados teóricos obtenidos indican que en esas condiciones se obtiene el mayor grado de supersaturación y el mayor coeficiente de transferencia de materia en la película del líquido.

ARTÍCULO

Experimental and theoretical analysis of the operating parameters for precipitating acetaminophen and tretinoin with solution enhanced dispersion by supercritical fluids

Industrial and Engineering Chemistry Research

52 (2013) 8745-8754

I&EC research
Industrial & Engineering Chemistry Research

Article

pubs.acs.org/IECR

Experimental and Theoretical Analysis of the Operating Parameters for Precipitating Acetaminophen and Tretinoin with Solution Enhanced Dispersion by Supercritical Fluids

Antonio Tabernero, Eva M. Martín del Valle,* and Miguel A. Galán

Department of Chemical Engineering, University of Salamanca, P/Los Caídos S/N, 37008 Salamanca, Spain

Supporting Information

ABSTRACT: The aim of this work is to analyze the experimental conditions for particle production with solution enhanced dispersion by supercritical fluids. Thermodynamics, atomization process, and mass transfer are separately studied in terms of phase equilibria, disintegration regimes, and mass transfer coefficients of liquid and vapor phases. These calculations are correlated with the precipitation data of acetaminophen and tretinoin. According to experimental results, the smallest and more spherical particles (with fewer aggregates) for both solids are obtained just above the mixture critical point of the antisolvent−solvent system with a high antisolvent−solvent mass flow rate ratio. Theoretical results indicate that a high mass transfer coefficient of the liquid phase and a high degree of supersaturation are produced at those conditions. That means a great antisolvent effect because of the low liquid side mass transfer resistance and a small particle size because of the high supersaturation. Furthermore, results highlight that the antisolvent effect is improved for smaller initial droplet sizes.

1. INTRODUCTION

Over the past decade, supercritical fluids (SCFs) as antisolvents have been used for particle formation. Techniques such as gas antisolvent (GAS), supercritical antisolvent (SAS), or solution enhanced dispersion of supercritical fluids (SEDS) have been employed to produce a wide range of particle size distributions (PSD), and without traces of residual solvents. SCF techniques with their fundamentals and characteristics have been reviewed in different articles.[1−4]

SAS and SEDS are the most used. In these semicontinuous processes the solution is atomized in a supercritical atmosphere. If the SCF is highly soluble in the solvent, and at the same time the solute is sparingly soluble in the SCF, the SCF is dissolved in the solvent droplets, providing an antisolvent effect. Great supersaturations are induced in the solutions, and the solid precipitates therefore in the form of small particles with narrow PSD. The only difference between SAS and SEDS processes is the nozzle design. A coaxial design is presented by SEDS, against the conventional nozzle for the SAS process.

Thermodynamics, hydrodynamic, mass transfer, and crystallization kinetics are involved in these type of processes, and they should be studied to get a complete understanding of this type of precipitation. Experimental conditions are very important regarding the precipitation mechanism.[4,5] Particularly, it is important to know the position of the mixture critical point (MCP) of the ternary system solute−antisolvent−solvent. In this context, the MCP of the ternary system usually matches with the MCP of the binary system antisolvent−solvent. However, these conditions can be displaced (or even the type of binary equilibria can change) when the solid is added to the binary system.[6] The MCP is defined at the pressure (for a certain temperature) at which the liquid and vapor phases merge in one single supercritical phase. The interphase vanishes theoretically at these conditions. However, according to visual studies, the surface tension above the MCP decreases progressively, and does not disappear completely until a certain time. On the other hand, the surface tension vanishes almost immediately far above the MCP. In any case, at any conditions above the MCP, the surface tension is known as dynamic surface tension and stabilizes the jet against aerodynamic perturbations.[5,7]

Different works have been performed in order to explain (and model) the SAS process and the influence of different parameters in size and morphology. Rantakylä et al.[8] correlated the initial droplet size with the final PSD. Although the initial droplet size was calculated with an equation for a blast atomization at high pressures, significant deviations were obtained, specifically when the conditions lie above the MCP. Tenorio et al.[9] explained the particle morphology depending on the different disintegration regimes (Rayleigh, sinous-wave, and atomization breakups), but a clear relationship morphology-regime was not found, although they established that certain hydrodynamic conditions are needed to get fine particles. Petit-Gas et al.[10] established the role of the hydrodynamic in a SAS process by studying at miscible conditions the dispersion of a solution in sc-CO_2. On the basis of visual observations, it was shown that the jet break-up is faster than the mass transfer, and finer particles are obtained mainly for the mixing process, not for the atomization process. More phenomena should be therefore taken into account to explain a supercritical antisolvent process, such as mass transfer. Werling and Debenedetti studied numerically the mass transfer (coupled with thermodynamics) between a stagnant droplet of toluene

Special Issue: Giulio Sarti Festschrift

Received: August 29, 2012
Revised: October 9, 2012
Accepted: October 15, 2012
Published: October 15, 2012

ACS Publications © 2012 American Chemical Society

dx.doi.org/10.1021/ie3022972 | Ind. Eng. Chem. Res. 2013, 52, 8745−8754

and a supercritical CO_2 atmosphere above and under the MCP. Their results indicate that under the MCP there is always droplet swelling.[11] However, above the MCP, droplet swelling or shrinking depend on the density difference of the solvent−antisolvent.[12] In any case, without considering hydrodynamic effects, mass transfer above the SCF is faster than under the MCP.

Droplet velocity with mass transfer and thermodynamics were taken into account by Lora et al.[13] Their work highlights the importance of the solute in explaining the morphology and particle size of the outcome. Depending on the solute, the evaporation effect (as well as the antisolvent effect) might be required to precipitate the solid of interest (naphthalene for instance). However, other solids only require an antisolvent effect (phenanthrene). Martín and Cocero[14] performed a complete study of the SAS process (thermodynamics, mass transfer, crystallization, and hydrodynamics). It was shown that the experimental conditions should be modified to increase the supersaturation, given that it is the main parameter to obtain the best PSD.

Reverchon et al.[5] studied mass transfer, phase equilibria, and jet hydrodynamics (observing the gas−liquid boundaries) in a SAS process. On the basis of visual observations and experimental results, they explained particle size and morphology depending on the time for breaking the jet (t_b) and the time for the complete disappearance of the surface tension (t_s). According to them, if t_s is less than t_b, there is a gas to solid nucleation (nucleation followed by a size reduction), and nanoparticles are obtained (conditions far above the MCP). On the other hand, if t_s is greater than t_b (under the MCP), the obtained microparticles present different morphologies depending on the mass transfer mechanism of the precipitation inside the droplet. A mixture between microparticles and nanoparticles can be produced due to a competition between the previous times. This theory was numerically explained by calculating t_b and t_s for different concentrations and pressure conditions.[15] If both times are plotted, a cross point can be observed, distinguishing the two different precipitation mechanisms, surface tension vanishing mechanism (nanoparticles), and jet break-up mechanism (microparticles). So far the studies on modeling works are either focused on understanding the precipitation mechanism or the associated phenomena with the droplet flight along the vessel. Moreover, these different results indicate that particle size for this type of precipitation depends mainly on the solid.

This work aims to establish a relation between experimental conditions and particle size and morphology for particle formation by using SEDS. Depending on the initial experimental conditions, the different atomization regimes are determined, and the initial droplet size and mass transfer coefficients for the SCF and liquid layers are calculated. Peng−Robinson equation of state is used to perform the thermodynamic calculations and provide the required equilibria knowledge. These results allow the correlation of the different values of mass transfer coefficients, atomization regimes, and dimensionless numbers (calculated depending on the initial conditions) with the PSD and morphology. In that way, particle size and morphology may be predicted by calculating these dimensionless numbers before performing experiments.

To compare theoretical and experimental results, tretinoin (all-*trans* retinoic acid) and acetaminophen are used as model solids. These solids were already precipitated with SEDS using ethanol as a solvent in a previous work,[16] but studying only the influence of the MCP in the particle size, keeping constant the SCF/solution mass flow rate ratio. Therefore, new experiments with SEDS are performed in order to change that ratio and study the effect of this change in particle size. XRD diagrams (the XRD patterns showed that the processed solids presented a reduced crystallinity) and the previous visual thermodynamic study were already published in the previous article,[16] and they are not included here.

2. EXPERIMENTAL AND THEORETICAL SECTION

2.1. Materials. Acetaminophen with a purity of 99.0% was purchased from Sigma-Aldrich, whereas tretinoin with a richness of 100.8% was supplied by Fagron Iberica. Ethanol (purity of 99.9%) was obtained from BDH Prolabo. Carbon dioxide at 99.5% was purchased from Air Liquide.

2.2. Precipitation Apparatus and Procedure. The experimental apparatus for precipitating both solids has been previously described.[16] It comprises a high pressure jacketed vessel of 500 mL, an air booster (SPRAGUE products) to feed the CO_2 to the vessel, and a diaphragm pump (SERA) to pump the dissolution to the vessel. The nozzle presents a concentric design, with a mixing length to provide a previous mixture of the antisolvent and the solution. A mass flow meter (Bronckhorst) is used to control and measure the antisolvent mass flow. There are different heating systems to heat the vessel, the nozzle, the CO_2, and the SCF. Finally, different pressure and temperature controllers are used to observe all the experimental conditions inside the nozzle and inside the vessel during the experiments. These controllers can be modified by using a control box (RFL Electricite Tableautier). Particles are collected in a 0.1 μm isopore membrane filter (Millipore) placed at the end of the vessel.

Figure 1 describes the used nozzle, with a diameter of 80 μm and with a mixing length to provide a mixing between the antisolvent and the solvent. The outer and inner diameters of the mixing length tube are respectively 0.00152 and 0.00102 m. These diameters are used to calculate the antisolvent and solvent velocities.

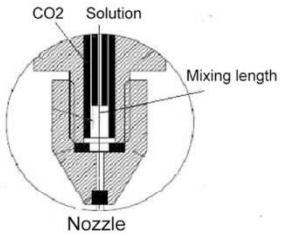

Figure 1. SEDS nozzle geometry.

Experiments start by adding CO_2 to the vessel. CO_2 is pressurized with the booster by using a back pressure regulator for controlling the pressure inside the vessel. After that, vessel, CO_2 lines, nozzle and solution conducts are heated with the different heat exchangers. The solution is pumped subsequently to the vessel and the precipitated particles are collected on the filter. The solution flow rate is controlled by changing the pump's frequency, whereas the CO_2 flow rate is modified by the mass flow meter. Solid concentration is 5 mg/mL for the acetaminophen and 1 mg/mL for the RA.

Images of the particles were taken by using scanning electron microscope (model ZEISS DSM 940). PSD was determined by using ImageJ software.[17] More details of this analysis process can be found elsewhere.[16]

2.3. Phase Equilibrium. Phase equilibria studies give information about the MCP of the system and the conditions at which the induced supersaturation is the maximum. The different binary and ternary diagrams for the systems of interest were determined in previous articles.[16,18] No immiscibilities liquid−liquid were not found in the previous systems. For both systems it was shown that the molar fraction of the solid in the liquid phase (in the antisolvent−solvent−solute system) reaches a minimum. The maximum induced degree of supersaturation is therefore achieved at these conditions. After that minimum, if the pressure increases, the solubility increases and the degree of supersaturation is reduced. At the same time, this minimum matches with the MCP of the system antisolvent−solvent (in this case CO_2−ethanol).

Therefore, according to our previous results, the influence of the solid in the MCP can be neglected for these systems, and PR-EOS[19] (eq 1) is used to determine only the vapor−liquid equilibria (VLE) diagram CO_2−ethanol.

$$P = \frac{RT}{v - b} - \frac{a(T)}{v^2 + 2bv - b^2} \tag{1}$$

In eq 1, v is the molar volume, R the gas constant, and P and T are the pressure and temperature of the system. For a pure component, the attractive parameter a (eq 2) and the repulsive term b (eq 3) are defined in function of its critical properties T_C and P_C.

$$a = 0.45724\frac{R^2{T_C}^2}{{P_C}^2}\alpha(T_R) \tag{2}$$

$$b = 0.07780\frac{RT_C}{P_C} \tag{3}$$

The dependence of the temperature of the attractive parameter a is treated with a corrector term α (eq 4), in which the acentric factor w takes into account the no esfericity of the molecule:

$$\alpha(T_R) = [1 + (0.374 + 1.542w + -0.269w^2)(1 - T_R)^{0.5}]^2 \tag{4}$$

In multicomponent systems, it is necessary to use a mixing rule to consider the interactions between the different components. In this study, van der Waals mixing rules with one single interaction parameter k_{ij} are used (considering l_{ij} as a null value). This parameter should be determined for each binary system by regressing experimental data against theoretical data:

$$a_m = \sum_i \sum_j x_i x_j \sqrt{a_i a_j}(1 - k_{ij}) \tag{5}$$

$$b_m = \sum_i \sum_j x_i x_j \left(\frac{b_i + b_j}{2}\right)(1 - l_{ij}) \tag{6}$$

The VLE diagram and the corresponding molar fractions at equilibrium were calculated by using the previous equations and the well-known algorithm previously explained elsewhere.[20]

2.4. Disintegration Regimes. The classical disintegration regimes for a jet liquid under atmospheric pressure, as well as their corresponding boundaries, were classified by Lefebvre.[21] However, the influence of the high pressure should be taken into account due to the solution of the gas in the liquid, varying kinetic and surface tension forces. Therefore, disintegration boundaries should be modified.

Disintegration regimes boundaries at high pressure were defined by Cwerzonatis and Eggers.[22] They established different correlations to distinguish between Rayleigh, sinous-wave and atomization breakups depending on the experimental conditions. Different dimensionless numbers were used for this identification. Reynolds (at the nozzle) of the solution (Re_L) for considering the inertia of the liquid phase, Weber (We_G) number for taking into account the relation between kinetic and surface tension forces and the modified Ohnesorge number (Z^{**}) to consider the viscosity.

According to that work, the different regimes at high pressure were distinguished depending on the value of the Re_L and Z^{**} (eq 7 and eq 8).

Rayleigh breakup—sinous wave breakup boundary:

$$Z^{**} = 10^{3.9} \times {Re_L}^{-1.66} \tag{7}$$

Sinous wave breakup—atomization boundary:

$$Z^{**} = 10^{5} \times {Re_L}^{-1.73} \tag{8}$$

On the other hand, Z^{**} and Re_L are calculated with eq 9 and eq 10. The relative velocity between the antisolvent and solvent was used in Reynolds number because it is the main contribution for the jet breakup.[8,23] The used Weber number is defined by eq 11.

$$Re_L = \rho_L D_b (V_a - V_d)/\mu_L \tag{9}$$

$$Z^{**} = \left(\mu_L \frac{V_a}{\sigma}\right)\sqrt{\frac{\rho_G}{\rho_L}}\sqrt{\frac{\mu_L}{\mu_G}} \tag{10}$$

$$We_G = \rho_G D_b (V_a - V_d)^2/\sigma \tag{11}$$

Different experimental conditions or physical properties, such as ethanol density (ρ_L), antisolvent density (ρ_G), nozzle diameter (D_b), antisolvent velocity (V_a), solution velocity (V_d), ethanol viscosity (μ_L), antisolvent viscosity (μ_G), and surface tension (σ) are included in the previous dimensionless numbers.

Ethanol viscosity and density were taken respectively from literature.[24,25] Antisolvent density and viscosity were determined from the NIST webbook.[26] On the other hand, ethanol equilibrium surface tension under sc-CO_2 atmosphere was experimentally determined by Dittmar et al.[27] However, above the MCP, there is a surface tension vanishing phenomenon. Under these conditions, the dynamic surface tension ($\sigma_{t=0}$) was calculated using the correlation given by Macleod−Sudgen (eq 12). Parachor parameter ([Pi]) of ethanol and ethanol should be previously determined for that equation.[24] Equilibrium liquid molar fraction x_i and vapor molar fraction y_i are included in the expression, and they were calculated with PR-EOS.

$${\sigma_{t=0}}^{1/4} = \sum_{i=1,\ldots,n}^{n} [Pi](\rho_L x_i - \rho_G y_i) \tag{12}$$

The theoretical initial droplet Sauter diameter d_{32t} can be estimated with Jasuja's empirical equation (eq 13). That equation was, according to Rantakylä et al.,[8] defined for an airblast atomization at high pressure. After making a comparison with several equations in order to correlate initial droplet diameter and PSD for a SAS process, the best fit was

obtained with the previous equation.[23] In eq 13, L/G is the mass ratio of liquid flow to gas flow.

$$d_{32t} = 0.17(\sigma/\rho_G)^{0.45}(1/(V_a - V_d))^{0.9}(1 + L/G)^{0.5}D_b^{0.55} + 0.015[(\mu_L)^2/(\sigma\rho_L)]^{0.5}D_b^{0.5}(1 + L/G) \quad (13)$$

2.5. Mass Transfer Coefficients. There is a simultaneous two-way mass transfer between the liquid side of the droplet and the SCF atmosphere in this type of semicontinuous antisolvent processes, as it is illustrated in Figure 2.

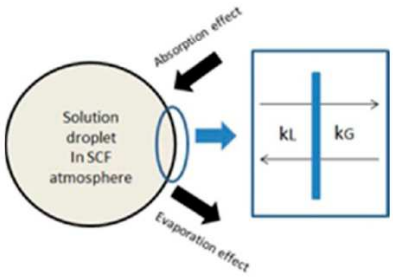

Figure 2. Simultaneous mass transfer occurring in a semicontinuous antisolvent process.

The existing mass transfer coefficients can be therefore calculated, but only after determining the diffusion coefficients for both liquid and SCF phases. Since the SCFs can be treated as a liquid due to the high density, Wilke-Chang's correlation (eq 14) for diffusion coefficient for dilute solutions can be used.[28] Moreover, this equation provides, according to different works,[29,30] a good fit for this property.

$$D^0_{BA} = \frac{7.4 \times 10^{-8}(\phi M_A)^{0.5}T}{\mu_A V^{0.6}} \quad (14)$$

D_{BA} is the diffusion coefficient at infinite dilution ($cm^2 \cdot s^{-1}$) of compound B in the compound A, M is molecular weight ($g \cdot mol^{-1}$), μ is viscosity (cP), ϕ is the association factor of the solvent (the value for the ethanol is 1.5) and V is the volume molar ($cm^3 \cdot mol^{-1}$) of the solvent at its normal boiling temperature.

However, the diffusion of the antisolvent in the droplet modifies the droplet composition. Therefore, there is a variation of both two-way coefficients depending on the equilibrium conditions. This phenomenon is taken into account by the approach of Vignes,[31] proposing a correction (eq 15) for the initial equation, by using the molar fraction of the SCF in the liquid solvent (x_A):

$$D_{BA} = (D^0_{BA})^{(1-X_A)}(D^0_{BA})^{X_A} \quad (15)$$

Mass transfer coefficients of the liquid (k_L) and vapor sides (k_G) are strongly dependent on the diffusion coefficients and droplet diameter d_d, and are calculated by using different dimensionless numbers, such as Sherwood (Sh), Schmidt (Sc), and the Reynolds number for theoretical droplet diameter (Re_{Ld}). It can be observed that the Sh number is directly related to the mass transfer coefficient, although in this equation the definition is given for the vapor mass transfer coefficient.

$$Re_{Ld} = \rho_L d_d(V_a - V_d)/\mu_L \quad (16)$$

$$Sh = k_G d_d/D_{21} \quad (17)$$

$$Sc = \frac{\mu_G}{\rho_G D_{21}} \quad (18)$$

Therefore, an appropiate estimation for the Sh number should be chosen. We chose a Sh correlation that was defined for a spraying process of oils into sc-CO_2 (eq 19).[32] On the other hand, the liquid side mass transfer coefficient k_L was considered as an effective internal mass transfer coefficient, calculated for a stagnant droplet (eq 20).[33] These equations were used by Rantäkyla to calculate these coefficients for a SAS process.[23]

$$Sh = 2.0 + 0.6Sc^{1/3}Re_{Ld}^{1/2} \quad (19)$$

$$k_L = (10D_{12})/d_d \quad (20)$$

3. RESULTS AND DISCUSSION

3.1. Precipitation Results. Table A.1 (provided in the Supporting Information) shows the precipitation results and the experimental conditions for the tretinoin and for the acetaminophen. Experimental Sauter mean diameter d_{32}, morphology, and position with respect to the MCP for each experiment are given as well. It should be specified that the experimental results from our previous article[16] in mean diameter were transformed to Sauter mean diameter d_{32}. Figure 3 illustrates different pictures for both solids at different experimental conditions. In this context, in Table A.1, M_a/M_d is the ratio between the antisolvent flow rate (M_a) and the solution flow rate (M_d)

3.2. Phase Equilibria. Critical properties and acentric factors of ethanol and CO_2 were taken from Knez et al.[34] and are given in Table 1. The binary interaction parameter k_{ij} was calculated by regressing experimental data against theoretical data,[34] using eq 21 as an objective function. The best fit is obtained for a value of 0.080 for k_{ij}.

$$\sum_{i=1}^{N}\frac{1}{N}(x_{expti} - x_{calci})^2 + (y_{expti} - y_{calci})^2 \quad (21)$$

The MCP can be determined upon the vapor−liquid equilibrium CO_2−ethanol (Figure 4). It can be observed that the MCP is located close to 75 bar at 313 K, and close to 80 bar at 318 K.

From the experimental PSD and the VLE diagram, several conclusions can be obtained. The narrowest PSD (without taking into account the antisolvent−solvent mass flow rates) is obtained just above the MCP. These results agree with different experimental works.[35,36] At these conditions there is nucleation in one single phase, and the supersaturation is close to the maximum. Conditions under the MCP and far above the MCP provide largest PSD given that the molar fraction of the solid in the liquid phase of the ternary system is higher, and consequently the supersaturation ratio decreases.

On the other hand, it is possible to observe on the pictures that more spherical particles (and fewer aggregates) are produced above the MCP. This can be explained in terms of mixing enthalpy CO_2−ethanol, nucleation kinetics, and mass transfer mechanisms[5].

3.3. Disintegration Results. Supporting Information, Table A.2 shows the values for the surface tension, antisolvent (V_a) and solution velocities (V_d), Z^{**} and Re_L (eq 9) for each

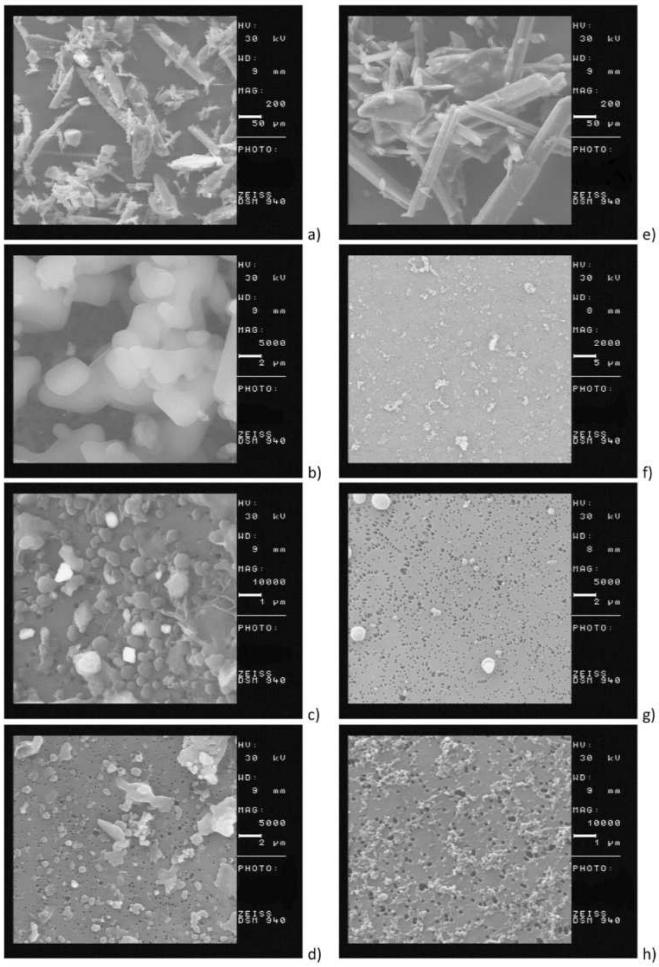

Figure 3. SEM images of different experiments collected in Table 1: (a) unprocessed acetaminophen; (b) run 2; (c) run 6; (d) run 12; (e) unprocessed tretinoin; (f) run 15; (g) run 20; (h) run 25.

Table 1. Critical Properties and Acentric Factors of CO_2 and Ethanol

compound	P_c (MPa)	T_c (K)	w
CO_2	7.38	304.10	0.225
ethanol	6.14	513.90	0.644

experiment (nozzle diameter 80 μm). The calculated theoretical droplet diameter (d_{32t} calculated with eq 13) and the experimental particle size (d_{32}) are also shown in this table.

Finally, Figure 5 illustrates the chart for the different atomization regimes. Only 13 points can be seen given that these experimental conditions are repeated for both solids.

By means of Supporting Information, Table A.2 and Figure 5 the effect of the disintegration regime on the particle size can be determined. First, it can be observed that there is no clear relationship disintegration regimes-morphology. Different morphologies can be found for atomization, sinous wave, and Rayleigh breakups for conditions either above or under the

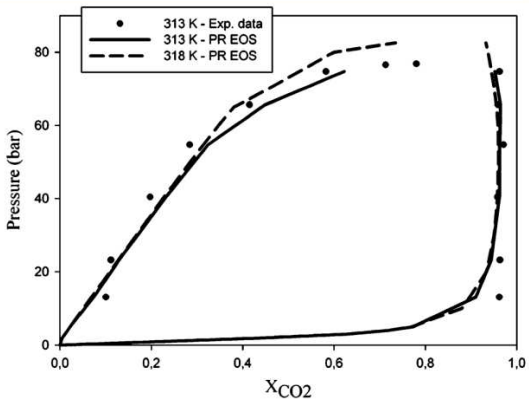

Figure 4. VLE CO_2–ethanol. Experimental data from Knez et al.[34]

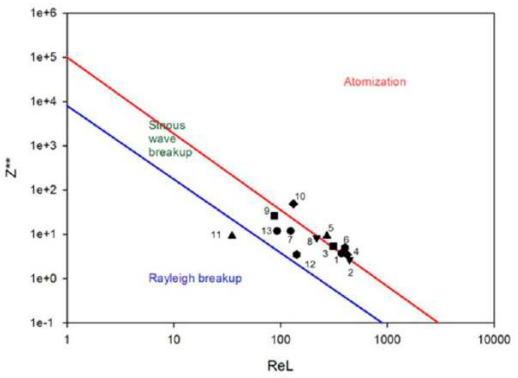

Figure 5. Chart of different atomization regimes.

MCP. For instance, run 6 (Figure 3c) and run 20 (Figure 3g) are above the MCP and present similar morphology, but different disintegration regimes. Experiments with different regimes and same morphology can be also found (run 2 (Figure 3b) and run 25 (Figure 3h) for instance).

At the same time, it can be observed that for experiments with the same regime, an increase (run 1−2) or decrease (run 2−4) of the particle size can be produced (these experiments were performed under an atomization regime).

It is possible to notice that the theoretical droplet diameter only predicts the tendency (with pressure and temperature) of the particle size at conditions under MCP. This result was already found for SAS process.[8]

In our case, higher deviations are found for conditions above the MCP with a Rayleigh disintegration regime. The explanation lies mainly on the surface tension vanishing, that cannot be considered by the used equation. Rayleigh regime indicates a strong influence of the capillary forces and the formation of bigger droplets. However, at these conditions droplets disappear after a fast surface tension vanishing process.

In addition, the calculated theoretical droplet diameter does not correlate well with particle size, mainly for low ratios antisolvent/solvent mass flow rates (experiments 11, 12, 13, 24, 25, 26). That can be due to the empirical character of the equation and phenomena such as secondary atomization, coalescence effects, or mass transfer between droplet and supercritical atmosphere.

The previous calculations highlight that above the MCP this type of initial droplet size predictions cannot be used to predict the experimental particle size for a SEDS process. However, results indicate that they can be useful for a rough prediction of the particle size for experiments with high ratios antisolvent/solvent mass flow rates as long as there is either atomization or sinous wave regime at conditions under the MCP.

It seems therefore that thermodynamic equilibrium has a predominant influence on the particle size and morphology than the atomization process. Nevertheless, best results in term of PSD are obtained for experiments with a higher ratio antisolvent/solvent mass flow rate. Increasing this ratio improves the turbulence, and consequently the mixing antisolvent−solvent. Therefore, the PSD is narrower, although this ratio does not have any influence in the morphology.

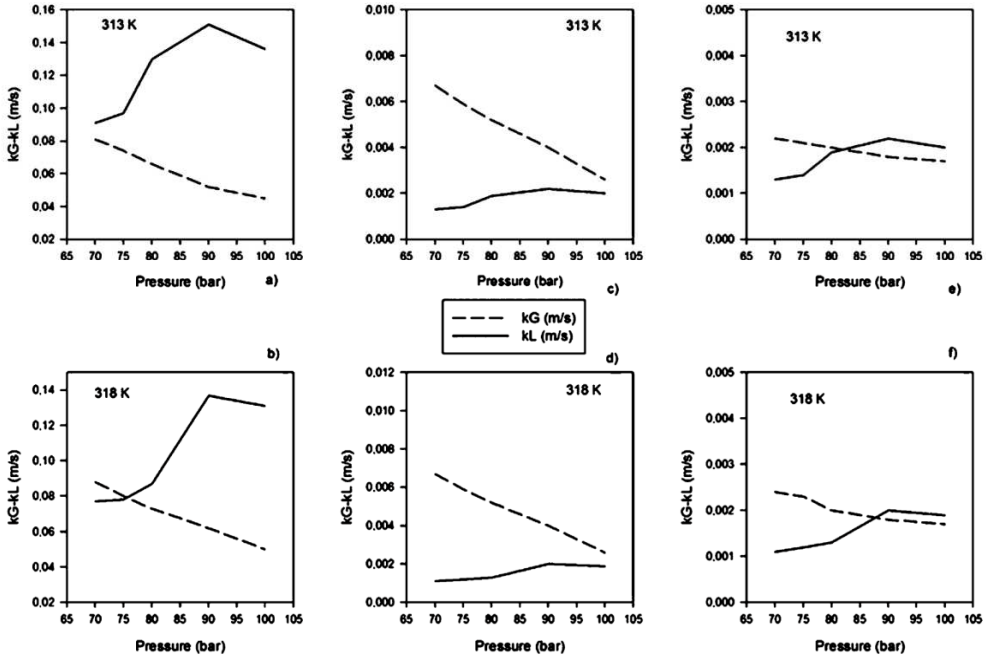

Figure 6. Influence of the pressure and temperature on the mass transfer coefficients k_G and k_L for the different sets of values at different temperatures (set 1, a and b; set 2, c and d; set 3, e and f).

According to these results, controlling the supersaturation by means of the phase equilibria, accompanied by high turbulence, is the most important regarding PSD.

Morphology is also given by thermodynamic considerations, because the mass transfer mechanism and the crystallization will be different whether the experiments are performed under or above the MCP.

However, the atomization process plays an important role in the mechanism of particle formation with a SEDS process, mainly under the MCP. At those conditions, the theoretical droplet size follows the same tendency of the particle size. Therefore, it is convenient to produce finer droplets to precipitate fine particles. That means that (at constant conditions of pressure, temperature and antisolvent/solvent mass flow ratio), an atomization regime is preferred over regimes that can produce bigger droplets (Rayleigh or sinous-wave).

The situation is different at conditions above the MCP because the mixing process is produced in the entire jet.[5] In this case, according to our results the used equation for calculating the initial droplet size cannot be used for predicting the tendency of the particle above the MCP, and the morphology does not vary in a great extent depending on the disintegration regime. The reason can be that at these conditions the jet dispersion is very similar due to the fast surface tension vanishing.

We have found a similar morphology at conditions near and above the MCP for different solution velocities, despite the existence of short-time phase boundaries. That means that probably similar jet dispersions were produced. This might be due to the increasing of the turbulence in the mixing length of the nozzle before the atomization, or that the critical atomization velocity was not reached. However, visual studies inside the nozzle and inside the vessel with the systems would have to be performed to check the explanation for that phenomenon.

3.4. Mass Transfer Results. Liquid and vapor side mass transfer coefficients were calculated using eq 14−20. Droplet diameter and velocity values are required for these equations. This fact allows the study of the influence of the velocity and the droplet diameter in the mass transfer coefficients. Specifically, three different set of values were used.

For the first set, a velocity of 5 $m \cdot s^{-1}$ and a diameter of 1.5 μm (d_d) were chosen to perform the different calculations. These values were taken because the average experimental velocity $V_a - V_d$ and the theoretical initial droplet size d_{32t} lie close to these values.

Diameter and velocity of 100 μm and 5 $m \cdot s^{-1}$ were chosen for the second set. Therefore, it can be observed the effect of the initial droplet diameter on the mass transfer coefficients. Finally, the third set of data is proposed to study the change on the mass transfer coefficients with the velocity, varying it from 5 $m \cdot s^{-1}$ to 0.5 $m \cdot s^{-1}$ but keeping the droplet diameter constant (100 μm).

Results for the different sets are given in Supporting Information, Table A.3 and Figure 6.

Mass transfer coefficient k_G decreases with pressure and increases with temperature for all sets, following the same tendency that the diffusion coefficient of the liquid in the supercritical fluid. According to Figure 6, the decrease of the value of the slope of the k_G is more pronounced for conditions close to the MCP, increasing the resistance of the evaporation of the droplet. For conditions far above the MCP, the value of the mass transfer coefficient can remain almost identical (this phenomenon is more noticeable for bigger initial droplet sizes) due to the surface tension vanishing. On the other hand, mass transfer coefficient k_L increases with pressure and decreases with temperature. However, there is a decrease of the k_L after the MCP due to the surface tension vanishing, and the mass transfer resistance on the liquid phase is increased. As occurs with the k_G, the same tendency is found for all the sets of values.

The influence of the velocity can be observed between set 2 and set 3. If the velocity difference between the antisolvent and solution is increased, the value of the mass transfer coefficient k_L increases. Therefore, the penetration effect of the SCF in the droplet is improved because the mass transfer resistance on the liquid phase is reduced. Same tendency is observed for the k_G, obtaining an almost constant value for high velocity difference.

The effect of the diameter is observed between set 1 and set 2. If the theoretical droplet diameter is reduced, both mass transfer coefficients increase, and as a consequence the mass transfer resistances on both sides of the droplet decrease.

In general, k_G is higher than k_L, which means that mass transfer rate is controlled by the SCF phase. However, there are particular cases in which the liquid phase controls the mass transfer rate. Set 1 and set 3 highlight that the k_L can be higher than the k_G. Under these conditions, the antisolvent tends to dissolve in a greater extent in the droplet solution and the antisolvent effect is improved. According to Figure 6, the combination of smaller initial droplet size and higher velocity difference (set 1) is the best for getting the greatest liquid side mass transfer coefficient.

On the other hand, although the same phenomenon is found in set 3, this situation is not very convenient, because the values of the mass transfer coefficients are very low and the global mass transfer is reduced.

Mass transfer coefficient results indicate that the value of the k_L is the most important regarding the particle size. The smallest particle size is obtained at conditions at which the k_L is the maximum (always above the MCP), indicating that the antisolvent tends to dissolve faster in the solvent at these conditions. In this case, the liquid side tends to control the mass transfer. Further, the k_G reaches almost its minimum value at these conditions. Therefore, at the same time, the mass transfer resistance of the gas phase increases.

Relationship between k_{G1} and k_{L1} (R) for both temperatures is illustrated in Figure 7. It can be seen how this value decreases with pressure and increases with temperature because of the opposite tendency of each mass transfer coefficient. The smallest particle size is found when the curve decreases drastically because of the previous considerations (just above the MCP). It can be seen how R for both temperatures reaches almost the same value for a certain pressure far above the MCP. At this pressure, the mass transfer antisolvent−solvent remains constant because of the fast and complete vanishing of the droplet.

The values of the mass coefficients are not an exact indication of droplet swelling or shrinking. The absorption or evaporation processes are depending on the respective molar flux of antisolvent and solvent. These fluxes are at the same time depending on the equilibrium concentrations, the concentration inside the droplet, and the flying time of the droplet along the vessel. These absorption/evaporation phenomena are not calculated here and can be found in different modeling articles.

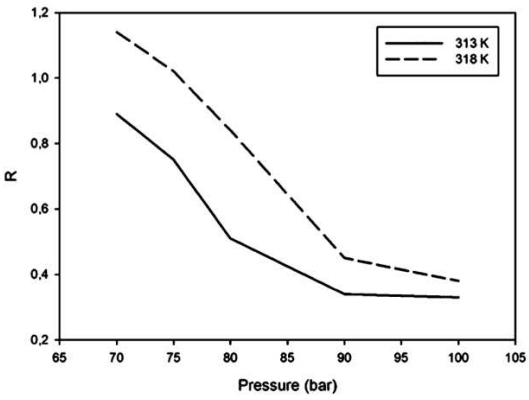

Figure 7. Relationship R for set 1 (5 m·s^{-1} and a 1.5 μm diameter).

3.5. Interactions between Thermodynamic, Disintegration Regime, and Mass Transfer Results. According to the previous results, SEDS experimental conditions just above the MCP provide the maximum supersaturation according to thermodynamic considerations (together with a nucleation in one single phase), and as a result fine particles with few aggregates are obtained. Mass transfer coefficient on the liquid phase is the maximum at these conditions, and consequently the penetration of the antisolvent inside the droplet is the maximum attainable because the mass transfer resistance in the liquid phase is the minimum. Moreover, a high mass flow ratio antisolvent/solution improves the turbulence, obtaining a smaller particle size.

The disintegration regime can affect the particle size, given that the mass transfer coefficient strongly depends on the initial droplet size. As long as there are phase boundaries, the calculated initial droplet size follows the tendency of the particle size, and therefore an atomization regime is preferred over bigger droplet regimes such as Rayleigh or sinous wave break-up. Nevertheless, under the MCP, the disintegration regime did not affect in a great extent the morphology because there is a nucleation in a biphasic phase, leading to the appearance of aggregates. The same happened for the investigated conditions above and near and above the MCP. It seems, that in our case, similar jet dispersions were produced for those conditions.

In concordance with that, parameters that can affect the initial droplet size have been proved very important regarding the particle size. Smaller theoretical droplet size and a higher difference between antisolvent/solvent velocities can give as a result a higher penetration of the antisolvent into the droplet.

3.6. Modification of the Theoretical Droplet Size to Predict the PSD. As it is possible to observe, Jasuja's equation predicts roughly the PSD. In fact, the average relative deviation AARD (eq 22) with Jasujás equations can be higher than 100% (Table 4) mainly due to the experiments above the MCP with Rayleigh disintegration regime.

$$\mathrm{AARD}(\%) = \frac{100}{N}\frac{\sum_{i=1}^{N}\mathrm{PSD}_{\mathrm{calc}} - \mathrm{PSD}_{\mathrm{expt}}}{\mathrm{PSD}_{\mathrm{expt}}} \quad (22)$$

Different phenomena such as droplet coalescence, secondary atomization, and surface tension vanishing can be a source of deviation. Moreover, parameters such as fluids viscosity or density, surface tension, nozzle diameter, and velocities play an important role in this process. To take into account all these parameters, a simple and empirical modification for the initial droplet size diameter has been proposed in order to improve the fit of this equation.

This equation is modified by adding different terms to the initial droplet diameter calculation (eq 23). Dimensionless numbers We_G, Z^{**}, and Re_L, together with the mass transfer parameter R are included in this term. Considering these numbers, it is possible to take into account the parameters that can affect the relationship between initial droplet size-PSD for each system and for each experimental device. At the same time, all the terms included in the modification are multiplied by a coefficient that should be calculated by regressing experimental data against theoretical data.

$$\mathrm{PSD} = d_0((AWe_G) + (BZ^{**}) + (CR) + (DRe_L)) \quad (23)$$

Table 2 shows the obtained parameters for both acetaminophen and tretinoin. The AARD for both solids are also included in this table. It can be seen how the AARD is reduced until a 20%, avoiding great deviations for conditions above the MCP. Therefore, the PSD for these solids can be predicted by knowing the experimental initial conditions and the corresponding experimental coefficients.

4. CONCLUSIONS

This work tries to elucidate the relation experimental conditions−particle size-morphology in order to perform a precipitation process with SEDS. Thermodynamics, atomization considerations, (initial droplet size diameter and disintegration regimes), and mass transfer are separately taken into account.

Results indicate that supersaturation and phase equilibria are the main phenomena to control particle size and morphology. According to these phenomena, the narrowest PSD with spherical morphology is obtained at conditions just above the MCP. At the same time, the supersaturation can be enhanced by improving turbulence in the nozzle mixing length by increasing the velocity difference between the gas and the liquid.

In our case, the disintegration regime did not have any influence in the morphology although it is important for the mechanism of the particle formation and the resulting particle size. According to the results, under the MCP, the disintegration regime should be chosen in order to get the smallest droplet size given that there is a relationship between droplet size and particle size. Therefore, atomization regime is preferred over other regimes such as Rayleigh, because smaller droplets are produced.

Table 2. Modeling Results with eq 13 and eq 23

solid	A	B	C	D	AARD (%) (eq 13)	AARD (%) (eq 23)
acetaminophen	0.00229	0.00727	−0.19587	0.00287	110.32	17.18
tretinoin	0.00374	0.00456	0.0667	0.00084	127.36	24.36

Mass transfer coefficients on both sides of the droplet were calculated. The liquid side mass transfer coefficient reaches the maximum value close to the MCP and at the same time the vapor mass transfer coefficient reaches the minimum value. That involves a better dissolution of the SCF in the droplet although the evaporation of the solvent into the SCF medium gets more difficult. The antisolvent effect is improved as a consequence. This effect is improved for smaller initial droplet size diameter and higher velocity difference.

Therefore, from these results, it can be concluded that conditions just above the MCP, accompanied by small initial droplet size diameter and high difference velocity in the mixing length of the nozzle are the optimum to get small and mainly spherical particles without aggregates.

■ ASSOCIATED CONTENT

Supporting Information

Tables A1−A3 with experimental details and calculations. This material is available free of charge via the Internet at http://pubs.acs.org.

■ AUTHOR INFORMATION

Corresponding Author

*E-mail: emvalle@usal.es. Tel.: (+34) 923-294479. Fax: (+34) 923-294579.

Notes

The authors declare no competing financial interest.

■ ACKNOWLEDGMENTS

This research was supported by funds from the Ministerio de Ciencia e Innovación (Spain), project CTQ2009-08222 (PPQ Subprogram).

■ REFERENCES

(1) Jung, J.; Perrut, M. Particle design using supercritical fluids: Literature and patent survey. *J. Supercrit. Fluids* **2001**, *20*, 179−219.

(2) Tabernero, A.; Martín del Valle, E. M.; Galán, M. A. Supercritical fluids for pharmaceutical particle engineering: Methods, basic fundamentals and modelling. *Chem. Eng. Process.* **2012**, *60*, 9−25.

(3) Reverchon, E. Supercritical antisolvent precipitation of micro- and nano-particles. *J. Supercrit. Fluids* **1999**, *15*, 1−21.

(4) Martín, A.; Cocero, M. J. Micronization processes with supercritical fluids: Fundamentals and mechanisms. *Adv. Drug Delivery Rev.* **2008**, *60*, 339−350.

(5) Reverchon, E.; Torino, E.; Dowy, S.; Brauer, A.; Leipertz, A. Interactions of phase equilibria, jet fluid dynamics and mass transfer during supercritical antisolvent precipitation. *Chem. Eng. J.* **2010**, *156*, 446−458.

(6) Reverchon, E.; De Marco, I. Supercritical antisolvent micronization of Cefonicid: Thermodynamic interpretation of results. *J. Supercrit. Fluids* **2004**, *31*, 207−215.

(7) Dukhin, S. S.; Zhu, Z.; Dave, R.; Pfeffer, R.; Luo, J. J.; Chavez, F.; Shen, Y. Dynamic interfacial tension near critical point of a solvent-antisolvent mixture and laminar jet stabilization. *Colloids Surf. A* **2003**, *229*, 181−199.

(8) Rantakylä, M.; Jäntti, A.; Aaltonen, O.; Hurme, M. The effect of initial droplet size on particle size on the supercritical antisolvent precipitation (SAS) technique. *J. Supercrit. Fluids* **2000**, *24*, 251−263.

(9) Tenorio, A.; Jaeger, P.; Gordillo, M. D.; Pereyra, C. M.; Martínez de la Ossa, E. On the selection of limiting hydrodynamic conditions for the supercritical (SAS) antisolvent processes. *Ind. Eng. Chem. Res.* **2009**, *48*, 9224−9232.

(10) Petit-Gas, T.; Boutin, O.; Raspo, I.; Badens, E. Role of hydrodynamics in supercritical antisolvent processes. *J. Supercrit. Fluids* **2009**, *51*, 248−255.

(11) Werling, J. O.; Debenedetti, P. G. Numerical modeling of mass transfer in the supercritical antisolvent process. *J. Supercrit. Fluids* **1999**, *16*, 167−181.

(12) Werling, J. O.; Debenedetti, P. G. Numerical modeling of mass transfer in the supercritical antisolvent process: Miscible conditions. *J. Supercrit. Fluids* **2000**, *18*, 11−24.

(13) Lora, M.; Bertucco, A.; Kikic, I. Simulation of the semi-continuous supercritical antisolvent recrystallization process. *Ind. Eng. Chem. Res.* **2000**, *39*, 1487−1496.

(14) Martín, A.; Cocero, M. J. Numerical modeling of jet hydrodynamics, mass transfer, and crystallization kinetics in the supercritical antisolvent (SAS) process. *J. Supercrit. Fluids* **2004**, *32*, 203−219.

(15) Marra, F.; De Marco, I.; Reverchon, E. Numerical analysis of the characteristic times controlling supercritical antisolvent micronization. *Chem. Eng. Sci.* **2012**, *71*, 39−45.

(16) Tabernero, A.; Martín del Valle, E. M.; Galán, M. A. Precipitation of tretinoin and acetaminophen with solution enhanced dispersion by supercritical fluids (SEDS). Role of phase equilibria to optimize particle diameter. *Powder Technol.* **2012**, *217*, 177−188.

(17) Rasband, W. S. *ImageJ*; U.S. National Institutes of Health: Bethesda, MD, USA, 1997−2011; http://imagej.nih.gov/ij/.

(18) Tabernero, A.; Martín del Valle, E. M.; Galán, M. A. On the use of semiempirical models of (solid+supercritical fluid) systems to determine solid sublimation properties. *J. Chem. Thermodyn.* **2011**, *43*, 711−718.

(19) Peng, D. Y.; Robinson, D. B. A new two constant equation of state. *Ind. Eng. Chem. Fundam.* **1976**, *15*, 59−64.

(20) Prausnitz, J. M.; Lichtenthaler, R. N.; De Azevedo, E. G. *Molecular Thermodynamics of Fluid-Phase Equilibria*, 2nd ed.; Prentice-Hall: Upper Saddle River, NJ, 1986.

(21) Lefebvre, A. H. *Atomization and Sprays*; Taylor & Francis: New York, 1989.

(22) Czerwonatis, N.; Eggers, R. Disintegration of liquid jets and drop drag coefficients in pressurized nitrogen and carbon dioxide. *Chem. Eng. Technol.* **2001**, *24*, 619−624.

(23) Rantakylä, M. *Particle production by supercritical antisolvent techniques*. Ph.D. Dissertation, Laboratory of Chemical Engineering and Plant Design, Helsinki, Finland, 2004.

(24) Poling, B. E.; Prausnitz, J. M.; O'Connell, J. P. *The Properties of Gases and Liquids*, 5th ed.; McGraw-Hill: New York, 2001.

(25) Perry, R. H.; Green, D. W. *Perry's Chemical Engineer's Handbook*; 7th ed. McGraw-Hill: New York, 1997.

(26) Linstrom, P. J., Mallard, W. G., Eds. *NIST Chemistry Webbook, NIST Standard Reference Database Number 69*; National Institute of Standards and Technology: Gaithersburg, MD, http://webbook.nist.gov, accessed May 2, 2012.

(27) Dittmar, D.; Oei, S. B.; Eggers, R. Interfacial tension and density of ethanol in contact with carbon dioxide. *Chem. Eng. Technol.* **2002**, *25*, 23−27.

(28) Wilke, C. R.; Chang, P. Correlation of diffusion coefficients in dilute solution. *AIChE J.* **1955**, *1*, 264−270.

(29) Silva, C. M.; Macedo, E. A. Diffusion coefficients of ethers in supercritical carbon dioxide. *Ind. Eng. Chem. Res.* **1998**, *37*, 1490−1498.

(30) Debenedetti, P. G.; Reid, R. C. Diffusion and mass transfer in supercritical fluids. *AIChE J.* **1986**, *37*, 2034−2046.

(31) Vignes, A. Diffusion in binary solutions, variation of diffusion coefficient with composition. *Ind. Eng. Chem. Fundam.* **1966**, *5*, 189−196.

(32) Roh, R.; Trepp, Ch. *High Pressure Chemical Engineering*; Elsevier: Amsterdam, The Netherlands, 1996.

(33) McCabe, W.; Smith, J.; Harriot, P. *Unit Operations of Chemical Engineering*, 4th ed.; McGraw-Hill: Singapore, 1985.

(34) Knez, Z.; Skerget, M.; Ilic, I.; Lutge, C. Vapor−liquid equilibrium of binary CO_2−organic solvents systems (ethanol, tetrahydrofuran, *ortho*-xylene, *meta*-xylene, *para*-xylene). *J. Supercrit. Fluids* **2008**, *45*, 338−345.

(35) Miguel, F.; Martín, A.; Gamse, T.; Cocero, M. J. Supercritical antisolvent precipitation of lycopene. Effect of the operating parameters. *J. Supercrit. Fluids* **2006**, *36*, 225−235.
(36) Miguel, F.; Martín, A.; Mattea, F.; Cocero, M. J. Precipitation of lutein and co-precipitation of lutein and poly-lactic acid with the supercritical antisolvent process. *Chem. Eng. Process.* **2008**, *47*, 1594−1602.

Supporting information for the article:

Experimental and theoretical analysis of the operating parameters for precipitating acetaminophen and tretinoin with solution enhanced dispersion by supercritical fluids.

Antonio Tabernero, Eva M. Martín del Valle*, Miguel A. Galán

Department of Chemical Engineering, University of Salamanca, P/Los Caídos S/N, 37008 Salamanca, Spain

Tables

Table A.1. Experimental results.

Run	Solute	P (bar)	T (K)	*Ma/Md*	d_{32} (μm.)	SEM image	Position with respect to the MCP
1	Acet	70	313	3	2.73	-	Under
2	Acet	70	318	3	2.88	2b	Under
3	Acet	75	313	3	1.83	-	Near
4	Acet	75	318	3	1.91	-	Under
5	Acet	80	313	3	1.08	-	Near and above
6	Acet	80	318	3	1.21	2c	In the MCP
7	Acet	90	313	3	1.36	-	Above
8	Acet	90	318	3	1.49	-	Above
9	Acet	100	313	3	1.81	-	Above
10	Acet	100	318	3	1.93	-	Above
11	Acet	80	313	0.5	1.25	-	Near and above
12	Acet	75	318	0.5	2.16	2d	Under
13	Acet	90	313	0.5	1.71	-	Above
14	RA	70	313	3	1.59	-	Under
15	RA	70	318	3	1.71	2f	Under
16	RA	75	313	3	1.27	-	Near and above
17	RA	75	318	3	1.39	-	Under
18	RA	80	313	3	0.94	-	Near and above
19	RA	80	318	3	1.05	-	In the MCP
20	RA	90	313	3	1.84	2g	Above
21	RA	90	318	3	1.92	-	Above
22	RA	100	313	3	1.96	-	Above
23	RA	100	318	3	2.13	-	Above
24	RA	80	313	0.5	1.09	-	Near and above
25	RA	75	318	0.5	1.86	2h	Under
26	RA	90	313	0.5	2.78	-	Above

Table A.2. Experimental conditions for the experiments.

Run	MCP	*Va* *(m·s^{-1})*	*Vd* *(m·s^{-1})*	d_{32} (µm.)	d_{32t} (µm.)	σ(N·m^{-1}) x 10^3	We_G	Z**	Re_L	Dis. Regime
1	Under	5.61	0.58	2.73	1.86	3.53	114	3.68	373	Atom
2	Under	6.08	0.59	2.88	1.93	4.21	105	2.66	444	Atom
3	Near	4.80	0.58	1.83	1.67	2.28	145	5.38	312	Atom
4	Under	5.32	0.59	1.91	1.81	3.08	122	3.48	383	Sin
5	Near and above	3.99	0.58	1.08	1.41	1.22	213	9.18	253	Atom
6	In the MCP	4.61	0.59	1.21	1.62	2.01	156	5.02	326	Atom
7	Above	2.26	0.58	1.36	1.50	0.60	185	11.90	124	Sin
8	Above	3.28	0.59	1.49	1.45	0.99	199	8.27	218	Sin
9	Above	1.76	0.58	1.81	1.12	0.20	352	26.1	87	Sin
10	Above	2.22	0.59	1.93	0.75	0.12	886	48.9	132	Atom
11	Near and above	3.99	3.51	1.25	12.5	1.22	408	9.18	350	Ray
12	Under	5.32	3.56	2.16	6.64	3.08	17	3.47	142	Sin
13	Above	3.51	2.26	1.71	2.93	0.60	111	18.6	96	Sin
14	Under	5.61	0.58	1.59	1.86	3.53	114	3.68	373	Atom
15	Under	6.08	0.59	1.71	1.93	4.21	105	2.66	444	Atom
16	Near and above	4.80	0.58	1.27	1.67	2.28	145	5.38	312	Atom
17	Under	5.32	0.59	1.39	1.81	3.08	122	3.48	383	Sin
18	Near and above	3.99	0.58	0.94	1.41	1.22	213	9.18	253	Atom
19	In the MCP	4.61	0.59	1.05	1.62	2.01	156	5.02	326	Atom
20	Above	2.26	0.58	1.84	1.50	0.60	185	11.9	124	Sin
21	Above	3.28	0.59	1.92	1.45	0.99	199	8.27	218	Sin
22	Above	1.76	0.58	1.96	1.12	0.20	352	26.1	87	Sin
23	Above	2.22	0.59	2.13	0.75	0.12	886	48.9	132	Atom
24	Near and above	3.99	3.51	1.09	12.5	1.22	408	9.18	350	Ray
25	Under	5.32	3.56	1.86	6.64	3.08	17	3.47	142	Sin
26	Above	3.51	2.26	2.78	2.93	0.60	111	18.6	96	Sin

Table A.3. Mass transfer coefficients for different diameters and velocities. (Set 1: 1.5 µm. and 5 $m \cdot s^{-1}$) (Set 2: 100 µm. and 5 $m \cdot s^{-1}$) (Set 3: 100 µm. and 0.5 $m \cdot s^{-1}$).

Run	k_{G1} ($m \cdot s^{-1}$)	k_{L1} ($m \cdot s^{-1}$)	$R = k_{G1}/k_{L1}$	k_{G2} ($m \cdot s^{-1}$)	k_{L2} ($m \cdot s^{-1}$)	k_{G3} ($m \cdot s^{-1}$)	k_{L3} ($m \cdot s^{-1}$)
1	0.081	0.091	0.89	0.0060	0.0014	0.0023	0.0014
2	0.088	0.077	1.14	0.0067	0.0012	0.0024	0.0012
3	0.074	0.098	0.76	0.0052	0.0015	0.0021	0.0015
4	0.081	0.079	1.02	0.0059	0.0012	0.0023	0.0012
5	0.069	0.131	0.51	0.0045	0.0020	0.0020	0.0020
6	0.073	0.087	0.84	0.0052	0.0013	0.0021	0.0013
7	0.052	0.151	0.35	0.0030	0.0023	0.0019	0.0023
8	0.062	0.137	0.45	0.0041	0.0021	0.0020	0.0021
9	0.045	0.136	0.33	0.0025	0.0020	0.0017	0.0020
10	0.050	0.131	0.38	0.0029	0.0020	0.0018	0.0020
11	0.046	0.131	0.35	0.0020	0.0020	0.0020	0.0020
12	0.063	0.079	0.80	0.0038	0.0012	0.0023	0.0012
13	0.050	0.151	0.33	0.0027	0.0023	0.0019	0.0023
14	0.081	0.091	0.89	0.0060	0.0014	0.0023	0.0014
15	0.088	0.077	1.14	0.0067	0.0012	0.0024	0.0012
16	0.074	0.098	0.76	0.0052	0.0015	0.0021	0.0015
17	0.081	0.079	1.02	0.0059	0.0012	0.0023	0.0012
18	0.069	0.131	0.51	0.0045	0.0020	0.0020	0.0020
19	0.073	0.087	0.84	0.0052	0.0013	0.0021	0.0013
20	0.052	0.151	0.35	0.0030	0.0023	0.0019	0.0023
21	0.062	0.137	0.45	0.0041	0.0021	0.0020	0.0021
22	0.045	0.136	0.33	0.0025	0.0020	0.0017	0.0020
23	0.050	0.131	0.38	0.0029	0.0020	0.0018	0.0020
24	0.046	0.131	0.35	0.0020	0.0020	0.0020	0.0020
25	0.063	0.079	0.80	0.0038	0.0012	0.0023	0.0012
26	0.050	0.151	0.33	0.0027	0.0023	0.0019	0.0023

9.4. Conclusiones.

En el artículo anterior se ha estudiado la relación condiciones experimentales-tamaño de partícula-morfología en un proceso de precipitación de fármacos con un proceso SEDS, mediante el estudio de forma separada del equilibrio de fases de los diferentes sistemas, hidrodinámica (regímenes de desintegración y tamaño inicial de gota) y transferencia de materia.

El grado de supersaturación obtenido (y por tanto el equilibrio de fases) es el principal fenómeno que controla el tamaño de partícula. La óptima distribución de tamaño de partícula es obtenida en condiciones ligeramente superiores al punto crítico de mezcla del sistema antisolvente-disolvente. Este grado de sobresaturación puede incrementarse mediante incrementar la turbulencia en la longitud de mezcla de la boquilla al aumentar la relación de caudales entre el fluido supercrítico y el disolvente.

En nuestro proceso, los regímenes de desintegración no influenciaron la morfología de las partículas obtenidas, aunque pueden resultar importantes en el mecanismo de formación de partículas y su correspondiente tamaño. De hecho, en condiciones inferiores al punto crítico de mezcla, un régimen de atomización es preferible para conseguir un pequeño tamaño inicial de gota que dará como resultado una distribución de tamaño de partícula más pequeña.

Mediante el cálculo de los coeficientes de transferencia de materia en la película del líquido y del fluido supercrítico, se pudo observar que el valor máximo de k_L fue obtenido en condiciones cercanas al punto crítico de mezcla. Esto implica que a estas condiciones exista una mayor penetración del fluido supercrítico en el disolvente, y por tanto su efecto antisolvente sea incrementado.

A partir de estos resultados tanto experimentales como teóricos, se ha concluido que operar a condiciones ligeramente superiores al punto crítico de mezcla con una alta relación de caudales antisolvente-disolución es lo óptimo para obtener la mejor distribución de tamaño de partícula sin la aparición de agregados en nuestro proceso SEDS.

• Referencias también citadas

[1] A. H. Lefebvre, Atomization and sprays, 1º Ed.- Estados Unidos: Ed. Taylor and Francis, 1988.

[2] E. Badens; O. Boutin; G. Charbit, Laminar jet dispersion and jet atomization in pressurized carbon dioxide. J. Supercrit. Fluids 36 (2005) 81-90.

[3] Y. Sun; B. Y. Shekunov, Surface tension of ethanol in supercritical CO_2, J. Supercrit. Fluids 27 (2003) 73-83.

[4] S. S. Dukhin; C. Zhu; R. Dave; R. Pfeffer; J. J. Luo; F. Chavez; Y. Shen, Dynamic interfacial tension near critical point of a solvent-antisolvent mixture and jet estabilization, Colloid: Surf. A: Physicochem. Eng. Asp. 229 (2003) 181-199.

[5] E. Reverchon; E. Torino; S. Dowy; A. Brauer; A. Leipertz, Interactions of phase equilibria and mass transfer during supercritical antisolvent micronization, Chem. Eng. J. 156 (2010) 446-458.

[6] N. Czerwonatis; R. Eggers, Disintegration of liquid jets and drop drag coefficients in pressurized nitrogen and carbon dioxide, Chem. Eng. Technol. 24 (2001) 619-624.

[7] M. Mukhopadhyay; S. Dalvi, Mass and heat transfer analysis of SAS: effects of thermodynamics states and flow rates on droplet size, J. Supercrit. Fluids 30 (2004) 333-348.

CAPÍTULO 10.

Conclusiones

10.1. Conclusiones

Teniendo en cuenta el trabajo realizado y descrito a lo largo de esta tesis doctoral, pueden extraerse las siguientes conclusiones.

● Se ha estudiado un proceso de precipitación de fármacos mediante un proceso con CO_2sc como antisolvente (SEDS) a fin de determinar las condiciones óptimas de operación. Asimismo, se han determinado los equilibrios de fase involucrados en este proceso (estudiando más detalladamente los equilibrios sólido-fluido supercrítico).

● Para ello, se ha realizado un estudio de la influencia de las variables termodinámicas (presión y temperatura), regímenes de atomización y transferencia de materia en las partículas generadas de acetaminofén y tretinoína mediante un proceso SEDS, utilizando etanol como disolvente para ambos fármacos.

● Se ha realizado un estudio teórico-experimental de los equilibrios de fases binarios y ternarios de los sistemas CO_2-etanol-acetaminofén y CO_2-etanol-tretinoína mediante la ecuación de Peng-Robinson y utilizando una celda de equilibrio.

A partir de este estudio se determinaron las condiciones a las cuáles se obtenía el máximo grado de supersaturación, que coincidían con el punto crítico de mezcla antisolvente-disolvente. Se observó además que la adición del sólido no modificaba las condiciones del punto crítico de mezcla.

● Se han empleado diversas ecuaciones semiempíricas para modelar la solubilidad de fármacos en CO_2sc, a fin de estudiar la influencia de las condiciones experimentales en el error de ajuste obtenido. La ecuación de

Sparks producía el mejor ajuste a esos datos experimentales. Sin embargo, se observó, para todas las ecuaciones, que el error de ajuste aumentaba notablemente cuando se producía un alto incremento grande de temperatura debido a la dificultad para modelar datos de solubilidad en la cercanía del punto crítico final superior (*"upper critical end point"* (UCEP)).

● Se utilizaron diversas ecuaciones semiempíricas para modelar la solubilidad de fármacos en CO_2sc en presencia de cosolventes. Las ecuaciones de González y Reddy-Madras resultaron ser las más versátiles dado que pueden ser utilizadas en un intervalo amplio de concentraciones de cosolvente, además de no tener un gran número de parámetros ajustables. Se observó un incremento generalizado en el error si las condiciones experimentales se acercaban a las condiciones del punto crítico de mezcla cosolvente-CO_2sc debido a la transición de un sistema bifásico a un monofásico.

● Se estudió la modificación de los modelos semiempíricos para la solubilidad de sólidos en CO_2sc puro y con cosolventes mediante el concepto de entropía de Tsallis, obteniendo los modelos *q*. En los modelos *q* no aparecía la inconsistencia teórica con la temperatura de las ecuaciones sin modificar, aunque tanto los modelos originales como los modelos *q* proporcionaban el mismo error de ajuste de la solubilidad.

● Se desarrolló un método para la determinación de la presión de sublimación de moléculas complejas mediante el modelado de la solubilidad del sólido objeto de estudio en CO_2sc con ecuaciones semiempíricas. Dicho método fue validado calculando la presión de sublimación de diferentes sólidos de forma exitosa.

Posteriormente, la presión de sublimación calculada con el método desarrollado en esta tesis fue utilizada en diversas aplicaciones relacionadas con

la investigación en la industria farmacéutica, como puede ser el cálculo de las propiedades de solvatación.

● Se procedió al desarrollo de un modelo robusto mediante el empleo de la contribución de grupos para la estimación de las entalpías de sublimación de compuestos orgánicos compuestos por anillos aromáticos y/o policíclicos sustituidos con un error menor del 9%.

● Se desarrolló un test de consistencia para analizar datos de solubilidad de fármacos en CO_2sc basado en la entalpía de sublimación del sólido y en un factor de mejora modificado. Este test fue desarrollado mediante el estudio de más de 2000 datos experimentales obtenidos de bibliografía, y fue probado de forma satisfactoria con varios fármacos. Este método posibilita el análisis de exactitud de los datos experimentales para nuevos fármacos en CO_2sc.

● Las condiciones óptimas experimentales para la generación de partículas con un equipo SEDS son ligeramente superiores al punto crítico de mezcla antisolvente-disolvente. En estas condiciones se obtiene la menor resistencia a la transferencia de materia en la película del líquido y el mayor grado de supersaturación.

● De entre los tres regímenes de desintegración descritos a un proceso de desintegración de un chorro a alta presión, el régimen de atomización se presenta como el óptimo para llevar a cabo los experimentos. Esto es debido a que este régimen produce el menor tamaño de gota inicial y el mejor grado de dispersión del chorro atomizado. Estas características son las más adecuadas para la obtención de una mejor distribución de tamaño de partícula sin la aparición de agregados.

10.2. Trabajo futuro

Finalizado este trabajo, quedan abiertas una serie de posibles líneas de investigación, que se describen a continuación:

• La aplicación de la técnica SEDS para la microencapsulación de la tretinoína y el acetaminofén en polímeros biodegradables y biocompatibles. Para ello se debería operar inicialmente a las condiciones para las que se obtuvo la mejor distribución de tamaño de partícula (y determinadas en esta tesis doctoral), pero variando la cantidad de polímero y los respectivos flujos de antisolvente y disolución. Estas variaciones de flujos y de concentraciones de polímero tendrían que ser correlacionadas con el rendimiento de microencapsulación.

• Caracterización de la boquilla. En esta tesis se ha trabajado con una longitud fija de mezcla de la boquilla. Sería interesante el estudio del efecto de la variación de esa longitud en los resultados experimentales obtenidos.

• Realización de un estudio computacional del proceso SEDS con el fin de incorporar la cinética de precipitación. Para ello, se debería modificar el diseño de la vasija, que debería tener un cristal a fin de realizar la grabación de la ruptura del chorro.

Posteriormente, una vez aplicadas las condiciones iniciales y las ecuaciones convenientes en el programa de elementos finitos, se procedería a la comparación entre la fotografía obtenida y el resultado computacional. En caso de ser positiva, se podría conocer el perfil de sobresaturación. Conociendo este perfil se podría conseguir la predicción del tamaño de partícula obtenido.

• Predicción de la solubilidad de fármacos en fluidos supercríticos. Actualmente no existe ninguna metodología para la predicción de este tipo de solubilidad, ya que todas las ecuaciones necesitan de parámetros de interacción

que deben ser calculados mediante una regresión de datos experimentales frente a datos teóricos. La posibilidad de realizar esa predicción sería de una importancia considerable para procesos de extracción supercrítica o de generación de partículas, porque se podría determinar la viabilidad del proceso sin experimentos previos de solubilidad.